A high-density electroencephalographic investigation of sleep brain oscillations: a unique window to explore neuropsychiatric disorders

A doctoral dissertation presented by

Anna Castelnovo

Under the supervision of

Prof. Dr. Med. Mauro Manconi

Submitted to the

Faculty of Biomedical Sciences

Università della Svizzera italiana

For the degree of

Ph.D. in Biomedical Sciences (Human Neurosciences)

October 2022

Contents

1. INTRODUCTION

1.1. Preface

This is a cumulative thesis articulated in 5 different projects to show the potential use of sleep high-density EEG analysis in different in neuro-psychiatric disorders.

Sleep is a recurring and rapidly reversible behavioural state characterized by altered consciousness and awareness, reduced muscle activity and almost absent interactions with the environment. Despite being a highly risky behaviour, sleep evolved ubiquitously throughout the animal kingdom due to its essential role for life. Indeed, sleep plays a crucial role in many physiological functions, such as brain development, neuroplasticity, memory, learning (Diekelmann and Born, 2010), tissue growth and repair (Bellesi et al., 2016), immune system (Imeri and Opp, 2010), autonomic and emotion regulation (Walker, 2009), and probably much more.

The study of sleep has therefore implications not solely in the sleep-field but also for a wealth of other disciplines, like neuroscience, neurology, psychiatry, psychology, and even apparently more distant disciplines, like immunology or pneumology. Moreover, sleep studies offer several advantages over wake studies, like fewer muscular artifacts and no biases related to inattention. Last but not least, the growing knowledge on sleep circuits from animal studies, are destined to inform and guide human studies in many ways. Of specific interest for this thesis, the disruption of specific sleep oscillations in humans indirectly suggests the involvement of the underlying brain structures and networks responsible for their generation. Thus, sleep oscillations can be considered a proxy for brain connectivity and excitability.

The general **aim** was to take advantage of sleep brain oscillations recorded non-invasively using scalp high density electroencephalography (hdEEG) to inform specific pathological processed in the field of sleep and psychiatry. To reach this goal, sophisticated signal processing techniques were used to build-up a hdEEG pipeline for sleep data analysis (pre-processing and post processing) in the Matlab environment. The first project represents a first important methodological effort to develop a solid, structured and fluent hdEEG pipeline (**Project 1)**. This effort was also meant as a necessary step to favour and implement the use of hdEEG, currently mainly used for research porpoises, into clinical practice. The hdEEG pipeline developed for this thesis was mainly tailored to study slow waves, sleep slow oscillations in the range of 0.5-4 Hz. I selected this specific frequency range because it represents the most prominent feature of “deeper” and more restorative sleep, which has been associated with many fundamental sleep functions, like experience-dependent plasticity (Huber et al., 2004; Massimini et al., 2009). As a second step, this pipeline was applied to study several slow wave properties in a group of healthy subjects (**Project 2**) composed of both young adolescents and young adults. As a third step, hdEEG slow wave analysis was applied to sleep and psychiatric disorders. More specifically, I selected Attention Deficit Hyperactivity (ADHD) disorder as a representative pathological condition in child psychiatry (**Project 3**), first-episode psychosis (FEP) as a representative pathological condition in adult psychiatry (**Project 4**), and Disorders of Arousal (DOA) as a representative pathological condition in sleep medicine (**Project 5**). Each project includes a short overview on the study sample, the study aim(s) and results, a copy of the related original paper(s) that resulted from each experiment, and a short discussion of possible future directions.

Before moving to the description of each project, key basic concepts on sleep and EEG will be reviewed in this first thesis chapter.

1.2. EEG

Invented in 1924 by a German psychiatrist, Hans Berger, EEG is one of the oldest technologies that measure neuronal activity in humans. Scalp EEG is now part of the clinical routine in the neurologic/epileptological field and the technique of choice to study sleep. (Figure 1).

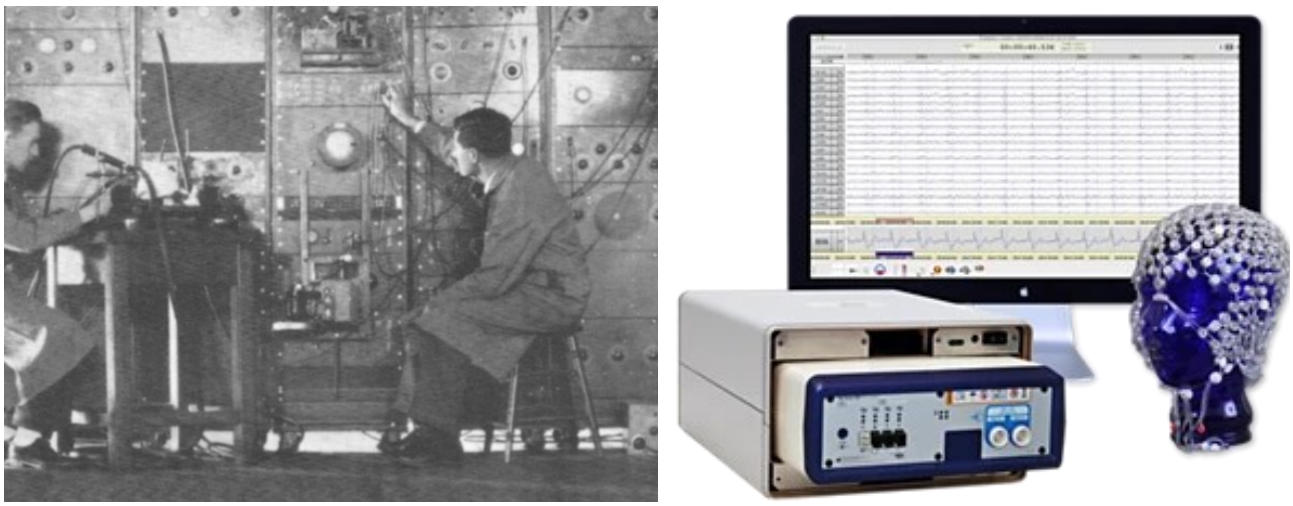

Figure 1. EEG models throughout history. *EEG equipment used in 1934. Taken from* (Stone and Hughes, 2013). *Right*: current high density EEG system used for research (https://www.philips.com.qa/).

Contrary to other neuro-imaging techniques, like PET, SPECT and MRI, EEG offers a unique opportunity to image the brain with exquisite temporal resolution (sub-seconds) throughout

the entire sleep period and without restriction of normal or pathologic nocturnal movements. Furthermore, in contrast to other imaging procedures, EEG is relatively inexpensive, portable, and can be performed repeatedly. In addition, with digitalization and technological advancement, EEG signal analysis changed from pure visual inspection (still valuable and fundamental for clinical practice) to a comprehensive evaluation of the temporal and spatial dynamics of the recorded signals.

Although EEG has been traditionally hampered by a low spatial resolution, the implementation of high-density EEG (hdEEG) for research purposes – meaning EEG systems with an increased number of scalp electrodes (up to 256) - marked the full title entrance of hdEEG in the list of neuroimaging modalities. hdEEG high spatial resolution allows to localize more precisely and more reliably the brain generators of the recorded activity at the scalp surface, using a combination of precise head anatomical information by magnetic resonance imaging (MRI) and sophisticated source localization algorithms (see Chapter 2). With 256 channels hdEEG systems, the current resolution is ~ 1-2 cm. This resolution is surely below the one offered by MRI (~1 mm, or even less with current ultra-high magnetic field MRI scanners). The accuracy the EEG source reconstruction is affected by a number of factors including head-modelling errors, source-modelling errors and EEG instrumental or biological noise (Grech et al., 2008).

Despites technological advantages, the physiology behind EEG recording did not change. EEG basically detects and amplifies the electrical activity of the brain using small, metal electrodes on the scalp. EEG systems are composed of recording electrodes, an amplifier,

analogical and/or digital filters, a system to acquire data, and a screen to visualize the signal. The signal is always compared to the signal recorded by an electrode chosen as reference.

This signal measures the electrical activity of a living brain, and more in particular – if the measurement is performed on the scalp - it measures the sum of post-synaptic (dendritic) potentials produced by the pyramidal cells located in the brain cortex (Figure 2).

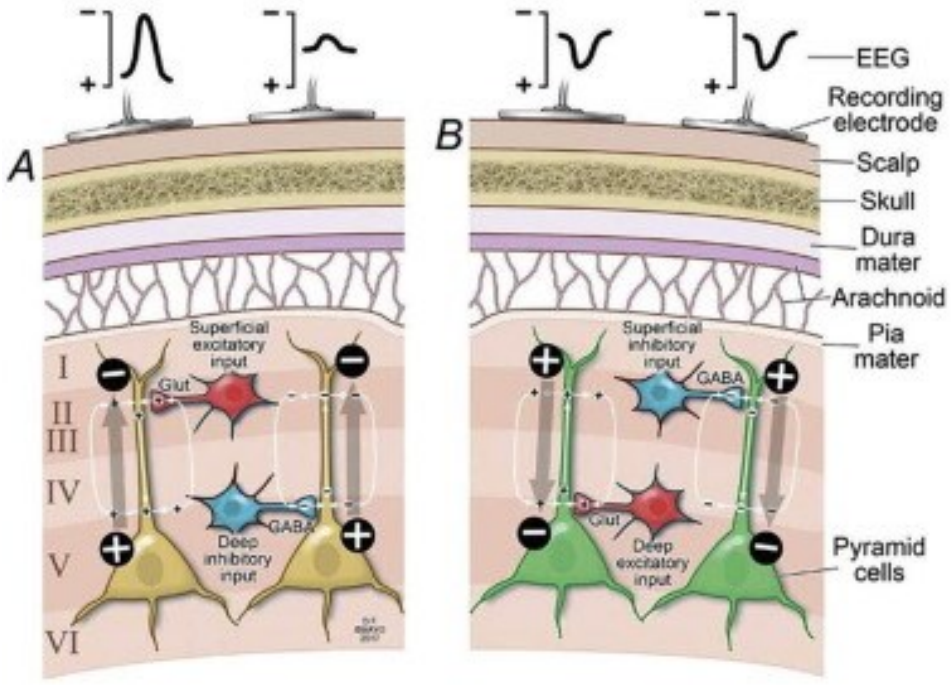

Figure 2. Physiological mechanisms of EEG signal. *Since these neurons are organized in columns which are located perpendicularly to the scalp, the sum of the potentials recorded by the electrode is different from zero. Taken from* (Tatum et al., 2018).

The measured activity is traditionally divided in multiple frequency bands: delta or slow wave activity (SWA, 0.5-4 Hz), theta (4-8 Hz), alpha (8-16 Hz), beta (16-30 Hz), gamma (>30 Hz).

When cells firing is desynchronized (during wakefulness, see Figure 3), scalp EEG is dominated by high frequency low voltage oscillations. The more neuronal firing is synchronized and coordinated (during specific phases of sleep), the higher is the EEG voltage and the slower are the rhythms that appear in sleep recordings.

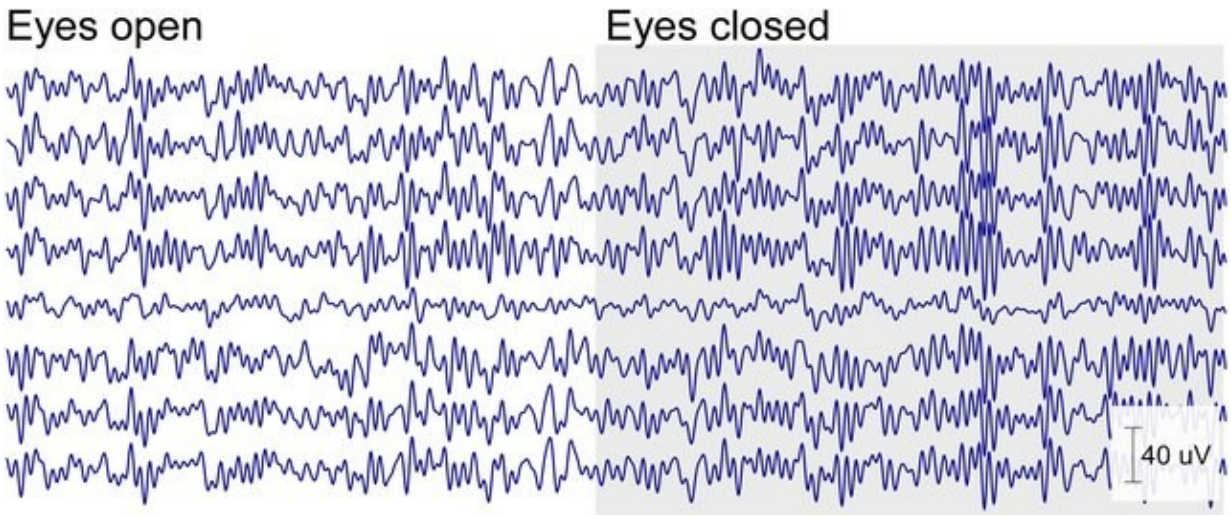

Figure 3. EEG during wakefulness. *The upper panel illustrates one EEG trace during wakefulness, when eyes are open (left side) and when eyes are closed (right side). The lower panel shows the spectrogram of the signal (power in different frequency bands over time). When eyes are closed, a sharp increase of alpha rhythm could be appreciated, especially in occipital electrodes. Taken from* (Bleichner and Debener, 2017).

1.3. EEG in sleep

During sleep the EEG is extremely different from wakefulness due to subtle but significant changes in the mechanisms that govern neuronal firing and excitability (Figure 4).

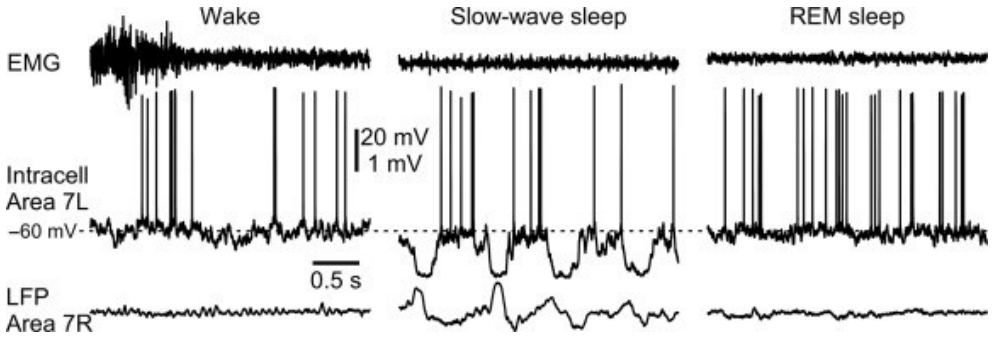

Figure 4. Recording of single neuronal units and local field potentials (LFP). The figure exemplifies the difference in firing between waking and sleep. *During waking the firing is irregular but always present, instead during sleep there is an alternation of ON and OFF periods. During ON periods the firing is stronger or as strong as waking firing, during OFF periods there is almost no firing. Taken from* (Timofeev and Chauvette, 2019).

The identification of different sleep stages is based on the coordinated recording of EEG, electromyography (EMG), and electrooculography (EOG). All three are needed, reminding us that sleep is primarily a behavioral state, and EEG just a way to measure it under a particular perspective.

NREM sleep (NREM) is composed of 3 stages (Figure 4) according to traditional scoring rules (Berry RB, Brooks R, Gamaldo CE, Harding SM, Lloyd RM, Marcus CL, 2020):

1) Stage 1 (N1) is the stage of transition from wake to sleep and it is characterized by a low voltage EEG activity and the attenuation of the alpha rhythm (produced by the brain activity when eyes are closed), so that less than 50 % of the waves are in the alpha range in every 30 seconds epoch (sleep scoring is usually approximated to 30 secs epochs windows).

2) Stage 2 (N2) typically presents two specific brain oscillations, meaning sleep spindles and

K-complexes.

3) Stage 3 (N3) - which is often called Slow Wave Sleep (SWS), Delta Sleep or Deep Sleep – is characterized by a slow and synchronized activity, which occupies at least the 20% of a 30 seconds epoch. During this stage sleep spindles can be a common finding, although slow waves are more typical and tend to mask them.

REM (Rapid Eye Movement) sleep typically presents a desynchronized, fast, low voltage EEG activity, similar to waking EEG (Figure 5). In addition, it is characterized by muscle atony (low EMG voltage), and conjugated rapid eye movements usually initiated by an EOG deflection <500 milliseconds (ms).

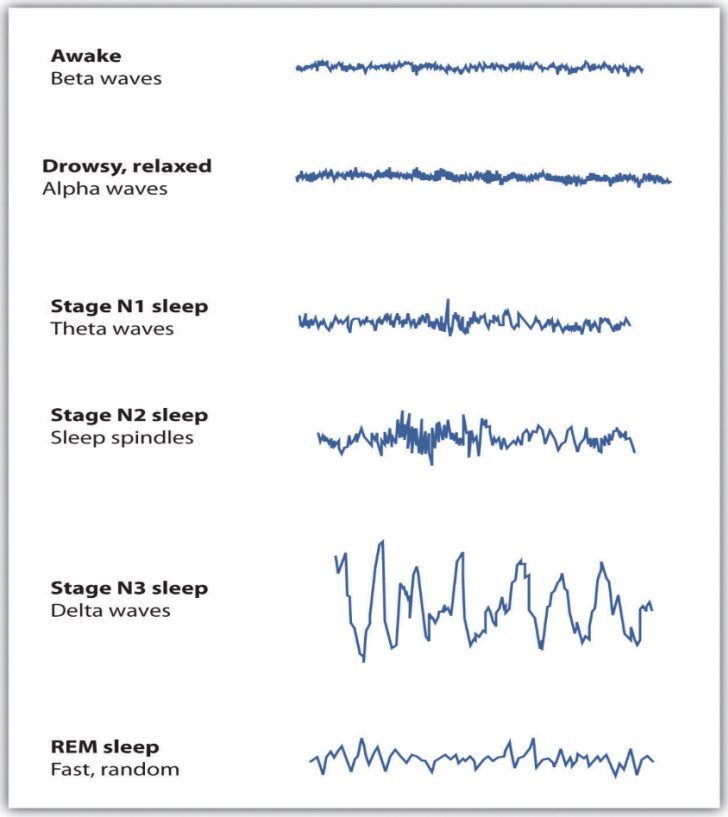

Figure 5. Graphic explicative representation of EEG during wakefulness and sleep.

Taken from (Stangor and Walinga, 2014).

During the night, these stages rotate in around 90 minutes cycles, as described in the hypnogram below (Figure 6).

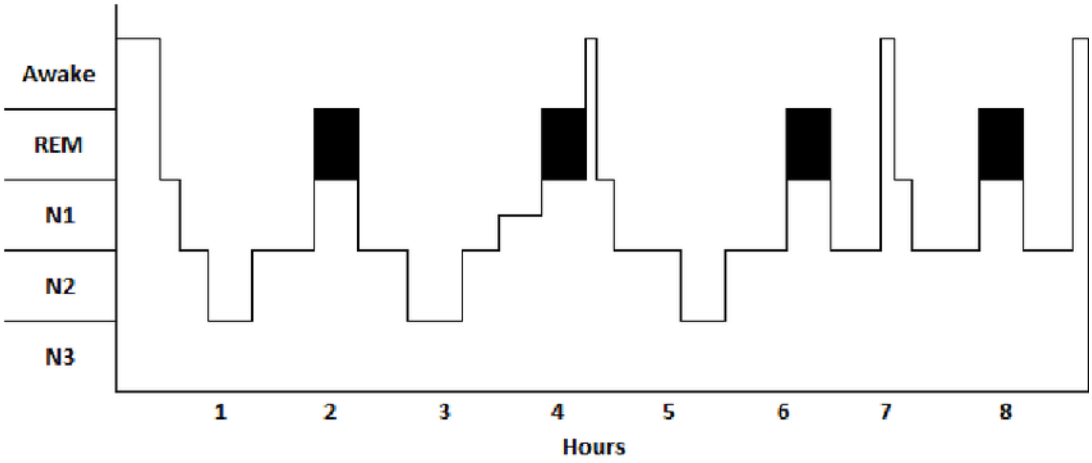

Figure 6. Hypnogram of a typical night sleep of a healthy young adult*. The hypnogram shows the typical alternation of NREM and REM sleep cycles (the average is 4-5 cycles each night). Throughout the night there's a progressive reduction of NREM (N3 in particular), and an increase of REM. Taken from* (Miller et al., 2015).

While NREM sleep has long been connected to unconsciousness and synaptic downscaling (meaning the decrease of the strength of each synapsis by the same factor and the potential loss of less connected synapses) (Tononi and Cirelli, 2014), REM sleep has been typically connected to dreams and to the regulation of emotions and emotional memories (Ackermann and Rasch, 2014).

However, several studies have now shown that sleep is not a global phenomenon (Nobili et al., 2012), and that small isles of neuros may locally produce sleep during wakefulness

(D'Ambrosio et al., 2019), or wake during sleep (Nobili et al., 2011) or while falling asleep (Magnin et al., 2010; Marzano et al., 2013; Sarasso et al., 2014), or NREM sleep into REM sleep (Baird et al., 2018; Bernardi et al., 2019; Funk et al., 2016), or probably even REM sleep in the context of NREM sleep (Nielsen, 2000; Siclari et al., 2017). Similarly, mental activity during sleep may occur independently of the sleep stage, as demonstrated in one third or more of the awakenings out of NREM sleep (Siclari et al., 2013).

This physiological co-occurrence of different sleep and wake states is particularly evident during transitional states, like the arousal process (Peter-Derex et al., 2015; Ruby et al., 2021). This may sometimes turn into pathology (Mahowald and Schenck, 2005, 2001, 1992; Siclari and Tononi, 2017) (see Figure 7 for a graphical representation of the concept), for example during NREM sleep parasomnia episodes (Castelnovo et al., 2018), where wakefulness largely intrudes into NREM sleep, in different brain regions or even in the same brain areas, as I will discuss in project 4.

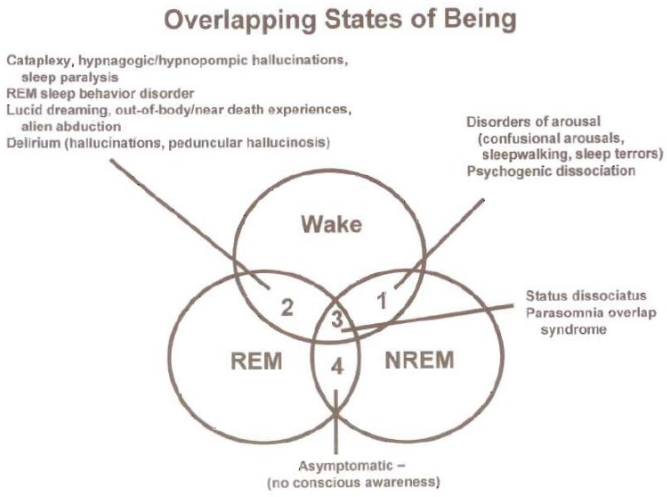

Figure 7. Areas of overlap among states of being. *Taken from* (Mahowald and Schenk, 2001).

1.4. Sleep slow waves

Slow waves are the most prominent electroencephalographic (EEG) signature of non-rapid eye movement (NREM) sleep. Slow waves are defined as slow EEG oscillations at a frequency of 0.5-4 Hz (Figure 8). For sleep scoring porpoises, slow wave negative peak amplitude should be equal or higher than 75 μV (as measured over the frontal cortex). Their rate of occurrence increases progressively after sleep onset, reaching almost once per second as sleep deepens.

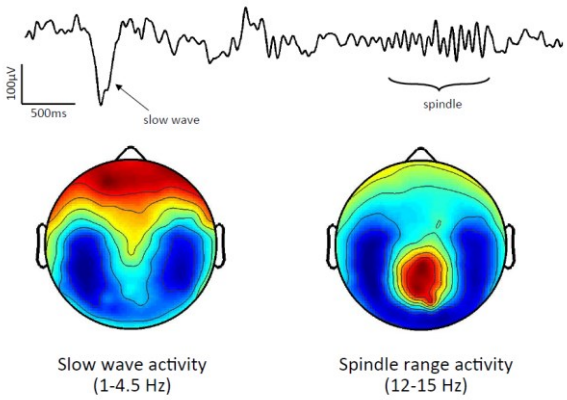

Figure 8. Graphic representation of a slow wave and a spindle in a typical EEG recording and of their topographic distribution. *Red indicates a higher density while blue indicates a lower density of these two elements. Taken from* (Tononi et al., 2009).

Slow waves are markers of, and probably have a direct role in a variety of fundamental functions, including the maintenance of disconnection from the external environment during sleep (Pigorini et al., 2015), synaptic plasticity and learning (de Vivo et al., 2017; González-Rueda et al., 2018; Tononi, 2009), cellular restoration and the clearance of neurotoxic metabolites (Xie et al., 2013). Even more notably, extensive changes in slow waves have been also observed in association with brain maturation, from childhood through adolescence. Indeed, sleep depth measured as the absolute SWA power progressively

decreases, in parallel with massive synaptic remodeling (Buchmann et al., 2011b). Even more strikingly, SWA peak activity migrates along the postero-anterior axis during development (Kurth et al., 2010) (see Figure 9).

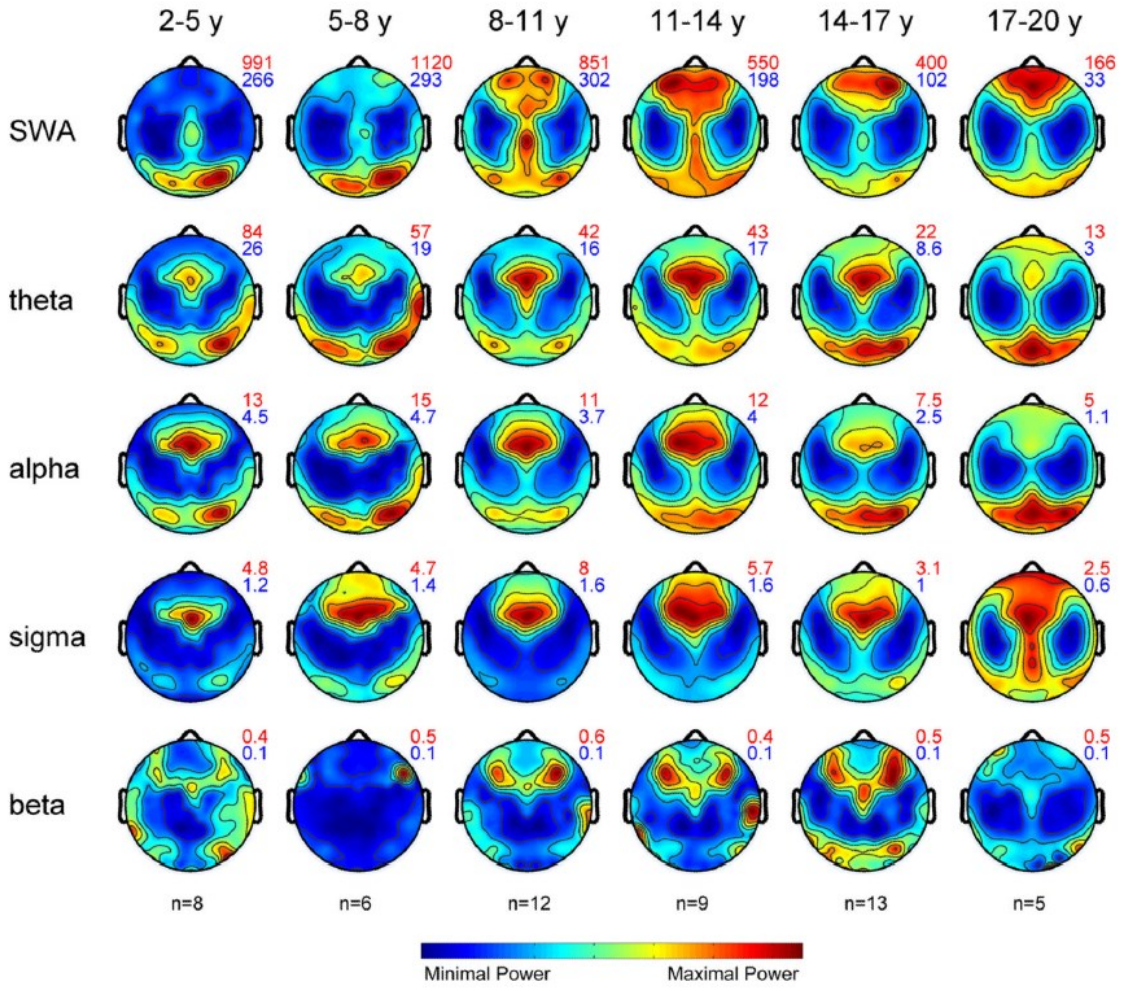

Figure 9. EEG power during NREM sleep throughout development.

Maps were normalized for each individual and then averaged for each age group. Values are color coded (maxima in red, minima in blue) and plotted on the planar projection of the hemispheric scalp model. At the top right of the maps, numbers indicate maxima and minima (in square microvolts) for each plot. Figure taken from (Kurth et al., 2010).

Slow waves derive from the summed activity of large ensembles of cortical neurons, whose membrane potentials during NREM sleep become “bistable”. Indeed, instead of firing tonically, cortical neurons start to fluctuate between hyperpolarized “silent” phases (or down-states) and depolarized “active” firing phases (or up-states) (Steriade et al., 1993a, 1993b), due to the reduction of wake-promoting neuro-modulators. Thus, each time a slow wave is produced, cortical cells hyperpolarize and remain silent for a dozen or hundreds of milliseconds (corresponding to the wave down-state or negative peak). This is then followed by a tonic depolarization, which is often associated with an action potential generation (corresponding to the slow wave up-state). This process is almost synchronous over large cortical sections, so that sleep slow waves can be recorded using the scalp EEG. However, this process is not perfectly synchronous. Using hdEEG recordings in humans, Massimini et al. showed that there is a small delay (of few milliseconds) between the negative peak of each slow wave, meaning that, at a macroscale level, slow waves behave as traveling waves (Massimini et al., 2004). In other words, these slow bursts of neuronal excitation and depolarization spread across the cortex following specific patterns at an estimated speed of 1.2–7.0 m/sec (Figure 10). The pattern of origin and propagation of sleep slow oscillations is reproducible across nights and subjects and provides a blueprint of cortical excitability and connectivity (Murphy et al., 2009). More specifically, in adults, slow waves seem to originate more frequently in orbitofrontal regions and tend to propagate mainly following antero-posterior direction. Such a long-range synchronization and propagation is assumed to reflect the structural integrity and maturation of cortico-cortical white matter connections (Buchmann et al., 2011a; Kurth et al., 2017; Murphy et al., 2009; Piantoni et al., 2013),

including the corpus callosum (Avvenuti et al., 2020; Bernardi et al., 2021), which is the main route responsible for cross-hemispheric slow wave propagation.

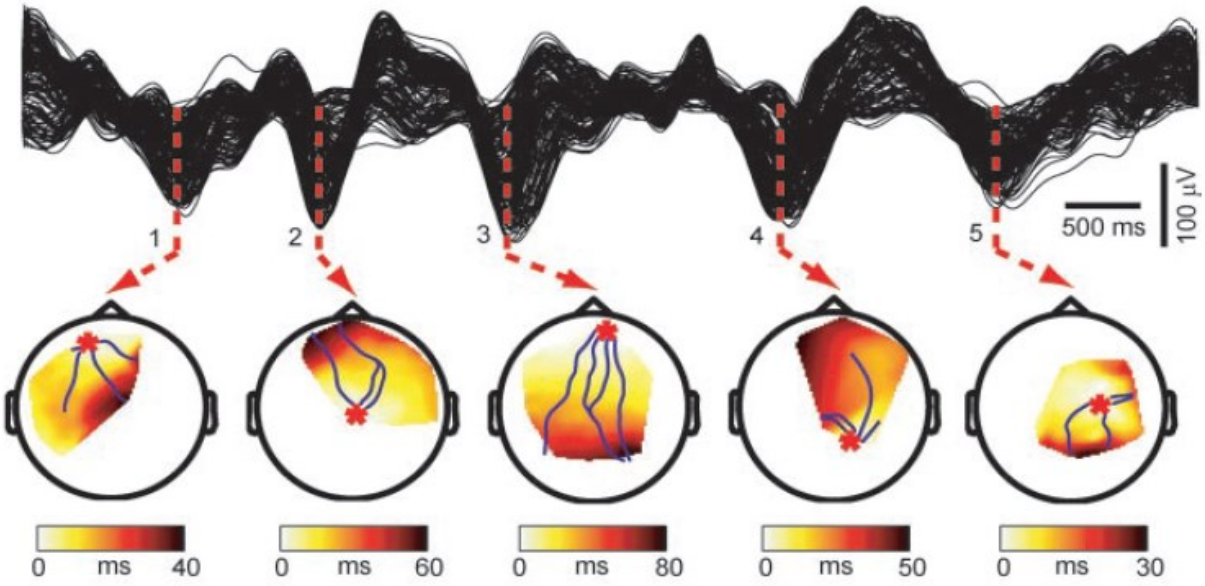

Figure 10. Visual representations of slow wave traveling. *Signal recorded from 256 scalp electrodes during 5 consecutive cycles of the slow oscillation and their corresponding delay maps. Each wave has a different origin and spreads over the scalp with a distinct pattern of propagation (from Massimini et al., 2004).*

Slow waves can be generated by the cortex when it is isolated from thalamic input (Steriade et al., 2001, 1993b). The excitatory cortical neurons located in the 5th layer may play a fundamental role in the generation and spread of cortical up states (Sanchez-Vives et al., 2000; Wester et al., 2012; Beltramo et al., 2013), although a recent study clearly pointed also to the role of GABAergic somatostatin positive neurons - but not of parvalbumin positive ones (Funk et al., 2017).

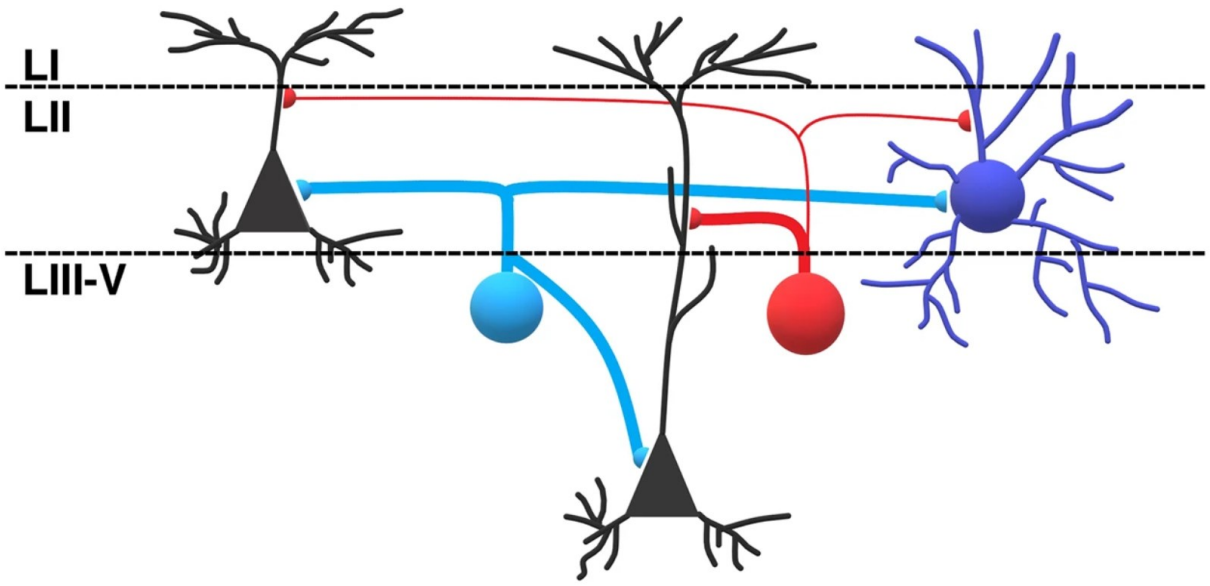

Figure 11. Graphic representation of the complex interactions between pyramidal excitatory neurons and GABAergic interneurons. *Layer II: pyramidal (black, left), stellate (black, right). Layer III–V: pyramidal (black, bottom), PV+ interneuron (PV, blue), and SOM+ interneuron (SOM, red). Taken from* (Kecskés et al., 2020).

The most common (~70%) GABAergic SOM+ are the so-called cells of Martinotti. These cells are diffusely represented in every part of the cortex. Their somas are located in the 5th layer of the neocortex and their axons characteristically extend to the cortex surface (1st layer), which is the area where numerous cortico-cortical and TC connections converge. In layer 1 they create a kind of functional syncytium through complex synaptic arborizations and gap junctions. These cells activation comes as a consequence of the pyramidal cells synchronous firing that takes place at the end of the up states. Their activation causes a powerful and synchronous inhibition of the excitatory transmission across many pyramidal cells located over large brain sections. This mechanism is able to explain the OFF period and the down states that can be observed during NREM sleep, as well as the slow wave tendency to travel throughout the cortex (at least over short distances).

However, growing literature has shown that the thalamus can also generate slow waves, as suggested by the following observations:

1) In vitro, both thalamo-cortical (TC) neurons and neurons in the thalamic reticular nucleus (TRN) show a strong rhythmic alternation of up and down states, when they are isolated from the rest of the central nervous system (Blethyn et al., 2006; Crunelli and Hughes, 2010; Hughes et al., 2002);
2) In vivo, TC neurons firing is strictly associated with EEG slow waves (and in specific thalamic nuclei, precede cortical up states) (Sheroziya and Timofeev, 2014; Slézia et al., 2011).
3) Moreover, the selective activation of TC neurons using optogenetic techniques can induce slow waves occurrence in mice and rats (David et al., 2013; Fernandez, 2012). More specifically, while the tonic activation of centro-medial thalamus induces wakefulness, its burst activation induces up-states in the cingulate cortex and finally in the cerebral cortex though the relay of the anterior thalamic nucleus (Gent et al., 2018b, 2018a);
4) Studies performed on rats and cats conclusively demonstrated the presence of significant slow waves alterations during anesthesia and physiologic sleep after optogenetic or pharmacologic thalamic inactivation (David et al., 2013; Lemieux et al., 2014);
5) In humans, thalamic nuclei lesions can impair slow waves slope renormalization (Jaramillo et al., 2021).

Taken together, these data show that both cortical and thalamic neurons can generate and influence slow rhythms.

Thus, which come first: the chick or the egg?

As neither the isolated cortex nor the isolated thalamus can express slow waves identical to those observed in vivo, slow wave full expression seems to require an intact thalamocortical network, although their full complex interplay is still not completely uncovered (Adamantidis et al., 2019; Crunelli et al., 2015).

1.5. References

Ackermann, S., Rasch, B., 2014. Differential effects of non-REM and REM sleep on memory consolidation? Curr Neurol Neurosci Rep 14, 1–10. https://doi.org/10.1007/S11910-013-0430-8/TABLES/1

Adamantidis, A.R., Gutierrez Herrera, C., Gent, T.C., 2019. Oscillating circuitries in the sleeping brain. Nat Rev Neurosci 20, 746–762. https://doi.org/10.1038/S41583-019-0223-4

Avvenuti, G., Handjaras, G., Betta, M., Cataldi, J., Imperatori, L.S., Lattanzi, S., Riedner, B.A., Pietrini, P., Ricciardi, E., Tononi, G., Siclari, F., Polonara, G., Fabri, M., Silvestrini, M., Bellesi, M., Bernardi, G., 2020. Integrity of Corpus Callosum Is Essential for theCross-Hemispheric Propagation of Sleep Slow Waves:A High-Density EEG Study in Split-Brain Patients. J Neurosci 40, 5589–5603. https://doi.org/10.1523/JNEUROSCI.2571-19.2020

Baird, B., Castelnovo, A., Riedner, B.A., Lutz, A., Ferrarelli, F., Boly, M., Davidson, R.J., Tononi, G., 2018. Human Rapid Eye Movement Sleep Shows Local Increases in Low-Frequency Oscillations and Global Decreases in High-Frequency Oscillations Compared to Resting Wakefulness. eNeuro 5. https://doi.org/10.1523/ENEURO.0293-18.2018

Bellesi, M., Bushey, D., Chini, M., Tononi, G., Cirelli, C., 2016. Contribution of sleep to the repair of neuronal DNA double-strand breaks: Evidence from flies and mice. Sci Rep. https://doi.org/10.1038/srep36804

Bernardi, G., Avvenuti, G., Cataldi, J., Lattanzi, S., Ricciardi, E., Polonara, G., Silvestrini, M., Siclari, F., Fabri, M., Bellesi, M., 2021. Role of corpus callosum in sleep spindle synchronization and coupling with slow waves. Brain Commun 3, fcab108. https://doi.org/10.1093/braincomms/fcab108

Bernardi, G., Betta, M., Ricciardi, E., Pietrini, P., Tononi, G., Siclari, F., 2019. Regional delta waves in human rapid eye movement sleep. Journal of Neuroscience 39, 2686–2697. https://doi.org/10.1523/JNEUROSCI.2298-18.2019

Berry RB, Brooks R, Gamaldo CE, Harding SM, Lloyd RM, Marcus CL, V.B., 2020. The AASM Manual for the Scoring of Sleep and Associated Events: Rules, Terminology and Technical Specifications, 2.6 versio. ed.

Bleichner, M.G., Debener, S., 2017. Concealed, unobtrusive ear-centered EEG acquisition: Ceegrids for transparent EEG. Front Hum Neurosci 11. https://doi.org/10.3389/FNHUM.2017.00163

Blethyn, K.L., Hughes, S.W., Tóth, T.I., Cope, D.W., Crunelli, V., 2006. Neuronal Basis of the Slow (<1 Hz) Oscillation in Neurons of the Nucleus Reticularis Thalami In Vitro. Journal of Neuroscience 26, 2474–2486. https://doi.org/10.1523/JNEUROSCI.3607-05.2006

Buchmann, A., Kurth, S., Ringli, M., Geiger, A., Jenni, O.G., Huber, R., 2011a. Anatomical markers of sleep slow wave activity derived from structural magnetic resonance images. J Sleep Res 20, 506–513. https://doi.org/10.1111/J.1365-2869.2011.00916.X

Buchmann, A., Ringli, M., Kurth, S., Schaerer, M., Geiger, A., Jenni, O.G., Huber, R., 2011b. EEG sleep slow-wave activity as a mirror of cortical maturation. Cereb Cortex 21, 607–615. https://doi.org/10.1093/CERCOR/BHQ129

Castelnovo, A., Lopez, R., Proserpio, P., Nobili, L., Dauvilliers, Y., 2018. NREM sleep parasomnias as disorders of sleep-state dissociation. Nat Rev Neurol 14, 470–481. https://doi.org/10.1038/s41582-018-0030-y

Crunelli, V., David, F., Lorincz, M.L., Hughes, S.W., 2015. The thalamocortical network as a single slow wave-generating unit. Curr Opin Neurobiol 31, 72–80. https://doi.org/10.1016/j.conb.2014.09.001

Crunelli, V., Hughes, S.W., 2010. The slow (<1 Hz) rhythm of non-REM sleep: a dialogue between three cardinal oscillators. Nat Neurosci 13, 9. https://doi.org/10.1038/NN.2445

D'Ambrosio, S., Castelnovo, A., Guglielmi, O., Nobili, L., Sarasso, S., Garbarino, S., 2019. Sleepiness as a Local Phenomenon. Front Neurosci 13, 1086. https://doi.org/10.3389/fnins.2019.01086

David, F., Schmiedt, J.T., Taylor, H.L., Orban, G., di Giovanni, G., Uebele, V.N., Renger, J.J., Lambert, R.C., Leresche, N., Crunelli, V., 2013. Essential thalamic contribution to slow waves of natural sleep. J Neurosci 33, 19599–19610. https://doi.org/10.1523/JNEUROSCI.3169-13.2013

de Vivo, L., Bellesi, M., Marshall, W., Bushong, E.A., Ellisman, M.H., Tononi, G., Cirelli, C., 2017. Ultrastructural Evidence for Synaptic Scaling Across the Wake/sleep Cycle. Science 355, 507. https://doi.org/10.1126/SCIENCE.AAH5982

Diekelmann, S., Born, J., 2010. The memory function of sleep. Nat Rev Neurosci 11, 114–126. https://doi.org/10.1038/nrn2762

Fernandez, L., 2012. Thalamic control of cortical states Related papers. https://doi.org/10.1038/nn.3035

Funk, C.M., Honjoh, S., Rodriguez, A. v., Cirelli, C., Tononi, G., 2016. Local slow waves in superficial layers of primary cortical areas during REM sleep. Current Biology 26, 396–403. https://doi.org/10.1016/j.cub.2015.11.062

Funk, X.C.M., Peelman, K., Bellesi, M., Marshall, X.W., Cirelli, X.C., Tononi, G., 2017. Role of Somatostatin-Positive Cortical Interneurons in the Generation of Sleep Slow Waves 37, 9132–9148. https://doi.org/10.1523/JNEUROSCI.1303-17.2017

Gent, T.C., Bandarabadi, M., Herrera, C.G., Adamantidis, A.R., 2018a. Thalamic dual control of sleep and wakefulness. Nat Neurosci 21, 974–984. https://doi.org/10.1038/S41593-018-0164-7

Gent, T.C., Bassetti, C. la, Adamantidis, A.R., 2018b. Sleep-wake control and the thalamus. Curr Opin Neurobiol 52, 188–197. https://doi.org/10.1016/j.conb.2018.08.002

González-Rueda, A., Pedrosa, V., Feord, R.C., Clopath, C., Paulsen, O., 2018. Activity-Dependent Downscaling of Subthreshold Synaptic Inputs during Slow-Wave-Sleep-like Activity In Vivo. Neuron 97, 1244-1252.e5. https://doi.org/10.1016/J.NEURON.2018.01.047

Grech, R., Cassar, T., Muscat, J., Camilleri, K.P., Fabri, S.G., Zervakis, M., Xanthopoulos, P., Sakkalis, V., Vanrumste, B., 2008. Review on solving the inverse problem in EEG source analysis. J Neuroeng Rehabil 5, 1–33. https://doi.org/10.1186/1743-0003-5-25/COMMENTS

Huber, R., Ghilardi, M.F., Massimini, M., Tononi, G., 2004. Local sleep and learning. Nature 430, 78–81. https://doi.org/10.1038/NATURE02663

Hughes, S.W., Cope, D.W., Blethyn, K.L., Crunelli, V., 2002. Cellular Mechanisms of the Slow (<1 Hz) Oscillation in Thalamocortical Neurons In Vitro. Neuron 33, 947–958. https://doi.org/10.1016/S0896-6273(02)00623-2

Imeri, L., Opp, M.R., 2010. Immune System Make Us Sleep. Nat Rev Neurosci.

Jaramillo, V., Jendoubi, J., Maric, A., Mensen, A., Heyse, N.C., Eberhard-Moscicka, A.K., Wiest, R., Bassetti, C.L.A., Huber, R., 2021. Thalamic Influence on Slow Wave Slope Renormalization During Sleep. Ann Neurol 90, 821–833. https://doi.org/10.1002/ANA.26217

Kecskés, M., Henn-Mike, N., Agócs-Laboda, Á., Szőcs, S., Petykó, Z., Varga, C., 2020. Somatostatin expressing GABAergic interneurons in the medial entorhinal cortex preferentially inhibit layerIII-V pyramidal cells. Communications Biology 2020 3:1 3, 1–13. https://doi.org/10.1038/s42003-020-01496-x

Kurth, S., Jenni, O.G., Riedner, B.A., Tononi, G., Carskadon, M.A., Huber, R., 2010. Characteristics of sleep slow waves in children and adolescents. Sleep 33, 475–480. https://doi.org/10.1093/sleep/33.4.475

Kurth, S., Riedner, B.A., Dean, D.C., O'Muircheartaigh, J., Huber, R., Jenni, O.G., Deoni, S.C.L., LeBourgeois, M.K., 2017. Traveling Slow Oscillations During Sleep: A Marker of Brain Connectivity in Childhood. Sleep 40. https://doi.org/10.1093/SLEEP/ZSX121

Lemieux, M., Chen, J.Y., Lonjers, P., Bazhenov, M., Timofeev, I., 2014. The impact of cortical deafferentation on the neocortical slow oscillation. J Neurosci 34, 5689–5703. https://doi.org/10.1523/JNEUROSCI.1156-13.2014

Magnin, M., Rey, M., Bastuji, H., Guillemant, P., Mauguière, F., Garcia-Larrea, L., 2010. Thalamic deactivation at sleep onset precedes that of the cerebral cortex in humans. Proc Natl Acad Sci U S A 107, 3829–3833. https://doi.org/10.1073/PNAS.0909710107

Mahowald, M.W., Schenck, C.H., 2005. Insights from studying human sleep disorders. Nature 437, 1279–1285. https://doi.org/10.1038/nature04287

Mahowald, M.W., Schenck, C.H., 2001. Evolving concepts of human state dissociation. Arch Ital Biol 139, 269–300. https://doi.org/10.4449/AIB.V139I3.504

Mahowald, M.W., Schenck, C.H., 1992. Dissociated states of wakefulness and sleep. Neurology 42, 44–51. https://doi.org/10.1201/9780429114373-10

Marzano, C., Moroni, F., Gorgoni, M., Nobili, L., Ferrara, M., de Gennaro, L., 2013. How we fall asleep: regional and temporal differences in electroencephalographic synchronization at sleep onset. Sleep Med 14, 1112–1122. https://doi.org/10.1016/J.SLEEP.2013.05.021

Massimini, M., Huber, R., Ferrarelli, F., Hill, S., Tononi, G., 2004. The sleep slow oscillation as a traveling wave. J Neurosci 24, 6862–6870. https://doi.org/10.1523/JNEUROSCI.1318-04.2004

Massimini, M., Tononi, G., Huber, R., 2009. Slow waves, synaptic plasticity and information processing: insights from transcranial magnetic stimulation and high-density EEG experiments. Eur J Neurosci 29, 1761–1770. https://doi.org/10.1111/J.1460-9568.2009.06720.X

Miller, C.B., Kyle, S.D., Melehan, K.L., Bartlett, D.J., 2015. Methodology for the Assessment of Sleep. Sleep and Affect: Assessment, Theory, and Clinical Implications 65–90. https://doi.org/10.1016/B978-0-12-417188-6.00004-9

Murphy, M., Riedner, B.A., Huber, R., Massimini, M., Ferrarelli, F., Tononi, G., 2009. Source modeling sleep slow waves. Proc Natl Acad Sci U S A 106, 1608–1613. https://doi.org/10.1073/pnas.0807933106

Nielsen, T.A., 2000. A review of mentation in REM and NREM sleep: "Covert" REM sleep as a possible reconciliation of two opposing models. Behavioral and Brain Sciences 23, 851–866. https://doi.org/10.1017/S0140525X0000399X

Nobili, L., de Gennaro, L., Proserpio, P., Moroni, F., Sarasso, S., Pigorini, A., de Carli, F., Ferrara, M., 2012. Local aspects of sleep: observations from intracerebral recordings in humans. Prog Brain Res 199, 219–232. https://doi.org/10.1016/B978-0-444-59427-3.00013-7

Nobili, L., Ferrara, M., Moroni, F., de Gennaro, L., Russo, G. lo, Campus, C., Cardinale, F., de Carli, F., 2011. Dissociated wake-like and sleep-like electro-cortical activity during sleep. Neuroimage 58, 612–619. https://doi.org/10.1016/J.NEUROIMAGE.2011.06.032

Peter-Derex, L., Magnin, M., Bastuji, H., 2015. Heterogeneity of arousals in human sleep: A stereo-electroencephalographic study. Neuroimage 123, 229–244. https://doi.org/10.1016/j.neuroimage.2015.07.057

Piantoni, G., Poil, S.S., Linkenkaer-Hansen, K., Verweij, I.M., Ramautar, J.R., van Someren, E.J.W., van der Werf, Y.D., 2013. Individual differences in white matter diffusion affect sleep oscillations. J Neurosci 33, 227–233. https://doi.org/10.1523/JNEUROSCI.2030-12.2013

Pigorini, A., Sarasso, S., Proserpio, P., Szymanski, C., Arnulfo, G., Casarotto, S., Fecchio, M., Rosanova, M., Mariotti, M., lo Russo, G., Palva, J.M., Nobili, L., Massimini, M., 2015. Bistability breaks-off deterministic responses to intracortical stimulation during non-REM sleep. Neuroimage 112, 105–113. https://doi.org/10.1016/J.NEUROIMAGE.2015.02.056

Ruby, P., Eskinazi, M., Bouet, R., Rheims, S., Peter-Derex, L., 2021. Dynamics of hippocampus and orbitofrontal cortex activity during arousing reactions from sleep: An intracranial electroencephalographic study. Hum Brain Mapp 42, 5188–5203. https://doi.org/10.1002/HBM.25609

Sarasso, S., Proserpio, P., Pigorini, A., Moroni, F., Ferrara, M., de Gennaro, L., de Carli, F., lo Russo, G., Massimini, M., Nobili, L., 2014. Hippocampal sleep spindles preceding neocortical sleep onset in humans. Neuroimage 86, 425–432. https://doi.org/10.1016/J.NEUROIMAGE.2013.10.031

Sheroziya, M., Timofeev, I., 2014. Systems/Circuits Global Intracellular Slow-Wave Dynamics of the Thalamocortical System. https://doi.org/10.1523/JNEUROSCI.4460-13.2014

Siclari, F., Baird, B., Perogamvros, L., Bernardi, G., LaRocque, J.J., Riedner, B., Boly, M., Postle, B.R., Tononi, G., 2017. The neural correlates of dreaming. Nat Neurosci 20, 872–878. https://doi.org/10.1038/nn.4545

Siclari, F., LaRocque, J.J., Postle, B.R., Tononi, G., 2013. Assessing sleep consciousness within subjects using a serial awakening paradigm. Front Psychol 4. https://doi.org/10.3389/fpsyg.2013.00542

Siclari, F., Tononi, G., 2017. Local aspects of sleep and wakefulness. Curr Opin Neurobiol 44, 222–227. https://doi.org/10.1016/j.conb.2017.05.008

Slézia, A., Hangya, B., Ulbert, I., Acsády, L., 2011. Phase Advancement and Nucleus-Specific Timing of Thalamocortical Activity during Slow Cortical Oscillation. Journal of Neuroscience 31, 607–617. https://doi.org/10.1523/JNEUROSCI.3375-10.2011

Stangor, C., Walinga, J., 2014. 6.1 Sleeping and Dreaming Revitalize Us for Action.

Steriade, M., Nunez, A., Amzica, F., 1993a. Intracellular analysis of relations between the slow (<1 Hz) neocortical oscillation and other sleep rhythms of the electroencephalogram. Journal of Neuroscience 13, 3266–3283. https://doi.org/10.1523/jneurosci.13-08-03266.1993

Steriade, M., Nunez, A., Amzica, F., 1993b. A novel slow (. J Neurosci 13, 3252–3265. https://doi.org/10.1523/JNEUROSCI.13-08-03252.1993

Steriade, M., Timofeev, I., Grenier, F., 2001. Natural waking and sleep states: a view from inside neocortical neurons. J Neurophysiol 85, 1969–1985. https://doi.org/10.1152/JN.2001.85.5.1969

Stone, J.L., Hughes, J.R., 2013. Early history of electroencephalography and establishment of the American Clinical Neurophysiology Society. J Clin Neurophysiol 30, 28–44. https://doi.org/10.1097/WNP.0B013E31827EDB2D

Tatum, W.O., Rubboli, G., Kaplan, P.W., Mirsatari, S.M., Radhakrishnan, K., Gloss, D., Caboclo, L.O., Drislane, F.W., Koutroumanidis, M., Schomer, D.L., Kastelijn-Nolst Trenite, D., Cook, M.,

Beniczky, S., 2018. Clinical utility of EEG in diagnosing and monitoring epilepsy in adults. Clinical Neurophysiology 129, 1056–1082. https://doi.org/10.1016/J.CLINPH.2018.01.019

Timofeev, I., Chauvette, S., 2019. Neuronal Activity During the Sleep-Wake Cycle. Handb Behav Neurosci 30, 3–17. https://doi.org/10.1016/B978-0-12-813743-7.00001-3

Tononi, G., 2009. Slow Wave Homeostasis and Synaptic Plasticity. Journal of Clinical Sleep Medicine 5. https://doi.org/10.5664/JCSM.5.2S.S16

Tononi, G., Cirelli, C., 2014. Sleep and the price of plasticity: from synaptic and cellular homeostasis to memory consolidation and integration. Neuron 81, 12–34. https://doi.org/10.1016/J.NEURON.2013.12.025

Walker, M.P., 2009. The role of sleep in cognition and emotion. Ann N Y Acad Sci. https://doi.org/10.1111/j.1749-6632.2009.04416.x

Xie, L., Kang, H., Xu, Q., Chen, M.J., Liao, Y., Thiyagarajan, M., O'Donnell, J., Christensen, D.J., Nicholson, C., Iliff, J.J., Takano, T., Deane, R., Nedergaard, M., 2013. Sleep drives metabolite clearance from the adult brain. Science (1979) 342, 373–377. https://doi.org/10.1126/SCIENCE.1241224/SUPPL_FILE/XIE-SM.PDF

2. PROJECT 1

In this chapter, I describe step by step the pipeline for hdEEG sleep data acquisition, pre-processing and post-processing procedures. The practical application of this pipeline is illustrated in the subsequent projects.

2.1. Data acquisition

HdEEG data were recorded using an EGI amplifier connected with a 256-channel head net (Electrical Geodesics Inc., Eugene, OR) in a controlled sleep laboratory setting. The signal was vertex-referenced (meaning that was referenced to the central electrode Cz at the head's vertex), unfiltered and sampled at 250 Hz or higher. According to the Nyquist's theorem, a periodic signal must be sampled at more than twice the highest frequency component of interest. In practice, because of the finite time available, a sample rate 5 times higher is the typical choice.

HdEEG was coupled with traditional Polysomnography (PSG) collected using the Embla system. PSG included the following channels:

- electro-oculogram (electrodes placed 1 cm above the right outer cantus and 1 cm below the left outer cantus and referred to the left mastoid)
- electromyogram of the submentalis muscle (electrodes placed 2 centimetres apart, 1 centimetre below the mandibular edge)
- electromyogram of the right and left tibialis anterior muscles (bipolar derivations with 2 electrodes placed 3 cm apart on the belly of the tibialis anterior muscle of each leg)

- electrocardiogram (CM4 derivation: anode in position V4 and cathode attached to the manubrium of the sternum)
- oral and nasal airflow thermistors and/or nasal pressure cannula
- wearable piezo-electric thoracic and abdominal bands to detect respiratory movements
- pulse-oxymetry
- snoring sensor
- position sensor
-

Sleep stages and sleep events were scored visually using the Embla ® RemLogic TM Software (Neurolite AG) by sleep medicine expert physicians according to international criteria (Berry RB, Brooks R, Gamaldo CE, Harding SM, Lloyd RM, Marcus CL, 2020).

HdEEG data were exported from the EGI system in the ".mff" format, which contains both raw data and meta information like the date of the recording, the sampling rate, the position and impedance of the EEG sensors.

PSG raw data were used directly in the Remlogic ".ebm" format, while PSG meta data (essentially the sleep scoring files) were exported as ".txt" files.

2.2. Data pre-processing

Data pre-processing steps are summarized in Figure 1.

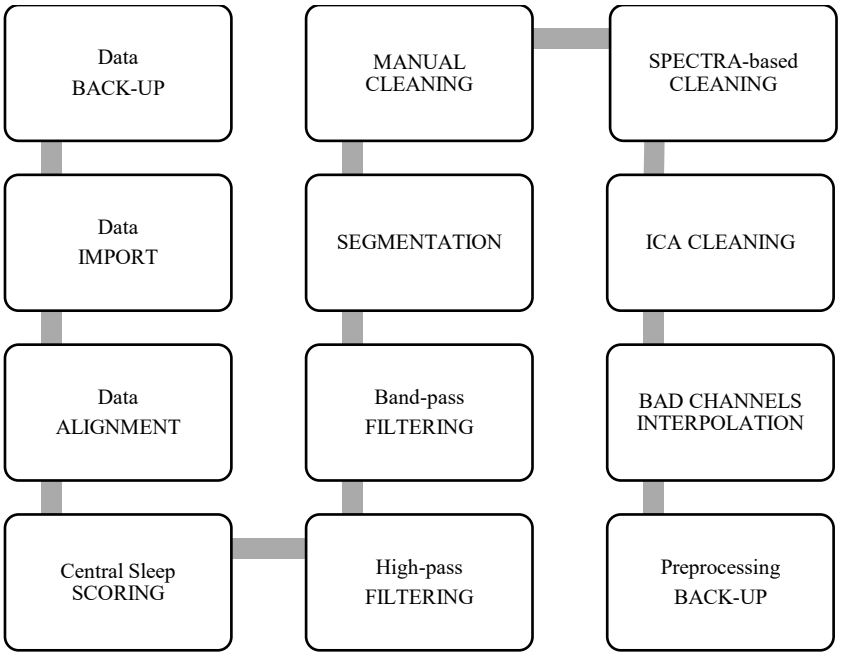

Figure 1. Summary of data pre-processing steps

Each step of data pre-processing is briefly summarized below.

2.2.1. Data backup

Mff, ebm and txt files were codified and stored in a protected Network Attached Storage (NAS) with 2 storage drives (10 TB each) arranged into redundant array of independent disks (RAID) to prevent data loss. The results of subsequent analyses were stored in the same drives.

2.2.2. Data import

Coded data were imported in Matlab using custom scripts. HdEEG files were converted in the EEGlab format (.set files containing meta-data coupled with .fdt files containing the raw

data). Sleep scoring information from text files was extracted and converted from 30 second epoch format to a data-point format (one scoring information per each data point of the recording file). This information was appended to the set files. PSG data were instead added to the fdt files.

2.2.3. Alignment

hdEEG and PSG data were collected with 2 different systems. Thus, I aligned hdEEG and PSG data so that they started at the same exact time. However, this could not be achieved through a simple translation of the starting point of one of the 2 signals. Indeed, the clock in our computers is controlled by the vibration of crystal oscillators that are not all created equal. This adds up to seconds or milliseconds per day/night. Thus, I collected the same ECG signal with both recording systems (essentially creating a mechanical bridge). Then, I plotted both of the ECG signals in EEGLAB, visually identified specific ECG artifacts at the beginning and at the end of the night and marked the time difference for each ECG artifact between the 2 systems. Finally, I translated one of the 2 signals of the average time difference between the artifacts. The same process could be potentially repeated to align with 0 delay specific nocturnal events (e.g., parasomnias episodes).

2.2.4. Central scoring

Being an expert in sleep medicine, I personally supervised central scoring after data import, using an open-source Matlab toolbox (Figure 2, https://github.com/Mensen/swa-matlab).

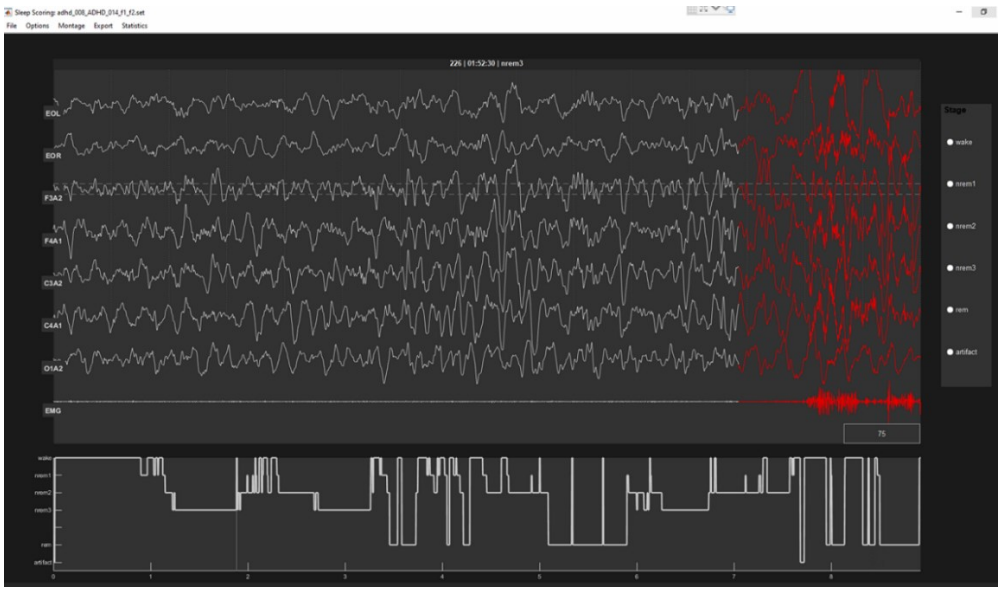

Figure 2. Screenshot of the Matlab toolbox used for central sleep scoring.

1: NREM stage 1, 2: NREM stage 2, 3: NREM stage 3, 5: REM, 0 wakefulness, 6: unscored epochs. In RED: artifacts.

After sleep staging and the scoring of related events, I also scored sleep cycles using a custom-graphical user interface (GUI) that I created in Matlab (Figure 3).

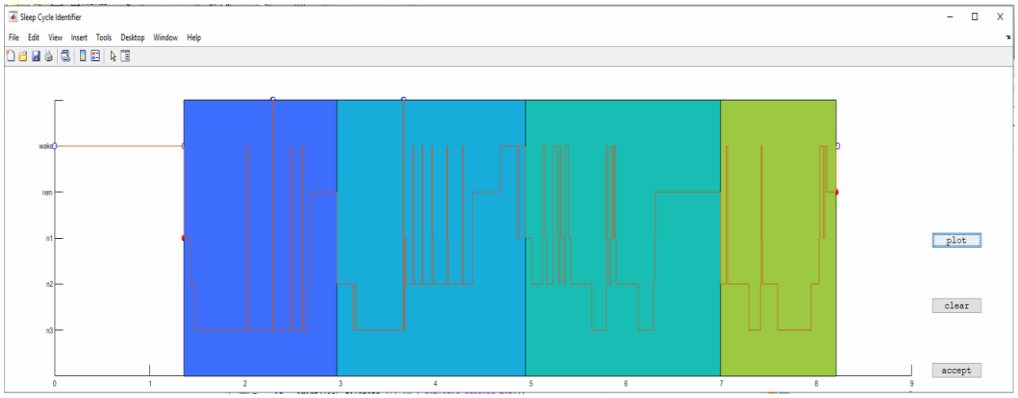

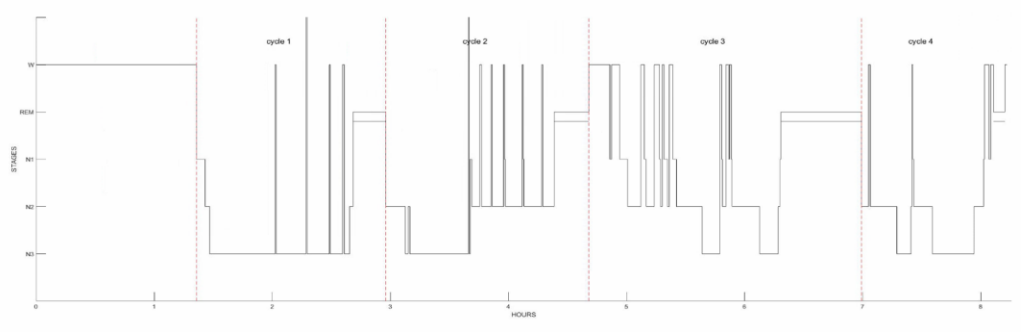

Figure 3. Screenshot of the Matlab GUI used to identify sleep cycles.

This GUI allows to mark the beginning of each NREM and REM cycle by clicking directly on the hypnogram edges.

2.2.5. High-pass and band-pass filtering

Filters are basically tools for spectral separation, which remove unwanted components or features from the EEG signal. This effect is obtained convolving the EEG signal and a reversed Kernel function (a wavelet or sine wave). Convolution basically works by computing the dot-product, meaning the sum of the products of the corresponding entries of the two functions.

EEG filters can be divided in 2 groups: Finite Impulse Response (FIR) and Infinite Impulse Response (IIR), which main features are summarized in the following table.

FILTERING TYPES		
	FIR	**IIR**
Method	Multiply data with Kernel	Multiply data with data
Kernel Length	Long	Short

Speed	Slower	Faster
Stability	High	Data dependent

FIR filters have an impulse response for a finite duration, and produce equal delays at all frequencies. IIR filters have an infinite impulse response where part of the output of the filter is recursively used as feedback. This results in unequal delays at different frequencies, meaning that the output is shifted in time with respect to the input, with some frequency components shifted more than others. In short, FIR filters are more accurate but computationally less efficient, while IIR filters create larger distortions but are computationally more efficient.

Digital filtering is a complicate and delicate step in signal analysis. This step may cause a distortion of the shape/temporal structure of EEG signals and affect all subsequent analyses. Thus, it must be tailored for the specific planned analysis.

In line with typical practice in EEG signal processing, for this thesis, each EEG signal was first-order high-pass filtered at 0.1 Hz (IIR filter reproducing a single resistor capacity) to filter out slow and large data drifts due to skin potentials. The EEG signal was subsequently band-pass filtered (0.5 – 45 Hz, Kaiser window-based FIR with zero-phase distortion).

2.2.6. Segmentation

Data epochs corresponding to NREM sleep stage 3 and NREM stage 2 (and to REM sleep and wake for project 3) were extracted and cleaned separately. For the last project on NREM sleep parasomnia episodes, only specific short segments of 4-minute length were selected

(based on the motor onset of each event) and extracted (3 minutes before up to 1 minute after the motor onset of each episode). See project 6 for further details.

2.2.7. Manual cleaning

An interactive open-source tool for data visualization and data-cleaning (https://github.com/CSC-UW/csc-eeg-tools.git) was used to visually inspect data (Figure 4).

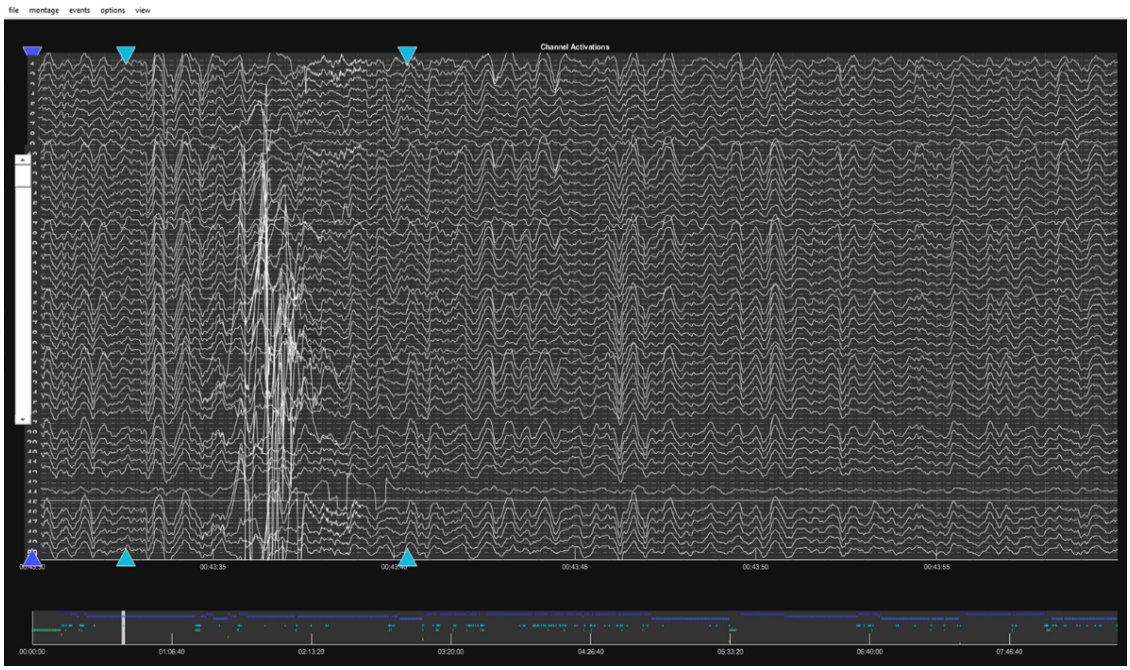

Figure 4. EEG GUI used for manual cleaning.

This tool allows to scroll quickly the hdEEG signal across channels and across time, and to interactively select bad channels and mark bad epochs (as the one between the 2 sky-blue triangles) by clicking directly on the data. The bar at the bottom allows to quickly visualize the marked artifacts across the time domain.

Channels with clear artifacts were removed, while data segments containing artifacts affecting the majority of channels were marked as “bad” and not considered in subsequent analyses.

2.2.8. Spectra-based cleaning

Furthermore, I removed channels with distinctly greater power (see paragraph 1.4.1 for a clarification on the concept of EEG power) relative to neighbouring channels upon visual inspection of power spectra and topographic power maps using a custom GUI.

I created this GUI in order to interactively select individual channels from the EEG power spectrum, and mark them as bad when clearly different from the others. Topographical power maps were plotted before and after bad channels removal (Figure 5).

I am currently developing a more sophisticated tool in the Python environment, in collaboration with the Department of Informatics of the University of Southern Switzerland (USI). This new tool allows to directly check at the same time the EEG raw signal, topographical power maps (in different frequency bands) and power spectrum, as well as to mark bad channels in red (see Figure 6).

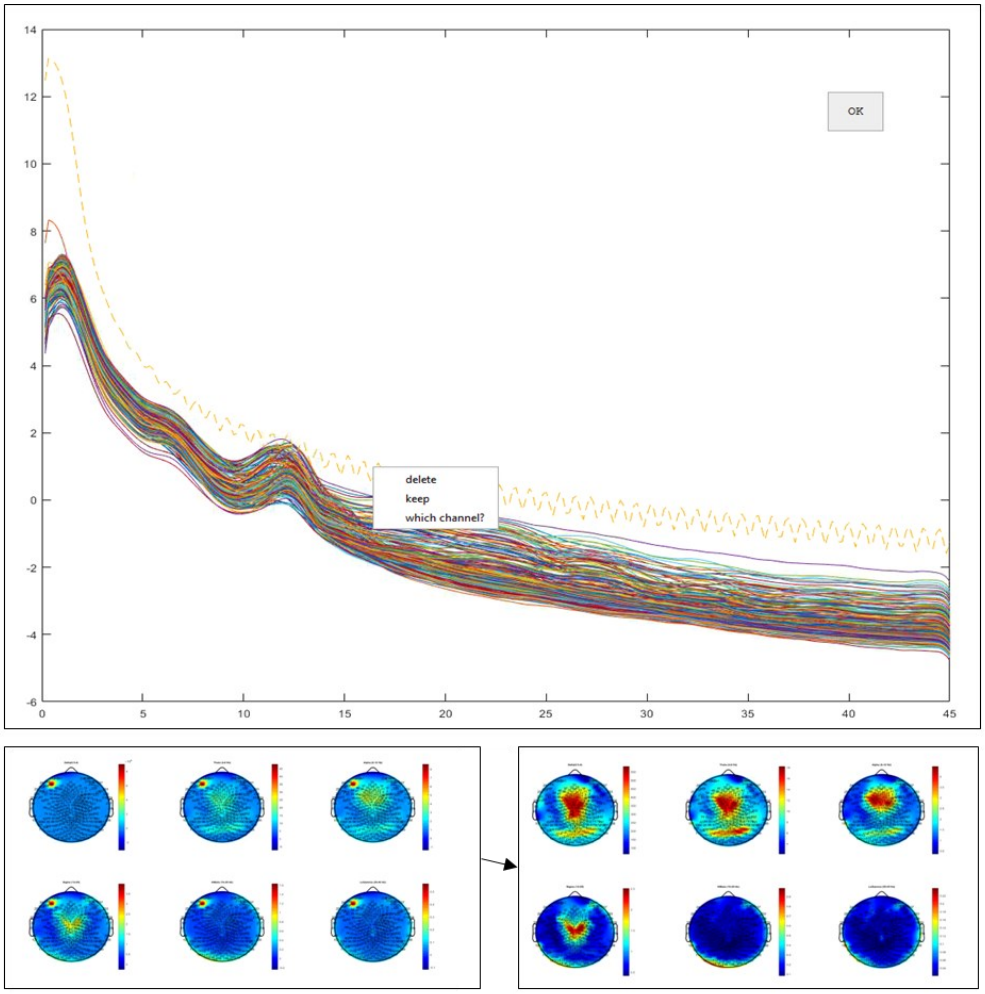

Figure 5. Spectra-based GUI

Upper panel: power spectrum of all 256 channels. One single bad channel is marked as bad (yellow dotted line). Lower left panel: power topography in 6 traditional frequency bands. This map is plotted before opening the spectra-based GUI. One single bad channel can be easily detected as a red spot over the right frontal area. Lower right panel: power topography plotted after the removal of the yellow dotted line with the GUI.

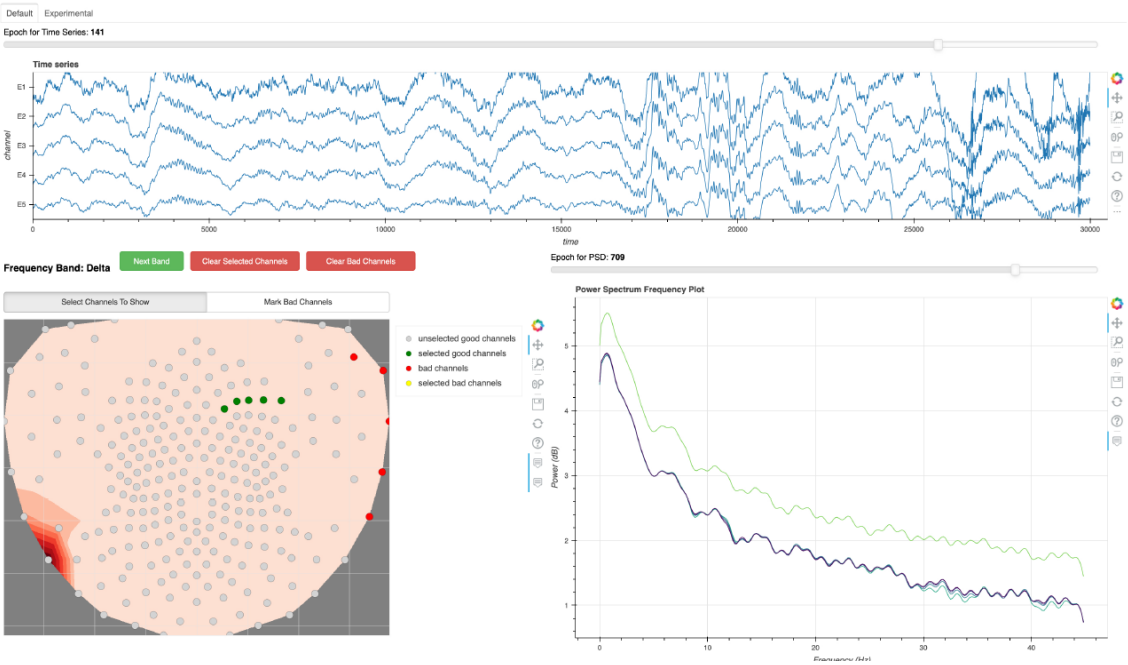

Figure 6. Spectra-based GUI

Upper panel: EEG raw signal. It can be scrolled in the time-domain using the bar at the top, and across channels using the bar on the right.

Lower left panel: power map in the delta range. A bad channel can be clearly identified over the left posterior area (red spot). Channels can be selected (green color) and visualized in the left right panel, and can be marked as bad (red color). Other frequency ranges can be visualized by clicking on the green button.

Lower right panel: power spectrum.

We are working to improve the graphical design and interactivity of the tool. We are also planning to add a spectrogram to represent the distribution of energy in both the time and frequency domain, and to add the possibility to easily visualize and mark bad epochs.

2.2.9. ICA-based cleaning

Independent Component Analysis (ICA) is a special type of blind source separation that decomposes the signal into additive subcomponents. ICA works well on multi-channel hdEEG signal due to its realistic assumptions: 1) the observed multi-channel EEG signals are a linear mixture of unknown sources; 2) sources are linearly and mutually independent 3) and non-Gaussian. To limit the intrinsic risk of removing sources that also carry information about real brain activity, I removed only ICA components with activity patterns and component maps characteristic of clear artifactual activity (see Figures 7 and 8). More specifically, only ocular, electrocardiographic, sweating, and residual muscular artifacts (or possible epileptic spikes in ADHD patients) were removed with ICA. For this step, I used both EEGLAB routines (to plot ICA components' power) and the previously mentioned EEG data visualization GUI (to plot ICA components in the time domain).

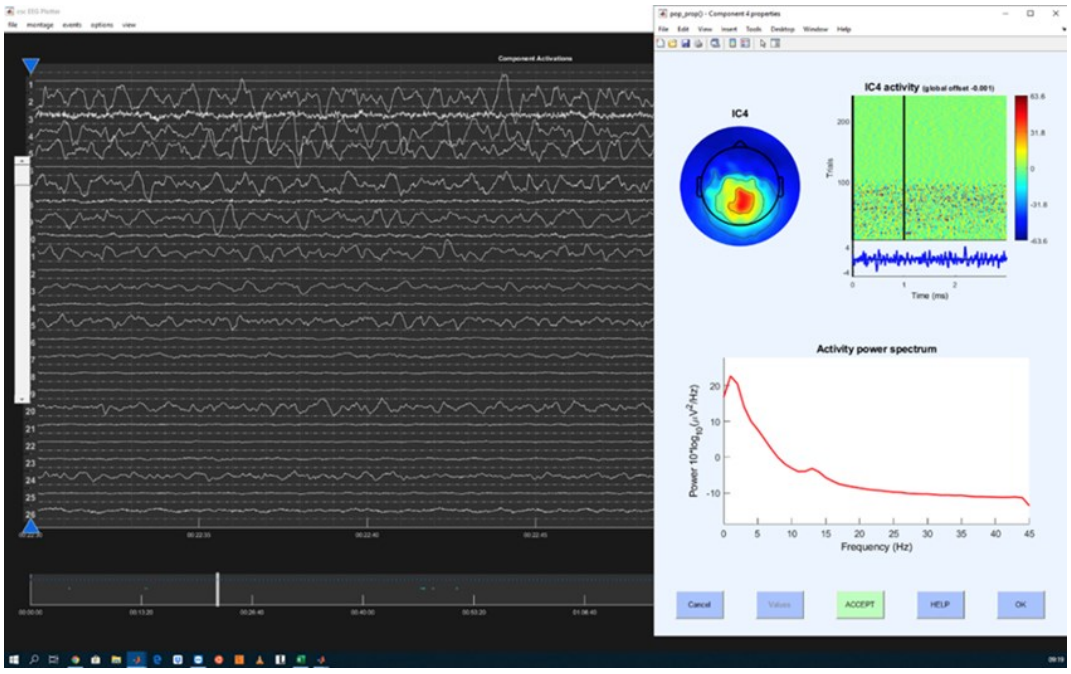

Figure 7. Example of a 'good' ICA component

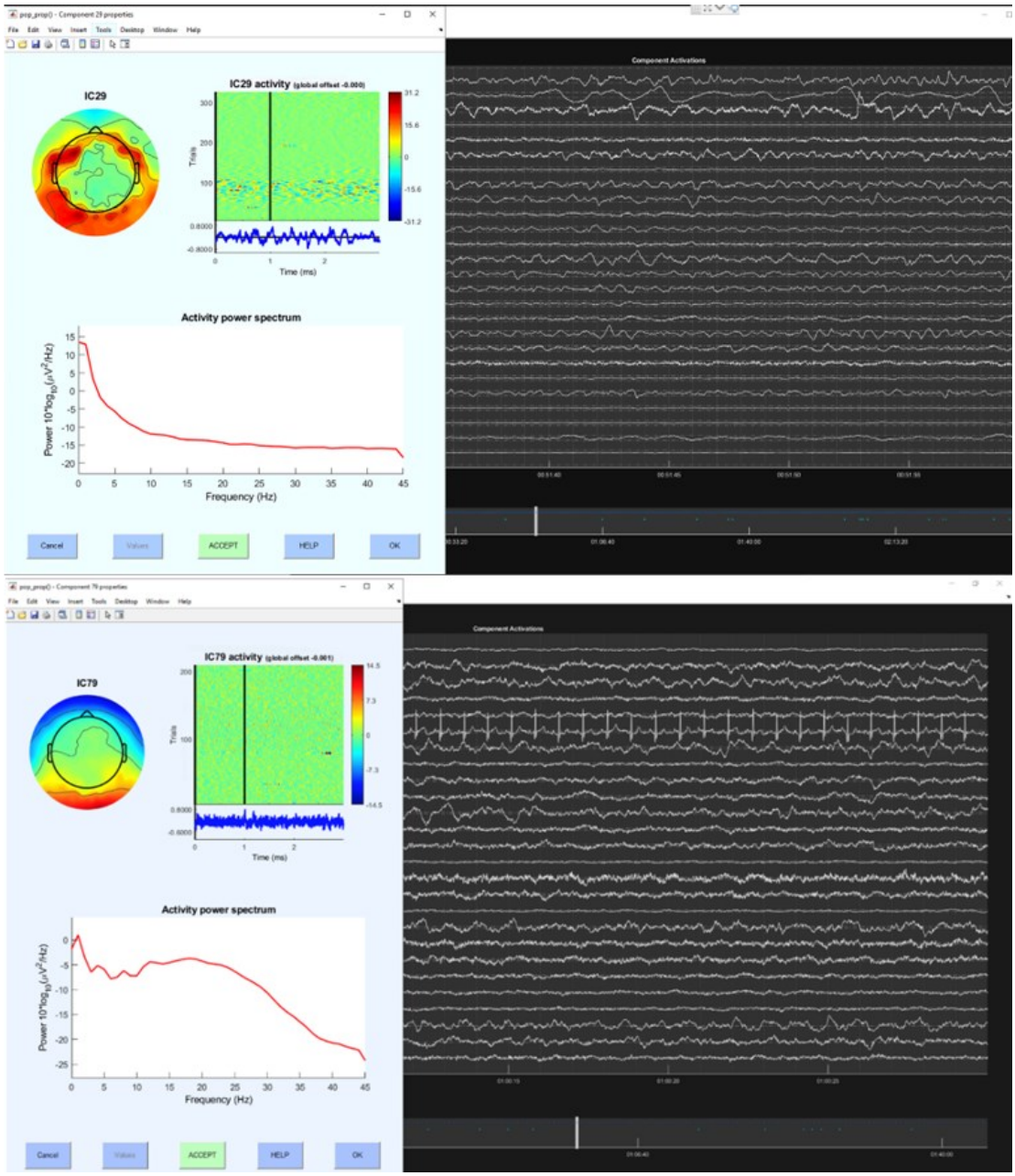

Figure 8. Examples of a 'bad' ICA components.

Upper panel: typical sweating artifact. Lower panel: typical ECG artifact.

I am planning to create a specific GUI to improve ICA components visualization and cleaning, in collaboration with the USI department of informatics.

2.2.10. Bad-channel interpolation

Subsequently, as a last pre-processing step, I replaced selected bad channels with virtual healthy channels created by the interpolation from neighbouring channels. Among different interpolation methods for channel reconstruction (spherical splines, higher-order polynomials, nearest-neighbour averaging and radial basis function), I selected the EEGLAB "pop_interpol" function, which uses as default method the spherical splines. This method allows for an accurate estimation of scalp potentials if the electrode mapping is sufficiently dense (Perrin et al., 1989).

2.3. Data post-processing

2.3.1. Scalp spectral analysis

From the earliest stages of EEG research, different EEG frequencies were believed to reflect different states of the brain, as suggested for example by the strong association between occipital alpha rhythm and eye-closure. Broadly speaking, lower frequency bands, which dominate during sleep or drowsiness, are believed to reflect subconscious states, while higher frequency bands have been connected to more alerted, active states and higher cognitive functions.

Scalp spectral analysis is one of the most basic and widely used quantitative EEG analysis. Spectral analysis allows to decompose the signal from the time domain to the frequency domain thanks to the Fourier Transform (see Figure 9).

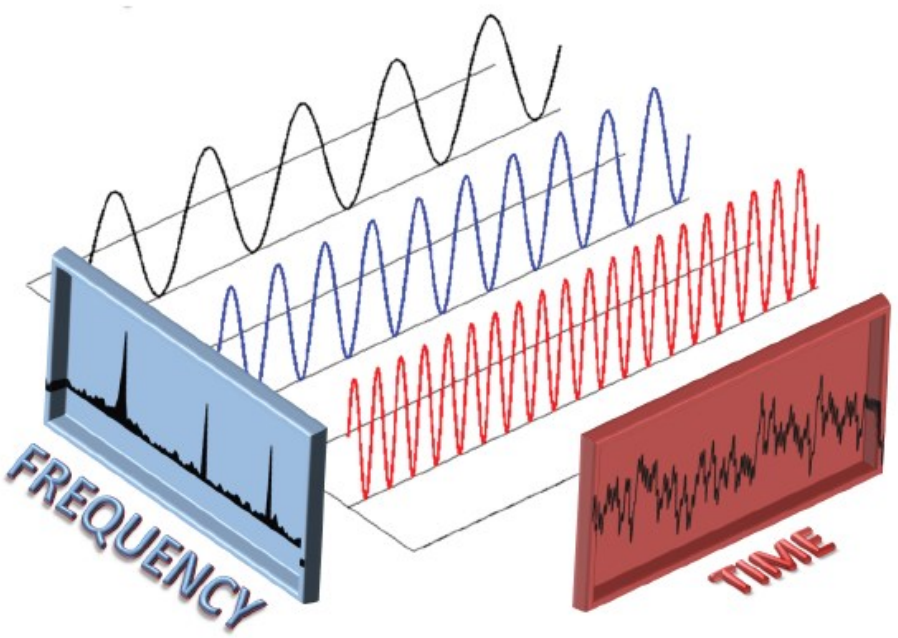

Figure 9. Fourier transform (FT). *Taken from* (Kalhara et al., 2018).

The *continuous Fourier transform* (CFT) of a function $x(t)$ is basically a correlation between the signal $x(t)$ and the complex sinusoidal functions $e^{-j\omega t} = \cos \omega t - j \sin \omega t$, where ω is the angular frequency corresponding to the linear frequency f ($\omega = 2\pi f$). The highest is the correlation, the higher is the influence of the frequency ω in the original signal $x(t)$. In other words, Fourier transform represents how similar the given signal is to the complex exponential of a given frequency.

Contrary to CFT, the *discrete Fourier transform (DFT)* does not assume that the signal is infinite or continuous in time, but just that its input signal is one period of a periodic signal. Therefore, DFT is used for any modern EEG recording, where the signal is recorded for a relatively short time interval and stored digitally.

The *fast Fourier transform* (FFT), currently used in EEG signal analysis (Cox and Fell, 2020), is a particular implementation of the DFT that assumes that the signal is stationary and slowly varying and gives identical results with reduced calculations (from N^2 to $N\log_2(N)$) and computational burden.

FFT returns, for each frequency bin and for each electrode, a complex number from which the amplitude and phase of the signal at that specific frequency can be easily extracted. The amount of the specific frequency band included in the signal (usually reported as power spectral density or Welch's periodogram, expressed in (micro)-Volts^2 per Hertz) and its spatial distribution (over different brain areas) are the 2 most important factors considered in traditional EEG spectral analysis (see Figure 10).

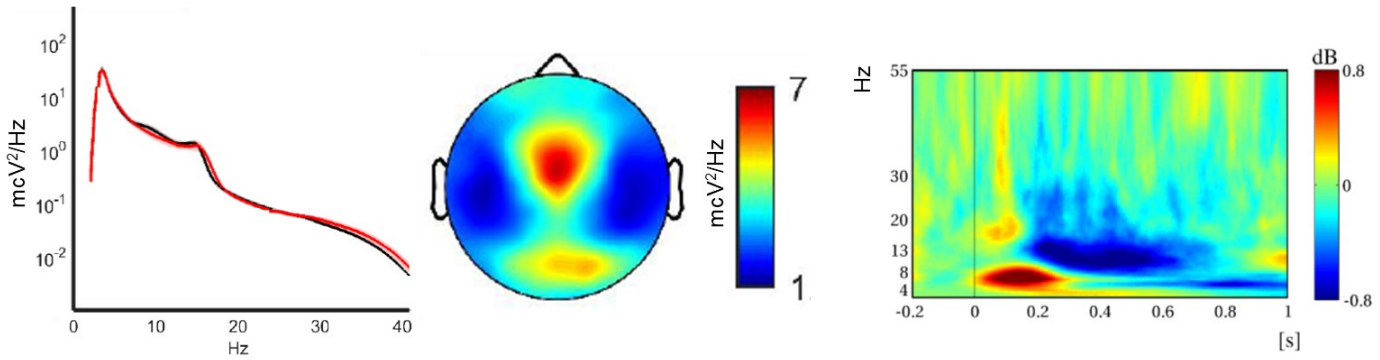

Figure 10. Different representation of the FFT output.

Left: power spectrum (power versus frequency), taken from (Castelnovo et al., 2016). *Middle: topo-plot (power topography), taken from* (Castelnovo et al., 2016). *Right: spectrogram (time versus frequency). Taken from* (Kang et al., 2015).

2.3.2. Slow wave detection analysis

Slow wave detection analysis refers to the identification of individual slow waves and to the analysis of their parameters. This analysis offers both more sensitivity and specificity compared to spectral analysis for the analysis of sleep oscillations in the 0.5-4 Hz range (Mensen et al., 2016a).

The detection of slow waves is usually conducted via automatic algorithms, which may vary in terms of conceptual methodology or in terms of parameters used for slow wave detection. For example, using the **"zero-crossing" method**, slow waves can be detected at the single channel level by first band-pass filtering the EEG signal in the delta range, then identifying filtered EEG data-points that cross the zero line, and the positive and negative peaks as the second-derivative between the identified consecutive zero-crossings. In this context, amplitude can be evaluated as the distance between the negative peak and the 0 line along the y-axis (negative-peak amplitude) or as the distance between consecutive positive and negative peaks (peak-to-peak amplitude), while up- and down-slopes are computed as the amplitude of the most negative (or positive) peak (a) divided by the time until the next (or previous) zero-crossing (t) (see Figure 11, left panel).

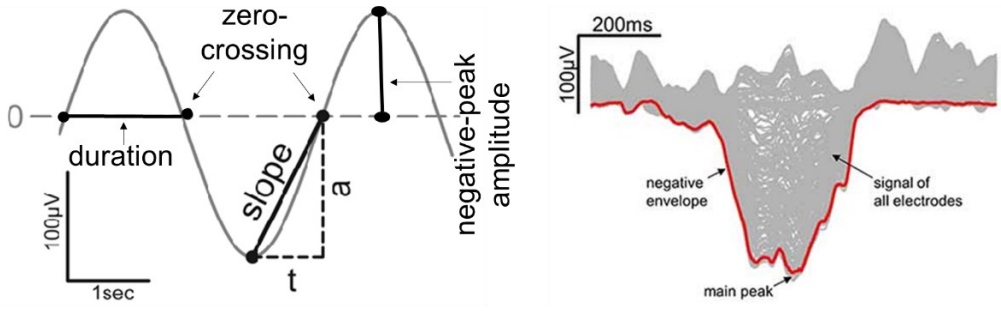

Figure 11. Simplified graphical representation of slow waves parameters.

Left - Adjusted from (Kurth et al., 2010)*. Right – taken from* (Bernardi et al., 2018).

Another common strategy consists in:

1) identifying a **“canonical”** (most representative) **signal or wave**

2) then individual slow waves within the canonical signal, and subsequently

3) computing slow waves in individual channels. Finally, one can also decide whether or not

4) to explore slow wave traveling properties (see chapter 1 for an introduction to this last concept).

First step

A canonical wave can be calculated according to conceptually distinct approaches:

- a “regional” method, i.e., taking the mean activity over a specified brain region, or
- a “negative envelope” method, i.e., examining the butterfly plot of overlaying channels, tracing its negative contour, and taking the most negative values (e.g., < 2.5%) at each data sample (Figure 13, right panel).

The negative envelope has the advantage of not losing regional (local) slow waves and being computationally faster (the full detection criteria run once, on a single time series), but also has some limitations: 1) the waveform may be distorted and not closely correspond to any particular channel; 2) the peak-to-peak amplitude information is lost given that the positive portion of the signal is eliminated; 3) the negative peak amplitude is unpredictably altered as the negative envelope has rare zero-crossings and must be high-pass filtered or detrended to shift the mean activity to zero.

Second step

The second step, after the creation of the canonical wave, is the definition of an **"inspection point"** to detect slow waves at individual channels. The choice is usually between the 0 line or the local minima/maxima. In the first case, the procedure is the same as the above mentioned "zero-crossing" method. This method can be affected by slow EEG drifts and could be unreliable when using the negative envelope. An alternative is to examine the local minima of the canonical wave and consider as the start and end points of that particular wave the nearest local maxima. Furthermore, some crucial thresholds on different parameters (e.g., minimum amplitude, minimum and maximum wavelength) are usually selected to make sure to retain only "real" slow waves.

Third step

The same set of criteria applied to the canonical wave can be applied to individual channels. One could also use stricter criteria for the canonical wave to maximize specificity, and more relaxed criteria at the channel level to maximize sensitivity. Afterwards, for each slow wave, the delays at the time point of the minimum peak are computed for each channel.

An alternative is represented by the cross-correlation of the canonical wave with the individual channels over a specified time-window around each slow wave negative peak. This method is amplitude independent, and already implies the calculation of the temporal delay of the wave at each channel, in a way that it is robust to noise (as not only the negative peak but the entire waveform is considered for the calculation of the delay, see Figure 12).

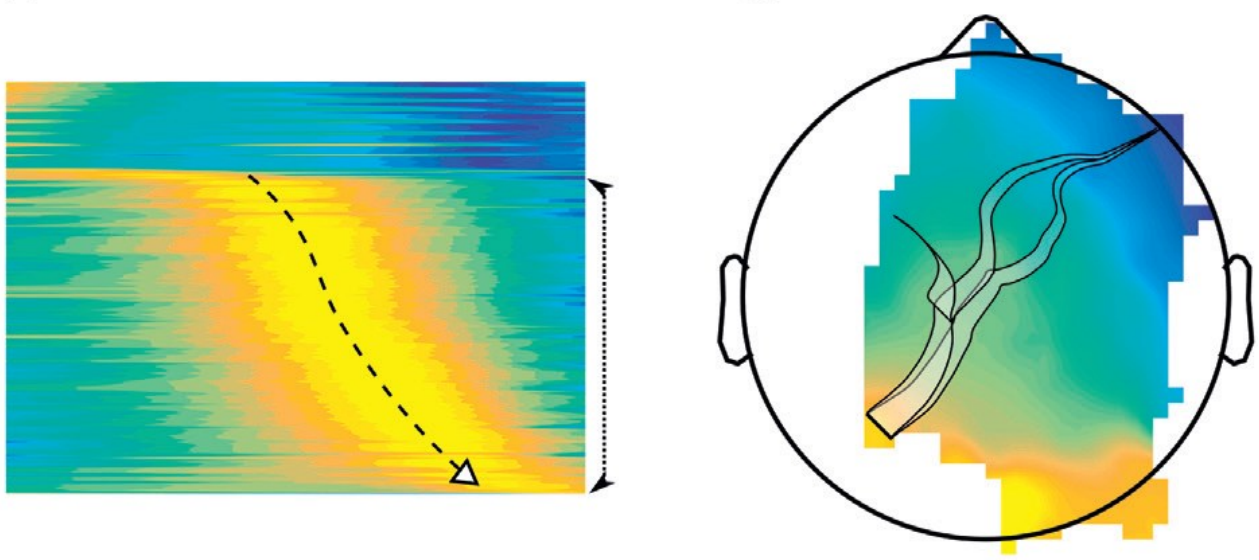

Figure 12. Slow wave traveling analysis

Left: Cross-correlation analysis allows to find: 1) whether a specific channel express a slow wave at the same time as the canonical slow wave (high positive correlation, in yellow); 2) what sampling delay they best fit giving an estimate of the channel origins of the wave and its propagation pattern. Right: graphical representation of a delay map created by interpolating on the scalp the delays of an individual slow wave, with over imposed 3 typical streamlines (see main text). Figure taken from (Mensen et al., 2016b).

When using the envelope as canonical wave, it might be useful to cross-correlate each channel with the channel displaying the largest negative peak (as the negative envelope may not correlate well with any particular channel).

Finally, to avoid “island channels”, not connected to the other channels, which are likely to be random artifacts, a cluster test can be performed on the active channel topography.

Fourth step

Traveling slow wave properties of individual waves are computed on the interpolated scalp delay map created using the individual delays across ‘active’ channels. Channels with a 0 or near zero delay are usually considered as slow wave origins. Slow wave streamlines are computed using a complex algorithm that defines the trajectory of each streamline based on each gradient of the delay map until a stopping condition is met: 1) the gradient at the next point does not exist or is equal to zero, 2) the change in gradient angle is greater than 90 degrees. Usually, only the streamline with the longest displacement (the distance between the start and endpoints of each wave) is retained for subsequent analyses, but other selection criteria can be applied. For example, one can decide to consider the longest distance traveled (taking into account the cumulative sum of the streamline’s datapoints).

As a last note, EEG data are traditionally average mastoid-referenced before slow-wave detection analysis, according to clinical sleep scoring criteria (Berry et al., 2013). It has to be noted that mastoid-reference may create a frontal bias (larger waves over frontal electrodes, being mastoids in a posterior-temporal position). However, this solution is likely better than average referencing, as this can invert the polarity for electrodes where the wave is smaller than the average and make the negative envelope of large, global slow waves especially tricky to interpret.

A practical application of slow wave analysis is described in detail in the second and in the fourth projects of this thesis.

2.3.3. Source analysis

Source imaging techniques (Song et al., 2015) try to overcome the limited EEG spatial resolution by reconstructing the cortical sources of the EEG signal. Source localization analysis can be broken down into 2 major parts called the “forward problem” and the “inverse problem” (see Figure 13). The forward problem consists of finding the scalp potentials that would result from a hypothetical model of currents/dipoles inside the head. The inverse problem consists in estimating brain activity sources that better fit the actual EEG data measured at specified scalp electrodes, using the hypothetical current models provided by the forward problem.

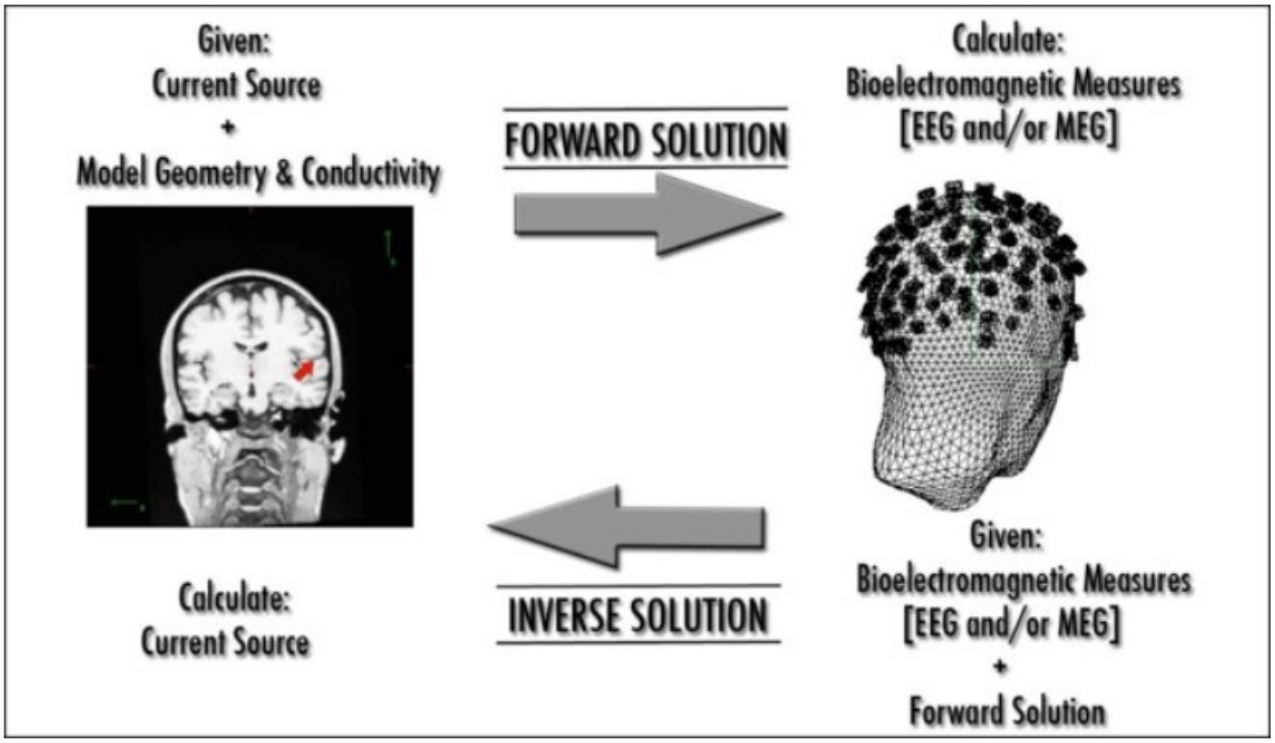

Figure 13. The forward and inverse problems of EEG source analysis.

Taken from (Bangera and Bhalchandra, 2008).

The **forward model** can be divided in 2 steps: 1) the identification of mathematical models of the head and 2) the assignment of appropriate properties to each layer. The head can be modeled as a single-layer homogenous, isotropic, conductive sphere. This oversimplified head model can be improved by establishing 3 (or 4) concentric, spherical regions representing the brain, (the cerebro-spinal fluid), the skull, and scalp and by assigning to each region an appropriate conductivity value (Figure 14, left panel). This ***3-(4)-shell concentric spherical head model*** can be further improved by integrating a second imaging modality, typically in the form of an MRI scan, to create a ***realistic-head model*** through segmentation algorithms (Figure 14, central panel). MRI structural scans of the brain can be segmented into multiple closed triangular meshes with a finite number of nodes, preserving the structural integrity of the actual head (Figure 14, right panel).

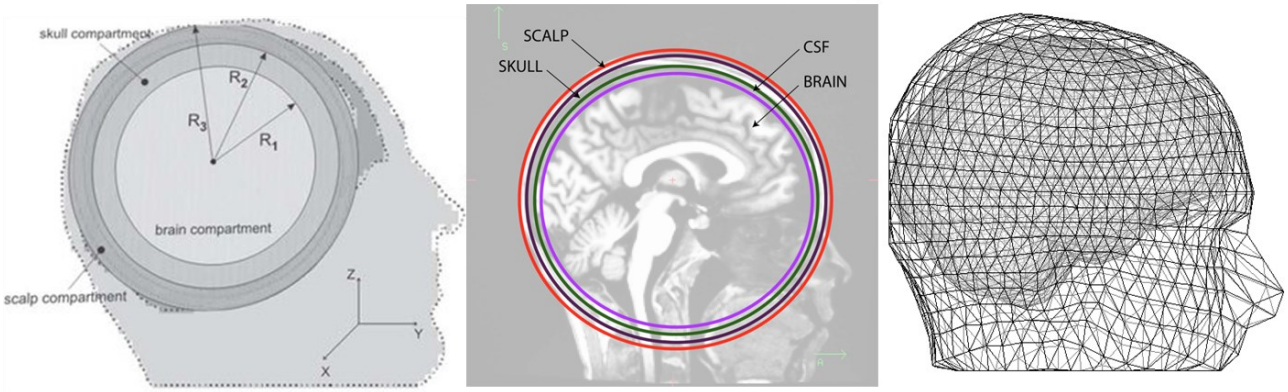

Figure 14. Head models

Left panel: 3-shell model, taken from (Gaignaire et al., 2010)*. Central panel: realistic 4 shell-model, taken from* (Bangera and Bhalchandra, 2008)*. Right panel: plot of the head model with the three meshes (brain, skull and scalp), taken from https://www.fieldtriptoolbox.org/workshop/oslo2019/forward_modeling/.*

The brain, skull, and skin surfaces are then used as boundary layers that encapsulate the 3 (or 4) tissue volumes with homogeneous volume conductive properties. Of note, while the brain to skull conductivity is reported in the literature with consistency, the soft tissue to skull conductivity ratio remains a subject of debate and a remaining degree of uncertainty may significantly impact on the accuracy of the forward model. Taking into account this possible limitation, the potential at any node on the mesh scalp surface, generated by the dipoles in the brain compartment can be estimated using a complex numerical technique called the *boundary element method* (BEM). The number of nodes and triangle meshes used to represent 3 (or 4) compartment surfaces partially affect the accuracy of this estimation. Moreover, constant conductivity values are assumed for the spaces in between these boundaries. Thus, the BEM modelling of the human head volume conductor may fail to capture local inhomogeneities and the anisotropic properties of biological brain tissues. This issue can be solved using more complex algorithms, like the finite element method (FEM).

The **inverse problem** is defined as “ill-posed” due to the non-uniqueness of its solution. Indeed, the number of unknown sources is much larger than the number of scalp measurements (Grech et al., 2008). There are 2 main mathematical optimization approaches to the EEG inverse problem: parametric and non-parametric optimization methods, which make different assumptions on the source space, and more specifically, on the number and/or the spatial distribution of the source current dipoles, and/or whether the positions, magnitudes, and orientations of potential dipoles are fixed or varied.

In **parametric methods**, the source space usually comprises a single dipole or a few dipoles with unknown position(s), magnitude(s), and orientation(s) like in the non-linear least-squares method or the beamformer method. The ***non-linear least-squares method*** finds

a solution for a single “equivalent dipole” with an unknown position and moment that result in a global minimization of the residual error between the estimated and observed EEG signals through an iterative process. The least-squares method has 3 significant limitations: 1) when extended for multiple dipoles the computational demand is high; 2) the true number of dipoles (that are chosen a priori by the operator) is actually unknown and probably too large to be represented by a single dipole; 3) the minimum least-squares error solution is not necessarily the closest solution to the underlying physiological sources. The ***beamforming method*** is a technique introduced originally for radar applications. Beamformers estimate the contribution of a single dipole to the detected field (this way the number of dipoles is not assumed a priori) by applying a spatial filter. The spatial filter is arranged in a specific way so as to enhance the incoming or outgoing signals in a preferred direction and to suppress the contributions from all other sources. The same filter can be applied at any location and to each of the measurement vectors to obtain the time-course of activity. The main limitation of beamforming techniques is the possible presence of highly correlated spatially distinct sources, which can be partially handled introducing longer time windows.

Non-parametric methods use *cortically distributed source* (CDS) models based on the assumption that the primary current sources are the cortical pyramidal neurons oriented normally to the brain surface. A current dipole is assigned at each of the mesh element of the cortical layer (so that the number of dipoles is of several thousands and the dipole locations are known). Dipole orientations are either fixed (normal to the local surface) or unknown. The ***minimum-norm estimates*** (MNE) solution produces (Pinto and Silva, 2007) the inverse solution that minimize the overall power of the estimated source activity. As MNE

is suitable for the estimation of superficially distributed sources but underestimate deeper sources, a *weighted minimum-norm estimates* (wMNE) algorithm was implemented to reduce the MNE depth-bias. The ***low-resolution electromagnetic tomography*** (LORETA) method (Pascual-Marqui et al., 2002) considers the physiological principle that neighboring neural sources are activated simultaneously. This is achieved by the implementation of a smoothing (Laplacian) operation on the source space. LORETA has superior deep source localization accuracy when compared to MNE or wMNE.

The ***dynamic statistical parametric mapping*** (dSPM) (Dale et al., 2000) method and ***standardized low-resolution electromagnetic tomography*** (sLORETA) (Pascual-Marqui, 2002) standardizes the solutions by the variance of the estimated current density. dSPM assumes that the source of variation in the estimated current is only from the measurement noise, while sLORETA also takes into account the variance within the actual source itself. sLORETA is claimed to be able to get the lowest localization error in noisy environments, but, as dSPM, usually results in much larger spatial dispersion than non-standardized solutions. Moreover, while sLORETA yields best accuracy in a single point source, LORETA may perform better in cases where multiple distinct sources are active.

In project 2 and 5, I used a 3-shell spherical BEM model for the forward problem and the sLORETA inverse model to model EEG sources in physiological and pathological states.

distribution of the source activation given the observed scalp potentials.

Last but not least, the **probabilistic Bayesian** methods is a recently developed approach to source localization that tries to solve for the inverse problem by identifying the probability

2.2.4. Connectivity analysis

Consciousness and information processing seem to be sustained by self-organized functional connections between brain regions. Such functional interactions are driven by synchronized neuronal activity, both locally and over distant brain regions. During NREM sleep, information processing and consciousness apparently fade away progressively, and re-emerge periodically in the form of dreams. In the last project of this thesis, I used EEG connectivity inference, to explore consciousness during NREM sleep-related abnormal complex behaviours (known as NREM sleep parasomnias).

Considering the intrinsic limited temporal resolution of fMRI, EEG is better suited for the dynamic connectivity analysis in the millisecond scale. The growing interest in connectivity among different brain areas lead to the development of a host of methods and models of connectivity measures (Cao et al., 2022; Sakkalis, 2011) summarized in Table 1.

Category		CCF	COH	PLV	PLI	MI	GC	PDC	TE	DCM
Directionality	Non-directed	√	√	√	√	√				
	Directed						√	√	√	√
Theoretical basis	Data-driven	√	√	√	√		√	√		
	Information-based					√			√	
	Model-based									√
Signal domain	Amplitude	√	√			√	√	√	√	√
	Phase		√	√	√					

Table 1. Summary of main EEG connectivity methods. *CCF: cross-correlation function, COH: coherence, PLV: phase locking value, PLI: phase lag index, MI: mutual information, GC: Granger's causality, PDC: partial directed coherence, TE: transfer entropy, DCM: dynamic causal modelling. Taken from* (Choi and Kim, 2018).

The first distinction to be made is between functional connectivity (FC) and effective connectivity (EC).

FC is defined as the temporal coincidence of spatially distant neurophysiological events and is basically a statistical description of the relationship between the EEG activity recorded at different channels. FC is based on the intuitive notion that 2 events occurring together should be somehow related to each other. While FC represents a simple approach to the analysis of functional networks that requires few a priori assumptions, it suffers from biological and technical confounds. Indeed, FC is purely correlative in nature and does not imply any causal relationship or direct connection between 2 brain regions.

On the other hand, EC relies on more complex assumptions regarding the underlying neurobiological substrates and models to estimate the causal effects that generate data, which are usually computational demanding (and partially unknown). The choice of a connectivity analysis method over another can dramatically affect the reconstructed brain networks and activity and is not always straightforward, as each method has its own pros and cons.

Cross correlation function (CCF) method is the linear correlation between 2 signals in the time domain.

Coherence (COH) is the linear correlation between 2 signals in the frequency domain. Several variants of coherence, inherently robust to volume conduction, have been developed, like the imaginary coherence (ImCHO).

Phase locking value (PLV) was designed to be independent from signal amplitude (unlike CCG and CHO) and measures the degree of phase synchrony between 2 signals over time. Phase locking is calculated after bandpass filtering, by averaging the phase angle difference over N time points between 2 signals, thus measuring the stability of phase differences across EEG time segments. Values ranges between 0 (no synchronization) and 1 (perfect synchronization).

Phase lag index (PLI) quantifies the asymmetry of the distribution of phase differences between 2 signals. When considering phase asymmetry, the likelihood that the phase difference in the interval -π to 0 is considered as different from the likelihood in the interval 0 to π. See Figure 15.

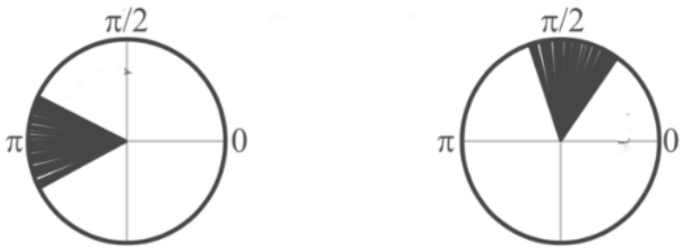

Figure 15. Differences between PLV and PLI. *In the left figure the distribution of phase differences is uniform around π and will thus give a PLI of 0, while in the right figure, the distribution of the phase differences between 0 and π, in this case more specifically entered around π/2, will give a PLI of 1.*

PLI values ranges between 0 and 1. Zero indicates either no coupling or coupling with a phase difference centered around 0 mod π (meaning around 0, π, 2π and so on). One indicates perfect phase locking at a value of phase difference different from 0 mod π. Thus,

PLI overcomes spurious phase locking synchrony from volume conduction or active reference electrodes by disregarding phase locking that is centered around 0 mod π phase differences (at the risk of ignoring true instantaneous interactions). The weighted PLI (wPLI) was suggested to take into account the magnitude as well as the distribution of the phase differences and to be less statistically biased for small sample sizes.

Mutual information (MI) quantifies the amount of information that 2 signals share with each other, where information is computed with the *Shannon entropy* formula. MI is computed as the sum of the entropies of the 2 signals *X* and *Y*, minus their joint entropy. If *X* and *Y* are independent, the MI equals zero. Otherwise, the MI is positive (with unit in bits) and shows the maximum value when 2 signals are equal. CCF, COH, ImCOH, PLV, PLI, MI do not give any information about the direction of interaction. For this porpoise, other connectivity measures have been developed.

Granger causality (GC) is a statistical hypothesis test that allows to determine whether one time series X can be used to predict another time series Y. Signal X is interpreted as causal of signal Y if the predictions of Y estimated by autoregressive (AR) modeling are significantly better (meaning that the prediction error is reduced) when based on past values of Y plus past values of X (joint bivariate AR modeling of X and Y) than when based only on past values of Y alone (univariate AR model of Y). If no causal influence of X to Y exists, GC is close to 0, and vice versa. GC is directional and interpreted as bidirectional if GCs of both directions are high.

Partial directed coherence (PDC) is an equivalent of the GC in the frequency-domain, based on multivariate autoregressive (MVAR) modeling of multichannel signals.

Dynamic causal modeling (DCM) is a Bayesian model-comparison procedure designed to answer questions about the architecture of underlying hidden neuronal dynamics (Kiebel et al., 2009). The basic idea is to construct reasonably realistic “dynamic models”, meaning models of interaction between cortical regions or “sources”. In the EEG field, a source is described using a “neural mass model”, a sort of simplified macro-column model. This model includes average post-membrane potentials and average firing rates of 3 neuronal populations (spiny stellate cells in the granular layer, pyramidal cells and inhibitory interneurons in the infra-granular and supra-granular layers). Each neuronal population has intrinsic dynamics and internal connections with the other 2 populations. Moreover, each source receives extrinsic input, from other sources or from the external environment. Dynamic causal models, meaning the models of the dynamics of the sources and their interactions are specified by a set of first-order differential equations. Bayesian model comparison is used to select the best model and its connected parameters, given the observed evidence (meaning the recorded EEG signal). DCM has not been used for full-scale connectivity analyses, because of the high computational cost and the complexity in selecting the *a priori* model parameters and connections.

Transfer entropy (TE) is an alternative measure of effective (directed) connectivity based on information theory that measures the amount of directed transfer of information (where information is calculated using Shannon entropy) between 2 random processes (Vicente et al., 2011). Like GC, TE estimates whether including the past of both source (X) and target (Y) time-series influences the ability to predict the future of the target time-series (Y). TE is model-free and makes no assumptions on signal or interaction structure but requires large amounts of continuous data. Phase TE (PTE) is a phase-based TE metric suitable for large-

scale directed connectivity analysis, which is very robust with respect to noise and linear mixing typical of EEG data (Lobier et al., 2014).

Finally, connectivity analyses can be conducted at the cortical source space. This provides time-series of cortical current densities at numerous vertices on cortical surface that allow for the better explanation of the connectivity results. Indeed, each connection has am anatomical interpretation and the effects of volume conduction are sensibly reduced (Choi and Kim, 2018).

For these reasons, in project 4, I opted for using PTE on source data, using Brainstorm, a collaborative open-source Matlab-based software dedicated to the analysis of neuro-physiological recordings, which has e very nice graphical interface and support both source and connectivity analyses, as well as complex statistical analyses with adjustments for multiple comparisons.

2.4. References

Bangera, Bhalchandra, N., 2008. Development and validation of a realistic head model for EEG. PhDT 273.

Bernardi, G., Siclari, F., Handjaras, G., Riedner, B.A., Tononi, G., 2018. Local and Widespread Slow Waves in Stable NREM Sleep: Evidence for Distinct Regulation Mechanisms. Front Hum Neurosci 12. https://doi.org/10.3389/FNHUM.2018.00248

Berry RB, Brooks R, Gamaldo CE, Harding SM, Lloyd RM, Marcus CL, V.B., 2020. The AASM Manual for the Scoring of Sleep and Associated Events: Rules, Terminology and Technical Specifications, 2.6 versio. ed.

Berry, R.B., Brooks, R., Gamaldo, C.E., Harding, S.M., Marcus, C.L., Vaughn, B. v., Vaughn, V.B., 2013. The AASM Manual for the Scoring of Sleep and Associated Events. American Academy of Sleep Medicine 53, 1689–1699. https://doi.org/10.1017/CBO9781107415324.004

Cao, J., Zhao, Y., Shan, X., Wei, H. liang, Guo, Y., Chen, L., Erkoyuncu, J.A., Sarrigiannis, P.G., 2022. Brain functional and effective connectivity based on electroencephalography recordings: A review. Hum Brain Mapp 43, 860–879. https://doi.org/10.1002/HBM.25683

Castelnovo, A., Riedner, B.A., Smith, R.F., Tononi, G., Boly, M., Benca, R.M., 2016. Scalp and Source Power Topography in Sleepwalking and Sleep Terrors: A High-Density EEG Study. Sleep 39, 1815–1825. https://doi.org/10.5665/sleep.6162

Choi, J.W., Kim, K.H., 2018. Methods for Functional Connectivity Analysis 125–145. https://doi.org/10.1007/978-981-13-0908-3_6

Cox, R., Fell, J., 2020. Analyzing human sleep EEG: A methodological primer with code implementation. Sleep Med Rev 54, 101353. https://doi.org/10.1016/J.SMRV.2020.101353

Dale, A.M., Liu, A.K., Fischl, B.R., Buckner, R.L., Belliveau, J.W., Lewine, J.D., Halgren, E., 2000. Dynamic statistical parametric mapping: combining fMRI and MEG for high-resolution imaging of cortical activity. Neuron 26, 55–67. https://doi.org/10.1016/S0896-6273(00)81138-1

Gaignaire, R., Crevecoeur, G., Dupré, L., Sabariego, R. v., Dular, P., Geuzaine, C., 2010. Stochastic uncertainty quantification of the conductivity in eeg source analysis by using polynomial chaos decomposition. IEEE Trans Magn 46, 3457–3460. https://doi.org/10.1109/TMAG.2010.2044233

Grech, R., Cassar, T., Muscat, J., Camilleri, K.P., Fabri, S.G., Zervakis, M., Xanthopoulos, P., Sakkalis, V., Vanrumste, B., 2008. Review on solving the inverse problem in EEG source analysis. J Neuroeng Rehabil 5, 1–33. https://doi.org/10.1186/1743-0003-5-25/COMMENTS

Kalhara, P.G., Jayasinghearachchd, V.D., Dias, A.H.A.T., Ratnayake, V.C., Jayawardena, C., Kuruwitaarachchi, N., 2018. TreeSpirit: Illegal logging detection and alerting system using audio identification over an IoT network. International Conference on Software, Knowledge Information, Industrial Management and Applications, SKIMA 2017-December. https://doi.org/10.1109/SKIMA.2017.8294127

Kang, J.H., Kim, S.J., Cho, Y.S., Kim, S.P., 2015. Modulation of Alpha Oscillations in the Human EEG with Facial Preference. PLoS One 10, e0138153. https://doi.org/10.1371/JOURNAL.PONE.0138153

Kiebel, S.J., Garrido, M.I., Moran, R., Chen, C.C., Friston, K.J., 2009. Dynamic causal modeling for EEG and MEG. Hum Brain Mapp 30, 1866–1876. https://doi.org/10.1002/HBM.20775

Kurth, S., Jenni, O.G., Riedner, B.A., Tononi, G., Carskadon, M.A., Huber, R., 2010. Characteristics of sleep slow waves in children and adolescents. Sleep 33, 475–480. https://doi.org/10.1093/sleep/33.4.475

Lobier, M., Siebenhühner, F., Palva, S., Palva, J.M., 2014. Phase transfer entropy: A novel phase-based measure for directed connectivity in networks coupled by oscillatory interactions. Neuroimage 85, 853–872. https://doi.org/10.1016/J.NEUROIMAGE.2013.08.056

Mensen, A., Riedner, B., Tononi, G., 2016a. Optimizing detection and analysis of slow waves in sleep EEG. J Neurosci Methods 274, 1–12. https://doi.org/10.1016/J.JNEUMETH.2016.09.006

Mensen, A., Riedner, B., Tononi, G., 2016b. Optimizing detection and analysis of slow waves in sleep EEG. J Neurosci Methods 274, 1–12. https://doi.org/10.1016/j.jneumeth.2016.09.006

Pascual-Marqui, R D, Esslen, M., Kochi, K., Lehmann, D., Pascual-Marqui, Roberto D, n.d. Functional imaging with low resolution brain electromagnetic tomography (LORETA): a review.

Pascual-Marqui, R.D., 2002. Standardized low-resolution brain electromagnetic tomography (sLORETA): technical details. Methods Find Exp Clin Pharmacol 24 Suppl D, 5–12.

Perrin, F., Pernier, J., Bertrand, O., Echallier, J.F., 1989. Spherical splines for scalp potential and current density mapping. Electroencephalogr Clin Neurophysiol 72, 184–187. https://doi.org/10.1016/0013-4694(89)90180-6

Pinto, B., Silva, C.Q., 2007. A simple method for calculating the depth of EEG sources using minimum norm estimates (MNE). Med Biol Eng Comput 45, 643–652. https://doi.org/10.1007/S11517-007-0204-Z/FIGURES/4

Sakkalis, V., 2011. Review of advanced techniques for the estimation of brain connectivity measured with EEG/MEG. Comput Biol Med 41, 1110–1117. https://doi.org/10.1016/J.COMPBIOMED.2011.06.020

Song, J., Davey, C., Poulsen, C., Luu, P., Turovets, S., Anderson, E., Li, K., Tucker, D., 2015. EEG source localization: Sensor density and head surface coverage. J Neurosci Methods 256, 9–21. https://doi.org/10.1016/J.JNEUMETH.2015.08.015

Vicente, R., Wibral, M., Lindner, M., Pipa, G., 2011. Transfer entropy-a model-free measure of effective connectivity for the neurosciences. J Comput Neurosci 30, 45–67. https://doi.org/10.1007/S10827-010-0262-3/FIGURES/8

3. PROJECT 2

3.1. Preface

This project is entirely dedicated to sleep physiology. Herein, I describe a hdEEG sleep study on typically developing young adolescents and young adults. For this study, I fully developed the hdEEG pipeline for slow wave detection analysis.

3.2. Adolescence

Adolescence is a transitional phase of life characterized by specific and drastic phycological and physical changes that lead a child to adulthood. There is no agreement about the precise age span interested by these modifications and current more inclusive definitions encompass ages before 10 and after 20.

While the most rapid and dramatic brain development occurs in the first few years of life, during adolescence the brain is still highly dynamic. White matter connections are locally strengthened or weakened in response to environmental stimuli, the overall white matter volume progressively increases, and at the same time the gray matter decreases asynchronously in different cortical regions due to neuronal loss (‘pruning’) and/or intra-cortical myelination (Paus, 2005). Fronto-parietal associative brain regions are the most massively involved by these processes (Piekarski et al., 2017).

Interestingly, the peak of incidence of onset for the most common psychiatric disorders occurs during adolescence. Thus, the understanding of what goes wrong in subjects who

develop a psychiatric condition during this age span is one of the most compelling questions in the field of psychiatry (Galván, 2017).

A recent longitudinal fMRI study (Kaufmann et al., 2017) has drawn attention to functional connections, rather than functional brain regions. Most specifically, the study showed that adolescence is the life period characterized by the most rapid transformation of the functional connectome distinctiveness (how well it discriminates an individual from the others) during which individuals develop their own stable connectivity fingerprint (Figure 1). Subjects with higher clinical symptoms (of ADHD, schizophrenia or even depression) displayed a delay in this fine network tuning and had less individualized connectomes compared to age-related peers. This and similar researches inspired the current and the next 2 projects.

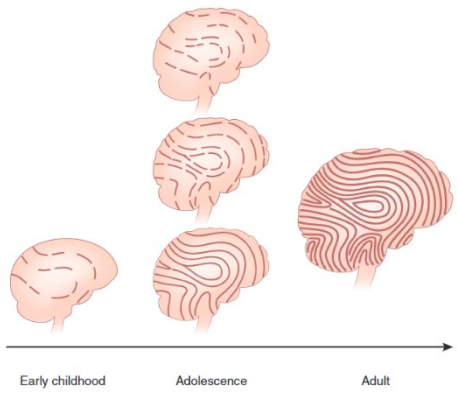

Figure 1. The human connectome.

The brain connectome fingerprint, ill-defined in early childhood, progressively develops a clear signature (distinct to each person) during adolescence. Taken from (Galván, 2017).

3.3. Sleep during the transition between childhood and adolescence

Adolescence is marked by significant changes in sleep habits (reduced sleep-time and phase-delay), in face of unchanged sleep-needs (Gradisar et al., 2011; Tarokh et al., 2016). At EEG, the most striking change is a reduction in amplitude and power (up to 40% pre- and post-puberty), across all EEG frequencies, during both wakefulness and

sleep (Campbell et al., 2012; Campbell and Feinberg, 2009a; Tarokh et al., 2011a; Tarokh and Carskadon, 2010a). This reduction is particularly marked for delta and theta and parallels a significant decline in cortical grey matter over a wide range of brain regions (Buchmann et al., 2011a). Even most notably, a separate study that used hdEEG to map cortical spectral activity pointed to a developmental progression of maximal sleep SWA from posterior to anterior scalp regions (Kurth et al., 2010b). Once again, this progression goes along with the trajectory of regional maximal cortical grey matter observed with longitudinal MRI studies (Shaw et al., 2008). Recent studies also suggested that sleep may play an active role in modeling our brain during adolescence. For example, synaptic spine elimination was found to be higher during sleep than wakefulness in adolescent but not adult mice (Maret et al., 2011). In humans, correlational studies pointed to an association between sleep duration and brain development of both local grey matter and white matter integrity (Taki et al., 2012; Telzer et al., 2015).

3.4. Study aim

Most sleep studies in children and adolescents focused on delta power (SWA), and rarely investigated specific individual slow waves properties (Jaramillo et al., 2020; Kurth et al., 2017, 2010a; Schoch et al., 2018; Spiess et al., 2018; Timofeev et al., 2020). Thus, in this project, I investigated maturation-dependent changes in slow-wave traveling parameters, with a particular attention to the left-right and anterior-posterior slow wave asymmetry by comparing sleep hdEEG data (256 channels) of 21 young adolescents and 18 young adults.

3.5. Original paper

I enclose here the original article from this project, submitted to Sleep.

Origin, synchronization, and propagation of sleep slow waves in children

Anna Castelnovo [1,2,3], Althea Lividini [4], Brady A. Riedner [5], Giulia Avvenuti [6], Stephanie G. Jones [7], Silvia Miano [1,2], Giulio Tononi [7], Mauro Manconi [1,2,8], Giulio Bernardi [6]

[1]*Sleep Medicine Unit, Neurocenter of Southern Switzerland, Ospedale Civico, Lugano, Switzerland.*

[2]*Faculty of Biomedical Sciences, Università della Svizzera Italiana, Lugano, Switzerland.*

[3]*University Hospital of Psychiatry and Psychotherapy, University of Bern, Bern, Switzerland.*

[4]*Epilepsy Center - Sleep Medicine Center, Childhood and Adolescence Neuropsychiatry Unit, ASST SS. Paolo e Carlo, San Paolo Hospital, Milan, Italy*

[5]*Center for Sleep and Consciousness, Department of Psychiatry, University of Wisconsin - Madison, Madison, WI, USA.*

[6]*MoMiLab Research Unit, IMT School for Advanced Studies Lucca, Lucca, Italy.*

[7]*Department of Psychiatry, Wisconsin Institute for Sleep and Consciousness, University of Wisconsin-Madison, Madison, WI, USA*

[8]*Department of Neurology, University Hospital, Inselspital, Bern, Switzerland.*

**Corresponding author: Anna Castelnovo, via Tesserete 46, 6900 Lugano, anna.castelnovo@eoc.ch; *Co-corresponding author: Giulio Bernardi, Piazza San Francesco, 19, Lucca 55100, Italy. Electronic address: giulio.bernardi@imtlucca.it.*

Abstract

Study Objectives

Slow waves undergo significant changes throughout development, mirroring changes in brain function and anatomy. However, most current knowledge on age-dependent slow-wave changes is based on the analysis of delta power (<4 Hz). Here we aimed at characterizing individual slow wave properties such as origin, synchronization, and cortical propagation at the transition between childhood and adulthood.

Methods

We analyzed overnight high-density (256 electrodes) EEG recordings of healthy typically developing children (N=21, 10.3±1.5 years old) and young healthy adults (N=18, 31.1±4.4 years old). All recordings were preprocessed to reduce artifacts, and NREM slow waves were detected and characterized using validated algorithms. The threshold for statistical significance was set at p=0.05.

Results

The slow waves of children were larger and steeper, but less widespread than those of adults. Moreover, they tended to mainly originate from and spread over more posterior brain areas. Relative to those of adults, the slow waves of children also displayed a tendency to more strongly involve and originate from the right than the left hemisphere. The separate analysis of slow waves characterized by high and low synchronization efficiency showed that these waves undergo partially distinct maturation patterns,

consistent with their possible dependence on different generation and synchronization mechanisms.

Conclusions

Changes in slow wave origin, synchronization, and propagation at the transition between childhood and adulthood are consistent with known modifications in cortico-cortical and subcortico-cortical brain connectivity. In this light, changes in slow-wave properties may provide a valuable yardstick to assess, track, and interpret physiological and pathological development.

Keywords

Development, maturation, slow wave activity, SWA, traveling

Introduction

During childhood and adolescence, the human brain undergoes several significant structural and functional adaptations. White-matter volume increases with age till young adulthood (Keshavan et al., 2002) according to region-specific trajectories (Lynch et al., 2020). Vice versa, starting after 7 years of age, gray matter volume declines massively and asynchronously, especially over fronto-parietal associative areas, following a posterior-anterior trajectory (Piekarski et al., 2017). This decline seems to result from the combination of selective synaptic pruning, programmed cell death, and progressive intra-cortical myelination (Paus, 2005). Importantly, a derangement of such delicate and complex processes is supposed to underlie several psychiatric disorders that typically emerge during adolescence (Paus et al., 2008).

Sleep electroencephalography (EEG) has been proposed as a reliable tool to track maturation-dependent brain adaptations occurring from infancy to young adulthood (Gorgoni et al., 2020; Ricci et al., 2021; Ringli and Huber, 2011; Schoch et al., 2018; Timofeev et al., 2020). Indeed, brain activity recorded during the sleep state is only marginally affected by confounds related to motivational, attentional, and contextual influences, thus allowing for an unbiased assessment of brain activity. Moreover, properties of sleep hallmarks such as NREM slow waves (<4 Hz) and spindles (10-16 Hz) appear to directly reflect brain organization and connectivity and may thus allow to track physiological and pathological maturational changes (Buchmann et al., 2011; Shaw et al., 2008). Sleep slow waves are especially interesting in this respect because of their dependence on short- and long-range connectivity. Specifically, local changes in synaptic strength and efficiency are thought to affect neuronal synchronization and thus slow wave

properties such as amplitude, slope, and number of negative peaks (Esser et al., 2007; Riedner et al., 2007a; Vyazovskiy et al., 2007). Differently, long-range (e.g., transcallosal) connectivity seems to affect long-range slow wave traveling at the cortical level (Avvenuti et al., 2020; Massimini et al., 2004; Murphy et al., 2009).

In line with these considerations, slow wave activity (SWA) - expressed as the mean EEG signal power within in the delta range (<4 Hz) - decreases progressively with age (Campbell and Feinberg, 2009; Jenni and Carskadon, 2004; Kurth et al., 2010), while its topographic distribution displays a shift from posterior to anterior scalp regions (Kurth et al., 2010). These changes occur in parallel with (micro)structural variations in regional myelination and cortical volume, as well as with the acquisition of region-specific skills (Kurth et al., 2012). In addition, changes in the myelination of longitudinal and interhemispheric fibers are associated with an increase in the speed and distance traveled by slow waves (Kurth et al., 2017).

Interestingly, previous work suggested the existence of at least two slow wave sub-types that are presumably generated by distinct synchronization processes (Siclari et al., 2014),(Bernardi et al., 2018) : 1) a likely subcortical-cortical, arousal-related process (type I) may be responsible for the emergence of widespread, large, and steep slow waves that predominate early in the falling asleep period and tend to originate from centro-frontal areas; 2) a cortico-cortical process may underlie the generation of more circumscribed, smaller, and shallower slow waves (type II) that predominate during stable NREM sleep and may originate everywhere in the cortex. The study of these slow wave sub-types across development could offer an important window on the maturation of both cortical and subcortical structures involved in sleep and slow-wave regulation.

While the above observations hint at a potential value of slow waves as markers of brain maturation, a detailed and comprehensive analysis of how topographic slow-wave characteristics and different slow-wave sub-types change from childhood to adulthood has never been performed. Notably, a better understanding of the mechanisms that regulate slow waves in relation to developmental processes could have more general implications for the use of slow waves as a marker of neurodevelopmental disorders. Therefore, here we analyzed and compared night-sleep high-density EEG data (256 electrodes) collected in healthy children and young adults to investigate potential maturation-dependent changes in topographic slow-wave characteristics. In particular, we used automated methods to detect individual slow waves and analyzed their origin, regional synchronization, and propagation patterns. The following hypotheses were tested. First, both slow wave origin and involvement shift from posterior to anterior areas, thus reflecting changes in the ability of frontal areas to generate and be reached by traveling slow waves. Second, slow waves of children are less widespread and more asymmetric across the two hemispheres, as a possible consequence of an incomplete development of inter-hemispheric white-matter tracts [16,46] (Bernardi et al., 2018; Siclari et al., 2014; Spiess et al., 2018). Third, different slow waves sub-types present dissociable properties and maturation patterns in line with their predominant dependence on distinct synchronization mechanisms and brain structures (subcortical and cortical, respectively) (Bernardi et al., 2018; Siclari et al., 2014; Spiess et al., 2018).

Methods

2.1 Participants

For this observational, cross-sectional investigation, we studied healthy children and young adults recorded for one single night with the same EEG system and with similar procedures. Children were recruited at the Sleep Unit of the Civic Hospital of Lugano (Castelnovo et al., 2022; Miano et al., 2019), while young adults were drawn from a study conducted at the University of Wisconsin-Madison sleep laboratory (Dentico et al., 2016; Ferrarelli et al., 2013).

Physicians board-certified in Sleep Medicine thoroughly interviewed children and adults to screen for any known sleep disorder, or any medical condition affecting sleep. Selected subjects were then referred to the sleep laboratory for a sleep video-PSG with extended EEG monitoring to screen for the presence of obstructive sleep apnea syndrome (OSAS) and periodic limb movements (PLM).

Selection criteria were: 1) age between 7 and 14 for the pediatric group and between 20 and 40 for the adult group; 2) negative personal history for sleep disorders; 3) good technical quality of the sleep recordings; 4) a respiratory disturbance index (RDI) < 5 events/hour.

The pediatric group was composed of 21 subjects (10.3 ± 1.5 years old, 9 females), while the adult group consisted of 18 subjects (31.1 ± 4.4, 11 females).

All study procedures were reviewed and approved by the local Independent Ethics Committee ‘Comitato Etico Cantonale’ (02.26.2015 – n.2881) and by the University of Wisconsin Health Sciences Institutional Review Board. All participants provided written consent upon participation. All research activities were conducted in accordance with the Helsinki Declaration.

2.2 Sleep recordings

All participants underwent an in-laboratory overnight hd-EEG recording (256 channels; Electrical Geodesics Inc., Eugene, OR) with a 250 Hz or 500 Hz sampling rate, coupled with traditional video-PSG (Berry RB, Brooks R, Gamaldo CE, Harding SM, Lloyd RM, Marcus CL, 2020). Recordings performed at 500 Hz were down-sampled to 250 Hz before data preprocessing and analysis. Lights out was within one hour of the participants most consistently reported bedtime, and wake-up time was between 6 and 7 am for all participants.

Sleep stages and sleep events were scored according to standard criteria by a board-certified sleep physician using the Embla® Remlogic Software (Neurolite), based on 30-second epochs for 6 bipolar re-referenced EEG channels (F3/M2, F4/M1, C3/M2, C4/M1, O1/M2, O2/M1), electrooculogram (EOG), and submental electromyogram (EMG) (Berry RB, Brooks R, Gamaldo CE, Harding SM, Lloyd RM, Marcus CL, 2020). Supplementary Table S1 reports the sleep macrostructure of children and adults.

2.3 EEG data preprocessing

Before spectral analysis, we pre-processed the data according to standard routines for hd-EEG. We imported all EEG signals and other relevant information (including sleep scoring) and analyzed them in MATLAB (The MathWorks Inc., Natick, MA). We first-order high-pass filtered at 0.1 Hz (IIR filter reproducing a single resistor capacity) and subsequently band-pass filtered the EEG signal (0.5 – 45 Hz, Kaiser window-based FIR with zero-phase distortion). An interactive open-source tool for data visualization and data-cleaning (https://github.com/CSC-UW/csc-eeg-tools.git) was used to visually inspect

data in MATLAB and mark bad channels and artifactual signals. Data segments containing an arousal or artifacts affecting the majority of the channels were marked as 'bad' and not considered for subsequent analyses. We additionally removed channels with distinctly greater power relative to neighboring channels upon inspection of power spectra and topographic power maps. An Independent Component Analysis (ICA) was performed to remove ocular, electrocardiograph, sweating, and muscular artifacts using EEGLAB routines (Delorme and Makeig, 2004). We excluded only ICA components with specific activity patterns and component maps characteristic of artifactual activity. Finally, we recovered removed bad channels using non-linear spherical interpolation.

2.4 EEG signal power in NREM sleep

Spectral analysis was performed on the average-referenced signal using artifact-free 6-second epochs (Welch's averaged modified periodogram with Hamming windows, 8 segments, 50% overlap). For topographic analyses, we computed the average delta power across epochs (SWA; 1-4 Hz) and examined both absolute and normalized power (z-score across channels).

2.5 Slow wave detection

The EEG signals were referenced to linked-mastoids and slow waves were detected automatically using a validated method [24,33]. First, we calculated the signal negative envelope by selecting for each time-point the fifth most negative sample across 191 'internal' electrodes, i.e., after exclusion of channels placed on the face and neck. This approach minimizes the risk of including in the envelope potential residual high-amplitude oscillations of artifactual origin.

We then applied a negative half-wave detection procedure based on the identification of consecutive zero-crossings on the zero-mean centered signal envelope (Vyazovskiy et al., 2007). Only half-waves with a duration of between 0.25 and 1.0 s were retained for further analyses. No amplitude thresholds were applied (Bernardi et al., 2019, 2018; Castelnovo et al., 2020, 2016; D'Agostino et al., 2018; Mensen et al., 2016; Spiess et al., 2018; Vyazovskiy et al., 2007). For all the detected slow waves, we computed and stored the following parameters of interest: duration (time between zero-crossings in seconds; s), amplitude of the maximum negative-peak (μV), down-slope (between the first zero-crossing and the maximum negative peak; μV/s), up-slope (between the maximum negative peak and the second zero-crossing; μV/s), involvement (mean EEG signal calculated across all electrodes in a 40 ms window centered on the wave peak; μV).

2.6 Slow wave origin and propagation

For each detected slow wave, we computed its pattern of propagation by determining the topographic distribution of each local maximum negative peak relative delay (Massimini et al., 2004). We used a 'likeness constraint' method (Menicucci et al., 2009) to discard channels in which the negative wave was excessively dissimilar from a 'prototype' slow wave, defined as the wave with the largest negative peak at the time of the maximum wave peak detected on the signal negative envelope. This method is based on the cross-correlation between the instantaneous phases (estimated using the Hilbert transform) of the prototype wave and the instantaneous phases of each EEG signal (within a symmetrical 300 ms time-window) (Menicucci et al., 2009). Events falling above the 25th percentile of the distribution of the maximal cross-correlation values were retained to create a scalp delay map. Then, we applied a spatiotemporal clusterization procedure to

exclude potential propagation gaps (islands of channels that likely reflect artifacts in the local EEG signal). According to this procedure, we considered the local peaks of two neighboring electrodes separated by less than 10 ms as part of the same propagation cluster. Finally, we identified the propagation cluster including the prototype wave, extracted the final delay map, and set to zero the minimum delay.

The obtained delay maps were used to compute slow-wave density, globality, probabilistic origin and termination. Specifically, slow-wave density was defined for each channel as the number of times the considered channel participated in a slow wave per minute. This index was computed in each sleep epoch after exclusion of artifactual or non-physiological activity and then averaged across epochs. Slow-wave globality was computed as the number of channels involved by individual slow waves, as extracted from the delay map. Slow-wave origin and termination were respectively defined for each slow wave as the channels showing the lowest (i.e., 0 ms) or the highest propagation delay. Thus, the probabilistic origin/termination is the percentage of slow waves that originate/terminate in each electrode.

In order to investigate whether slow waves originated with a different incidence across the two hemispheres, we classified individual slow waves as having a left (or right) hemisphere origin if 75% of the origin channels were located in the left (or right) hemisphere. Then, we determined the overall proportion of slow waves with a clear origin in the left or in the right hemisphere with respect to the total number of detected slow waves. Finally, we computed a ‘channel recruitment symmetry index’ (Avvenuti et al., 2020), defined as the number of channels in the hemisphere with less involved

electrodes, divided by the total number of involved channels (%). A value of 50% indicates a symmetric distribution, while a value of 0% indicates a unilateral wave.

2.7 Principal component analysis of slow wave involvement

In adults, 95% of the variance related to slow-wave scalp involvement is explained by 3 principal components (PCs) - with maxima in the centro-frontal area (~70% of total variance), anterior or posterior areas (~20%), and left or right hemispheres (~5%) (Bernardi et al., 2018). These PCs may reflect distinct modes of slow-wave expression depending on the involvement of different wave origins or propagation patterns. To investigate how maturational processes affect such modes of slow wave expression, here we analyzed the involvement distribution (across channels) of all slow waves using principal component analysis (PCA), as described in previous studies (Avvenuti et al., 2020; Bernardi et al., 2018). First, we confirmed through visual inspection that the same 3 main PCs observed in previous work were found in our samples of young adults and children. Then, the PC-space of each subject was rotated into a common PC space using the Procrustes transformation (Bernardi et al., 2018). The Procrustes transformation is an orthogonal transformation that minimizes the Euclidean distance between two sets of paired vectors. The reference space was selected by iteratively applying the transformation over pairs of subjects and then identifying the coordinate system (i.e., the subject) presenting the smallest distance with respect to the coordinate systems of all subjects (Haxby et al., 2011). Finally, we applied the Procrustes transformation to remap the original PC-space of each subject (adult and children subjects), into the new reference PC-space. This procedure allowed us to compare the explained variance of the PCs across individuals.

In addition, we performed source modeling of the first 100 slow waves that weighed the most on each PC using Brainstorm. For this, we selected age-appropriate MRI templates (Richards et al., 2016) segmented using the SPM12/CAT12 MATLAB toolbox (Tzourio-Mazoyer et al., 2002). A symmetric Boundary Element Model (BEM) of the head having 3 realistic layers (scalp, inner skull, outer skull)

(Maureen, 2010) and a standard co-registered set of electrode positions were used to construct the forward model. The inverse matrix was computed using the sLORETA Minimum Norm (Pascual-Marqui, 2002) with sources constrained to be perpendicular to the cortical surface and retaining only diagonal elements of the noise covariance matrix.

2.7 Slow wave synchronization

Previous work showed that, in adults, slow wave sub-types having distinct properties and regulation, and likely reflecting distinct synchronization mechanisms (type I/II), could be heuristically distinguished based on their synchronization efficiency (Bernardi et al., 2018). Specifically, a 'synchronization score' was computed for each wave as the percentage of channels showing a negative averaged current value of <-5 μV multiplied by the wave mean slope (i.e., the mean of down-slope and up-slope). Based on evidence derived from animal and computational models, this index may be expected to depend on both the number of areas/neurons contributing to the slow waves and the rapidity of their synchronization [18,19].

Here, the same approach was used to calculate the synchronization score of each detected slow wave. Then, in order to allow for interpretable comparisons between children and adults, we selected for each participant an identical number of slow waves

with high and intermediate synchronization efficiency, respectively assumed to be representative of type I and type II slow waves. From the whole distribution of synchronization scores, we identified those falling between the 90th and to the 100th percentile (top10% - putative type I), and those between the 45th and to the 55th percentile (mid10% - putative type II). We then computed the origin and scalp involvement of slow waves classified as mid10% or top10%. Involvement values of each slow wave were normalized through z-score transformation across electrodes to account for inevitable amplitude differences between slow wave sub-types. This analysis was performed only on data of the first NREM cycle to avoid possible confounds related to homeostatic changes in slow wave synchronization.

2.8 Statistical Analysis

Statistical between-group comparisons were performed using unpaired 2-tailed t-tests, Mann–Whitney U tests, or χ^2 tests, as appropriate. Normality of data and homogeneity of variance were first assessed using the Shapiro/Wilk's test and Levene's test, respectively. Mixed model analyses of variance (ANOVA) were used to investigate interaction effects between group (children, adult) and within-group factors.

For scalp topographic analyses, we corrected for multiple comparisons using a cluster-based method (Nichols and Holmes, 2002), as described in previous work (Castelnovo et al., 2022). Specifically, for each performed t-test, a null distribution was generated by randomly shuffling subjects across groups. At each iteration of the permutation procedure, the test-statistics was computed for each electrode and the size of the largest significant electrode-cluster (uncorrected $p<0.05$) was stored in a frequency table. Given the impracticality of computing all possible data re-combinations, the full null distribution

was approximated using 50,000 iterations. Finally, the 95th percentile (5% significance level) was used as the critical cluster-size threshold. Correlations were performed using Spearman correlation.

Alpha significance was set to $p < 0.05$. Partial Eta-squared (η^2) and Cohen's d were used as measures of effect size (Cohen, n.d.). All statistical analyses were performed in MATLAB.

3. Results

3.1 Slow wave activity

The children group showed higher absolute NREM SWA than the adult group over the entire scalp (cluster size = 256, $p < 0.05$; Supplementary Figure S1). After normalization, though, SWA was higher over centro-posterior regions (cluster size = 30, $p < 0.05$) and lower over frontal regions (cluster size = 69, $p < 0.05$) in the children group compared to the adult group (Supplementary Figure S1). We obtained similar results in additional exploratory analyses focusing on N2 or N3 separately (Supplementary Figure S1), and on the first sleep cycle (*data not shown*).

3.2 Slow wave density and involvement

Absolute slow-wave density (cluster size = 158, $p < 0.05$) and involvement (cluster size = 169, $p < 0.05$) were significantly higher in children than in adults (Figure 1, Supplementary Figure S2). After normalization across electrodes, we found significantly higher values of density and involvement over posterior regions (cluster size = 72, $p < 0.05$, cluster size = 83, $p < 0.05$, respectively) and lower values over frontal regions (cluster size = 86, $p <$

0.05, cluster size = 98, $p < 0.05$, respectively) in children compared to adults. In addition, we found that slow-wave negative amplitude (2-tailed paired t-test, $p < 0.001$, $|t(1,37)| = 11.685$; M children = 73.2 ± 10.2, M adult = 38.8 ± 7.7, mean difference = 34.4, C.I. = 28.4 to 40.4, Eta-squared = 0.785), down-slope ($p < 0.001$, $|t(1,37)| = 7.989$; M children = 1846.6 ± 263.4, M adult = 1220.1 ± 219.4, mean difference = 626.5, CI = 467.7 to 785.5, Eta-squared = 0.63), and up-slope ($p < 0.001$, $|t(1,37)| = 9.664$; M children = 1620.1 ± 206.8, M adult = 1035.8 ± 163.7, mean difference = 584.3, C.I. = 461.8 to 706.8, Eta-squared = 0.72) were significantly higher in children compared to adults (Figure 1). On the other hand, slow-wave globality was lower in children than in adults ($p < 0.001$, $|t(1,37)| = - 6.130$; M children = 31.9 ± 1.9, M adult = 36.9 ± 3.1, mean difference = 6, C.I. = -6.7 to -3.4, Eta-squared = 0.504). Given that slow-wave slope and globality are thought to respectively reflect short-range and long-range synchronization efficiency, we further explored the relationship between these properties in the two age groups. When adjusted for age, slow wave down-slope positively correlated with globality in adults ($p = 0.012$, $r = 0.594$), but not in children ($p = 0.665$, $r = 0.103$), and the correlation coefficients differed significantly between groups ($p = 0.049$, Fisher's $z = 1.66$; see Supplementary Figure S3).

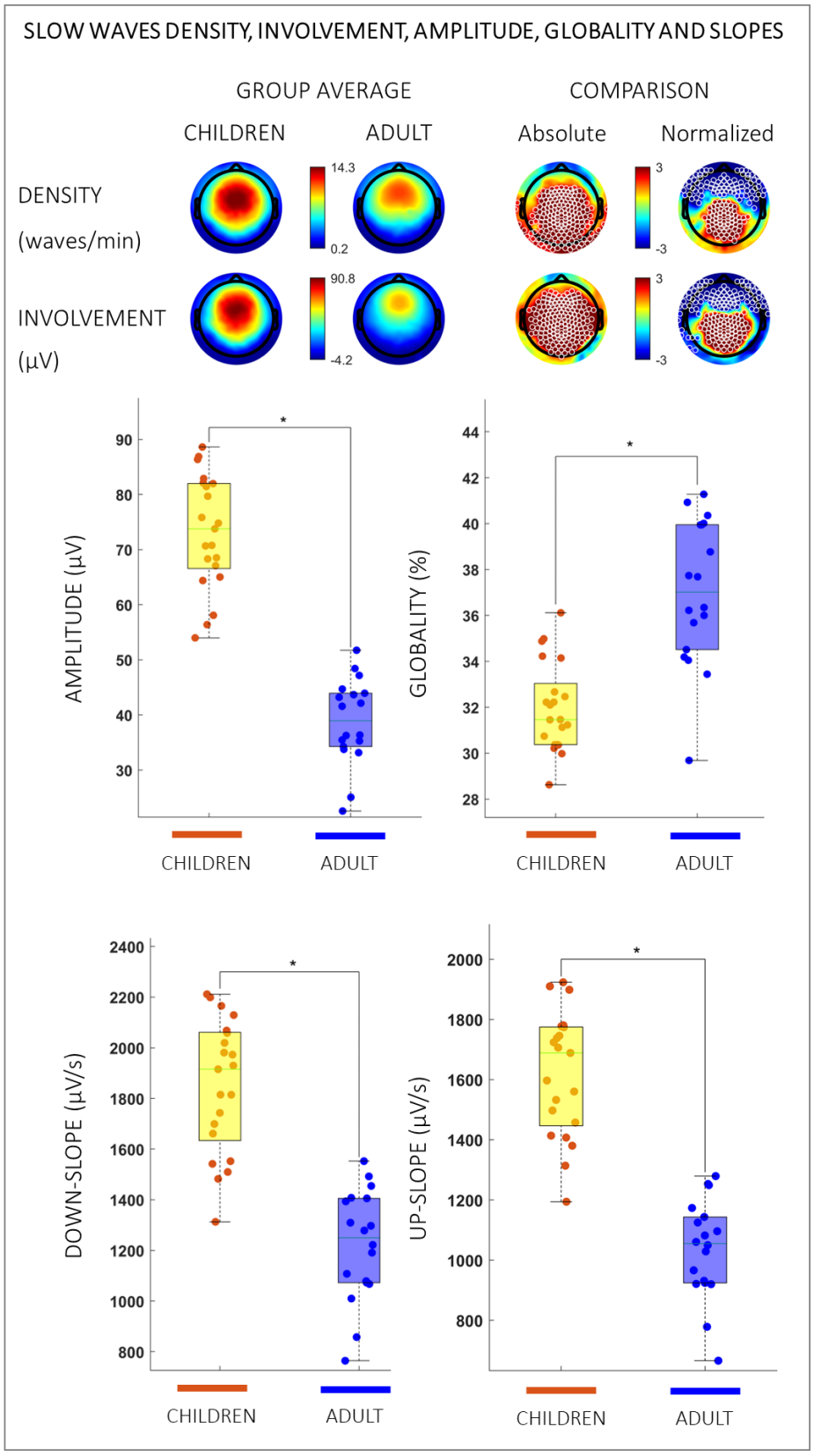
SLOW WAVES DENSITY, INVOLVEMENT, AMPLITUDE, GLOBALITY AND SLOPES
GROUP AVERAGE
COMPARISON
CHILDREN
ADULT
Absolute
Normalized
DENSITY
(waves/min)
INVOLVEMENT
(µV)
14.3
0.2
90.8
-4.2
3
-3
AMPLITUDE (µV)
GLOBALITY (%)
DOWN-SLOPE (µV/s)
UP-SLOPE (µV/s)
*
CHILDREN
ADULT

Figure 1. Slow wave density, involvement, globality, amplitude and slopes

Upper panel: Slow wave density and involvement topography. Values are color coded and plotted on the planar projection of the hemispheric scalp model. First row: slow wave density (waves/minute). Second row: slow wave involvement (μV). First and second column: average values for children and adults, respectively. Higher values are shown in red, lower in blue. Third and fourth column: t-value (two-tailed, unpaired) maps for the comparison between the two groups in terms of absolute and normalized (z-score across all electrodes) values, respectively. Blue: children < adult. Red: children > adult. White circles: significant electrodes (p < 0.05, cluster-size correction).

Lower panel: Boxplots for specific slow-wave properties: top-left, maximum negative-peak amplitude *(μV); top-right, slow wave globality (%); bottom-left, down-slope (μV/s), bottom-right: up-slope (μV/s). Orange dots: children. Blue dots: adults. The bottom and top of each boxplot are the 25th and 75th percentiles of the sample, respectively. The distance between the bottom and top of each box is the interquartile range. The green line in the middle of each box is the sample median. The whiskers extending above and below each box go from the end of the interquartile range to the furthest observation. The asterisks represent statistical significance at p<0.05.*

3.3 Principal component analysis of slow wave involvement

In both children and adults, most of the variance related to slow-wave involvement was explained by 3 PCs, with maxima in the centro-frontal area (adult group: 72.4%; range 63.0% - 84.0%; children group: 52.2%; range 36.4% - 67.1%), anterior or posterior area (adult group: 21.0%; range 12.5% - 31.2%; children group: 38.5%; range, 22.5% - 55.5%), and the left or right hemisphere (adult group: 6.7%, range: 3.5% - 10.6%; children group: 9.3%; range, 5.4% - 11.4%), respectively (Figure 2, Supplementary Figure S4). Figure 3 shows the cortical distribution of representative slow waves for each PC and group. Of note, all PCs were characterized by a maximal slow wave expression in inferior frontal

and inferior temporal areas, though they differed in terms of overall extent and relative distribution (also see Supplementary Figure S5-7).

In the children group, compared to the adult group, we observed a significant increase in the variance explained by the second (anterior/posterior: $p < 0.0001$, Cohen's $d = 2.52$) and third (left/right: $p < 0.0001$, Cohen's $d = -2.22$) PCs, at the expense of the first PC (centro-frontal: $p < 0.001$, Cohen's $d = -1.60$; Figure 2). Moreover, in children, the variance explained by the first and second PCs respectively showed a positive ($p = 0.034$, $r = 0.463$) and a negative correlation with age ($p = 0.027$, $r = -0.482$). No correlation with age was found for the third PC ($p = 0.804$, $r = 0.058$). In the adult group, none of the PCs were correlated with age (first PC: $p = 0.343$, $r = -0.237$; second PC: $p = 0.670$, $r = 0.118$; third PC: $p = 0.282$; $r = 0.268$; Figure 2).

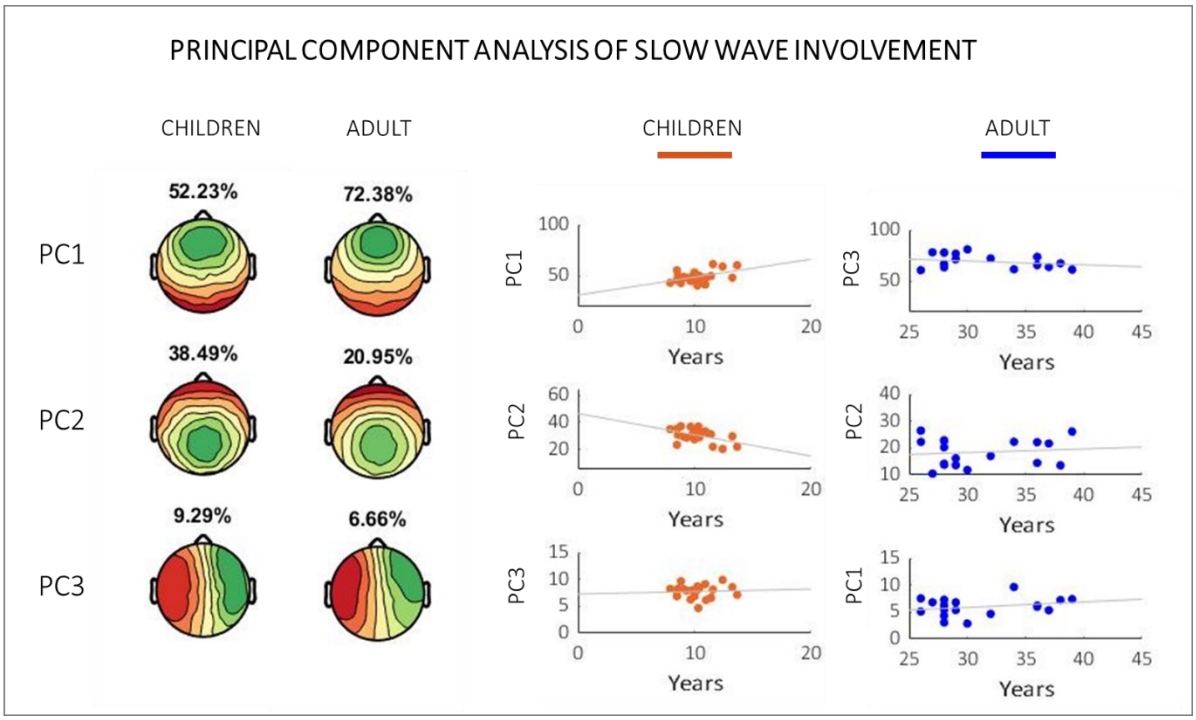

Figure 2. PC-based analysis of slow-wave involvement.

Left panel: The involvement distribution (mean EEG signal calculated across all electrodes in a 40 ms window centered on the wave peak) of all slow waves was entered in a PC analysis. The average variance explained is shown for each PC and group (after the Procrustes transformation computed to 'align' PCs across subjects and groups). PC1: first component; PC2: second component; PC3: third component. Right panel: correlation between age and variance explained by each PC. Orange dots: children. Blue dots: adults. Gray Line: least-squares regression line.

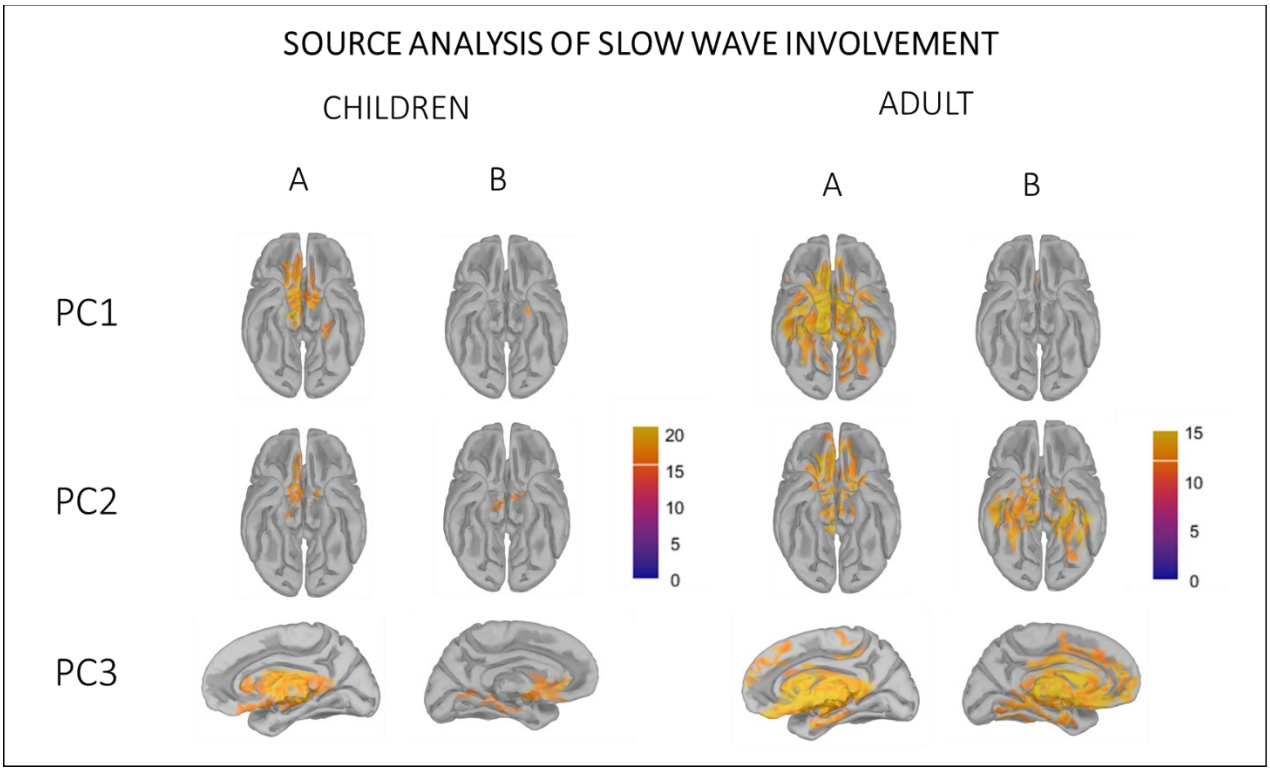

Figure 3. Source modeling of representative slow waves for each PC

First and second columns: children. Third and Fourth columns: adults. A: positive weights. B: negative weights. The figure represents the average peak of slow wave involvement (>75th percentile) in source space obtained from 3 most representative slow waves of each PC. Yellow: areas with larger overlap between subjects (>75% of subjects). The sources of PC1 included the orbito-frontal cortex and gyrus rectus, the occipital-temporal gyrus (lateral: fusiform gyrus and medial: para-hippocampus), the inferior temporal gyrus (right>left), and the temporal poles. The source of PC2 included the orbito-frontal cortex

and gyrus rectus. The source of PC3 included the rectus gyri, the para-hippocampus and the postero-ventral cingulate or middle cingulate, anterior cingulate, and subcallosal gyrus.

3.4 Recruitment symmetry index

The left-right symmetry (channel recruitment symmetry index) was significantly different between children and adults (2-tailed unpaired t-test, $p < 0.001$, $|t(1,37)| = -5.583$; M children = 29.9 ± 1.2, M adult = 32.4 ± 1.6, mean difference = 2.5, C.I.: -3.5 to -1.6, Eta-squared = 0.647; Figure 4). In addition, the symmetry index computed over anterior channels was significantly higher than the symmetry index computed for posterior channels in both groups (2-tailed paired t-tests; children: $p < 0.001$, $|t(20)| = 10.262$; M anterior = 28.7 ± 1.6, M posterior = 23.9 ± 1.6, mean difference = 4.8%, C.I. = -3.8 to 5.8, Eta-squared = 0.804; adults: $p < 0.001$, $|t(17)| = 22.519$; M anterior = 32.3 ± 1.8, M posterior = 23.9 ± 2.1, mean difference = 8.4, C.I. = 7.6 to 9.2, Eta-squared = 0.968).

There was a significant interaction (Wilks-lambda = 0.510, $F(1,37) = 35.489$, $p < 0.001$, partial Eta squared = 0.490) between group (children, adults) and region (anterior, posterior). Indeed, the symmetry index computed for anterior channels was higher in adults relative to children (2-tailed unpaired t-test, $p <0.001$, $|t(1,37)| = -6.565$; M anterior = 28.7 ± 1.6, M posterior = 32.3 ± 1.8, mean difference = 3.6, C.I. = -4.7 to -2.5, Eta-squared = 0.717), while no statistically significant difference emerged in the symmetry index computed over posterior channels (2-tailed unpaired t-test, $p = 0.932$, $|t(1,37)| = 0.086$; M anterior = 23.9 ± 1.6, M posterior = 23.9 ± 2.1, mean difference = 0.0, C.I. = -1.1 to 1.2, Eta-squared = 0.0002; Figure 4). Thus, anterior slow waves were more

asymmetric in children relative to adults, while the degree of hemispheric asymmetry was similar across groups for posterior areas.

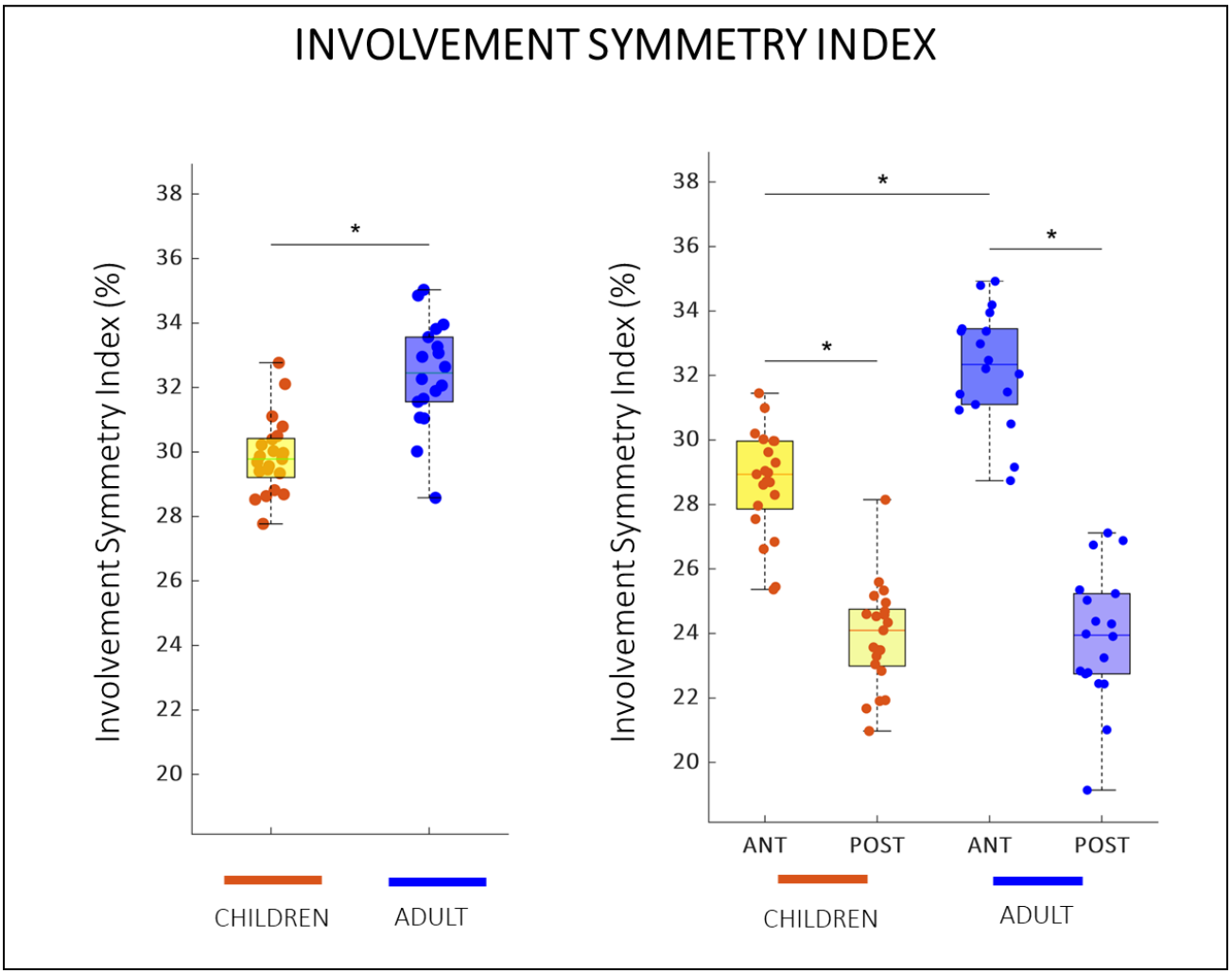

Figure 4. Slow wave channel recruitment symmetry index

Left Panel: Symmetry index computed taking into account all channels involved in each slow wave. Right Panel: Symmetry index computed separately for channels posterior to Cz (ANT: anterior, POST: posterior). Orange dots: children. Blue dots: adults. The bottom and top of each boxplot are the 25th and 75th percentiles of the sample, respectively. The distance between the bottom and top of each box is the interquartile range. The line in the middle of each box is the sample median. The whiskers extending above

and below each box go from the end of the interquartile range to the furthest observation. The asterisks represent statistical significance at p<0.05.

3.5 Slow-wave origin and termination

While the topographic distribution of slow-wave termination did not differ significantly between children and adults ($p > 0.05$), slow-waves appeared to originate significantly more often from frontal areas in adults relative to children (cluster size = 85, $p < 0.05$; Figure 5, Supplementary Figure S8-9). A complementary statistical trend was also observed in posterior electrodes, which showed a higher origin probability in children relative to adults ($p < 0.05$, uncorrected). In line with these observations, we found that the coordinates of the probabilistic origin peak on the anterior-posterior axis differed significantly between children and adults (2-tailed unpaired t test, $p = 0.005$, $|t(1,37)| = -3.007$; M children = 2.1 ± 4.7, M adult = 2.7 ± 2.6, mean difference = 2.1, C.I.: -4.3 to -0.8, Eta-squared = 0.227; Figure 5).

There was a significant interaction (Wilks-lambda = 0.868, $F(1,37) = 5.644$, $p = 0.023$, partial Eta squared = 0.132) between group (children, adults) and hemispheric origin probability (left, right). In fact, the percentage of waves that originated in the right hemisphere was significantly higher than the percentage of waves that originated in the left hemisphere in children (2-tailed paired t-test, $p = 0.029$, $|t(20)| = 2.351$; M left = 43.0 ± 3.3, M right = 46.0 ± 3.5, mean difference = 3.0, C.I. = -0.3 to 5.6, Eta-squared statistic = 0.217) but not in adults ($p = 0.386$, $|t(17)| = -0.889$, M left = 43.3 ± 6.0, M right = 42.7 ± 5.8, C.I.s = -2.0 to 0.8, mean difference = 0.6, partial-Eta-squared = 0.044). The percentage of slow waves that originated in the right hemisphere was higher in children

compared to adults (2-tailed unpaired t-test, $p = 0.040$, $|t(20)| = 2.129$; M children = 45.7 ± 3.5, M adult = 42.5 ± 3.3, mean difference = 3.2, C.I. = -0.2 to 6.3, Eta-squared = 0.185), while the percentage of slow waves that originated in the left hemisphere was similar between groups ($p = 0.827$, $|t(17)| = -0.221$; M children = 28.7 ± 1.6, M adult = 23.9 ± 1.6, mean difference = 0.33, C.I. = -3.4 to 2.7, Eta-squared = 0.003; Figure 5).

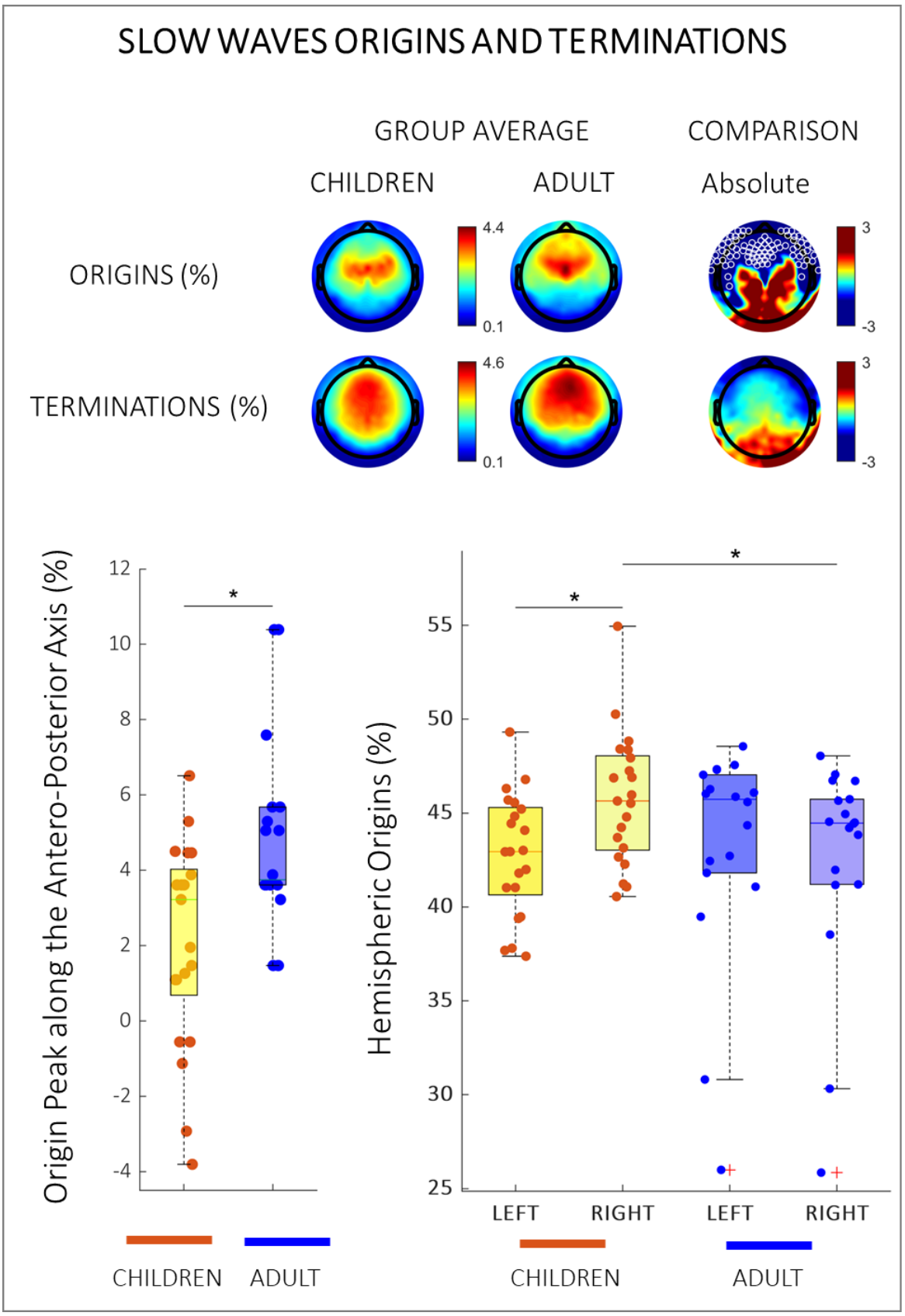
SLOW WAVES ORIGINS AND TERMINATIONS
GROUP AVERAGE
COMPARISON
CHILDREN
ADULT
Absolute
ORIGINS (%)
TERMINATIONS (%)
4.4
0.1
4.6
0.1
3
-3
3
-3
Origin Peak along the Antero-Posterior Axis (%)
12
10
8
6
4
2
0
-2
-4
*
CHILDREN
ADULT
Hemispheric Origins (%)
55
50
45
40
35
30
25
*
*
LEFT
RIGHT
LEFT
RIGHT
CHILDREN
ADULT

Figure 5. Slow wave origins and terminations

Upper panel: Slow wave origin and termination. Values are color coded and plotted on the planar projection of the hemispheric scalp model. First row: distribution of slow-wave origins (% of the total). Second row: distribution of slow wave terminations (% of the total). First and second columns: average values for the children group and the adult group, respectively. Higher values are shown in red, lower in blue. Third column: t-value (two-tailed, unpaired) maps for the comparison between the two groups. Blue: children < adult. Red: children > adult. White circles: significant electrodes ($p < 0.05$, cluster-size correction).

Lower panel: Slow-wave origin distribution along the antero-posterior axis (left lower panel) and in the right compared to the left hemisphere (right lower panel). Orange dots: children. Blue dots: adults. The bottom and top of each boxplot are the 25th and 75th percentiles of the sample, respectively. The distance between the bottom and top of each box is the interquartile range. The line in the middle of each box is the sample median. The whiskers extending above and below each box go from the end of the interquartile range to the furthest observation within the whisker length. Observations beyond the whisker length (more than 3 times the interquartile range away from the bottom or top of the box) are marked as outliers (red crosses). The asterisks represent statistical significance at $p<0.05$.

3.6 Slow waves with high and low synchronization efficiency

For each slow wave, a synchronization score was computed based on the mean slope and proportion of involved electrodes. The synchronization score distribution was non-Gaussian and right skewed in both groups (Figure 6). However, on average, children had higher synchronization scores (Median = 1.6, range = 0.3-4.5) compared to adults (Median = 0.9, range = 1.3-2.2; Mann-Whitney U Test, $z = - 5.225$, $U = 174$, $p < 0.001$, Eta-squared = 0.848). The synchronization score distributions remained similar across NREM cycles, but also showed a clear leftward shift compatible with the effects of homeostatic changes in slow-wave amplitude and globality (Figure 6). Thus, to avoid possible confounds related to homeostatic changes, we focused further analyses on the

first NREM cycle only. We then classified and separately analyzed slow waves with high (top10%) and intermediate (mid10%) synchronization efficiency.

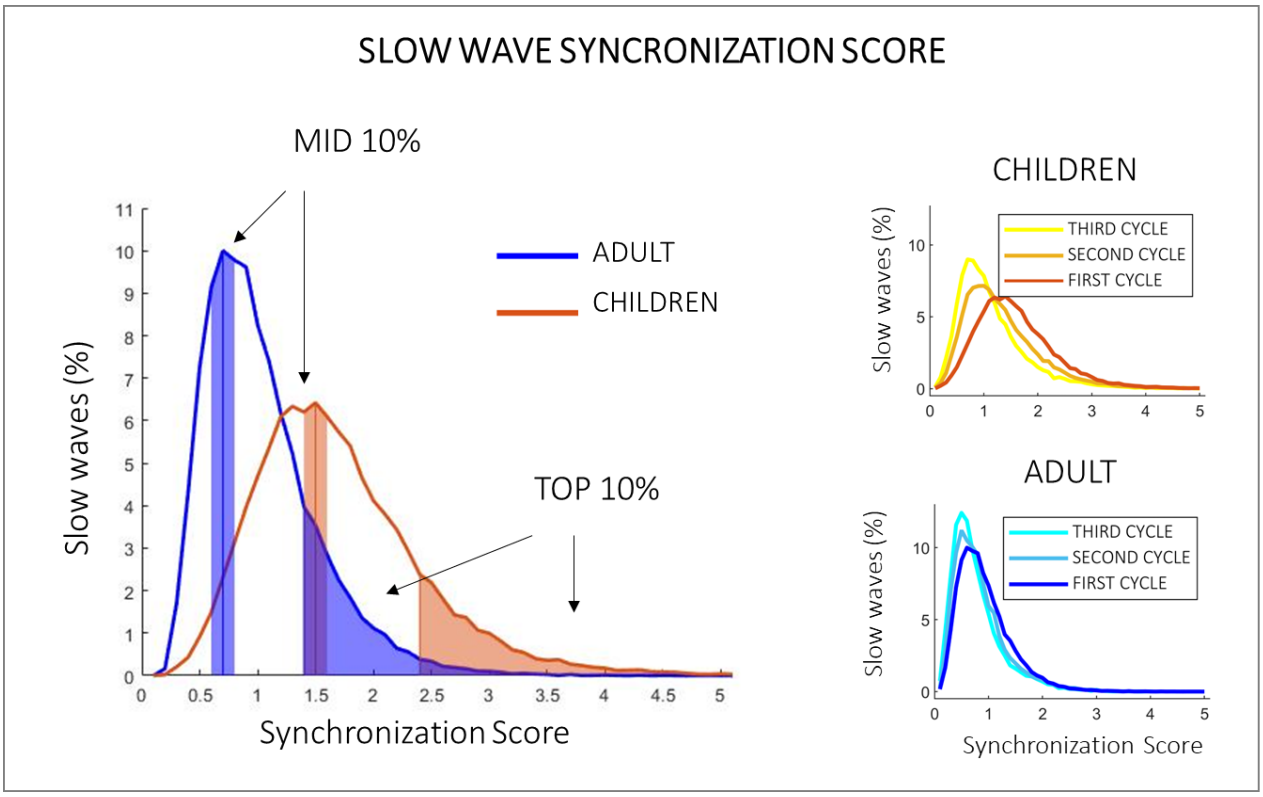

Figure 6. Slow wave synchronization score

Left panel: The two curves represent the distribution of synchronization scores (group average) during the first NREM sleep cycle in children (orange) and adults (blue). Right panels: The three curves represent the average distribution of synchronization scores during the first, second and third NREM sleep cycle in children (upper right panel) and adults (right lower panel).

Given that slow waves were classified based on their slope and globality, we first analyzed the relative contribution of these two parameters to synchronization efficiency (Supplementary Figure S10). We found no significant interaction between group (children, adults) and slow-wave sub-type (mid10%, top10%) for globality (Wilks- lambda = 0.988,

F(1,37) = 0.466, p = 0.499, partial Eta squared = 0.012). However, we identified a significant main effect of group (F(1,37) = 21.653, p < 0.001, partial Eta squared = 0.369) indicating that slow waves were overall more global in adults compared to children, and a main effect of wave sub-type (Wilks- lambda = 0.109, F(1,37) = 301.163, p < 0.001, partial Eta squared = 0.891), with both groups showing more global top10% slow waves than mid10% slow waves.

We then analyzed slow-wave down-slope and found a significant interaction (Wilks-lambda = 0.510, F(1,37) = 35.542, p < 0.001, partial eta squared = 0.490) between group (children, adults) and slow wave sub-type (mid10%, top10%). We also found a main effect of group (F(1,37) = 62.196, p < 0.001, partial Eta squared = 0.627), indicating that slow waves were overall steeper in children compared to adults (top10%: p <0.001, |t(37)| = -7.475; M children = 4005.5 ± 645.1, M adults = 2564.7 ± 542.3, C.I.: -1831.3 to 1050.2, Eta-squared: 0.607; mid10%, p <0.001, |t(37)| = -8.347; M adults = 1210.3 ± 225.0, M children = 1973.6 ± 327.0, C.I.: -948.6 to -578.0, Eta-squared: 0.653), and a main effect of slow-wave sub-type (Wilks-lambda = 0.868, F(1,37) = 888.043, p < 0.001, partial Eta squared = 0.960), with both the adult (2-tailed paired t-test, p <0.001, |t(17)| = 17.156, C.I.: 1188.0 to 1521.0, Eta-squared: 0.946) and the children (tailed paired t-test, p <0.001, |t(20)| = 25.232, C.I.: 1863.9 to 2199.9, Eta-squared: 0.969) groups showing steeper top10% than mid10% slow waves.

Slow waves with high and intermediate synchronization efficiency were then analyzed and compared for probabilistic origin and normalized scalp involvement (Figure 7). Both mid10% and top10% slow waves had a more posterior involvement in children than in adults. We found a significant interaction between group (children, adults) and wave type

(mid10%, top10%) for normalized involvement in a frontal (63 channels, $p < 0.05$) and a parieto-occipital cluster (77 channels, $p < 0.05$, Figure 7). Specifically, adults had higher involvement values compared to children in the frontal cluster for both top10% (2-tailed unpaired t-test, $p < 0.001$, $|t(37)| = 7.466$; M children = 0.4 ± 0.2, M adults = 0.8 ± 0.1, C.I. = from 0.1 to 0.2, Eta-squared = 0.601) and mid10% slow waves (2-tailed paired t-test, $p < 0.001$, $|t(37)| = 6.171$; M right = 0.4 ± 0.1, M adults = 0.6 ± 0.1, C.I. = from 0.3 to 0.5, Eta-squared = 0.507). Moreover, adults displayed significantly higher involvement values for top10% compared to mid10% slow waves within the same cluster ($p < 0.001$, $|t(17)| = 5.202$; C.I. = from 0.1 to 0.2, Eta-squared = 0.615), while no difference emerged in children ($p = 0.120$, $|t(20)| = -1.624$; C.I. = from -0.1 to 0.0, Eta-squared = 0.113; Figure 7C). Similar differences - though opposite in sign - were found in the posterior cluster (Supplementary Figure S10).

Both mid10% and top10% slow waves showed a tendency to originate from central and frontal electrodes, but a clear origin hot-spot was evident only for top10% slow waves of adults. We found a significant interaction between group and wave sub-type for slow-wave probabilistic origin in a central cluster of electrodes (14 channels, $p < 0.05$, Figure 7). Post-hoc analyses showed that, within this cluster, adults had a higher origin probability compared to children for top10% (2-tailed unpaired t-test, $p < 0.001$, $|t(37)| = 4.807$; M children = 3.0 ± 1.1, M adults = 4.9 ± 1.3, C.I. = from 1.1 to 2.6, Eta-squared = 0.461) but not for mid10% slow waves ($p = 0.9713$, $|t(37)| = -0.036$; M children = 3.0 ± 0.9, M adults = 3.0 ± 0.8, C.I. = from -0.6 to 0.5, Eta-squared = 0.00005). Moreover, adults were characterized by a significantly higher origin probability for top10% than mid10% slow waves within the same electrode cluster ($p < 0.001$, $|t(20)| = 6.295$, C.I. = from 1.2

to 2.5, Eta-squared = 0.665). A similar difference was not found in children (p = 0.935, |t(20)| = -0.0832; C.I. = from -0.5 to 0.4, Eta-squared = 0.0005; Figure 7, Supplementary Figures S11-12).

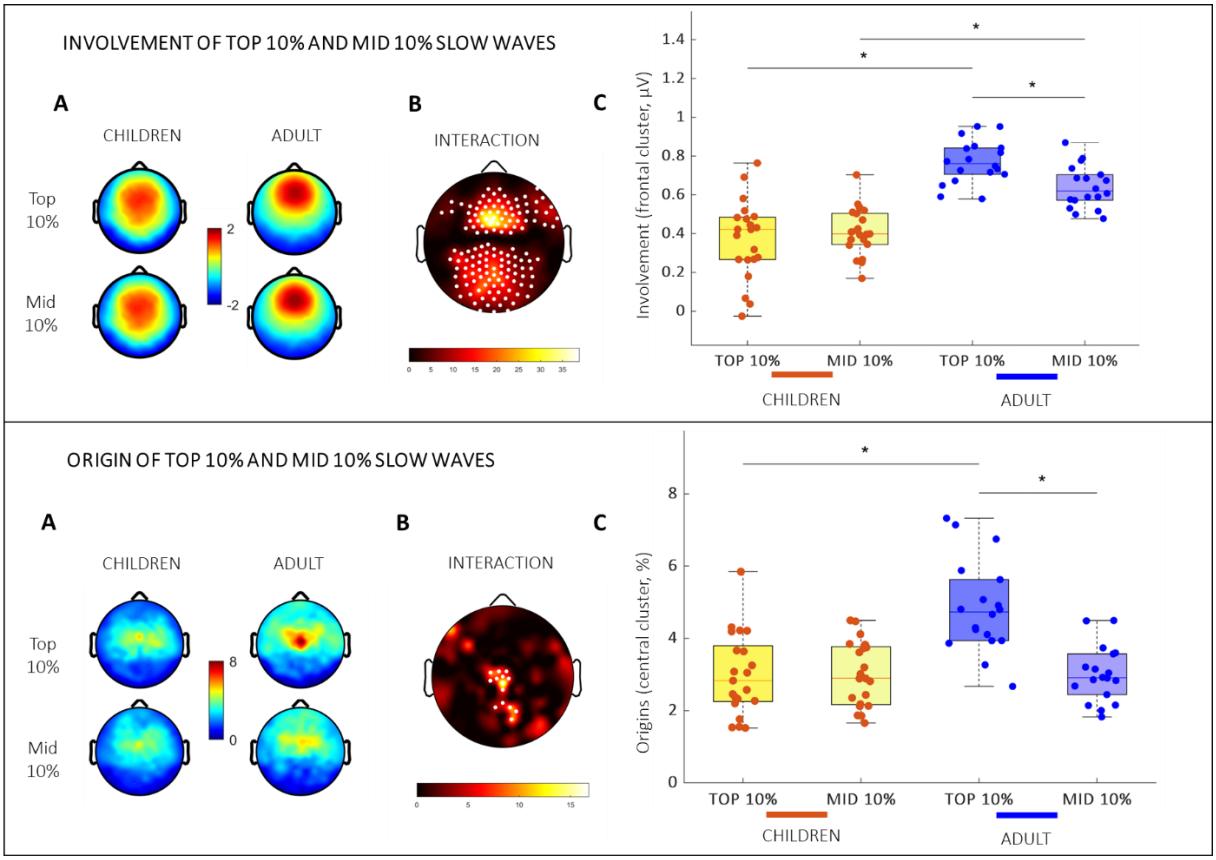

Figure 7. Origin and involvement of slow waves with high and intermediate synchronization efficiency

Involvement (top) and origin (bottom) of slow waves with high (top10%) and intermediate (mid10%) synchronization scores. Values are color coded and plotted on the planar projection of the hemispheric scalp model.

A| Topographic analysis - Average distribution of involvement/origin values for slow waves with high (top10%; first row) and intermediate (mid10%; second row) synchronization efficiency. Higher values are shown in red, lower in blue.

B| Interaction effect of the mixed-model within/between groups ANOVA. Lower F-values are represented in dark-red/black, while higher F- values in yellow/white. White circles indicate significant electrodes ($p < 0.05$, cluster-size correction).

C| Dots represent the average of channels within significant clusters of electrodes in Figure B (as two clusters were significant for the involvement, only the frontal cluster is represented here, while the posterior cluster is represented in Supplementary Figure 11). Orange dots: children; blue dots: adults. The bottom and top of each boxplot are the 25th and 75th percentiles of the sample, respectively. The distance between the bottom and top of each box is the interquartile range. The line in the middle of each box is the sample median. The whiskers extending above and below each box go from the end of the interquartile range to the furthest observation within the whisker length. The asterisks represent statistical significance at $p<0.05$.

Discussion

In the present study, we examined changes in slow-wave origin, synchronization and propagation from childhood to early adulthood using sleep hd-EEG. We found that, from childhood to adulthood: i) both the origin and topographic distribution of slow waves move towards more anterior brain regions; ii) slow waves become more global and more symmetric across hemispheres; iii) slow waves characterized by intermediate and high synchronization efficiency (putative type I and type II slow waves) display partially dissociated maturational changes.

Slow wave origin and involvement become more anterior from childhood to adulthood

Previous work demonstrated a progressive anteriorization of the SWA (delta power) peak during normal development (Kurth et al., 2010). Such a change has been suggested to

reflect a relative variation in inter-regional slow wave synchronization/propagation related to the maturation of frontal brain areas and their connectivity. More recently, preliminary observations suggested that the regional propensity to generate slow waves might also change following a posterior-to-anterior gradient from childhood to adulthood (Timofeev et al., 2020). Consistent with previous data, our present results show that both slow wave cortical distribution (involvement) and tendency to generate slow waves (origin) are stronger in anterior areas in young adults relative to children. In addition, our PCA-based analysis revealed that slow-wave scalp topography tends to follow a specific set of patterns that is common to both children and adults, and that the relative 'weight' of these patterns changes across development. Indeed, regardless of age, 95% of the variance related to slow wave involvement can be explained by 3 PCs, with maxima located in the central-frontal area, anterior or posterior areas, and left or right hemispheres (Bernardi et al., 2021). However, the relevance of the central-frontal PC appears to increase from childhood to adulthood at the expense of the other two PCs. These observations suggest that while most slow waves of children and adults may involve specific, partly overlapping brain networks, their relative propensity to 'reach' more anterior areas changes during development.

Together, our results indicate that in children, frontal areas have a lower propensity at both generating and being crossed by slow waves originating elsewhere relative to what is commonly observed in adults. Such modifications could reflect partially distinct maturational processes, such as local changes in microstructural organization and modifications in long-range connectivity, respectively (Spiess et al., 2018).

Slow wave interhemispheric asymmetry is more pronounced in children than in adults

The PCA-based analysis and the inter-hemispheric involvement analyses revealed that slow waves of children are characterized by a greater tendency to remain unilateral or at least more asymmetric on the left-right axis than slow waves of adults. Moreover, the involvement asymmetry was found to be stronger in anterior than in posterior areas.

Previous work showed that the degree of cross-hemispheric slow-wave propagation directly depends on the existence and integrity of interhemispheric (callosal) connections. Indeed, slow waves (but not spindles) of callosotomized epileptic adult patients typically remain circumscribed to the brain hemisphere in which they originate, while this is relatively uncommon in non-callosotomized individuals (Avvenuti et al., 2020; Bernardi et al., 2021). Based on this observation, our present results could be explained by an incomplete maturation of the corpus callosum in children (Giedd et al., 1999; Luders et al., 2010b). In fact, the size of the corpus callosum is known to increase throughout adolescence and up to the middle 20s (Keshavan et al., 2002), following a posterior-to-anterior gradient of maturation (Danielsen et al., 2020; Giedd et al., 1999; Luders et al., 2010a; Rajapakse et al., 1996; Thompson et al., 2000; Westerhausen et al., 2016) .

In addition, here we found in children (and not in adults) a significant interhemispheric origin asymmetry, with more slow waves originating in the right than in the left hemisphere. This is, again, consistent with findings obtained in callosotomized patients. Indeed, while previous work observed a tendency for slow waves to originate more often in the right than in the left hemisphere in both non-callosotomized and callosotomized individuals, the asymmetry appeared to be stronger in the latter group (Bernardi et al.,

2021). Interestingly, this effect could depend on an accentuation of otherwise small physiological asymmetries related to (micro)structural or functional factors due to a reduction in the synchronization between the two hemispheres. For instance, previous evidence indicates that the human brain may show lower SWA in the left than in the right hemisphere during the first night spent in a new environment (Tamaki et al., 2016), reminiscing the monitoring function of unihemispheric sleep in migratory birds and aquatic mammals (Mascetti, 2016). This relative asymmetry might become more pronounced when the coordination of activity between hemispheres is reduced. Alternatively, the observation of stronger origin asymmetries in individuals with an immature or absent corpus callosum could have a methodological explanation. Indeed, the reduced cross-hemispheric propagation in these individuals may lead to a more accurate localization of slow wave origin in the presence of EEG volume conduction. However, other explanations not involving the corpus callosum cannot be ruled out based on our current data. Indeed, for instance, previous work described an asymmetric maturation of higher-order association cortices that may contribute explaining our results (Gogtay et al., 2004). Future investigation should combine the assessment of electrophysiological and brain structural changes to determine specific mechanisms underlying slow-wave asymmetries in children.

Slow waves are larger but less widespread in children than adults

Consistent with findings indicating that slow waves of children are more often asymmetrical or even unihemispheric in children than in adults, we found that the number of channels involved by each slow wave (i.e., globality) is on average smaller in children.

Therefore, while slow waves of children are typically larger and steeper than those of adults, they are also less widespread (Kurth et al., 2017),(Mensen et al., 2016). In addition, we found that slope and globality are positively correlated in adults but not in children, indicating a dissociation between these slow-wave properties early during development.

We hypothesize that slow-wave slope and globality may reflect the (partially) independent maturation of local and long-range connectivity, respectively. Indeed, slow-wave slope is regarded as an electrophysiological marker for neuronal synchronization speed, which is in turn thought to depend on regional synaptic strength (Riedner et al., 2007b; Vyazovskiy et al., 2007). On the other hand, slow-wave globality likely reflects the efficacy of cortico-cortical spreading, being directly related to traveled distance (Kurth et al., 2017). Thus, slow waves of children may be locally more synchronous due to a still incomplete synaptic pruning and refinement (and thus, greater synaptic strength (Kurth et al., 2010)), but they are globally less widespread, due to an immature white matter connectome. This interpretation is consistent with the previously described correlation between distance traveled by slow waves and myelin content in whole-brain/interhemispheric connections [24], and between cortical involvement and myelin content in the superior longitudinal fascicle (Kurth et al., 2017). Moreover, our results are in line with the observation of an age-dependent increase in different functional and structural connectivity measures. For example, intra and inter-hemispheric delta and theta EEG coherence (a connectivity measure that was proposed to reflect white matter connectivity and myelination) (Kurth et al., 2013), as well as approximate entropy (an information-based connectivity measure) (Lee et al., 2013), positively correlate with age. Furthermore, local resting state functional

connectivity decreases with age as longer connections are formed (Kelly et al., 2009; Lopez-Larson et al., 2011), with a progressive increase in the strength of functional connectivity and in the extent of functionally connected regions (Jolles et al., 2011).

Maturation of slow wave synchronization processes from childhood to adulthood

Previous work demonstrated in adults that the transition to sleep is characterized by at least two main phases: i) an early phase dominated by large and widespread (type I) slow waves (likely including classically defined K-complexes) that originate around somatic sensory-motor areas and peak in frontal regions, and ii) a late phase characterized by the predominance of shallow, local (type II) slow waves that show variable origin and distribution (Siclari et al., 2014). This temporal dissociation was suggested to reflect the existence of distinct synchronization processes - an efficient, subcortical-cortical process and a less efficient cortico-cortical process - that come into play at different moments of the wake-sleep transition. Importantly, though, recent work revealed that the temporal dissociation between synchronization processes I and II at sleep onset is absent in children (Spiess et al., 2018). In line with this, here we found that slow waves characterized by a high synchronization efficiency (putative type I) do not present in children the same origin and distribution as those of adults. Specifically, putative type I slow waves of children do not present a clear origin hotspot in centro-frontal electrodes typically observed in adults and have a predominantly posterior rather than anterior involvement. In other words, while larger, steeper, and more global than most slow waves, highly synchronous slow waves of children are virtually indistinguishable in terms of origin and involvement from most other (type II) slow waves.

Overall, the above observations indicate that the process underlying the synchronization of type I slow waves might be largely immature in children. This conclusion is in line with previous evidence indicating that K-complexes, after their appearance at ~6 months of age, continue their maturation during childhood and reach their 'adult shape' only during adolescence (Spiess et al., 2018). Of note, while the origin and synchronization of type I slow waves is thought to be mediated by diffuse subcortico-cortical projections from arousal-related structures (Siclari et al., 2014) , their cortical spreading may still depend on the state and integrity of cortico-cortical connections. Therefore, in children, a relative immaturity of arousal-related structures or their connections to the cortex might explain the lack of a well-defined origin hot-spot as found in adults (Lynch et al., 2020), while the incomplete maturation of frontal connectivity may determine a preferential propagation to posterior areas (Gogtay et al., 2004).

From a more general perspective, our results suggest that previous evidence indicating a centro-frontal origin for NREM slow waves (Avvenuti et al., 2020; Bernardi et al., 2019; Massimini et al., 2004; Menicucci et al., 2009; Murphy et al., 2009) was actually driven for the most part, if not exclusively, by type I waves. Indeed, type I slow waves appear to have a more stereotyped origin and propagation pattern relative to type II slow waves [24,25], and their 'contribution' may thus emerge upon averaging even if they represent a relatively small percentage of all slow waves.

Limitations

Some limitations of our study are worth noting. The observational and cross-sectional nature of our study does not allow us to prove causality or exclude mediating factors between age and slow wave properties, nor to show the development of EEG activity, which would require a longitudinal investigation. The lack of brain structural measurements also prevented us from investigating specific associations between EEG and brain and white matter changes.

Conclusions and future directions

Taken together, present results indicate that a detailed characterization of slow-waves properties may offer valuable information regarding morpho-functional brain adaptations across childhood and adolescence that extend and complement those derived from the simple assessment of SWA (delta power). In addition, we provide evidence supporting the existence of at least two slow-wave sub-types characterized by different levels of synchronization efficiency, and show that these waves undergo partially distinct maturational changes. In light of previous observations indicating that the generation of such slow-wave subtypes may depend respectively on subcortico-cortical and cortico-cortical synchronization mechanisms, our present results suggest that their separate assessment could offer a valuable readout regarding the maturation of distinct anatomo-functional brain networks.

Overall, the present data support the view that sleep constitutes a unique window for observing and tracking brain physiological adaptations and their disruption and contribute

to the efforts aimed at providing an accurate yardstick to assess pathological development in clinical populations.

Acknowledgements

The authors are grateful to Giacomo Handjaras for his help in the definition of data analysis methodologies.

Funding sources

This study was in part supported by the ABREOC (Advisory Board of Scientific Research of the Ente Ospedaliero Cantonale, protocol EOC.NSI.14.12), and in part by the NCCAM (National Center for Complementary and Alternative Medicine, protocol P01AT004952. The funders had no involvement in study design, in the collection, analysis, and interpretation of data or in writing of the report and the decision to submit the article for publication.

Disclosure Statement

Declarations of interest: none

Author contributions

AC: Conceptualization; Data curation; Formal analysis; Investigation; Methodology; Writing - original draft; Software; Validation; Visualization; Project administration. AL: Data curation; Writing - review & editing. BR: Writing - review & editing; Methodology. GA: Writing - review & editing; Methodology. SGJ: Writing - review & editing. SM: Writing - review & editing; Funding acquisition. GT: MM: Writing - review & editing; Funding acquisition. MM: Writing - review & editing; Resources. GB: Conceptualization; Methodology; Writing - review & editing; Software; Supervision.

References

Avvenuti, G., Handjaras, G., Betta, M., Cataldi, J., Imperatori, L.S., Lattanzi, S., Riedner, B.A., Pietrini, P., Ricciardi, E., Tononi, G., Siclari, F., Polonara, G., Fabri, M., Silvestrini, M., Bellesi, M., Bernardi, G., 2020. Integrity of Corpus Callosum Is Essential for theCross-Hemispheric Propagation of Sleep Slow Waves:A High-Density EEG Study in Split-Brain Patients. J Neurosci 40, 5589–5603. https://doi.org/10.1523/JNEUROSCI.2571-19.2020

Bernardi, G., Avvenuti, G., Cataldi, J., Lattanzi, S., Ricciardi, E., Polonara, G., Silvestrini, M., Siclari, F., Fabri, M., Bellesi, M., 2021. Role of corpus callosum in sleep spindle synchronization and coupling with slow waves. Brain Commun 3, fcab108. https://doi.org/10.1093/braincomms/fcab108

Bernardi, G., Betta, M., Cataldi, J., Leo, A., Haba-Rubio, J., Heinzer, R., Cirelli, C., Tononi, G., Pietrini, P., Ricciardi, E., Siclari, F., 2019. Visual imagery and visual perception induce similar changes in occipital slow waves of sleep. J Neurophysiol 121, 2140–2152. https://doi.org/10.1152/JN.00085.2019

Bernardi, G., Siclari, F., Handjaras, G., Riedner, B.A., Tononi, G., 2018. Local and Widespread Slow Waves in Stable NREM Sleep: Evidence for Distinct Regulation Mechanisms. Front Hum Neurosci 12. https://doi.org/10.3389/FNHUM.2018.00248

Berry RB, Brooks R, Gamaldo CE, Harding SM, Lloyd RM, Marcus CL, V.B., 2020. The AASM Manual for the Scoring of Sleep and Associated Events: Rules, Terminology and Technical Specifications, 2.6 versio. ed.

Buchmann, A., Kurth, S., Ringli, M., Geiger, A., Jenni, O.G., Huber, R., 2011. Anatomical markers of sleep slow wave activity derived from structural magnetic resonance images. J Sleep Res 20, 506–513. https://doi.org/10.1111/J.1365-2869.2011.00916.X

Campbell, I.G., Feinberg, I., 2009. Longitudinal trajectories of non-rapid eye movement delta and theta EEG as indicators of adolescent brain maturation. Proc Natl Acad Sci U S A 106, 5177–5180. https://doi.org/10.1073/PNAS.0812947106

Castelnovo, A., Lividini, A., Bernardi, G., Pezzoli, V., Foderaro, G., Ramelli, G.P., Manconi, M., Miano, S., 2022. Sleep Power Topography in Children with Attention Deficit Hyperactivity Disorder (ADHD). Children (Basel) 9. https://doi.org/10.3390/CHILDREN9020197

Castelnovo, A., Riedner, B.A., Smith, R.F., Tononi, G., Boly, M., Benca, R.M., 2016. Scalp and Source Power Topography in Sleepwalking and Sleep Terrors: A High-Density EEG Study. Sleep 39, 1815–1825. https://doi.org/10.5665/sleep.6162

Castelnovo, A., Zago, M., Casetta, C., Zangani, C., Donati, F., Canevini, M., Riedner, B.A., Tononi, G., Ferrarelli, F., Sarasso, S., D'Agostino, A., 2020. Slow wave oscillations in Schizophrenia First-Degree Relatives: A confirmatory analysis and feasibility study on slow wave traveling. Schizophr Res 221, 37–43. https://doi.org/10.1016/J.SCHRES.2020.03.025

Cohen, J., n.d. Statistical Power Analysis for the Behavioral Sciences Second Edition.

D'Agostino, A., Castelnovo, A., Cavallotti, S., Casetta, C., Marcatili, M., Gambini, O., Canevini, M., Tononi, G., Riedner, B., Ferrarelli, F., Sarasso, S., 2018. Sleep endophenotypes of schizophrenia: slow waves and sleep spindles in unaffected first-degree relatives. NPJ Schizophr 4, 2. https://doi.org/10.1038/s41537-018-0045-9

Danielsen, V.M., Vidal-Piñeiro, D., Mowinckel, A.M., Sederevicius, D., Fjell, A.M., Walhovd, K.B., Westerhausen, R., 2020. Lifespan trajectories of relative corpus callosum thickness: Regional differences and cognitive relevance. Cortex 130, 127–141. https://doi.org/10.1016/J.CORTEX.2020.05.020

Delorme, A., Makeig, S., 2004. EEGLAB: An open source toolbox for analysis of single-trial EEG dynamics including independent component analysis. J Neurosci Methods 134, 9–21. https://doi.org/10.1016/j.jneumeth.2003.10.009

Dentico, D., Ferrarelli, F., Riedner, B.A., Smith, R., Zennig, C., Lutz, A., Tononi, G., Davidson, R.J., 2016. Short Meditation Trainings Enhance Non-REM Sleep Low-Frequency Oscillations. PLoS One 11. https://doi.org/10.1371/JOURNAL.PONE.0148961

Esser, S.K., Hill, S.L., Tononi, G., 2007. Sleep homeostasis and cortical synchronization: I. Modeling the effects of synaptic strength on sleep slow waves. Sleep 30, 1617–1630. https://doi.org/10.1093/SLEEP/30.12.1617

Ferrarelli, F., Smith, R., Dentico, D., Riedner, B.A., Zennig, C., Benca, R.M., Lutz, A., Davidson, R.J., Tononi, G., 2013. Experienced mindfulness meditators exhibit higher parietal-occipital EEG gamma activity during NREM sleep. PLoS One 8. https://doi.org/10.1371/JOURNAL.PONE.0073417

Giedd, J.N., Blumenthal, J., Jeffries, N.O., Rajapakse, J.C., Vaituzis, A.C., Liu, H., Berry, Y.C., Tobin, M., Nelson, J., Castellanos, F.X., 1999. Development of the human corpus callosum during childhood and adolescence: a longitudinal MRI study. Prog Neuropsychopharmacol Biol Psychiatry 23, 571–588. https://doi.org/10.1016/S0278-5846(99)00017-2

Gogtay, N., Giedd, J.N., Lusk, L., Hayashi, K.M., Greenstein, D., Vaituzis, A.C., Nugent, T.F., Herman, D.H., Clasen, L.S., Toga, A.W., Rapoport, J.L., Thompson, P.M., 2004. Dynamic mapping of human cortical development during childhood through early adulthood. Proc Natl Acad Sci U S A 101, 8174–8179. https://doi.org/10.1073/PNAS.0402680101

Gorgoni, M., D'Atri, A., Scarpelli, S., Reda, F., de Gennaro, L., 2020. Sleep electroencephalography and brain maturation: developmental trajectories and the relation with cognitive functioning. Sleep Med 66, 33–50. https://doi.org/10.1016/J.SLEEP.2019.06.025

Haxby, J. v., Guntupalli, J.S., Connolly, A.C., Halchenko, Y.O., Conroy, B.R., Gobbini, M.I., Hanke, M., Ramadge, P.J., 2011. A common, high-dimensional model of the representational space in human ventral temporal cortex. Neuron 72, 404–416. https://doi.org/10.1016/J.NEURON.2011.08.026

Jenni, O.G., Carskadon, M.A., 2004. Spectral analysis of the sleep electroencephalogram during adolescence. Sleep 27, 774–783. https://doi.org/10.1093/sleep/27.4.774

Jolles, D.D., van Buchem, M.A., Crone, E.A., Rombouts, S.A.R.B., 2011. A comprehensive study of whole-brain functional connectivity in children and young adults. Cereb Cortex 21, 385–391. https://doi.org/10.1093/CERCOR/BHQ104

Kelly, A.M.C., di Martino, A., Uddin, L.Q., Shehzad, Z., Gee, D.G., Reiss, P.T., Margulies, D.S., Castellanos, F.X., Milham, M.P., 2009. Development of anterior cingulate functional connectivity from late childhood to early adulthood. Cereb Cortex 19, 640–657. https://doi.org/10.1093/CERCOR/BHN117

Keshavan, M.S., Diwadkar, V.A., DeBellis, M., Dick, E., Kotwal, R., Rosenberg, D.R., Sweeney, J.A., Minshew, N., Pettegrew, J.W., 2002. Development of the corpus callosum in childhood, adolescence and early adulthood. Life Sci 70, 1909–1922. https://doi.org/10.1016/S0024-3205(02)01492-3

Kurth, S., Achermann, P., Rusterholz, T., Lebourgeois, M.K., 2013. Development of Brain EEG Connectivity across Early Childhood: Does Sleep Play a Role? Brain Sci 3, 1445–1460. https://doi.org/10.3390/BRAINSCI3041445

Kurth, S., Riedner, B.A., Dean, D.C., O'Muircheartaigh, J., Huber, R., Jenni, O.G., Deoni, S.C.L., LeBourgeois, M.K., 2017. Traveling Slow Oscillations During Sleep: A Marker of Brain Connectivity in Childhood. Sleep 40. https://doi.org/10.1093/SLEEP/ZSX121

Kurth, S., Ringli, M., Geiger, A., Lebourgeois, M., Jenni, O.G., Huber, R., 2010. High-Density Sleep Electroencephalogram Study. Journal of Neuroscience 30, 13211–13219. https://doi.org/10.1523/JNEUROSCI.2532-10.2010.Mapping

Kurth, S., Ringli, M., LeBourgeois, M.K., Geiger, A., Buchmann, A., Jenni, O.G., Huber, R., 2012. Mapping the electrophysiological marker of sleep depth reveals skill maturation in children and adolescents. Neuroimage 63, 959–965. https://doi.org/10.1016/J.NEUROIMAGE.2012.03.053

Lee, G.M.H., Fattinger, S., Mouthon, A.L., Noirhomme, Q., Huber, R., 2013. Electroencephalogram approximate entropy influenced by both age and sleep. Front Neuroinform 7. https://doi.org/10.3389/FNINF.2013.00033

Lopez-Larson, M.P., Anderson, J.S., Ferguson, M.A., Yurgelun-Todd, D., 2011. Local brain connectivity and associations with gender and age. Dev Cogn Neurosci 1, 187–197. https://doi.org/10.1016/J.DCN.2010.10.001

Luders, E., Cherbuin, N., Thompson, P.M., Gutman, B., Anstey, K.J., Sachdev, P., Toga, A.W., 2010a. When more is less: Associations between corpus callosum size and handedness lateralization. Neuroimage 52, 43–49. https://doi.org/10.1016/J.NEUROIMAGE.2010.04.016

Luders, E., Thompson, P.M., Toga, A.W., 2010b. The development of the corpus callosum in the healthy human brain. J Neurosci 30, 10985–10990. https://doi.org/10.1523/JNEUROSCI.5122-09.2010

Lynch, K.M., Cabeen, R.P., Toga, A.W., Clark, K.A., 2020. Magnitude and timing of major white matter tract maturation from infancy through adolescence with NODDI. Neuroimage 212, 116672. https://doi.org/10.1016/J.NEUROIMAGE.2020.116672

Mascetti, G.G., 2016. Unihemispheric sleep and asymmetrical sleep: behavioral, neurophysiological, and functional perspectives. Nat Sci Sleep 8, 221. https://doi.org/10.2147/NSS.S71970

Massimini, M., Huber, R., Ferrarelli, F., Hill, S., Tononi, G., 2004. The sleep slow oscillation as a traveling wave. J Neurosci 24, 6862–6870. https://doi.org/10.1523/JNEUROSCI.1318-04.2004

Maureen, C., 2010. An empirical evaluation of free BEM solvers for accurate M/EEG forward modeling. Front Neurosci. https://doi.org/10.3389/conf.fnins.2010.06.00065

Menicucci, D., Piarulli, A., Debarnot, U., d'Ascanio, P., Landi, A., Gemignani, A., 2009. Functional structure of spontaneous sleep slow oscillation activity in humans. PLoS One 4. https://doi.org/10.1371/JOURNAL.PONE.0007601

Mensen, A., Riedner, B., Tononi, G., 2016. Optimizing detection and analysis of slow waves in sleep EEG. J Neurosci Methods 274, 1–12. https://doi.org/10.1016/J.JNEUMETH.2016.09.006

Miano, S., Amato, N., Foderaro, G., Pezzoli, V., Ramelli, G.P., Toffolet, L., Manconi, M., 2019. Sleep phenotypes in attention deficit hyperactivity disorder. Sleep Med 60, 123–131. https://doi.org/10.1016/j.sleep.2018.08.026

Murphy, M., Riedner, B.A., Huber, R., Massimini, M., Ferrarelli, F., Tononi, G., 2009. Source modeling sleep slow waves. Proc Natl Acad Sci U S A 106, 1608–1613. https://doi.org/10.1073/pnas.0807933106

Nichols, T.E., Holmes, A.P., 2002. Nonparametric permutation tests for functional neuroimaging: a primer with examples. Hum Brain Mapp 15, 1–25. https://doi.org/10.1002/HBM.1058

Pascual-Marqui, R.D., 2002. Standardized low-resolution brain electromagnetic tomography (sLORETA): Technical details, in: Methods and Findings in Experimental and Clinical Pharmacology.

Paus, T., 2005. Mapping brain maturation and cognitive development during adolescence. Trends Cogn Sci 9, 60–68. https://doi.org/10.1016/J.TICS.2004.12.008

Paus, T., Keshavan, M., Giedd, J.N., 2008. Why do many psychiatric disorders emerge during adolescence? Nat Rev Neurosci 9, 947–957. https://doi.org/10.1038/NRN2513

Piekarski, D.J., Johnson, C.M., Boivin, J.R., Thomas, A.W., Lin, W.C., Delevich, K., Galarce, E.M., Wilbrecht, L., 2017. Does puberty mark a transition in sensitive periods for plasticity in the associative neocortex? Brain Res 1654, 123. https://doi.org/10.1016/J.BRAINRES.2016.08.042

Rajapakse, J.C., Giedd, J.N., Rumsey, J.M., Vaituzis, A.C., Hamburger, S.D., Rapoport, J.L., 1996. Regional MRI measurements of the corpus callosum: A methodological and developmental study. Brain Dev 18, 379–388. https://doi.org/10.1016/0387-7604(96)00034-4

Ricci, A., He, F., Fang, J., Calhoun, S.L., Vgontzas, A.N., Liao, D., Younes, M., Bixler, E.O., Fernandez-Mendoza, J., 2021. Maturational trajectories of non-rapid eye movement slow wave activity and odds ratio product in a population-based sample of youth. Sleep Med 83, 271–279. https://doi.org/10.1016/J.SLEEP.2021.05.002

Richards, J.E., Sanchez, C., Phillips-Meek, M., Xie, W., 2016. A database of age-appropriate average MRI templates. Neuroimage. https://doi.org/10.1016/j.neuroimage.2015.04.055

Riedner, B.A., Vyazovskiy, V. v., Huber, R., Massimini, M., Esser, S., Murphy, M., Tononi, G., 2007a. Sleep homeostasis and cortical synchronization: III. A high-density EEG study of sleep slow waves in humans. Sleep 30, 1643–1657. https://doi.org/10.1093/sleep/30.12.1643

Riedner, B.A., Vyazovskiy, V. v., Huber, R., Massimini, M., Esser, S., Murphy, M., Tononi, G., 2007b. Sleep homeostasis and cortical synchronization: III. A high-density EEG study of sleep slow waves in humans. Sleep 30, 1643–1657. https://doi.org/10.1093/SLEEP/30.12.1643

Ringli, M., Huber, R., 2011. Developmental aspects of sleep slow waves: linking sleep, brain maturation and behavior. Prog Brain Res 193, 63–82. https://doi.org/10.1016/B978-0-444-53839-0.00005-3

Schoch, S.F., Riedner, B.A., Deoni, S.C., Huber, R., Lebourgeois, M.K., Kurth, S., 2018. Across-night dynamics in traveling sleep slow waves throughout childhood. Sleep 41. https://doi.org/10.1093/sleep/zsy165

Shaw, P., Kabani, N.J., Lerch, J.P., Eckstrand, K., Lenroot, R., Gogtay, N., Greenstein, D., Clasen, L., Evans, A., Rapoport, J.L., Giedd, J.N., Wise, S.P., 2008. Neurodevelopmental trajectories of the human cerebral cortex. J Neurosci 28, 3586–3594. https://doi.org/10.1523/JNEUROSCI.5309-07.2008

Siclari, F., Bernardi, G., Riedner, B.A., LaRocque, J.J., Benca, R.M., Tononi, G., 2014. Two distinct synchronization processes in the transition to sleep: A high-density electroencephalographic study. Sleep 37, 1621-1637F. https://doi.org/10.5665/sleep.4070

Spiess, M., Bernardi, G., Kurth, S., Ringli, M., Wehrle, F.M., Jenni, O.G., Huber, R., Siclari, F., 2018. How do children fall asleep? A high-density EEG study of slow waves in the transition from wake to sleep. Neuroimage 178, 23–35. https://doi.org/10.1016/j.neuroimage.2018.05.024

Tamaki, M., Bang, J.W., Watanabe, T., Sasaki, Y., 2016. Night watch in one brain hemisphere during sleep associated with the first-night effect in humans. Curr Biol 26, 1190. https://doi.org/10.1016/J.CUB.2016.02.063

Thompson, P.M., Gledd, J.N., Woods, R.P., MacDonald, D., Evans, A.C., Toga, A.W., 2000. Growth patterns in the developing brain detected by using continuum mechanical tensor maps. Nature 2000 404:6774 404, 190–193. https://doi.org/10.1038/35004593

Timofeev, I., Schoch, S.F., LeBourgeois, M.K., Huber, R., Riedner, B.A., Kurth, S., 2020. Spatio-temporal properties of sleep slow waves and implications for development. Curr Opin Physiol 15, 172–182. https://doi.org/10.1016/J.COPHYS.2020.01.007

Tzourio-Mazoyer, N., Landeau, B., Papathanassiou, D., Crivello, F., Etard, O., Delcroix, N., Mazoyer, B., Joliot, M., 2002. Automated anatomical labeling of activations in SPM using a macroscopic anatomical parcellation of the MNI MRI single-subject brain. Neuroimage. https://doi.org/10.1006/nimg.2001.0978

Vyazovskiy, V. v., Riedner, B.A., Cirelli, C., Tononi, G., 2007. Sleep homeostasis and cortical synchronization: II. A local field potential study of sleep slow waves in the rat. Sleep 30, 1631–1642. https://doi.org/10.1093/SLEEP/30.12.1631

Westerhausen, R., Fjell, A.M., Krogsrud, S.K., Rohani, D.A., Skranes, J.S., Håberg, A.K., Walhovd, K.B., 2016. Selective increase in posterior corpus callosum thickness between the age of 4 and 11 years. Neuroimage 139, 17–25. https://doi.org/10.1016/J.NEUROIMAGE.2016.06.008

3.6. Supplementary Material

	CHILDREN GROUP n = 21	ADULT GROUP n = 18	COMPARISON p	Cohen's d
TRT (min)	506.6 ± 41.56	452.8 ± 49.56	0.001	1.7
TST (min)	435.5 ± 50.71	373.2 ± 82.56	0.007	1.3
SOL (min)	23.1 ± 14.65	26.2 ± 17.94	0.555	-0.3
REML (min)	104.4 ± 34.51	100.7 ± 70.18	0.835	0.1
WASO (min)	49.3 ± 44.02	53.4 ± 59.75	0.809	-0.1
SE (%)	86.2 ± 9.40	82.2 ± 14.76	0.315	0.5
N1 (min)	25.7 ± 10.53	26.0 ± 9.70	0.937	0.0
N1 (%)	6.0 ± 2.68	7.5 ± 4.59	0.228	-0.5
N2 (min)	160.5 ± 25.27	208.2 ± 52.47	0.001	-1.6
N2 (%)	36.9 ± 4.49	55.5 ± 7.04	0.000	-4.5
N3 (min)	148.9 ± 19.62	64.3 ± 21.61	0.000	5.8
N3 (%)	34.4 ± 4.12	18.1 ± 7.93	0.000	3.6
REM (min)	100.3 ± 28.50	74.8 ± 32.55	0.013	1.2
REM (%)	22.7 ± 4.84	18.9 ± 6.64	0.047	0.9
AI	12.8 ± 2.88	16.0 ± 6.70	0.056	-0.9

Supplementary Table 1 | Sleep architecture

TRT: total recording time. TST: total sleep time. SL: sleep onset latency. REML: REM latency. WASO: wake after sleep onset. SE: sleep efficiency. N1 (min): minutes spent in N1. N1 (%): percentage of total sleep time spent in N1; N2 (min): minutes spent in N2. N2 (%): percentage of total sleep time spent in N2. N3 (min): minutes spent in N3. N3 (%): percentage of total sleep time spent in N3. REM (min): minutes spent in REM. REM (%): percentage of total sleep time spent in REM. AI: arousal index (arousal count per hour of sleep).

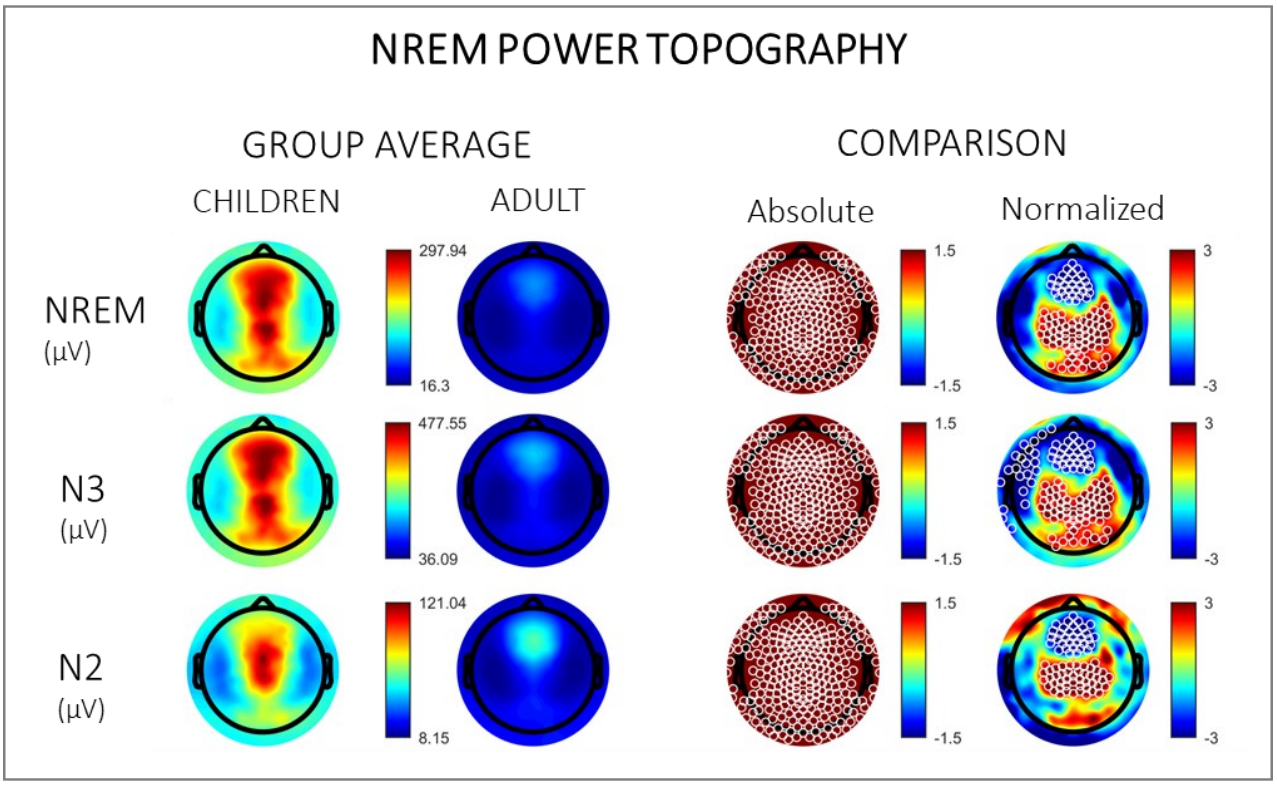

Supplementary Figure 1 | Comparison of the topographical distribution of SWA (1-4 Hz) power during NREM sleep in the children group and in the adult group.

Values are color coded and plotted on the planar projection of the hemispheric scalp model. First row: NREM sleep. Second row: N3. Third row: N2. First and second columns: average NREM sleep EEG topographies for children and adults, respectively. Higher values are shown in red, lower in blue. Third and fourth columns: single electrode t-value (two-tailed, unpaired) maps for the comparison between the two groups in terms of absolute and normalized (using the z-score across all electrodes) power. Blue: children < adult. Red: children > adult. White circles: significant electrodes ($p < 0.05$, cluster-size correction).

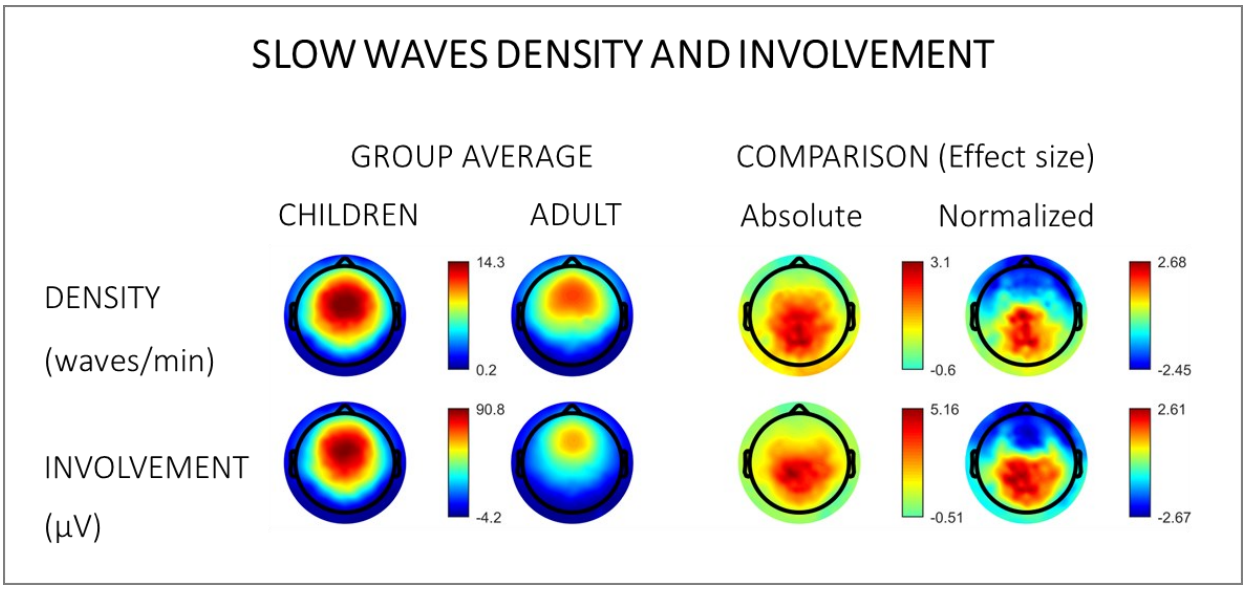

Supplementary Figure 2. Comparison of the topographical distribution of slow wave density and involvement during NREM sleep in the children group and in the adult group (effect size).

Values are color coded and plotted on the planar projection of the hemispheric scalp model. First row: density (waves/minute). Second row: slow wave involvement (µV). First and second columns: average values for the children group and the adult group. Higher values are shown in red, lower in blue. Third and fourth columns: single electrode effect size (Cohen's D) maps of the comparison between the two groups in terms of absolute and normalized (using the z-score across all electrodes) values. Blue: children < adult. Red: children > adult.

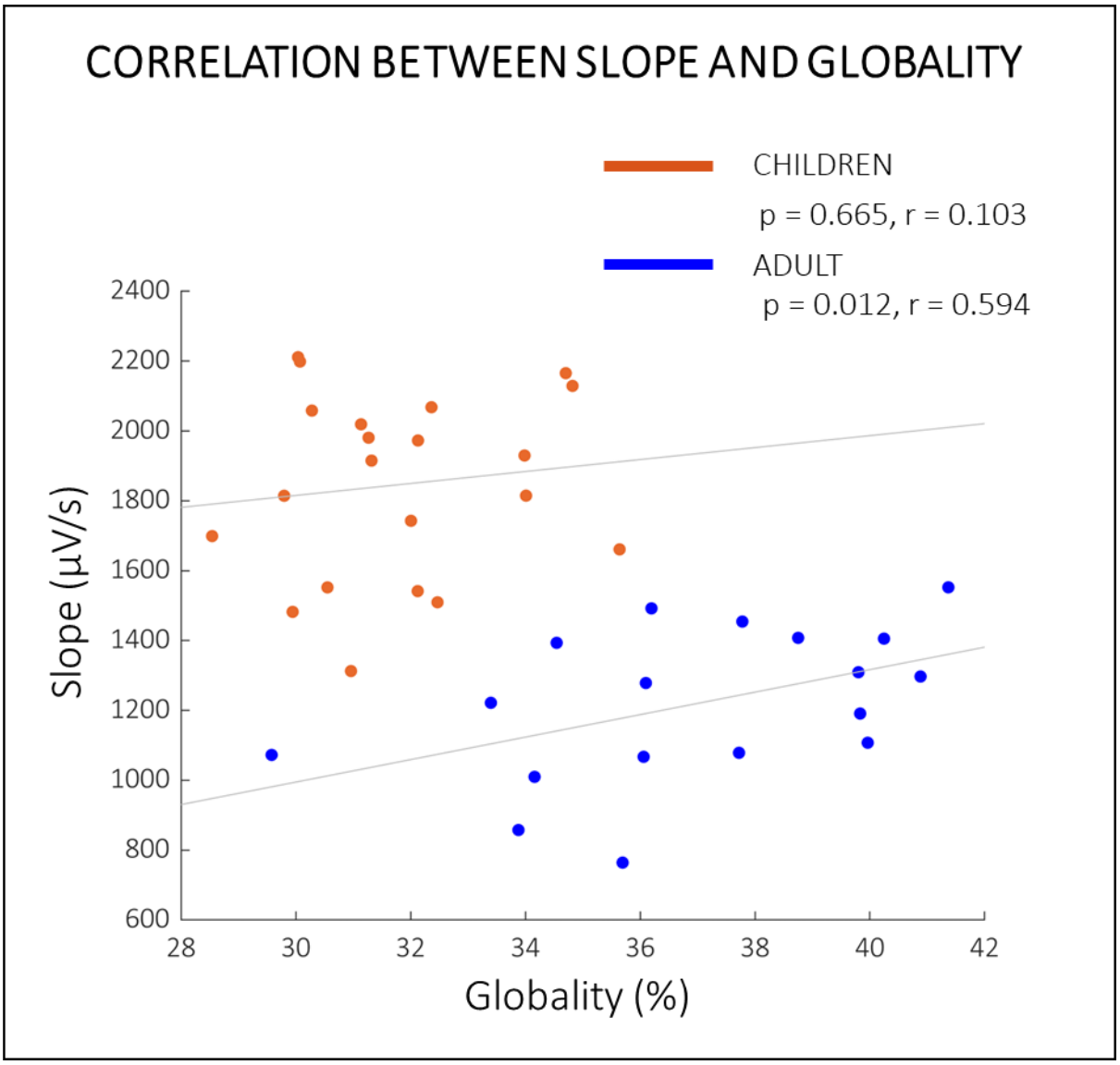

Supplementary Figure 3. Correlation between slow wave globality and slope.

Orange dots: children. Blue dots: adults. X-axis = globality (channels involved in individual slow waves divided by the total number of channels, %). Y-axis: down-slope (steepness of the line connecting between the first zero-crossing and the maximum negative peak, in mV/s). Gray Lines: least-squares regression lines for both groups.

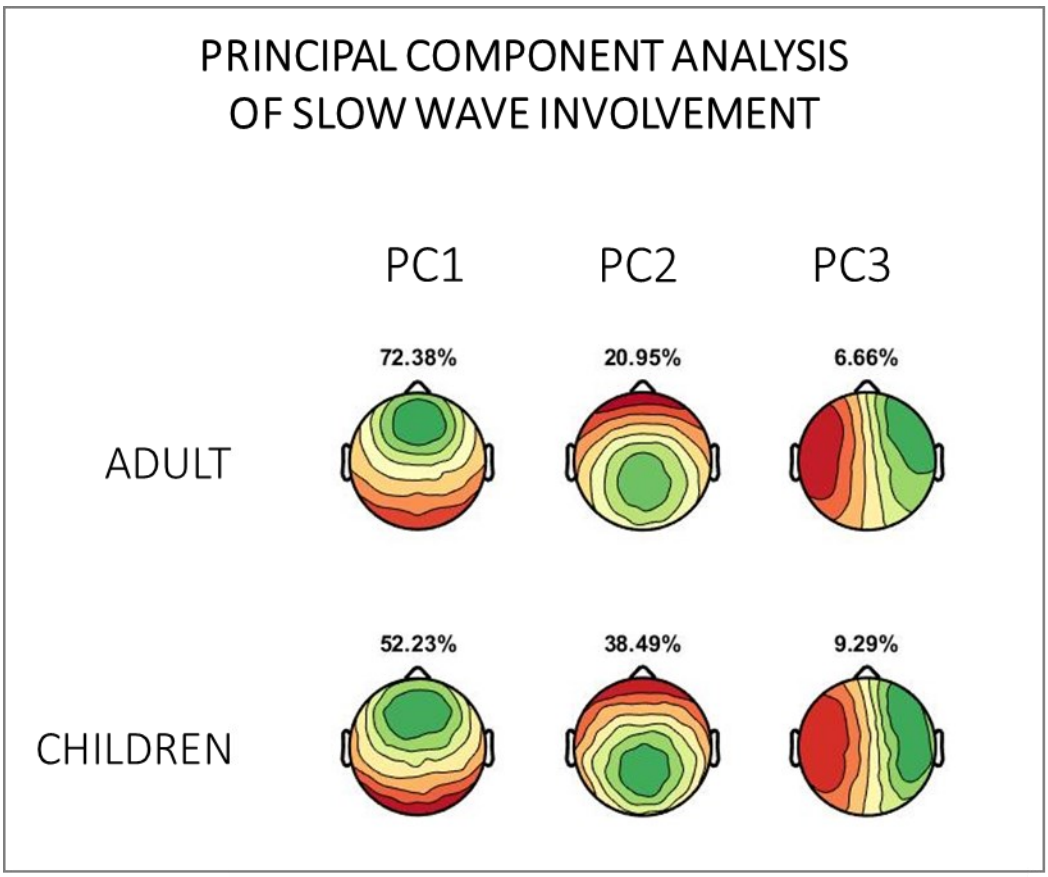

Supplementary Figure 4. Principal component analysis of slow-wave involvement.

The involvement distribution (mean EEG signal calculated across all electrodes in a 40 ms window centered on the wave peak; in microvolts) of all slow waves was entered in a PC analysis. The plot shows the average variance explained by each of the three PCs in the template subject for the adult group and for the children group (after the Procrustes transformation computed for each group separately). PC1: first component; PC2: second component; PC3: third component.

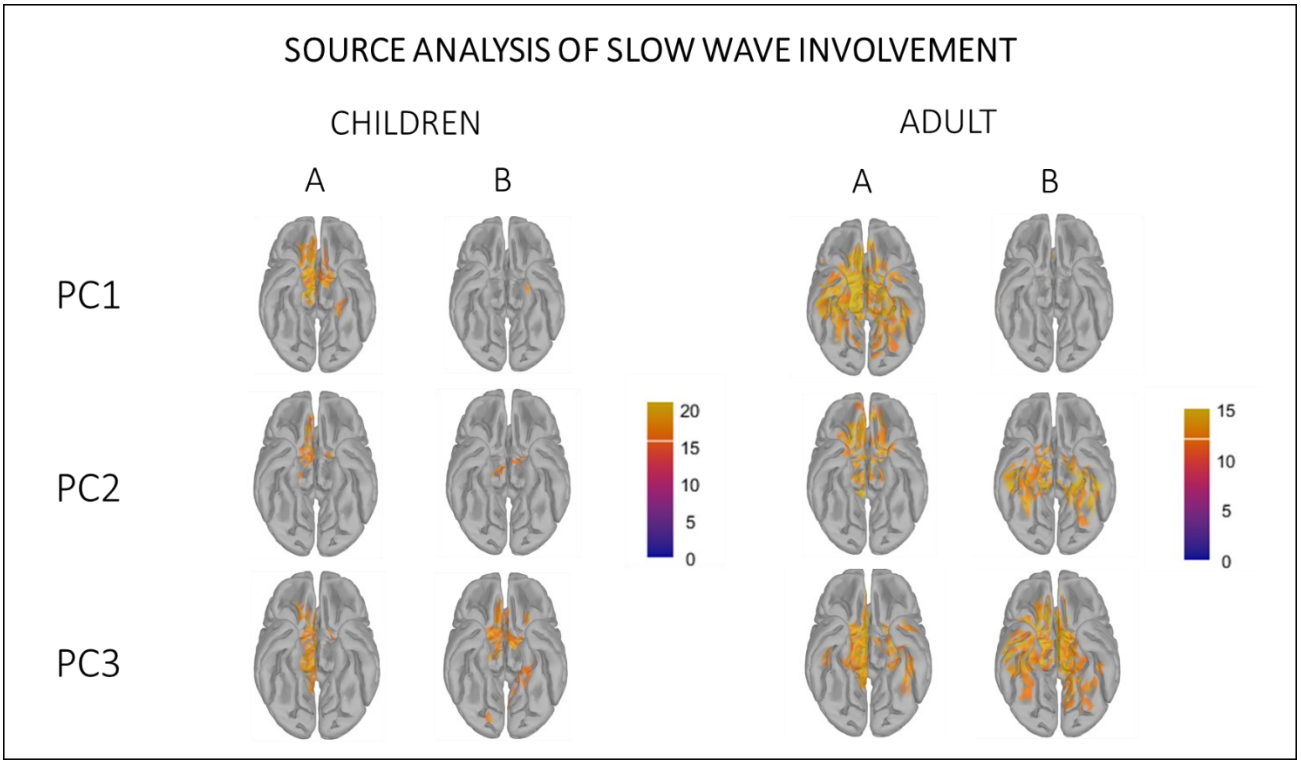

Supplementary Figure 5. Source modeling of slow waves (bottom view).

First and second columns: children. Third and Fourth columns: adults. A: positive weights. B: negative weights. First, second and third rows: horizontal plane (bottom) view of the brain cortex. The figure represents the average peak of slow wave involvement (>75th percentile) in source space obtained from 3 most representative slow waves of each PC. Yellow: areas with larger overlap between subjects (>75% of subjects).

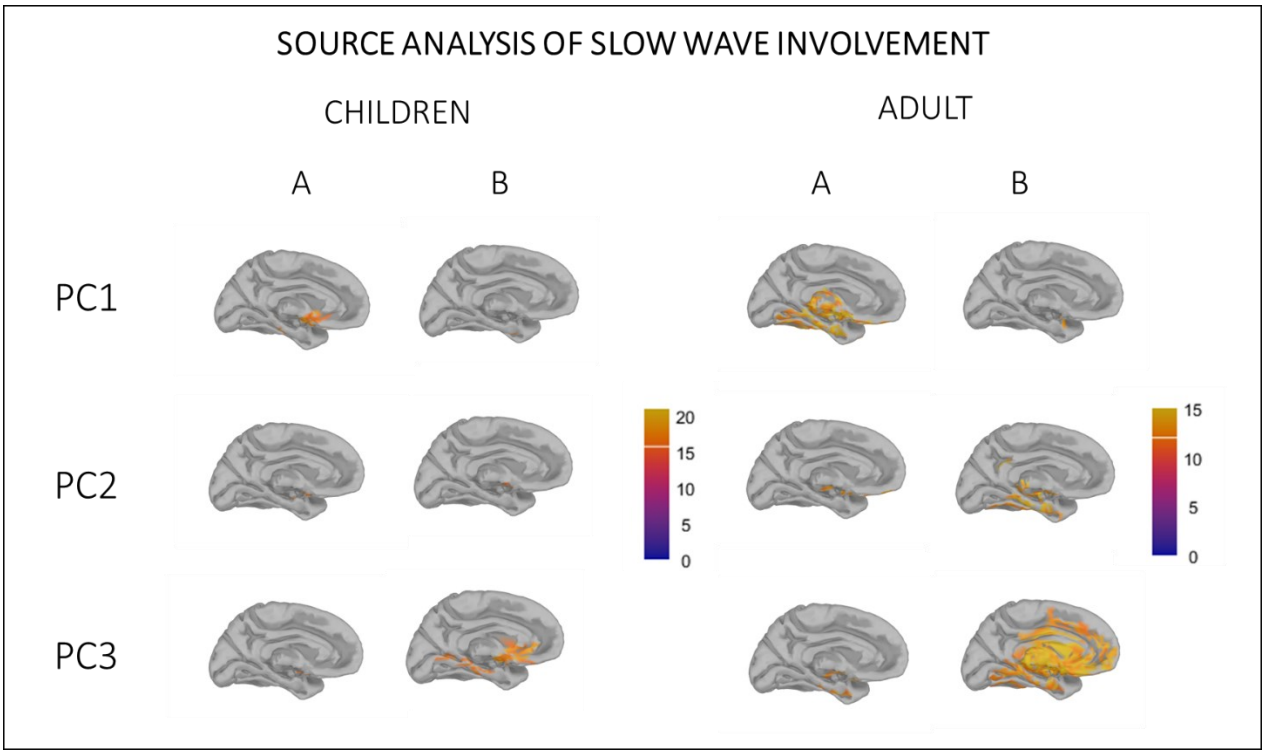

Supplementary Figure 6. Source modeling of slow waves (left medial view).

First and second columns: children. Third and Fourth columns: adults. A: positive weights. B: negative weights. First, second and third rows: sagittal plane, left hemisphere (medial) view of the brain cortex.

The figure represents the average peak of slow wave involvement (>75th percentile) in source space obtained from 3 most representative slow waves of each PC. Yellow: areas with larger overlap between subjects (>75% of subjects).

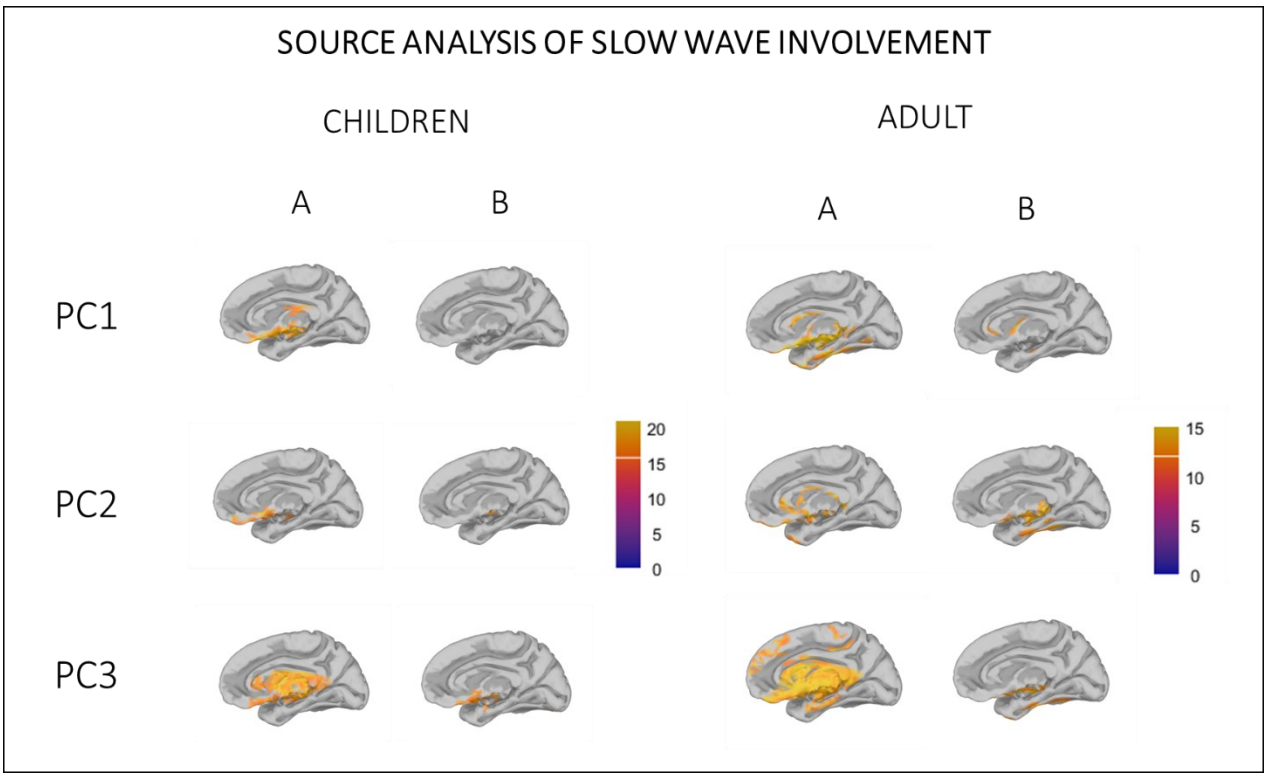

Supplementary Figure 7. Source modeling of slow waves in the children group (right medial view).

First and second columns: children. Third and Fourth columns: adults. A: positive weights. B: negative weights. First, second and third rows: sagittal plane, right hemisphere (medial) view of the brain cortex.

The figure represents the average peak of slow wave involvement (>75th percentile) in source space obtained from 3 most representative slow waves of each PC. Yellow: areas with larger overlap between subjects (>75% of subjects).

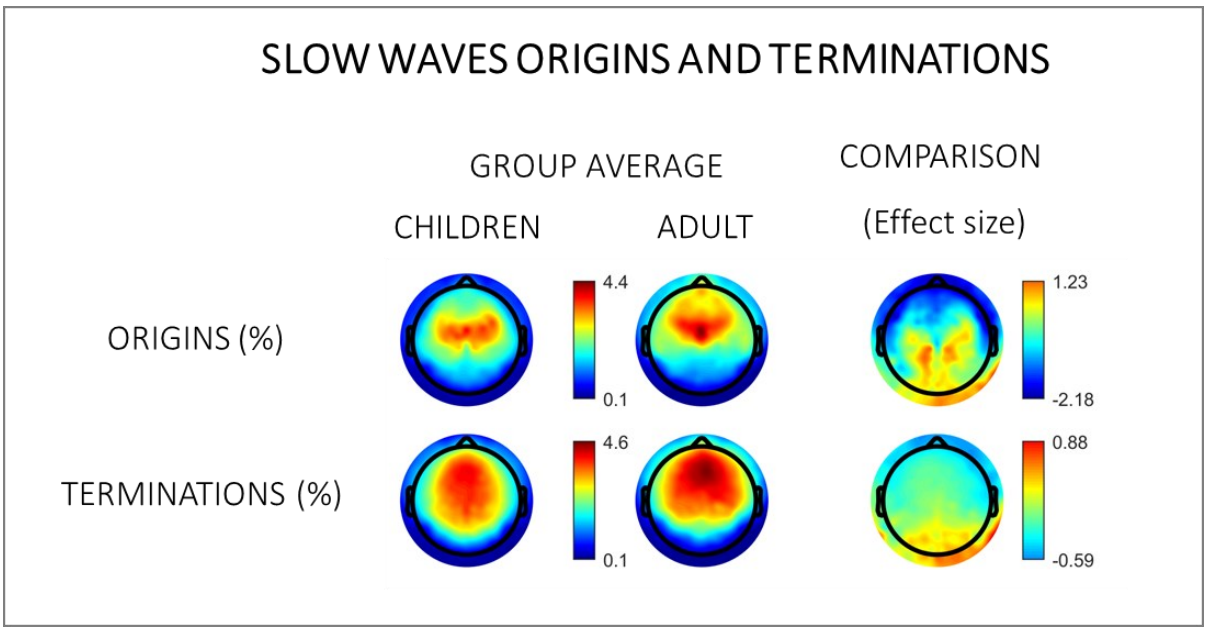

Supplementary Figure 8. Comparison of the topographical distribution of slow wave origins and terminations during NREM sleep in the children group and in the adult group (effect size).

Values are color coded and plotted on the planar projection of the hemispheric scalp model. First row: distribution of slow wave origins (channels with 0 delay, % of the total). Second row: distribution of slow wave terminations (channels with the maximum delay, % of the total). First and second columns: average values for children and adults. Higher values are shown in red, lower in blue. Third column: single electrode effect size (Cohen's D) map for the comparison between the two groups. Blue: children < adult. Red: children > adult.

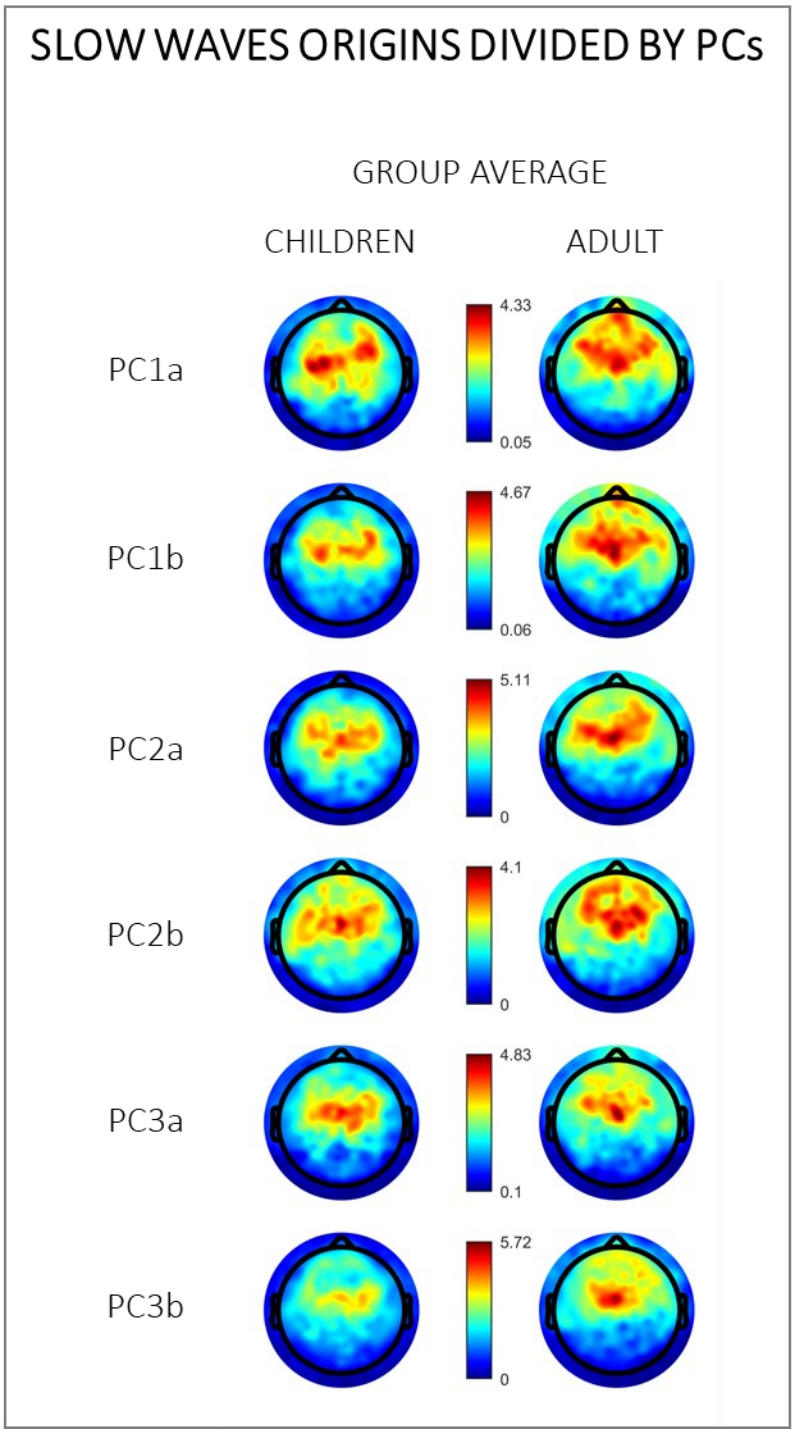

Supplementary Figure 9. Origin of slow waves with different involvement.

The plot shows the origin distribution for the 100 slow waves that weighed more for each PC of the involvement. First column: average origin topography in the children group, Second column:

average origin topography in the adult group. Rows: PC1a: first component – positive weight; PC1b: first component – negative weight; PC2a: second component – positive weight; PC2b: second component – negative weight; PC3a: third component– positive weight; PC3b: third component – negative weight.

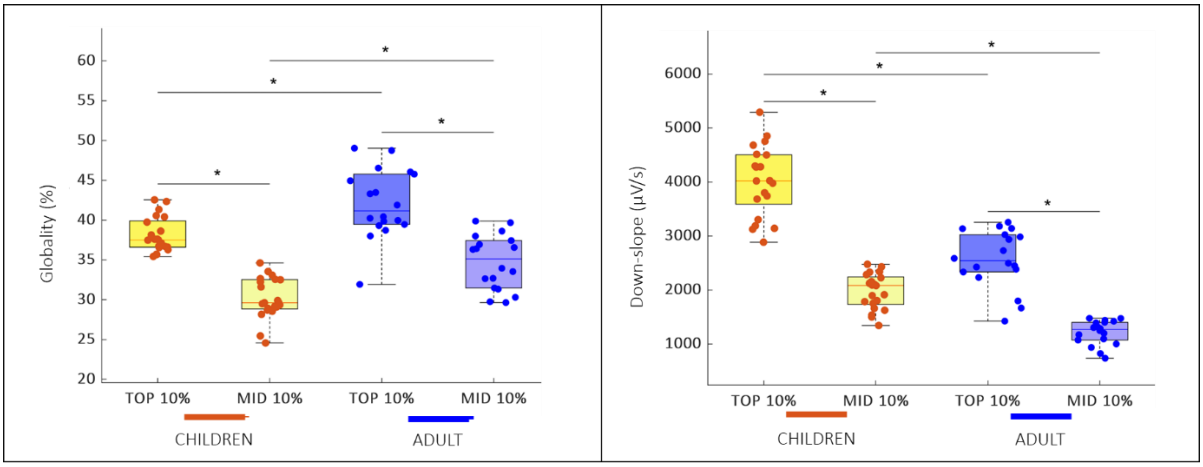

Supplementary Figure 10. Globality and slopes in top10% and mid10% slow waves.

Left panel: globality (% of channels interest by individual slow waves). Right panel: down-slopes. Orange dots: children, blue dots: adults. The bottom and top of each boxplot are the 25th and 75th percentiles of the sample, respectively. The distance between the bottom and top of each box is the interquartile range. The line in the middle of each box is the sample median. The whiskers extending above and below each box go from the end of the interquartile range to the furthest observation within the whisker length (more than 3 times the interquartile range away from the bottom or top of the box). The asterisks represent statistical significance at $p<0.05$.

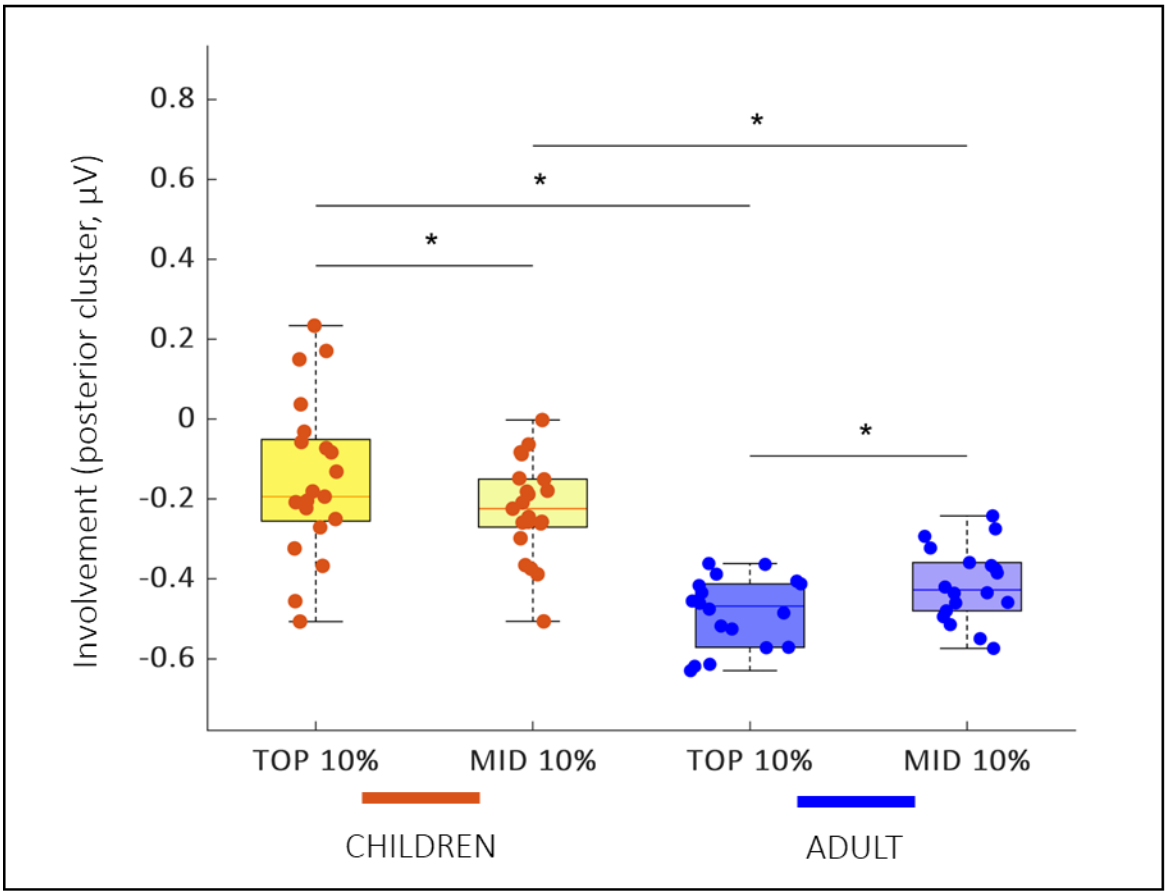

Supplementary Figure 11. Top10% and mid10% slow wave involvement: interaction effect between groups (children vs adults) and conditions (top10% and mid10% slow waves), posterior cluster.

Orange dots: children, blue dots: adults. The bottom and top10% of each boxplot are the 25th and 75th percentiles of the sample, respectively. The distance between the bottom and top of each box is the interquartile range. The line in the middle of each box is the sample median. The whiskers extending above and below each box go from the end of the interquartile range to the furthest observation within the whisker length (more than 3 times the interquartile range away from the bottom or top of the box). Observations beyond the whisker length are marked as outliers (red crosses). The asterisks represent statistical significance at p<0.05.

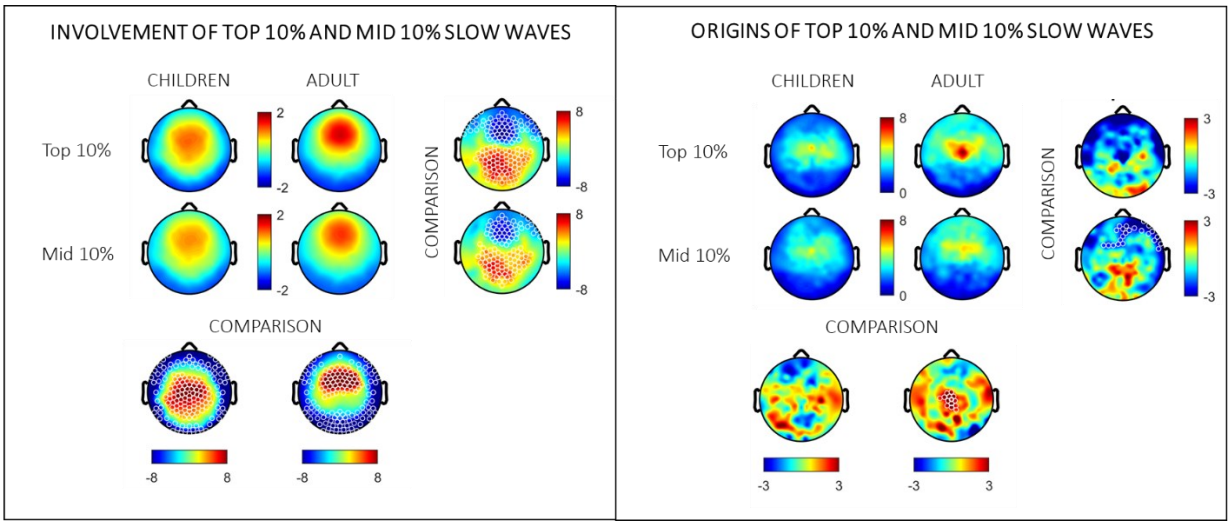

Supplementary Figure 12. Topographical analysis of involvement and origins in top10% and mid10% slow waves.

Left panel: Involvement (μV). Right panel: Origins (%). Top10%: putative Type I slow waves, i.e., slow waves with a synchronization score within the 90 and 100th percentile. Mid10%: putative Type II slow waves, i.e., slow waves with a synchronization score between the 45th and the 55th percentile. Values are color coded and plotted on the planar projection of the hemispheric scalp model. First row: average topography of top10% slow waves. Second row: average topography of mid10% slow waves. Third row: single electrode t-value (two-tailed, paired) maps for the comparison between top10% and mid10% slow waves. Blue: top10% < mid10%. Red: top10% > mid10%. First and second columns: average topographies for the children and adults, respectively. Higher values are shown in red, lower in blue. Third column: single electrode t-value (two-tailed, unpaired) maps comparison between children and adults. Blue, children < adult. Red: children > adult. White circles: p < 0.05, cluster-size correction.

3.7. References

Buchmann, A., Kurth, S., Ringli, M., Geiger, A., Jenni, O.G., Huber, R., 2011. Anatomical markers of sleep slow wave activity derived from structural magnetic resonance images. J Sleep Res 20, 506–513. https://doi.org/10.1111/J.1365-2869.2011.00916.X

Campbell, I.G., Feinberg, I., 2009. Longitudinal trajectories of non-rapid eye movement delta and theta EEG as indicators of adolescent brain maturation. Proc Natl Acad Sci U S A 106, 5177–5180. https://doi.org/10.1073/PNAS.0812947106

Campbell, I.G., Grimm, K.J., de Bie, E., Feinberg, I., 2012. Sex, puberty, and the timing of sleep EEG measured adolescent brain maturation. Proc Natl Acad Sci U S A 109, 5740–5743. https://doi.org/10.1073/PNAS.1120860109

Galván, A., 2017. Adolescence, brain maturation and mental health. Nature Neuroscience 2017 20:4 20, 503–504. https://doi.org/10.1038/nn.4530

Gradisar, M., Gardner, G., Dohnt, H., 2011. Recent worldwide sleep patterns and problems during adolescence: A review and meta-analysis of age, region, and sleep. Sleep Med 12, 110–118. https://doi.org/10.1016/J.SLEEP.2010.11.008

Jaramillo, V., Volk, C., Maric, A., Furrer, M., Fattinger, S., Kurth, S., Lustenberger, C., Huber, R., 2020. Characterization of overnight slow-wave slope changes across development in an age-, amplitude-, and region-dependent manner. Sleep 43, 1–10. https://doi.org/10.1093/SLEEP/ZSAA038

Kaufmann, T., Alnæs, D., Doan, N.T., Brandt, C.L., Andreassen, O.A., Westlye, L.T., 2017. Delayed stabilization and individualization in connectome development are related to psychiatric disorders. Nature Neuroscience 2017 20:4 20, 513–515. https://doi.org/10.1038/nn.4511

Kurth, S., Jenni, O.G., Riedner, B.A., Tononi, G., Carskadon, M.A., Huber, R., 2010a. Characteristics of sleep slow waves in children and adolescents. Sleep 33, 475–480. https://doi.org/10.1093/sleep/33.4.475

Kurth, S., Riedner, B.A., Dean, D.C., O'Muircheartaigh, J., Huber, R., Jenni, O.G., Deoni, S.C.L., LeBourgeois, M.K., 2017. Traveling Slow Oscillations During Sleep: A Marker of Brain Connectivity in Childhood. Sleep 40. https://doi.org/10.1093/SLEEP/ZSX121

Kurth, S., Ringli, M., Geiger, A., Lebourgeois, M., Jenni, O.G., Huber, R., 2010b. High-Density Sleep Electroencephalogram Study. Journal of Neuroscience 30, 13211–13219. https://doi.org/10.1523/JNEUROSCI.2532-10.2010.Mapping

Maret, S., Faraguna, U., Nelson, A.B., Cirelli, C., Tononi, G., 2011. Sleep and wake modulate spine turnover in the adolescent mouse cortex. Nat Neurosci 14, 1418. https://doi.org/10.1038/NN.2934

Paus, T., 2005. Mapping brain maturation and cognitive development during adolescence. Trends Cogn Sci 9, 60–68. https://doi.org/10.1016/J.TICS.2004.12.008

Piekarski, D.J., Johnson, C.M., Boivin, J.R., Thomas, A.W., Lin, W.C., Delevich, K., Galarce, E.M., Wilbrecht, L., 2017. Does puberty mark a transition in sensitive periods for plasticity in the associative neocortex? Brain Res 1654, 123. https://doi.org/10.1016/J.BRAINRES.2016.08.042

Schoch, S.F., Riedner, B.A., Deoni, S.C., Huber, R., Lebourgeois, M.K., Kurth, S., 2018. Across-night dynamics in traveling sleep slow waves throughout childhood. Sleep 41. https://doi.org/10.1093/sleep/zsy165

Shaw, P., Kabani, N.J., Lerch, J.P., Eckstrand, K., Lenroot, R., Gogtay, N., Greenstein, D., Clasen, L., Evans, A., Rapoport, J.L., Giedd, J.N., Wise, S.P., 2008. Neurodevelopmental trajectories of the human cerebral cortex. J Neurosci 28, 3586–3594. https://doi.org/10.1523/JNEUROSCI.5309-07.2008

Spiess, M., Bernardi, G., Kurth, S., Ringli, M., Wehrle, F.M., Jenni, O.G., Huber, R., Siclari, F., 2018. How do children fall asleep? A high-density EEG study of slow waves in the transition from wake to sleep. Neuroimage 178, 23–35. https://doi.org/10.1016/j.neuroimage.2018.05.024

Taki, Y., Hashizume, H., Thyreau, B., Sassa, Y., Takeuchi, H., Wu, K., Kotozaki, Y., Nouchi, R., Asano, M., Asano, K., Fukuda, H., Kawashima, R., 2012. Sleep duration during weekdays affects hippocampal gray matter volume in healthy children. Neuroimage 60, 471–475. https://doi.org/10.1016/J.NEUROIMAGE.2011.11.072

Tarokh, L., Carskadon, M.A., 2010. Developmental changes in the human sleep EEG during early adolescence. Sleep 33, 801–809. https://doi.org/10.1093/SLEEP/33.6.801

Tarokh, L., Saletin, J.M., Carskadon, M.A., 2016. Sleep in adolescence: physiology, cognition and mental health HHS Public Access. Neurosci Biobehav Rev 70, 182–188. https://doi.org/10.1016/j.neubiorev.2016.08.008

Tarokh, L., van Reen, E., LeBourgeois, M., Seifer, R., Carskadon, M.A., 2011. Sleep EEG provides evidence that cortical changes persist into late adolescence. Sleep 34, 1385–1393. https://doi.org/10.5665/SLEEP.1284

Telzer, E.H., Goldenberg, D., Fuligni, A.J., Lieberman, M.D., Gálvan, A., 2015. Sleep variability in adolescence is associated with altered brain development. Dev Cogn Neurosci 14, 16. https://doi.org/10.1016/J.DCN.2015.05.007

Timofeev, I., Schoch, S.F., LeBourgeois, M.K., Huber, R., Riedner, B.A., Kurth, S., 2020. Spatio-temporal properties of sleep slow waves and implications for development. Curr Opin Physiol 15, 172–182. https://doi.org/10.1016/J.COPHYS.2020.01.007

4. PROJECT 3

4.1. Preface

In this project, I will present a hdEEG study conducted on a group of ADHD children/adolescents and healthy control subjects.

This paper represents the first and the simplest application of the hdEEG pipeline previously described in project 1. Indeed, I herein performed, as a first step, a sleep power analysis at the scalp level. I believe this type of analysis already conveys relevant information, and powerfully illustrates how the existing and consolidated background on sleep EEG during development can inform research in child psychiatry. Furthermore, this analysis provided meaningful hypothesis to be tested in future research.

4.2. ADHD

ADHD is the most common neurodevelopmental disorder, with an average world-wide prevalence of about 5% (Polanczyk et al., 2014). It has a strong genetic predisposition, a typical onset in childhood and a chronic evolution. ADHD is broadly characterized by a persistent pattern of inattention, hyperactivity and/or impulsivity, inconsistent with the developmental level of the affected child. This pattern must be appreciated during early childhood (before 6-12 years), and must have a clear impact on the subject's functioning in two or more life settings (American Psychiatric Association, 2013). International diagnostic criteria are listed in Table 1. Due to these symptoms, often children with ADHD

struggle with education and social requirements, and/or develop other mental illness as adolescents and young adults.

	ICD-10	**DSM-V**
Name	Hyperkinetic Disorder (F90)	ADHD
Age of onset	By definition in childhood (more specifically, before the age of 7)	By definition in childhood (more specifically, before the age of 12)
Symptoms criteria for children	Must have a combination of impaired attention AND overactivity. A minimum of 6 of 10 symptoms of hyperactivity, 5 of 9 symptoms of inattention and 1 of 3 symptom of impulsivity	6 of 9 symptoms of inattention and/or hyperactivity/impulsivity
Symptoms criteria for adolescents and adults aged ≥ 17 years		5 of 9 symptoms of inattention and/or hyperactivity/impulsivity
Setting	Inattention and restlessness that are pervasive across situations at home and in school/nursery	Several inattentive or hyperactive-impulsive symptoms are present in two or more settings
Duration	≥ 6 months	≥ 6 months
Impairment	Clinically significant distress or impairment in social, academic, or occupational functioning	Interference with social, academic, or occupational functioning; includes severity specifiers: mild, moderate, severe
Subtypes	None ("hyperkinetic conduct disorder" for those who meet criteria for both disorders)	Three ADHD clinical presentations based on symptom profile: combined, predominantly inattentive and predominantly hyperactive/impulsive presentation
Comorbidity	Diagnosis of anxiety disorders, mood affective disorders, pervasive developmental disorders (autism) and schizophrenia must be excluded	A comorbid diagnosis with autism spectrum disorders is allowed

Table 1. *Comparison between ADHD (Diagnostic and Statistical Manual of Mental Disorders, 5th edition, DSM-5) and Hyperkinetic Disorder Diagnostic Criteria (International Classification of Diseases, 10th edition, ICD10).*

Despite being one of the most studied neurodevelopmental disorders in the last decades, pathogenetic hypotheses and clinical borderlands of ADHD remain poorly defined, as research on ADHD is severely hampered by clinical heterogeneity and the lack of unifying models.

4.3. Sleep in ADHD

Among other hypothesis, the connection between sleep and ADHD has been increasingly considered for the following reasons:

1. Sleep disorders are common in children with ADHD

   In clinical practice, sleep alterations are reported in 25–55% of children with ADHD (Hvolby, 2015; Wajszilber et al., 2018). Sleep issues may range from delayed sleep–wake disorder, higher bedtime resistance, more sleep onset difficulties, insomnia, sleep-disordered breathing (SDB), increased nocturnal motor activity, restless legs syndrome (RLS), sleep anxiety and teeth clenching (Bijlenga et al., 2019), sleep inertia and higher daytime sleepiness compared to typically developing children (Baddam, Canapari, van Noordt, et al., 2018; Cortese et al., 2009a; Lunsford-Avery et al., 2016a; Wajszilber et al., 2018).

2. ADHD symptoms resemble sleep-deprivation symptoms

Frontal lobes are particularly sensible to sleep deprivation and executive functions (attention, impulse control) are particularly compromised (Wu et al., 2006).

Moreover, sleepy children become often hyperactive. Thus, it has been hypothesized that excessive motor activity could be a strategy used by children with to stay awake and alert (Konofal et al., 2010).

3. Arousal-promoting are the most effective known-treatment for ADHD

Pharmacological first-line agents approved for ADHD treatment (Caye et al., 2019; Faraone et al., 2015; Sharma & Couture, 2014) are psychostimulants like Methylphenidate or amphetamine and lis-dexamfetamine (that act through inhibition of DA and NE reuptake). Second/third line medications are Atomoxetine, Guanfacine or Clonidine, Bupropion, Imipramine, Modafinil.

While many studies investigated sleep macro-structure with inconsistent findings (Baddam, Canapari, Noordt, et al., 2018; Cortese et al., 2009b; Díaz-Román et al., 2018; Gruber et al., 2009; Lunsford-Avery et al., 2016b), only few studies focused on sleep power in ADHD and mainly on SWA and theta (Gorgoni et al., 2020a) (see Table 2 and 3 for more details).

Author(s), Year	Age (min-max or mean±DS, y)	N° (Comorbi-dities)	Task-related	Sleep Stage	SW / Delta Power	Frequencies (Hz)	Power analysis	Results
Prehn-Kristensen et al., 2011	ADHD: 10–16; HC: 11–14	ADHD: 12; HC: 12 (ODD: 3)	Declarative Memory Task (DMT)	N2	Slow oscillations (SO) / Delta Power	SO: 0,5 - 1; Delta: 1-3	C3-A1	Positive correlations between sleep-associated memory consolidation and slow oscillation power in HC, but not

								in ADHD in the first sleep cycle
Prehn-Kristensen et al., 2013	ADHD and healthy children: 9-12; healthy adults: 20-28	ADHD: 16; healthy children: 16; healthy adults: 20	Emotional Memory Task (EMT)	SWS (N3)	Slow oscillations (SO) / Delta power	SO: 0.6–1; Delta: 1–4	F4 - (mean A1-A2)	SO/delta power negatively correlated with memory performance in children with ADHD but not in HC
Ringli et al., 201 3	ADHD: 9.7-13.4 HC: 9.6-14.2 * note: 2 ADHD treated with methylphenidate	ADHD: 9; HC: 9	No	first 60 min of N2 and N3	SWA (normalized)	1-4.5	128 channels - Cz	A local increase of SWA in a central cluster (6 electrodes) in children with ADHD compared to HC. This group difference was stable across the night.
Saletin et al., 2017,	ADHD and HC: 10–12.9	ADHD: 7; HC: 14	Motor Sequence Task (MST)	N2	SWA	1–4.6 Hz	average of C3/A2 and C4/A1	No significant differences in SWA between ADHD and HC
Cremone et al., 2017 No	ADHD and HC: 4-8	ADHD: 14; HC: 15	Go/No-go Task (2 sessions)	REM and NREM	SWA	0.5-4	F4-A1	No SWA differences between groups in NREM sleep. Higher SWA in ADHD compared to HC during REM sleep but not correlated with morning inhibitory control in HC
Furrer et al., 2019 Yes	ADHD and HC: 8-16 *note: 28 ADHD were treated with stimulants	ADHD. 50; HC: 86	No	first 60 min of N2 and N3	SWA (absolute)	1-4.5	128 channels - Cz	Lower whole brain SWA in ADHD compared to HC. The decrease was not significant in patients who were taking stimulant medication on a regular basis
Miano et al., 2019	ADHD: 10.1±2.1; HC: 10.34±1.54	ADHD: 30; HC: 25	No	first and last 60 min of N2 and N3	SWA (normalized)	1-4	256 channels- Cz	Higher SWA over fronto–central channels in ADHD compared to HC during the first-60-min of sleep

Table 2. *SWA/Delta power in children with ADHD.*

ADHD, attention-deficit/hyperactivity disorder; DISC-IV, Diagnostic Interview Schedule for Children IV; HC, healthy controls; EEG, electroencephalography; MSLT, multiple sleep latency test; ODD, oppositional-defiant disorder; PSG, polysomnography; REM, rapid eye movement; SWA, slow wave activity.

Author(s), Year	Age (min-max or mean±DS, y)	N°	Task-related	Comorbi-dities (n°)	Sleep Stage	Frequencies (Hz)	Power analysis	Results
Prehn-Kristensen et al., 2013	ADHD and healthy children: 9-12; healthy adults: 20-28	ADHD: 16; healthy children: 16; healthy adults: 20	Emotional Memory Task (EMT)	ODD (5)	REM	4-7	F4 - (mean A1-A2)	Children with and without ADHD showed higher theta power than healthy adults; theta oscillations correlated negatively with memory performance in children with ADHD but positively in healthy individuals (both children and adults)
Saletin et al., 2017	ADHD and HC: 10–12.9	ADHD: 7; HC: 14	Motor Sequence Task (MST)	-	N2	4–8	average of C3/A2 and C4/A1	Theta activity was marginally higher in ADHD than HC, but this difference was not statistically significant.
Cremone et al. 2017	ADHD and HC: 4-8	ADHD: 14; HC: 15	Go/No-go Task (2 sessions)	-	REM and NREM	4-7	F4-A1	Theta activity was significantly greater in the ADHD group compared to HC during REM sleep (but not during NREM sleep). Morning inhibitory control was positively correlated with REM theta activity only in HC.

Table 3. *Theta power in children with ADHD.*

ADHD, attention-deficit/hyperactivity disorder; HC, healthy controls; N2, non-rapid eye movement sleep stage 2; NREM, non-rapid eye movement; ODD, oppositional-defiant disorder; REM, rapid eye movement.

4.4. Study aims

Tables 2 and 3 clearly show that published articles on sleep power in ADHD are sparce, mainly based on one or few channels, task-related and focused on NREM sleep and/or hampered by medications. My study aimed to fill previous gaps in the literature, systematically investigating sleep power topography in all traditional frequency bands, in all sleep stages and across sleep cycles using hdEEG in 30 drug-naïve children/adolescents with ADHD and 23 typically developing children, in order to provide further support to the hypothesis of sleep abnormalities in ADHD.

4.5. Original paper

I herein enclose the original paper that resulted from this thesis project, recently published in Children (Castelnovo et al., 2022).

children

MDPI

Article

Sleep Power Topography in Children with Attention Deficit Hyperactivity Disorder (ADHD)

Anna Castelnovo [1,2,3,*], Althea Lividini [4], Giulio Bernardi [5], Valdo Pezzoli [6], Giuseppe Foderaro [6], Gian Paolo Ramelli [7], Mauro Manconi [1,2,8] and Silvia Miano [1,*]

1 Sleep Medicine Unit, Neurocenter of Southern Switzerland, Ospedale Civico, 6900 Lugano, Switzerland; mauro.manconi@eoc.ch
2 Faculty of Biomedical Sciences, Università della Svizzera Italiana, 6900 Lugano, Switzerland
3 University Hospital of Psychiatry and Psychotherapy, University of Bern, 3011 Bern, Switzerland
4 Department of Medical and Surgical Sciences, University of Bologna, 40126 Bologna, Italy; althea.lividini@asst-santipaolocarlo.it
5 MoMiLab Research Unit, IMT School for Advanced Studies Lucca, 55100 Lucca, Italy; giulio.bernardi@imtlucca.it
6 Department of Pediatrics, Ospedale Civico, 6900 Lugano, Switzerland; valdo.pezzoli@eoc.ch (V.P.); Giuseppe.Foderaro@eoc.ch (G.F.)
7 Department of Pediatrics, San Giovanni Hospital, 6500 Bellinzona, Switzerland; GianPaolo.Ramelli@eoc.ch
8 Department of Neurology, University Hospital, Inselspital, 3010 Bern, Switzerland
* Correspondence: anna.castelnovo@eoc.ch (A.C.); silvia.miano@eoc.ch (S.M.)

Abstract: Objective: Recent years saw an increasing interest towards sleep microstructure abnormalities in attention-deficit/hyperactivity disorder (ADHD). However, the existing literature on sleep electroencephalographic (EEG) power in ADHD is still controversial, often based on single electrode recordings, and mainly focused on slow wave activity (SWA) during NREM sleep. This study aimed to systematically investigate sleep power topography in all traditional frequency bands, in all sleep stages and across sleep cycles using high-density EEG (HD-EEG). Method: Thirty drug-naïve children with ADHD (10.5 ± 2.1 years, 21 male) and 23 typically developing (TD) control participants (mean age: 10.2 ± 1.6 years, 13 male) were included in the current analysis. Signal power topography was computed in classical frequency bands during sleep, contrasted between groups and sleep cycles, and correlated with measures of ADHD severity, cognitive functioning and estimated total sleep time. Results: Compared to TD subjects, patients with ADHD consistently displayed a widespread increase in low-frequency activity (between 3 and 10 Hz) during NREM sleep, but not during REM sleep and wake before sleep onset. Such a difference involved a wide centro-posterior cluster of channels in the upper SWA range, in Theta, and low-Alpha. Between-group difference was maximal in sleep stage N3 in the first sleep cycle, and positively correlated with average total sleep time. Conclusions: These results support the concept that children with ADHD, compared to TD peers, have a higher sleep pressure and altered sleep homeostasis, which possibly interfere with (and delay) cortical maturation.

Keywords: EEG; spectral analysis; power; topography; sleepiness; maturation

Citation: Castelnovo, A.; Lividini, A.; Bernardi, G.; Pezzoli, V.; Foderaro, G.; Ramelli, G.P.; Manconi, M.; Miano, S. Sleep Power Topography in Children with Attention Deficit Hyperactivity Disorder (ADHD). *Children* **2022**, *9*, 197. https://doi.org/10.3390/children9020197

Academic Editor: Marco Filardi

Received: 24 December 2021
Accepted: 28 January 2022
Published: 3 February 2022

1. Introduction

Attention-deficit/hyperactivity disorder (ADHD) is a common neurodevelopmental disorder broadly characterized by daytime symptoms of hyperactivity/impulsivity and inattention [1]. ADHD estimated prevalence in children and adolescence is around 5% worldwide [2–5]. ADHD high individual and societal impact have fueled intensive research over the last decades [2]. Nonetheless, the exact etiology of ADHD still remains largely unknown [6] and as a consequence, no objective/biological marker currently supports the diagnosis. Sleep problems are commonly reported by children-adolescents with ADHD and their parents in clinical settings [7]. This observation has led to a growing attention towards sleep [8] and its electroencephalographic (EEG) microstructure in ADHD [9,10].

Few quantitative EEG studies specifically investigated sleep power patterns in children with ADHD [9,11]. Older studies, which commonly focused only on one arbitrarily selected EEG channel, showed no abnormalities in the lower frequencies range (0.5–4.5 Hz) during non-rapid eye movement (NREM) sleep [12–15]. However, three later studies [16–18] have been performed in children with ADHD during sleep using high-density EEG (HD-EEG), which allows a higher level of spatial resolution of electrocortical activity in comparison to standard EEG. While two out of three studies found higher slow wave activity (SWA) over a centro-posterior cluster of electrodes [16,17], one found a global decrease in SWA in ADHD children compared to TD peers [18]. According to a recent meta-analysis, these apparently discrepant results might be explained by the negative association between SWA and both mean age and the use of medications [11].

Importantly, published results regarding frequency bands other than SWA were even more limited and contradictory, and were typically based only on the evaluation of a few scalp electrodes after cognitive demanding tasks. Previously mentioned HD-EEG studies focused only on SWA (mean signal power in the frequency range 0.5/1 to 4/4.5 Hz) during NREM sleep, since this parameter has a well-known role in synaptic, use-dependent plasticity and memory consolidation. However, all frequency bands have been found to undergo major modifications across typical development in both NREM and rapid eye movement (REM) sleep [9,19], and could thus reflect developmental alterations in children with ADHD. However, findings have been largely inconsistent across studies. These inconsistencies may be related to methodological issues and to the complexity and bidirectionality of the relationship between ADHD and sleep abnormalities [20,21]. Indeed, ADHD is a potential cause of sleep abnormalities per se [22,23], and sleep disorders are a potential source of ADHD-like symptoms [7,24]. In this regard, it is of utmost importance that quantitative EEG studies also consider PSG channels to assess major sleep comorbidities in ADHD.

In light of the above considerations, the aim of this study was to cover the aforementioned gaps in the literature, extending the analysis of common markers of ADHD using a previously collected dataset of overnight baseline HD-EEG/video-polysomnography (v-PSG) recordings [17]. In particular, while our previous study [17] focused on SWA in the first and last 60 min of NREM sleep, here we aimed to study all-night and all-frequency band power topography across sleep states (during both NREM stage 2—N2 and NREM stage 3—N3, REM sleep, and also pre-sleep-onset wakefulness), and across NREM sleep cycles, in order to explore candidate markers of disease.

2. Materials and Methods

This is an observational, prospective case-control single-center study carried out at the Neurocenter of Southern Switzerland on ADHD. All study procedures were reviewed and approved by the local Independent Ethics Committee "Comitato Etico Cantonale" (26 February 2015–n.2881), according to the regulatory requirements of Switzerland. All participants provided written consent before the study.

2.1. Participants

Thirty children with a clinical diagnosis of ADHD and 23 healthy control peers were included for analysis. This dataset overlaps with the one described in a recent publication by our group [17]. Demographics and clinical information are summarized in Table 1.

Table 1. Clinical and instrumental sleep data in the attention-deficit/hyperactivity disorder (ADHD) group and in the healthy control group.

	ADHD (n = 30)			CONTROL (n = 23)				
	M ± SD	**Median**	**Min–Max**	**M ± SD**	**Median**	**Min–Max**		
Age (y)	10.48 ± 2.06	10.33	7.80–13.83	10.15 ± 1.56	10.00	7.92–13.67		
BMI (kg/m^2)	18.71 ± 4.43	17.05	13.60–34.20	17.43 ± 2.71	17.10	13.80–23.60		
CPRS-R (tot)	76.11 ± 10.78	78	59–99					
WISC-IV (tot)	100.19 ± 9.02	98	84–114					
K-SADS-PL (tot)	2.93 ± 0.26	3	2–3					
Sex	Male		n = 21	Male		n = 12		
ADHD Subtypes	Inattentive		n = 6					
	Hyperactive		n = 2					
	Combined		n = 22					
Sleep Phenotypes	Epileptic EEG abnormalities		n = 10					
	Sleep onset insomnia		n = 5					
	PLMI > 5 events/hour		n = 8					
	OSAS		n = 15					
	Narcoleptic-like		n = 4					
	v-PSG [§]							
	M ± SD	**Median**	**Min–Max**	**M ± SD**	**Median**	**Min–Max**	**P**	**ES**
TIB (min)	493.40 ± 39.81	493.82	384.73–568.77	503.44 ± 41.04	506.55	390.00–567.80	0.377	
TST (min)	408.96 ± 58.73	423.00	215.95–478.50	430.69 ± 52.02	440.42	275.27–499.93	0.17	
SL (min)	29.72 ± 23.39	22.72	1.35–81.87	23.08 ± 14.32	23.98	3.29–58.58	0.578 *	
REML (min)	135.47 ± 56.75	116.38	55.50–299.57	111.01 ± 45.55	93.08	57.40–252.39	0.066 *	
WASO (min)	54.71 ± 55.31	28.58	7.24–216.45	50.84 ± 45.01	31.98	10.11–199.67	0.787	
SE (%)	83.12 ± 11.73	86.23	48.49–97.45	85.74 ± 9.44	89.02	55.22–97.45	0.388	
N1 (min)	23.16 ± 8.85	21.66	9.50–39.50	24.93 ± 10.48	23.70	11.00–56.01	0.512	
N1 (%TST)	5.89 ± 2.84	5.28	2.03–15.03	5.86 ± 2.62	5.49	2.89–12.36	0.971	
N2 (min)	151.47 ± 38.84	153.50	17.00–199.88	160.40 ± 24.71	165.48	93.00–199.70	0.343	
N2 (%TST)	36.51 ± 7.97	37.07	7.87–49.67	37.31 ± 4.51	35.46	29.58–46.87	0.668	
N3 (min)	141.45 ± 26.35	137.35	104.50–195.00	147.70 ± 19.14	144.50	109.50–181.96	0.345	
N3 (%TST)	35.12 ± 7.34	33.38	24.65–56.49	34.52 ± 4.08	34.35	27.20–42.47	0.727	
REM (min)	92.87 ± 23.56	97.25	44.50–129.13	97.66 ± 28.84	101.00	39.00–161.50	0.512	
REM (%TST)	22.48 ± 3.68	22.20	15.18–28.30	22.30 ± 4.82	22.01	14.03–33.00	0.881	
AI (n/h)	13.48 ± 3.44	13.90	7.42–19.67	12.74 ± 3.1	12.67	6.96–18.15	0.422	
AHI (n/h)	2.04 ± 1.70	1.40	0.00–6.90	0.67 ± 0.8	0.40	0.00–3.10	0.002	−1.002
PLMI (n/h)	2.96 ± 2.81	2.80	0.00–9.60	2.74 ± 3.55	1.50	0.00–12.70	0.807	

AI, arousal index; AHI, apnea-hypopnea index; BMI, body mass index; CPRS-R, Conners' Parent Rating Scale—Revised; K-SADS-PL, Schedule for Affective Disorders and Schizophrenia for School-Age Children Present and Lifetime Version; N1, non-REM sleep stage 1; N2, non-REM sleep stage 2; N3, non-REM sleep stage 3; OSAS, Obstructive sleep apnea syndrome (based on AHI >1 event/hour and at least one among snoring, labored sleep breathing and sleepiness); PLMI, periodic limb movements index; REM, rapid eye movement; REML, REM latency; SE, sleep efficiency; SL, sleep latency; TIB, time in bed; TST, total sleep time; WASO: wakefulness after sleep onset; WISC-IV, Wechsler Intelligence Scale for Children—IV. ES: effect size; M: median, min: minutes n: number; n/h: number/hour; P: p-value resulting from to 2-tailed independent t-test statistics unless otherwise specified (* Mann-Whitney U Test); SD: standard deviation. [§] only 29 patients considered as for 1 child with ADHD only the first sleep cycle was available.

2.1.1. Patient Group

Drug-naïve children with ADHD were recruited consecutively at the local Pediatric Department (in Lugano and Bellinzona) from April 2015 to May 2016. Each patient was evaluated by both a pediatrician and by a pediatric neuropsychiatrist (SM). The diagnostic protocol included a detailed medical history with both children and their parents, a neurological examination, a semi-structured psychiatric interview, i.e., the Schedule for Affective Disorders and Schizophrenia for School-Age Children Present and Lifetime Version (K-SADS-PL) [25], a paper-and-pencil version of the Conners' Parent Rating Scale—Revised (CPRS-R) [26] filled in by parents, and the Wechsler Intelligence Scale for Children—IV (WISC-IV) [27] and the Neuropsychological Developmental Assessment—Second Edition (NEPSY-II, a standardized neuropsychological battery for children) [28], administered to children with ADHD by a neuropsychologist and cognitive psychotherapist.

Inclusion criteria were: (1) a formal diagnosis of ADHD according to Diagnostic and Statistical Manual of Mental Disorders—5th Edition (DSM-V) criteria [29]; (2) age between 8 and 14 years. Exclusion criteria were: (1) a comorbid diagnosis of autistic spectrum disorder (ASD); (2) an intelligence quotient <70; (3) other known major neurological conditions; (4) previous treatment with stimulants or other medications used to treat ADHD.

The final group included 30 Caucasic research participants (mean age: 10.5 ± 2.1 years, range: 8–13 years, 21 male); of them, 22 were diagnosed with a combined ADHD presentation, 6 with a predominantly inattentive and 2 with a predominantly hyperactive presentation [17].

All research participants underwent a complete sleep assessment, which included a 1-week actigraphy recording, a nocturnal video-polysomnography (v-PSG) with extended EEG monitoring, and a multiple sleep latency test (MSLT) the day after the v-PSG. Good quality, all-night recordings were available for 29 participants. For one subject only the first cycle (NREM sleep plus a few epochs of REM sleep) was available and used for the current analysis.

According to a previous classification of the same group of patients, children with ADHD could be divided into 5 different phenotypes: (1) epileptic EEG abnormalities (n = 10); (2) sleep onset insomnia (n = 5), based on a reported sleep latency >20 min, for more than 3 times per week and more than three months; (3) periodic limb movements (PLM) >5 events/hour with no associated restless leg syndrome (RLS) (n = 8); (4) obstructive sleep apnea-hypopnea syndrome (OSAS), based on an apnea-hypopnea index (AHI) >1 events/hour and the presence of at least one of the following clinical features: snoring, labored sleep breathing, excessive daytime sleepiness (n = 15); (5) narcoleptic-like phenotype (n = 4), characterized by excessive daytime sleepiness as defined by an MSLT <8 min, and/or 2 sleep-onset REM-sleep periods at MSLT. For more details on the clinical features of this group, see Miano et al. [17].

2.1.2. Control Group

Twenty-five TD children were recruited by e-mail and word-of-mouth among all employees of the Civic Hospital of Lugano. A physician board-certified in both Pediatric Sleep Medicine and Child Psychiatrist (SM) thoroughly interviewed children and their parents to screen for any known sleep disorder, neuro-psychiatric comorbidity, or any medical condition affecting sleep. Selected children were then referred to the sleep laboratory for a sleep v-PSG with extended EEG monitoring.

Data collected from 2 participants were lost due to storage failure. Therefore, recordings from 23 participants were eventually used in the analysis (mean age: 10.2 ± 1.6 years, range: 8–13 years, 13 male). The control group did not significantly differ from the patient group for age ($t_{(51)} = -0.66$, $p > 0.05$, independent-samples 2-tailed t-test) and sex ($\chi^2_{(1,\, n = 53)} = 1.1$, $p > 0.05$, Chi-square test for independence with Yates Continuity Correction). Healthy control participants were also screened for sleep breathing disorders and PLM during sleep. None of them had symptomatic OSAS or an AHI >5 events/hour or reached the criteria for a PLM disorder or RLS.

2.2. Sleep Recordings

All participants underwent an in-laboratory overnight HD-EEG recording (256 channels; Electrical Geodesics Inc., Eugene, OR, vertex-reference, 250 Hz), coupled with traditional v-PSG [30]. Lights out was consistent with the participants' average bedtime, and wake-up time was between 6 and 7 am for all participants.

Sleep stages and sleep events were scored according to standard criteria by two board-certified sleep physicians using the Embla® Remlogic Software (Neurolite), based on 30-s epochs for 6 bipolar re-referenced EEG channels (F3/A2, F4/A1, C3/A2, C4/A1, O1/A2, O2/A1), electrooculogram (EOG), and submental electromyography (EMG) [30].

2.3. EEG Signal Power in NREM Sleep, in REM Sleep and Wake before Sleep Onset

Before spectral analysis, data were pre-processed according to standard routines for HD-EEG. All EEG signals and other relevant information (including sleep scoring) were imported and analyzed in MATLAB (The MathWorks Inc., Natick, MA, USA). Each signal was first-order high-pass filtered at 0.1 Hz (IIR filter reproducing a single resistor capacity) and subsequently band-pass filtered (0.5–45 Hz, Kaiser window-based FIR with

zero-phase distortion). Data epochs corresponding to NREM sleep N3 and N2, REM sleep and wake before sleep-onset (see below) were extracted and pre-processed separately. An interactive open-source tool for data visualization and data-cleaning (https://github.com/CSC-UW/csc-eeg-tools.git, accessed on 2 February 2021) was used to visually inspect data in MATLAB. Channels with clear artifacts were removed (and later recovered through interpolation; see below), while data segments containing artifacts affecting the majority of channels were marked as "bad" and not considered in subsequent analyses. Channels displaying a sharp difference in power relative to neighboring channels upon inspection of power spectra and topographic power maps were additionally removed. Quiet windows of wakefulness available in the time period between the end of electrode net setup and the beginning of the overnight recording (from 10 to 50 min before actual sleep onset) were selected. After the removal of artifactual data segments, a total of 8–16 min (M = 12.3, SD = 3.6) of wakefulness was retained for 27 patients and 18 control subjects. Three patients and 4 control subjects did not have artifact-free segments of wakefulness before sleep onset longer than 5 min and were therefore excluded. Independent Component Analysis (ICA) was performed on both sleep (REM and NREM) and wake data, in order to remove ocular, electrocardiograph, sweating, epileptic spikes and remaining muscular artifacts using EEGLAB routines [31]. Only ICA components with characteristic activity patterns typical of these artifactual activities were removed. Subsequently, the removed, bad channels were interpolated using spherical interpolation.

Spectral analysis was performed using all artifact-free 6-s epochs (Welch's averaged modified periodogram with a Hamming window, 8 segments with 50% of overlap) on the average-referenced signal. For topographic analysis, average signal power (across epochs) was computed for 6 classical frequency ranges [32]: delta/SWA (1–4 Hz), Theta (4–8 Hz), Alpha (8–12 Hz), Sigma (12–16 Hz) Beta (16–25 Hz), low Gamma (25–40 Hz). Both topographic maps of absolute average-referenced and normalized data (z-score across channels of the same participant) were examined. NREM sleep (more specifically stages N2 and N3, taken together and separately) and REM sleep all-night power maps as well as wake before sleep onset power maps were compared across groups (ADHD versus TD children) for all frequency bands.

2.4. NREM Sleep Homeostatic Regulation

Additional between-groups analyses were performed to compare the first, second and third sleep cycles separately, for the range of frequencies that significantly differed between groups in the all-night analysis. Of note, we specifically focused on the first three sleep cycles because this was the maximum number of cycles represented in the majority of our participants. In order to evaluate whether the physiological decline of low-frequency bands was preserved or altered in ADHD versus TD children, we also compared power in these frequencies across cycles and between groups.

2.5. Correlations between Power and Clinical Variables

The association between EEG power and clinical variables in the ADHD group was investigated for the frequency range that showed a significant difference between ADHD and TD children in the region of interest (ROI) of interest. Selected clinical variables were age, habitual total sleep time (TST) as estimated by parents and average sleep latency at the MSLT (as measures of sleep pressure), the global ADHD scores at the Conners Rating Scale, and global intellectual ability measured with the WISC-IV.

2.6. Statistical Analysis

Statistical between-group comparisons of demographic and polysomnographic variables, as well as power spectra, were performed using unpaired 2-tailed *t*-tests, Mann–Whitney U tests, or χ^2 tests, as appropriate. Normality of data and homogeneity of variance were evaluated using the Shapiro/Wilk's test and Levene's test, respectively. Comparisons of scalp power maps were performed separately for each frequency band. At the scalp level,

we corrected for multiple comparisons using a non-parametric cluster-based permutation test [33], as described in previous work [34–39]. Specifically, for each performed test, a null distribution was generated by randomly shuffling the group-label of each subject for comparisons. At each iteration of the permutation procedure, the test-statistics was computed for each electrode and the size of the largest significant electrode-cluster (uncorrected $p < 0.05$) was stored in a frequency table. Given the impracticality of computing all possible data re-combinations, the full null distribution was approximated using 10,000 iterations. Finally, the 95th percentile (5% significance level) was used as the critical cluster-size distribution threshold. Given the possible impact of age on these variables, an additional analysis was conducted with age introduced as a covariate. For the sake of simplicity, only results without using the covariate are detailed, except for cases where a discrepancy between the two analyses was observed. We did not correct for the issue of multiple testing across different comparisons (across bands and stages) due to the exploratory nature of this study.

In order to explore stage differences in average power comparisons, a mixed model analysis of variance (ANOVA) was used to determine the interaction effect between groups (ADHD and TD children) and sleep stages (N2 versus N3). In order to explore differences in the homeostatic regulation of sleep microstructural features, a mixed model ANOVA was used to assess the interaction effect between group (ADHD and TD children) and sleep cycle (first, second and third cycle), for the average power ROI identified by the cluster test analysis.

Correlation between power values and clinical variables in the patient group were performed using Spearman's correlation. As we performed 5 different correlations, the level of significance was adjusted for multiple comparisons (Bonferroni's correction, 0.05/5 = 0.01).

Statistical analyses were performed in MATLAB.

3. Results

3.1. EEG Signal Power in NREM Sleep, REM Sleep and Wake before Sleep Onset

3.1.1. NREM Sleep

During whole night NREM sleep children in the ADHD group showed a widespread, significant increase in absolute Theta power (cluster size = 124, $p < 0.05$) relative to the healthy control group (see Supplementary Figure S1). The increase was observed in most electrodes, with the notable exception of frontopolar ones.

No significant differences between children with ADHD and control participants were found in other frequency ranges and for normalized power except for a small frontal Beta cluster (cluster size = 18, $p < 0.05$), which was not confirmed after the introduction of age as covariate.

As there was a significant difference between the two groups (ADHD and TD) in the AHI, we also performed an exploratory analysis within the ADHD group between patients with ($n = 15$) and without ($n = 15$) the obstructive hypopneas/apneas phenotype. We could not observe any difference between these two groups in any frequency band (see Supplementary Figure S2).

In N2 sleep, many individual electrodes showed significantly higher absolute power values in the ADHD group relative to the control group, especially in low-frequency ranges (SWA, Theta, Alpha; $p < 0.05$, uncorrected). However, no significant effects were found for both absolute and normalized power maps (see Figure 1) after multiple comparison correction.

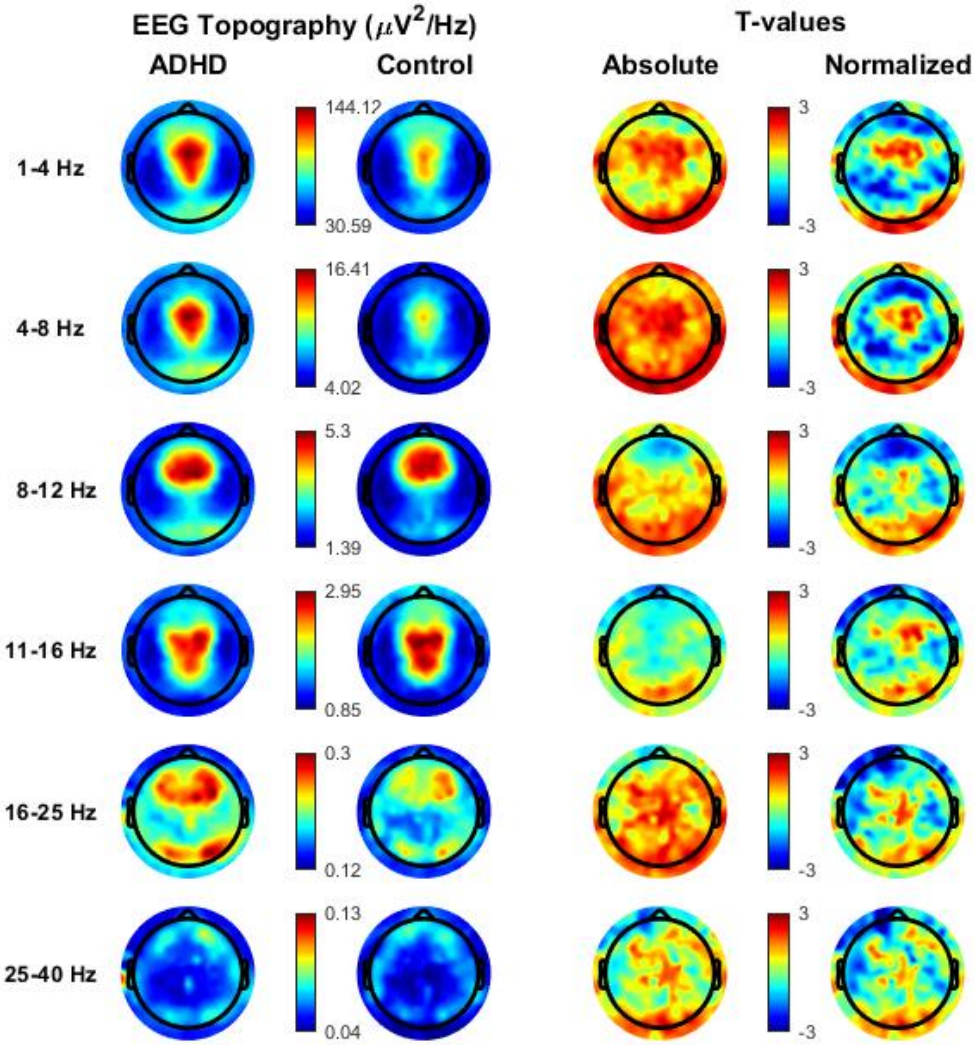

Figure 1. Topographical distribution of all frequency bands based on whole-night non-rapid eye movement (NREM) sleep stage 2 (N2) in the attention-deficit/hyperactivity disorder (ADHD) group and in the healthy control group. Values are color-coded and plotted on the planar projection of the hemispheric scalp model. Rows: frequency bands of interest. First and second column: average N2 sleep EEG topographies across frequency bands for children with ADHD and healthy control matches, respectively. Maxima are shown in red, minima in blue. Third and fourth column: single electrode *t*-value (2-tailed, unpaired) maps for the comparison between patients with ADHD and control subjects in terms of absolute and normalized (using the z-score across all electrodes) power, respectively. Blue color: decrease in EEG power in patients with ADHD relative to healthy controls (ADHDs < controls), red color: increase in EEG power in patients with ADHD relative to healthy controls (ADHD > controls). White circles indicate significant electrodes ($p < 0.05$ cluster-size correction).

In N3 sleep, a widespread significant increase in absolute Theta (cluster size = 143, $p < 0.05$) and Alpha (cluster size = 99, $p < 0.05$) was observed in the ADHD group relative to the healthy control group (see Figure 2). Differences were again observed in most central, parietal, temporal and occipital electrodes, and only spared frontopolar electrodes. When age was introduced as covariate, also the SWA range remained significant after multiple comparison correction (SWA range: cluster size = 134, $p < 0.05$, Theta range: cluster size = 197, $p < 0.05$, Alpha range, cluster size = 46 $p < 0.05$).

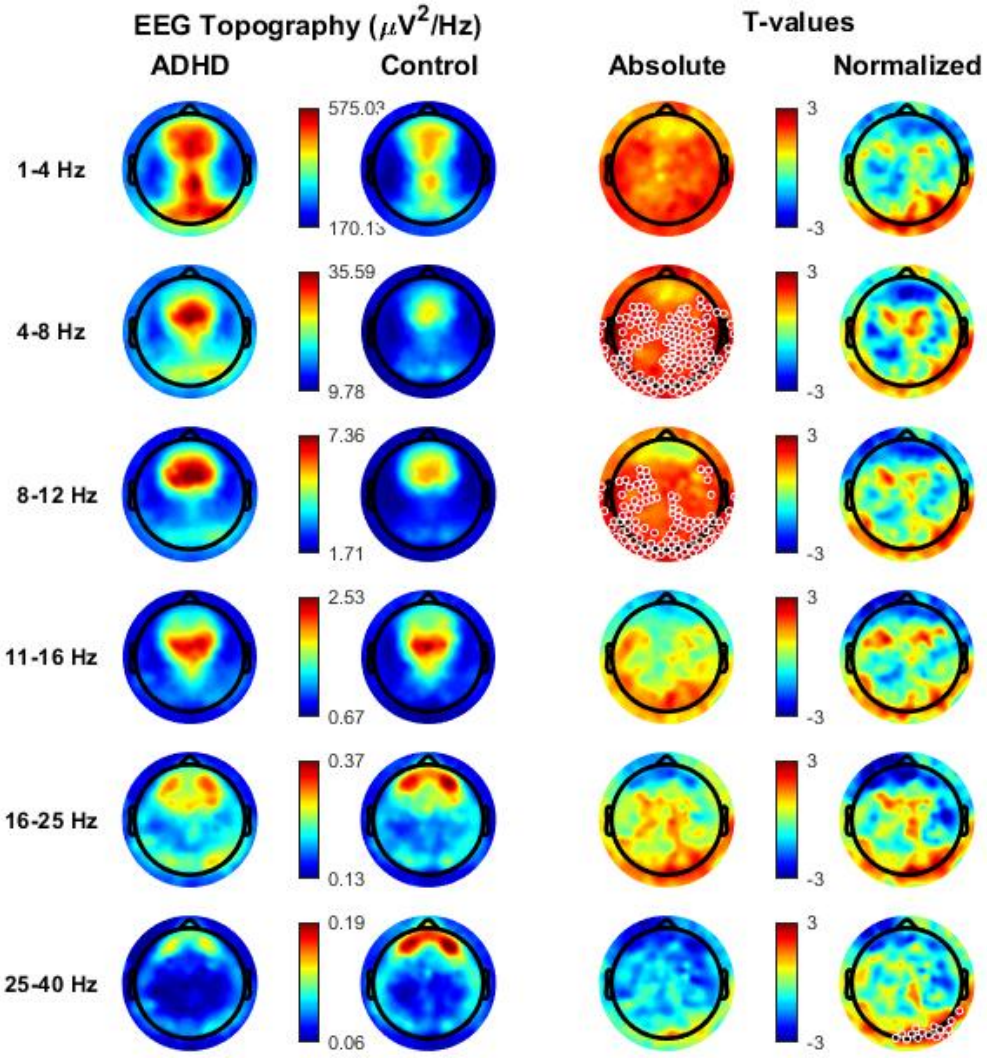

Figure 2. Topographical distribution of all frequency bands based on whole-night non-rapid eye movement (NREM) sleep stage 3 (N3) in the attention-deficit/hyperactivity disorder (ADHD) group and in the healthy control group. Values are color-coded and plotted on the planar projection of the hemispheric scalp model. Rows: frequency bands of interest. First and second column: average N2 sleep EEG topographies across frequency bands for children with ADHD and healthy control matches, respectively. Maxima are shown in red, minima in blue. Third and fourth column: single electrode *t*-value (2-tailed, unpaired) maps for the comparison between patients with ADHD and control subjects in terms of absolute and normalized (using the z-score across all electrodes) power, respectively. Blue color: decrease in EEG power in patients with ADHD relative to healthy controls (ADHDs < controls), red color: increase in EEG power in patients with ADHD relative to healthy controls (ADHD > controls). White circles indicate significant electrodes ($p < 0.05$ cluster-size correction).

No significant differences between ADHD and control children were found in other frequency ranges and for normalized power except for a small posterior Gamma cluster (cluster size = 15, $p < 0.05$), which was not confirmed after the introduction of age as covariate. It is however noteworthy that several individual posterior electrodes showed relatively higher levels of normalized SWA in ADHD, compared with control children ($p < 0.05$, uncorrected), in line with previous research.

Additional analyses were performed to better characterize the low-frequency increase observed during N3 sleep in ADHD relative to control children. In particular, we first compared the EEG power spectra (power spectral density averaged across all scalp channels) of the two groups and found a significant difference between 2.7 and 9.8 Hz

(Supplementary Figure S3). Consistent results also emerged from the analysis of topographical power maps when power was computed in 1 Hz bins (Figure 3). In particular, we found significant clusters with higher power in ADHD relative to control children in frequency bins from 3 to 10 Hz.

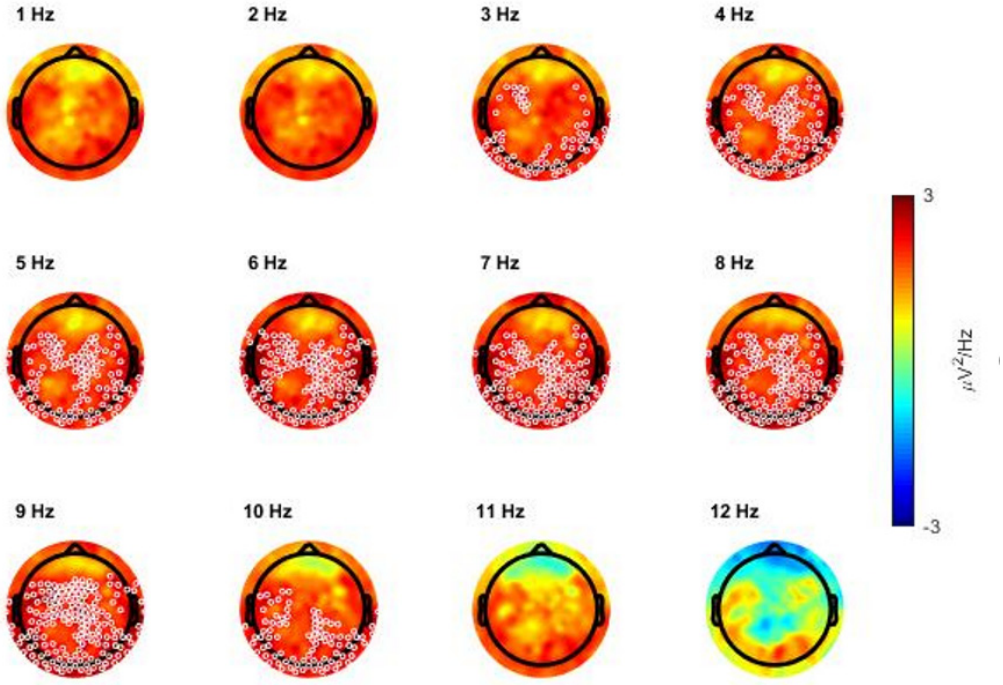

Figure 3. Topographical distribution of the comparison (single electrode *t*-value, 2-tailed, unpaired) between absolute power values of the attention-deficit/hyperactivity disorder (ADHD) group and of the healthy control group during whole-night non-rapid eye movement NREM sleep stage 3 (N3), represented per bin of frequency.

Each map represents the comparison for one bin of frequency centered on the value indicated above each map. Values are color-coded and plotted on the planar projection of the hemispheric scalp model. A lower EEG power in patients with ADHD relative to healthy controls (ADHDs < controls) is represented in blue, a higher power (ADHD > controls) in red. White circles indicate significant electrodes ($p < 0.05$ cluster-size correction).

Interestingly, observed differences involved most low-frequencies below 10 Hz, with the notable exception of frequencies below 2.5 Hz (Supplementary Figure S4). When slow (0.5–2.5 Hz) and fast SWA (2.5–4 Hz) were considered separately, a cluster of significance could be observed only in the fast SWA range (cluster size = 31, $p < 0.05$).

We then defined as ROI the cluster of electrodes that survived multiple comparison correction in the frequency range between 3 and 10 Hz. In order to investigate whether the low-frequency difference observed in N3 sleep (3–10 Hz range) was specific for this stage or also extended (and to which degree) to N2 sleep, we used an ANOVA model with group (ADHD versus TD) and stage (N2 versus N3) as factors to analyze the average signal power in the region of interest. There was a statistically significant two-way interaction between group and stage: $F_{(2, 50)} = 6.139$, $p < 0.05$, Huynh–Feldt correction for Epsilon > 0.75, partial eta squared = 0.109, see Figure 4, left panel). As expected, there was a significant effect of stage on power for both ADHD and TD groups (N3 > N2, $p < 0.001$, p Bonferroni-adjusted < 0.001 for both groups). Group comparisons were significant for both N2 (ADHD > TD, p Bonferroni-adjusted < 0.05) and N3 (ADHD > TD, p Bonferroni-adjusted < 0.05).

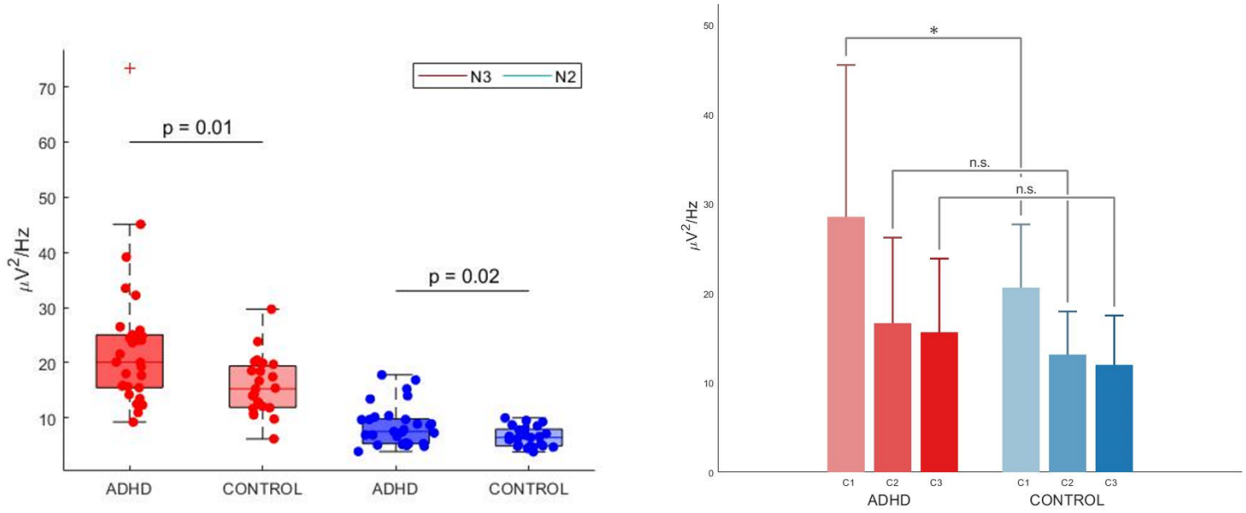

Figure 4. Left panel—Absolute spectral density averaged across channels within the significant Theta cluster in the attention-deficit/hyperactivity disorder (ADHD) and the control group in non-rapid eye movement (NREM) sleep stage 3 (N3) and NREM sleep stage 2 (N2). Red dots represent N3, blue dots N2. The bottom and top of each boxplot are the 25th and 75th percentiles of the sample, respectively. The distance between the bottom and top of each box is the interquartile range. The green line in the middle of each box is the sample median. The whiskers extending above and below each box go from the end of the interquartile range to the furthest observation within the whisker length. Observations beyond the whisker length (more than 3 times the interquartile range away from the bottom or top of the box) are marked as outliers. The cross (+) represents an outlier. The mean difference was significant between the ADHD group (N3: M = 22.90, SD = 12.65, N2: M = 8.60, SD = 3.73) and the control group (N3: M = 15.77, SD = 5.22, N2: M = 6.54, SD = 1.81) for both N3 ($p < 0.05$, also after the removal of the outlier in the ADHD group, Cohen's d = 0.70, meaning a medium effect size, independent samples *t*-test) and in N2 ($p = 0.018$, Cohen's d = 0.68, meaning a medium effect size, independent samples *t*-test). There was a significant interaction effect ($p < 0.05$) between stages (N3 versus N2) and groups (ADHD versus control) at a mixed between-within ANOVA model (not shown in the figure). Right panel—Absolute spectral density averaged across channels within the significant Theta cluster in the attention-deficit/hyperactivity disorder (ADHD) and the control group in different sleep cycles (first, second and third cycle). X-axes: time expressed in cycles, Y-axes: average power values in selected frequency range of 3–10 Hz, expressed in $\mu V/Hz^2$. Red bars: ADHD group. Blue bars: control group. C1: first cycle, C2: second cycle; C3: third cycle. There was a significant difference in 3–10 Hz power of the significant cluster of channels for the ADHD group (M = 28.55, SD = 16.97) and the control group (M = 20.63, SD = 7.06) in N3 of the first sleep cycle: t(51) = 2.10, ADHD > controls, $p < 0.05$, Cohen's d = 0.61, meaning a medium effect size, independent-samples *t*-test, two tailed). n.s.: not significant. (*): significant comparison.

3.1.2. REM Sleep Power

No differences were found between groups (ADHD versus TD) in terms of absolute or normalized power maps in REM sleep (see Supplementary Figure S5). No clusters of significance were found after multiple comparison correction also when considering the ROI emerged in NREM sleep analysis (data not shown).

3.1.3. Wake before Sleep Onset Power

No differences were found between groups (ADHD versus TD) in terms of absolute or normalized power in wake before sleep onset except for a small posterior Gamma cluster in normalized power maps (cluster size = 14, $p < 0.05$), which disappeared after the introduction of age as a covariate (see Supplementary Figure S6). No significant clusters were found after multiple comparison correction in 3–10 Hz power the ROI emerged from NREM sleep analysis (data not shown).

3.2. NREM Sleep Homeostatic Regulation

We first conducted separate group-level comparisons using 3–10 Hz power in the ROI of interest during the first, second and third cycle of N3 sleep, separately. Four research participants were removed from this analysis because they did not have N3 in the third cycle.

A 2-way mixed ANOVA used to investigate potential inter-group differences in 3–10 Hz power across cycles in the previously defined ROI revealed an interaction effect between group (ADHD versus TD) and cycle (cycle 1, cycle 2, cycle 3), within our significant cluster of channels: $F_{(1, 46)} = 3.318$, $p < 0.05$ (Huynh-Feldt correction for Epsilon > 0.75, partial eta squared = 0.066). Pairwise comparisons showed that power was significantly different between groups in cycle 1 (ADHD >TD, $p < 0.05$), but not in cycle 2 and 3 (although this effect did not stand multiple comparison correction with Bonferroni's adjustment, see Figure 4, right panel). There was a statistically significant effect of cycle on power for each group ($p < 0.05$ for both groups) which confirmed a physiological homeostatic decline in N3 power in both ADHD and TD. The pairwise comparisons cycle 1 versus cycle 2 and cycle 1 versus cycle 3 were significantly different for both groups ($p < 0.05$).

3.3. Correlation Analysis between Low-Frequency Activity and Clinical Variables

Given our observation of higher 3–10 Hz activity in ADHD relative to TD children during N3 sleep, we investigated whether this low-frequency power in the ROI of interest was correlated with demographic and clinical variables of children with ADHD. We found a significant negative correlation between low-frequency power and age, so that older children were characterized by lower signal power ($p < 0.001$, r = −0.515; Figure 5). In addition, we observed a significant positive correlation with the total sleep time as estimated by the parents ($p < 0.001$, r = 0.490). This correlation remained significant when the effect of age was partialled-out. No significant correlations were found between signal power in the 3–10 Hz range and MSLT mean sleep latency, overall ADHD symptoms measured by the Conners' scale ($p > 0.001$, r = 0.14), and the WISC-IV ($p > 0.001$, r = 0.29).

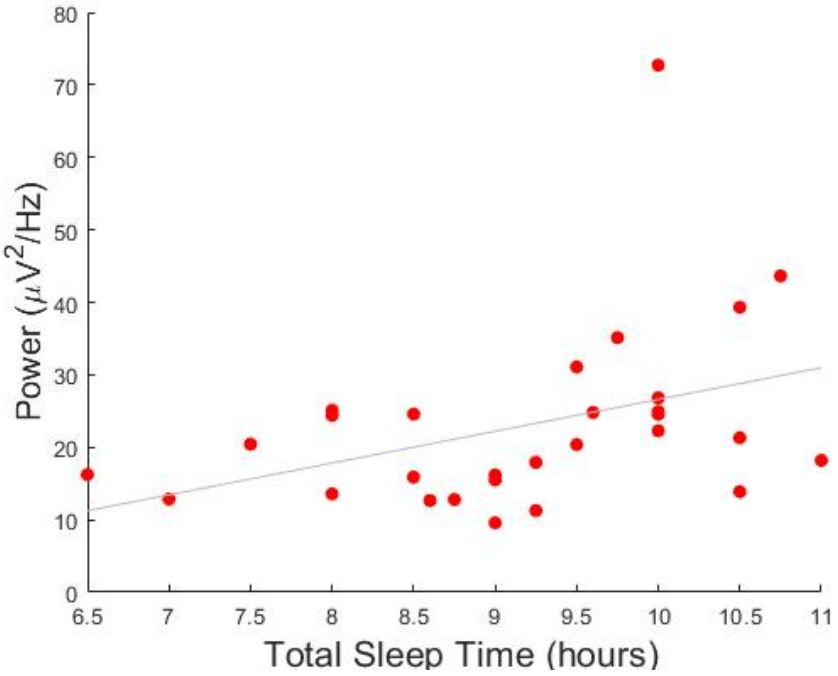

Figure 5. Correlation between power and total sleep time in children with attention deficit/hyperactivity disorder (ADHD). *Y*-axis represents the average power of all significant channels in the 3–10 Hz cluster. *X*-axis represents the habitual total sleep time estimated by parents.

4. Discussion

4.1. General Overview

This study expands our previous findings on normalized sleep power topography in ADHD children, which pointed to a relative increase of SWA power over centro–parietal–occipital regions in these subjects compared to TD children [18]. Here, we investigated systematically both absolute and normalized power density maps in all traditional frequency bands and in all sleep stages in the same dataset of drug-naive children with ADHD and healthy control peers, collected with HD-EEG coupled with a complete PSG monitoring [17]. Of note, contrary to previous studies investigating quantitative EEG differences in ADHD and TD children, this dataset was specifically tailored to investigate sleep problems in ADHD children but additionally demonstrated a higher prevalence of past and/or current sleep disorders in the ADHD children group compared to the control group. Despite the heterogeneity of sleep disorders in this patient population [17], our results consistently revealed a widespread increase in low-frequency activity, between 3 and 10 Hz, during NREM sleep in ADHD compared to TD children, but not during REM sleep and wake before sleep onset. We interpreted this effect as the common end-stage result of different sleep disorders on brain development. Such a difference involved the upper SWA range and peaked in the Theta range, encompassing a wide centro-posterior cluster of channels, sparing only fronto-polar regions. In addition, the difference was maximal in stage N3, although a similar trend could also be observed in N2 sleep. Between-group differences were more marked in the first sleep cycle, suggesting an increased homeostatic pressure in ADHD children. Average power values in the 3–10 Hz frequency range were positively correlated with estimated average total sleep time.

Overall, current results widen the perspective from previous sleep HD-EEG studies which focused exclusively on SWA in NREM sleep and clearly showed that all lower frequency bands (and mainly Theta band) are altered in children with ADHD during NREM sleep, paralleling findings during daytime "rested" wakefulness [40].

4.2. Interpretation of Results

This broad-band effect likely reflects the fact that the cut-offs of frequency bands, although based on the visual inspection of EEG activity, frequently do not correspond to the functional meaning of EEG rhythms [41]. Indeed, all lower EEG frequency bands are all homeostatically regulated in humans [42], meaning that their power increases with sleep deprivation and gradually dissipates during a good night of sleep [43,44]. Furthermore, the power of EEG slow frequencies during sleep varies significantly with brain maturation [40]. More specifically, global SWA activity during NREM sleep significantly increases in the first decade of life and then decreases during the second decade of life, both in cross-sectional and longitudinal studies [19,45–47]. Theta activity undergoes a similar trajectory, although its peak and decline begin significantly earlier compared to SWA (starting approximately at 9 years of age) [45]. The Alpha band has been less investigated, but the limited existing literature overall suggests a reduction in the Alpha band in the second decade of life [19,47,48]. Taken together these data contrast with the maturational trajectory of higher frequency bands [49] which seems to be less affected (Beta/Gamma) by age or to be modulated differently, as in the case of Sigma activity, following a bimodal curve with a first peak in the slow spindle range after the age of two years and a second, centro-parietal peak at high-Sigma frequencies during adolescence [42,50,51].

Therefore, an abnormality of lower EEG frequency bands in ADHD might both reflect a delay in brain maturation and/or an alteration in sleep homeostasis.

Delay in brain maturation—Higher power values from 3 to 10 Hz sparing more frontal areas may be consistent with ADHD children presenting a "younger" (i.e., less "mature") power pattern compared to their peers. This hypothesis is reinforced by the typical clinical evolution of the disorder, as symptoms tend to improve with age [52]. However, it should be noted that the results from previous longitudinal and cross-sectional, low-density EEG studies [47,53], reported a significant decrease with age of EEG power in

the delta/Theta/Alpha bands during both REM sleep and NREM sleep [47]. In this respect, consistency with the maturation delay hypothesis would imply a dissociation between NREM and REM sleep, with only maturational aspects reflected by NREM low-frequency activity actually altered in ADHD relative to TD children.

Sleep homeostasis impairment—At the same time, high levels of low-frequency activity may reflect a higher sleep pressure and an abnormal homeostatic process in children with ADHD. The homeostatic process is fundamental for brain plasticity [54] and is expressed by changes in the EEG power spectrum between the first and the second half of the night, mainly in the 1–9 Hz range [55], in face of a stable power topography. Our ADHD group displayed a specific increase in this frequency range, in the first sleep cycle, which rapidly and progressively dissipated throughout subsequent cycles. Interestingly, our results on SWA, the most commonly studied index of sleep pressure, are consistent with recent findings in animal models showing that higher-frequency SWA (2.5–3.5 Hz) respond to sleep loss with high initial power and fast, discontinuous decay during recovery sleep, while lower-frequency SWA (0.5–2.75 Hz) seems unrelated to time-spent-awake [56]. The increased sleep pressure in children with ADHD might be linked to the fact that subjective sleep complaints are common in persons with ADHD. Sleep disturbances were indeed confirmed objectively in our ADHD sample in a previously published paper [17]. It can be further speculated, on the basis of a positive correlation between estimated total sleep time and increased power in the 3–10 Hz range, that intrinsic abnormalities and/or underlying sleep disorders prevent these children from obtaining a fully restorative sleep, leading to a compensatory (but insufficient) increase in total sleep time. Finally, sleep abnormalities may impair neurodevelopmental and cortical maturational processes that are associated with sleep [57,58].

4.3. Limitations and Future Perspectives

To our knowledge, the analyzed dataset is the first that combined both quantitative EEG analysis and a full sleep evaluation (clinical interview, actigraphy, PSG and MSLT). This allowed us to discover an otherwise overlooked high prevalence of sleep disturbances in children with ADHD (as sleep assessments are not required for a formal diagnosis of ADHD). Notably, we found consistent results despite the heterogeneity of sleep disorders in our population. However, this heterogeneity prevented the possibility to explore the specific contribution of each sleep disorder to quantitative EEG findings. Although our sample was larger than those considered in many previous EEG studies in children with ADHD, increasing the sample size in future studies is warranted to investigate the impact of specific individual variables, such as gender, pharmacological treatment or sleep disturbances. Another potential limitation of this study was the lack of a detailed neuropsychological assessment and objective evaluation of daytime sleepiness/total sleep time (using MSLT and actigraphy) in the control group. This possible confounding bias should be ruled out in future studies. However, it should be noted that all control subjects underwent a sleep and neuropsychiatric screening interview and no sleep, cognitive or psychiatric complaint emerged from this clinical assessment.

Protocols involving a parallel acquisition of neurophysiological (EEG), anatomical (magnetic resonance imaging) and cognitive (executive functions) variables would ensure a deeper understanding of the neurobiological underpinnings and meaning of the findings we presented in this study. Furthermore, a longitudinal interventional study design (targeting sleep problems and/or ADHD per se with methylphenidate), would also help to elucidate both the causal relationship of sleep abnormalities on ADHD symptoms, as well as the impact of treatment strategies on ADHD prognosis.

5. Conclusions

In summary, we described for the first time, sleep power topography in ADHD on a broad range of frequencies during both NREM and REM sleep and across sleep cycles.

We found a global increase in low frequencies (high SWA, Theta and low Alpha, from 3 to 10 Hz) in NREM sleep of drug-naïve children with ADHD compared to TD children. This effect was specific for NREM sleep which could not be observed during REM sleep and pre-sleep-onset wakefulness and was more prominent in N3 in the first sleep cycle.

These findings reinforce the link between sleep neurophysiological abnormalities and ADHD. Moreover, our study found support for two recognized hypotheses regarding ADHD pathogenesis and suggests that they might not be in open contradiction: on one hand, cortical maturation seems to be delayed in children with ADHD, but on the other, a higher sleep pressure likely plays a role in this disease. Although these two hypotheses might appear to be independent from one another or even in open contradiction, upon closer study, they may represent two faces of the same phenomena. Indeed, sleep disorders during brain development, carefully evaluated and described in our dataset, might have interfered with both sleep quality (causing an increased sleep pressure) and with brain maturation, especially when chronic and early-onset. If confirmed, these results could guide future clinical research in ADHD, favoring the investigation of sleep disorders and their early therapeutic treatment.

Supplementary Materials: The following are available online at https://www.mdpi.com/article/10.3390/children9020197/s1, Figure S1: Topographical distribution of all frequency bands based on whole-night non-rapid eye movement (NREM) sleep stage 2 (N2) and stage 3 (N3) in the attention-deficit/hyperactivity disorder (ADHD) group and in healthy control group, Figure S2: Topographical distribution of all frequency bands based on whole-night non-rapid eye movement (NREM) sleep stage 3 (N3) in the attention-deficit/hyperactivity disorder (ADHD) group with and without the obstructive sleep apnea/hypo-apnea phenotype, Figure S3: Spectral power density average over all artifact free epochs in the attention-deficit/hyperactivity disorder (ADHD) group and in the healthy control group during whole-night non-rapid eye movement (NREM) sleep stage 3 (N3), Figure S4: Topographical distribution of alternative frequency bands based on whole-night non-rapid eye movement (NREM) sleep stage 3 (N3) in the attention-deficit/hyperactivity disorder (ADHD) group and in the healthy control group, Figure S5: Topographical distribution of all frequency bands based on whole-night rapid eye movement (REM) sleep in the attention-deficit/hyperactivity disorder (ADHD) group and in healthy control group, Figure S6: Topographical distribution of all frequency bands based on wake before sleep onset in the attention-deficit/hyperactivity disorder (ADHD) group and in healthy control group.

Author Contributions: Conceptualization, S.M.; Data curation, A.C.; Formal analysis, A.C. and A.L.; Funding acquisition, G.B. and S.M.; Investigation, V.P., G.F. and G.P.R.; Methodology, S.M.; Project administration, S.M.; Resources, S.M.; Supervision, G.B., M.M. and S.M.; Visualization, A.C.; Writing—original draft, A.C.; Writing—review & editing, A.C., A.L., G.B., V.P., G.F., G.P.R., M.M. and S.M. All authors have read and agreed to the published version of the manuscript.

Funding: All phases of this study were supported by an ABREOC grant (Advisory Board of Scientific Research of the Ente Ospedaliero Cantonale, protocol EOC.NSI.14.12), without any involvement in study design, in the collection, analysis and interpretation of data or in writing of the report and the decision to submit the article for publication.

Institutional Review Board Statement: All study procedures were reviewed and approved by the local Independent Ethics Committee "Comitato Etico Cantonale" (n.2881, approval date: 26th February 2015), according to the regulatory requirements of Switzerland. All participants provided written consent before the study.

Informed Consent Statement: Not applicable.

Data Availability Statement: The data presented in this study are available on request from the corresponding author.

Acknowledgments: We would like to thank all the parents of the recruited subjects and all the employees of the Sleep Medicine and the Pediatric Units of the Regional Hospital of Lugano for their help with the data collection and recruitment.

Conflicts of Interest: The authors declare no conflict of interest.

References

1. Cabral, M.D.I.; Liu, S.; Soares, N. Attention-Deficit/Hyperactivity Disorder: Diagnostic Criteria, Epidemiology, Risk Factors and Evaluation in Youth. *Transl. Pediatrics* **2020**, *9* (Suppl. 1), S104–S113. [CrossRef] [PubMed]
2. Doshi, J.A.; Hodgkins, P.; Kahle, J.; Sikirica, V.; Cangelosi, M.J.; Setyawan, J.; Erder, M.H.; Neumann, P.J. Economic Impact of Childhood and Adult Attention-Deficit/Hyperactivity Disorder in the United States. *J. Am. Acad. Child Adolesc. Psychiatry* **2012**, *51*, 990–1002.e2. [CrossRef] [PubMed]
3. Faraone, V.S.; Asherson, P.; Banaschewski, T.; Biederman, J.; Buitelaar, J.K.; Ramos-Quiroga, J.A.; Rohde, L.A.; Sonuga-Barke, E.J.S.S.; Tannock, R.; Franke, B. Attention-Deficit/Hyperactivity Disorder. *Nat. Rev. Dis. Primers* **2015**, *1*, 15020. [CrossRef] [PubMed]
4. Steinhausen, H.-C.; Metzke, C.W.; Meier, M.; Kannenberg, R. Prevalence of Child and Adolescent Psychiatric Disorders: The Zürich Epidemiological Study. *Acta Psychiatr. Scand.* **1998**, *98*, 262–271. [CrossRef] [PubMed]
5. Polanczyk, G.; de Lima, M.S.; Horta, B.L.; Biederman, J.; Rohde, L.A. The Worldwide Prevalence of ADHD: A Systematic Review and Metaregression Analysis. *Am. J. Psychiatry* **2007**, *164*, 942–948. [CrossRef] [PubMed]
6. Sharma, A.; Couture, J. A Review of the Pathophysiology, Etiology, and Treatment of Attention-Deficit Hyperactivity Disorder (ADHD). *Ann. Pharmacother.* **2014**, *48*, 209–225. [CrossRef]
7. Wajszilber, D.; Santiseban, J.A.; Gruber, R. Sleep Disorders in Patients with ADHD: Impact and Management Challenges. *Nat. Sci. Sleep* **2018**, *10*, 453–480. [CrossRef]
8. Baddam, S.K.R.; Canapari, C.A.; van Noordt, S.J.R.; Crowley, M.J. Sleep Disturbances in Child and Adolescent Mental Health Disorders: A Review of the Variability of Objective Sleep Markers. *Med. Sci.* **2018**, *6*, 46. [CrossRef]
9. Gorgoni, M.; Scarpelli, S.; Reda, F.; De Gennaro, L. Sleep EEG Oscillations in Neurodevelopmental Disorders without Intellectual Disabilities. *Sleep Med. Rev.* **2020**, *49*, 101224. [CrossRef]
10. Miano, S.; Castelnovo, A.; Bruni, O.; Manconi, M. Sleep Microstructure in Attention Deficit Hyperactivity Disorder According to the Underlying Sleep Phenotypes. *J. Sleep Res.* **2021**, *31*, e13426. [CrossRef]
11. Biancardi, C.; Sesso, G.; Masi, G.; Faraguna, U.; Sicca, F. Sleep EEG Microstructure in Children and Adolescents with Attention Deficit Hyperactivity Disorder: A Systematic Review and Meta-Analysis. *Sleep* **2021**, *44*, zsab006. [CrossRef] [PubMed]
12. Prehn-Kristensen, A.; Göder, R.; Fischer, J.; Wilhelm, I.; Seeck-Hirschner, M.; Aldenhoff, J.; Baving, L. Reduced Sleep-Associated Consolidation of Declarative Memory in Attention-Deficit/Hyperactivity Disorder. *Sleep Med.* **2011**, *12*, 672–679. [CrossRef] [PubMed]
13. Prehn-Kristensen, A.; Munz, M.; Molzow, I.; Wilhelm, I.; Wiesner, C.D.; Baving, L. Sleep Promotes Consolidation of Emotional Memory in Healthy Children but Not in Children with Attention-Deficit Hyperactivity Disorder. *PLoS ONE* **2013**, *8*, e65098. [CrossRef] [PubMed]
14. Saletin, J.M.; Coon, W.G.; Carskadon, M.A. Stage 2 Sleep EEG Sigma Activity and Motor Learning in Childhood ADHD: A Pilot Study. *J. Clin. Child Adolesc. Psychol.* **2017**, *46*, 188–197. [CrossRef]
15. Cremone, A.; Lugo-Candelas, C.I.; Harvey, E.A.; McDermott, J.M.; Spencer, R.M.C.C. REM Theta Activity Enhances Inhibitory Control in Typically Developing Children but Not Children with ADHD Symptoms. *Exp. Brain Res.* **2017**, *235*, 1491–1500. [CrossRef]
16. Ringli, M.; Souissi, S.; Kurth, S.; Brandeis, D.; Jenni, O.G.; Huber, R. Topography of Sleep Slow Wave Activity in Children with Attention-Deficit/Hyperactivity Disorder. *Cortex* **2013**, *49*, 340–347. [CrossRef]
17. Miano, S.; Amato, N.; Garbazza, C.; Abbafati, M.; Foderaro, G.; Pezzoli, V.; Ramelli, G.P.; Manconi, M.; Giuseppe, F.; Valdo, P. Shooting a High-Density Electroencephalographic Picture on Sleep in Children with Attention-Deficit/Hyperactivity Disorder. *Sleep* **2019**, *42*, zsz167. [CrossRef]
18. Furrer, M.; Jaramillo, V.; Volk, C.; Ringli, M.; Aellen, R.; Wehrle, F.M.; Pugin, F.; Kurth, S.; Brandeis, D.; Schmid, M.; et al. Sleep EEG Slow-Wave Activity in Medicated and Unmedicated Children and Adolescents with Attention-Deficit/Hyperactivity Disorder. *Transl. Psychiatry* **2019**, *9*, 324. [CrossRef]
19. Kurth, S.; Ringli, M.; Geiger, A.; LeBourgeois, M.; Jenni, O.G.; Huber, R. Mapping of Cortical Activity in the First Two Decades of Life: A High-Density Sleep Electroencephalogram Study. *J. Neurosci.* **2010**, *30*, 13211–13219. [CrossRef]
20. Miano, S.; Amato, N.; Foderaro, G.; Pezzoli, V.; Ramelli, G.P.; Toffolet, L.; Manconi, M. Sleep Phenotypes in Attention Deficit Hyperactivity Disorder. *Sleep Med.* **2019**, *60*, 123–131. [CrossRef]
21. Bioulac, S.; Taillard, J.; Philip, P.; Sagaspe, P. Excessive Daytime Sleepiness Measurements in Children With Attention Deficit Hyperactivity Disorder. *Front. Psychiatry* **2020**, *11*, 3. [CrossRef] [PubMed]
22. Scott, N.; Blair, P.S.; Emond, A.M.; Fleming, P.J.; Humphreys, J.S.; Henderson, J.; Gringras, P. Sleep Patterns in Children with ADHD: A Population-Based Cohort Study from Birth to 11 Years. *J. Sleep Res.* **2013**, *22*, 121–128. [CrossRef]
23. Scarpelli, S.; Gorgoni, M.; D'Atri, A.; Reda, F.; De Gennaro, L. Advances in Understanding the Relationship between Sleep and Attention Deficit-Hyperactivity Disorder (ADHD). *J. Clin. Med.* **2019**, *8*, 1737. [CrossRef]
24. Neto, F.K.; Noschang, R.; Nunes, M.L. The Relationship between Epilepsy, Sleep Disorders, and Attention Deficit Hyperactivity Disorder (ADHD) in Children: A Review of the Literature. *Sleep Sci.* **2016**, *9*, 158–163. [CrossRef] [PubMed]
25. Kaufman, J.; Birmaher, B.; Brent, D.; Rao, U.; Flynn, C.; Moreci, P.; Williamson, D.; Ryan, N. Schedule for Affective Disorders and Schizophrenia for School-Age Children-Present and Lifetime Version (K-SADS-PL): Initial Reliability and Validity Data. *J. Am. Acad. Child Adolesc. Psychiatry* **1997**, *36*, 980–988. [CrossRef] [PubMed]

26. Conners, C.K.; Sitarenios, G.; Parker, J.D.; Epstein, J.N. The Revised Conners' Parent Rating Scale (CPRS-R): Factor Structure, Reliability, and Criterion Validity. *J. Abnorm. Child Psychol.* **1998**, *26*, 257–268. [CrossRef]
27. Wechsler, D. *Wechsler Intelligence Scale for Children-Fourth Edition (WISC-IV)*; Giunti Organizzazioni Speciali; Italian Adaptation by Orsini, Pezzuti, Picone: Firenze, Italy, 2012.
28. Korkman, M.; Kirk, U.; Kemp, S.L. *NEPSY–II: Second Edition*; Giunti Organizzazioni Speciali; Italian Adaptation by Urgesi, Campanella and Fabbro: Firenze, Italy, 2011.
29. American Psychiatric Association. Neurodevelopmental Disorders: Attention-Deficit/Hyperactivity Disorder. In *Diagnostic and Statistical Manual of Mental Disorders, Fifth Edition (DSM-5)*; American Psychiatric Association: Washington, DC, USA, 2013. [CrossRef]
30. Berry, R.B.; Brooks, R.; Gamaldo, C.E.; Harding, S.M.; Marcus, C.L.; Vaughn, B.V.; Vaughn, V.B. The AASM Manual for the Scoring of Sleep and Associated Events. *Am. Acad. Sleep Med.* **2013**, *53*, 1689–1699. [CrossRef]
31. Delorme, A.; Makeig, S. EEGLAB: An Open Source Toolbox for Analysis of Single-Trial EEG Dynamics Including Independent Component Analysis. *J. Neurosci. Methods* **2004**, *134*, 9–21. [CrossRef] [PubMed]
32. Castelnovo, A.; Zago, M.; Casetta, C.; Zangani, C.; Donati, F.; Canevini, M.; Riedner, B.A.; Tononi, G.; Ferrarelli, F.; Sarasso, S.; et al. Slow Wave Oscillations in Schizophrenia First-Degree Relatives: A Confirmatory Analysis and Feasibility Study on Slow Wave Traveling. *Schizophr. Res.* **2020**, *221*, 37–43. [CrossRef]
33. Nichols, T.E.; Holmes, A.P. Nonparametric Permutation Tests for Functional Neuroimaging: A Primer with Examples. *Hum. Brain Mapp.* **2002**, *15*, 1–25. [CrossRef]
34. Riedner, B.A.; Hulse, B.K.; Murphy, M.J.; Ferrarelli, F.; Tononi, G. Temporal Dynamics of Cortical Sources Underlying Spontaneous and Peripherally Evoked Slow Waves. *Prog. Brain Res.* **2011**, *193*, 201–218. [CrossRef] [PubMed]
35. Castelnovo, A.; D'Agostino, A.; Casetta, C.; Sarasso, S.; Ferrarelli, F. Sleep Spindle Deficit in Schizophrenia: Contextualization of Recent Findings. *Curr. Psychiatry Rep.* **2016**, *18*, 72. [CrossRef] [PubMed]
36. Castelnovo, A.; Ferri, R.; Punjabi, N.M.; Castronovo, V.; Garbazza, C.; Zucconi, M.; Ferini-Strambi, L.; Manconi, M. The Paradox of Paradoxical Insomnia: A Theoretical Review towards a Unifying Evidence-Based Definition. *Sleep Med. Rev.* **2019**, *44*, 70–82. [CrossRef] [PubMed]
37. Spiess, M.; Bernardi, G.; Kurth, S.; Ringli, M.; Wehrle, F.M.; Jenni, O.G.; Huber, R.; Siclari, F. How Do Children Fall Asleep? A High-Density EEG Study of Slow Waves in the Transition from Wake to Sleep. *NeuroImage* **2018**, *178*, 23–35. [CrossRef]
38. Massimini, M.; Huber, R.; Ferrarelli, F.; Hill, S.; Tononi, G. The Sleep Slow Oscillation as a Traveling Wave. *J. Neurosci.* **2004**, *24*, 6862–6870. [CrossRef] [PubMed]
39. Huber, R.; Ghilardi, M.F.; Massimini, M.; Ferrarelli, F.; Riedner, B.A.; Peterson, M.J.; Tononi, G. Arm Immobilization Causes Cortical Plastic Changes and Locally Decreases Sleep Slow Wave Activity. *Nat. Neurosci.* **2006**, *9*, 1169–1176. [CrossRef]
40. Clarke, A.R.; Barry, R.J.; Johnstone, S.J.; Mccarthy, R.; Selikowitz, M. EEG Development in Attention Deficit Hyperactivity Disorder: From Child to Adult. *Clin. Neurophysiol.* **2019**, *130*, 1256–1262. [CrossRef]
41. Corsi-Cabrera, M.; Guevara, M.A.; Del Río-Portilla, Y.; Arce, C.; Villanueva-Hernández, Y. EEG Bands during Wakefulness, Slow-Wave and Paradoxical Sleep as a Result of Principal Component Analysis in Man. *Sleep* **2000**, *23*, 738–744. [CrossRef]
42. Gorgoni, M.; D'Atri, A.; Scarpelli, S.; Reda, F.; De Gennaro, L. Sleep Electroencephalography and Brain Maturation: Developmental Trajectories and the Relation with Cognitive Functioning. *Sleep Med.* **2020**, *66*, 33–50. [CrossRef]
43. De Gennaro, L.; Marzano, C.; Veniero, D.; Moroni, F.; Fratello, F.; Curcio, G.; Ferrara, M.; Ferlazzo, F.; Novelli, L.; Concetta Pellicciari, M.; et al. Neurophysiological Correlates of Sleepiness: A Combined TMS and EEG Study. *NeuroImage* **2007**, *36*, 1277–1287. [CrossRef]
44. Marzano, C.; Ferrara, M.; Curcio, G.; De Gennaro, L. The Effects of Sleep Deprivation in Humans: Topographical Electroencephalogram Changes in Non-Rapid Eye Movement (NREM) Sleep versus REM Sleep. *J. Sleep Res.* **2010**, *19*, 260–268. [CrossRef] [PubMed]
45. Campbell, I.G.; Feinberg, I. Longitudinal Trajectories of Non-Rapid Eye Movement Delta and Theta EEG as Indicators of Adolescent Brain Maturation. *Proc. Natl. Acad. Sci. USA* **2009**, *106*, 5177–5180. [CrossRef] [PubMed]
46. Ringli, M.; Huber, R. Developmental Aspects of Sleep Slow Waves: Linking Sleep, Brain Maturation and Behavior. *Prog. Brain Res.* **2011**, *193*, 63–82. [CrossRef] [PubMed]
47. Tarokh, L.; Carskadon, M.A. Developmental Changes in the Human Sleep EEG during Early Adolescence. *Sleep* **2010**, *33*, 801–809. [CrossRef] [PubMed]
48. Chu, C.J.; Leahy, J.; Pathmanathan, J.; Kramer, M.A.; Cash, S.S. The Maturation of Cortical Sleep Rhythms and Networks over Early Development. *Clin. Neurophysiol. Off. J. Int. Fed. Clin. Neurophysiol.* **2014**, *125*, 1360–1370. [CrossRef]
49. Somsen, R.J.; van't Klooster, B.J.; van der Molen, M.W.; van Leeuwen, H.M.; Licht, R. Growth Spurts in Brain Maturation during Middle Childhood as Indexed by EEG Power Spectra. *Biol. Psychol.* **1997**, *44*, 187–209. [CrossRef]
50. D'Atri, A.; Novelli, L.; Ferrara, M.; Bruni, O.; De Gennaro, L. Different Maturational Changes of Fast and Slow Sleep Spindles in the First Four Years of Life. *Sleep Med.* **2018**, *42*, 73–82. [CrossRef]
51. Novelli, L.; D'atri, A.; Marzano, C.; Finotti, E.; Ferrara, M.; Bruni, O.; De Gennaro, L. Mapping Changes in Cortical Activity during Sleep in the First 4 Years of Life. *J. Sleep Res.* **2016**, *25*, 381–389. [CrossRef]
52. Faraone, S.V.; Biederman, J.; Mick, E. The Age-Dependent Decline of Attention Deficit Hyperactivity Disorder: A Meta-Analysis of Follow-up Studies. *Psychol. Med.* **2006**, *36*, 159–165. [CrossRef]

53. Jenni, O.G.; Carskadon, M.A. Spectral Analysis of the Sleep Electroencephalogram during Adolescence. *Sleep* **2004**, *27*, 774–783.
54. Tononi, G.; Cirelli, C. Sleep Function and Synaptic Homeostasis. *Sleep Med. Rev.* **2006**, *10*, 49–62. [CrossRef]
55. Riedner, B.A.; Vyazovskiy, V.V.; Huber, R.; Massimini, M.; Esser, S.; Murphy, M.; Tononi, G. Sleep Homeostasis and Cortical Synchronization: III. A High-Density EEG Study of Sleep Slow Waves in Humans. *Sleep* **2007**, *30*, 1643–1657. [CrossRef] [PubMed]
56. Hubbard, J.; Gent, T.C.; Hoekstra, M.M.B.; Emmenegger, Y.; Mongrain, V.; Landolt, H.-P.; Adamantidis, A.R.; Franken, P. Rapid Fast-Delta Decay Following Prolonged Wakefulness Marks a Phase of Wake-Inertia in NREM Sleep. *Nat. Commun.* **2020**, *11*, 3130. [CrossRef] [PubMed]
57. Buchmann, A.; Ringli, M.; Kurth, S.; Schaerer, M.; Geiger, A.; Jenni, O.G.; Huber, R. EEG Sleep Slow-Wave Activity as a Mirror of Cortical Maturation. *Cereb. Cortex* **2011**, *21*, 607–615. [CrossRef] [PubMed]
58. Touchette, E.; Petit, D.; Séguin, J.R.; Boivin, M.; Tremblay, R.E.; Montplaisir, J.Y. Associations between Sleep Duration Patterns and Behavioral/Cognitive Functioning at School Entry. *Sleep* **2007**, *30*, 1213–1219. [CrossRef] [PubMed]

4.6. Supplementary material

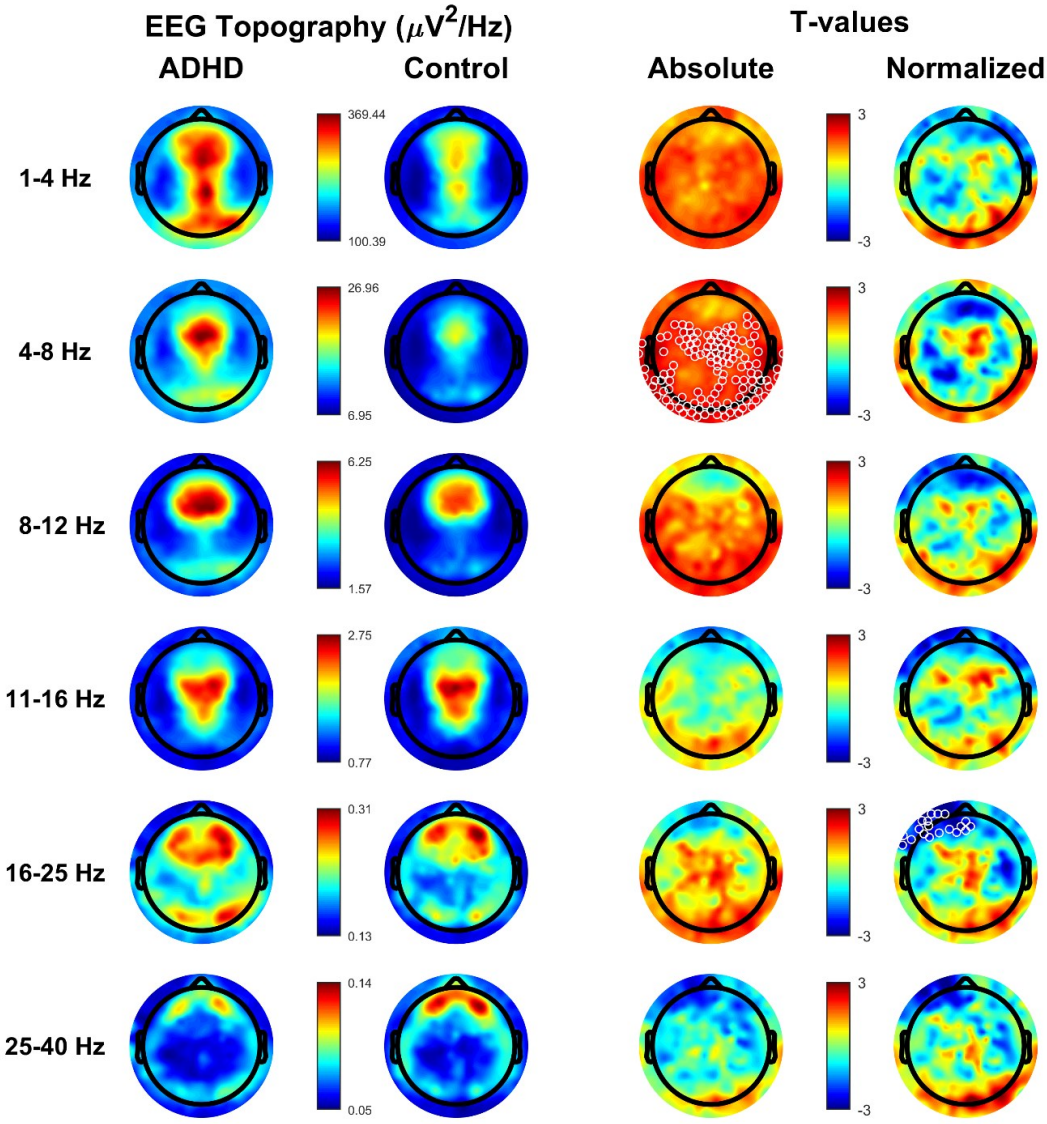

Supplementary Figure 1. Topographical distribution of all frequency bands based on whole-night non-rapid eye movement (NREM) sleep stage 2 (N2) and stage 3 (N3) in the attention-deficit/hyperactivity disorder (ADHD) group and in healthy control group.

Values are color coded and plotted on the planar projection of the hemispheric scalp model. Rows represent frequency bands of interest as indicated: Slow wave activity (SWA, 1-4 Hz), Theta (4-8 Hz), Alpha (8- 12 Hz), Sigma (11-16 Hz), Beta (18-25 Hz), Gamma (25-40 Hz). First and second column: average NREM sleep electroencephalographic (EEG) topographies across frequency bands for children with ADHD and healthy control matches, respectively. Maxima are

shown in red, minima in blue. Third and fourth column: single electrode t-value (two-tailed, unpaired) maps for the comparison between ADHD and control subjects in terms of absolute and normalized (using the z-score across all electrodes) power, respectively. A decrease in EEG power in patients with ADHD relative to healthy controls (ADHDs < controls) is represented in blue, an increase (ADHD > controls) in red. White circles indicate significant channels ($p < 0.05$, cluster-size correction).

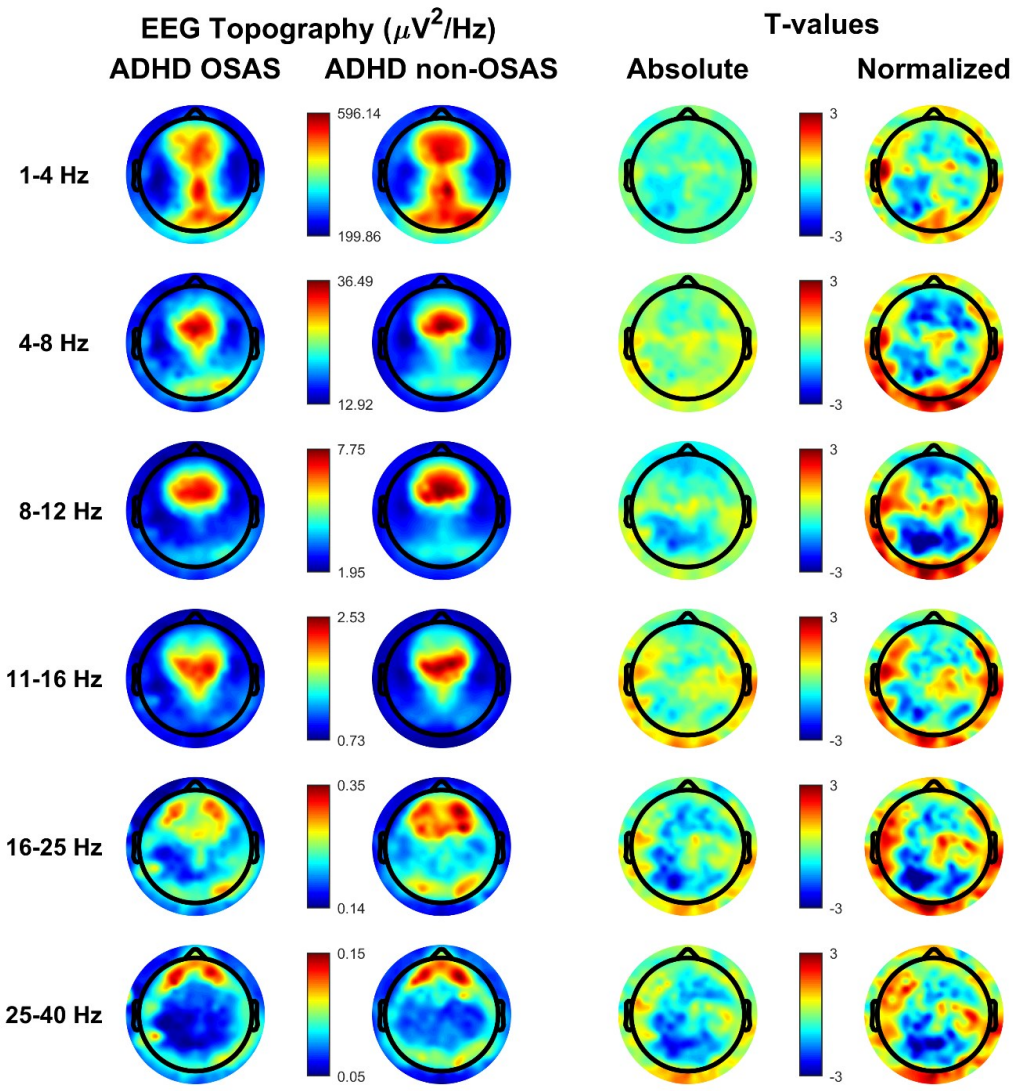

Supplementary Figure 2. Topographical distribution of all frequency bands based on whole-night non-rapid eye movement (NREM) sleep stage 3 (N3) in the attention-deficit/hyperactivity disorder (ADHD) group with and without the obstructive sleep apnea/hypo-apnea phenotype.

Values are color coded and plotted on the planar projection of the hemispheric scalp model. Rows represent frequency bands of interest as indicated: Slow wave activity (SWA, 1-4 Hz), Theta (4-8 Hz), Alpha (8- 12 Hz), Sigma (11-16 Hz), Beta (18-25 Hz), Gamma (25-40 Hz). First and second column: average N3 sleep electroencephalographic (EEG) topographies across frequency bands for children with ADHD with and without an obstructive sleep apnea/hypo-apnea phenotype, respectively. Maxima are shown in red, minima in blue. Third and fourth column: single electrode t-value (two-tailed, unpaired) maps for the comparison between ADHD and control subjects in terms of absolute and normalized (using the z-score across all electrodes) power, respectively. A decrease in EEG power in patients with ADHD with the apnea/hypo-apnea phenotype relative to in patients with ADHD without the apnea/hypo-apnea phenotype is represented in blue, an increase in red. White circles indicate significant channels ($p < 0.05$, cluster-size correction).

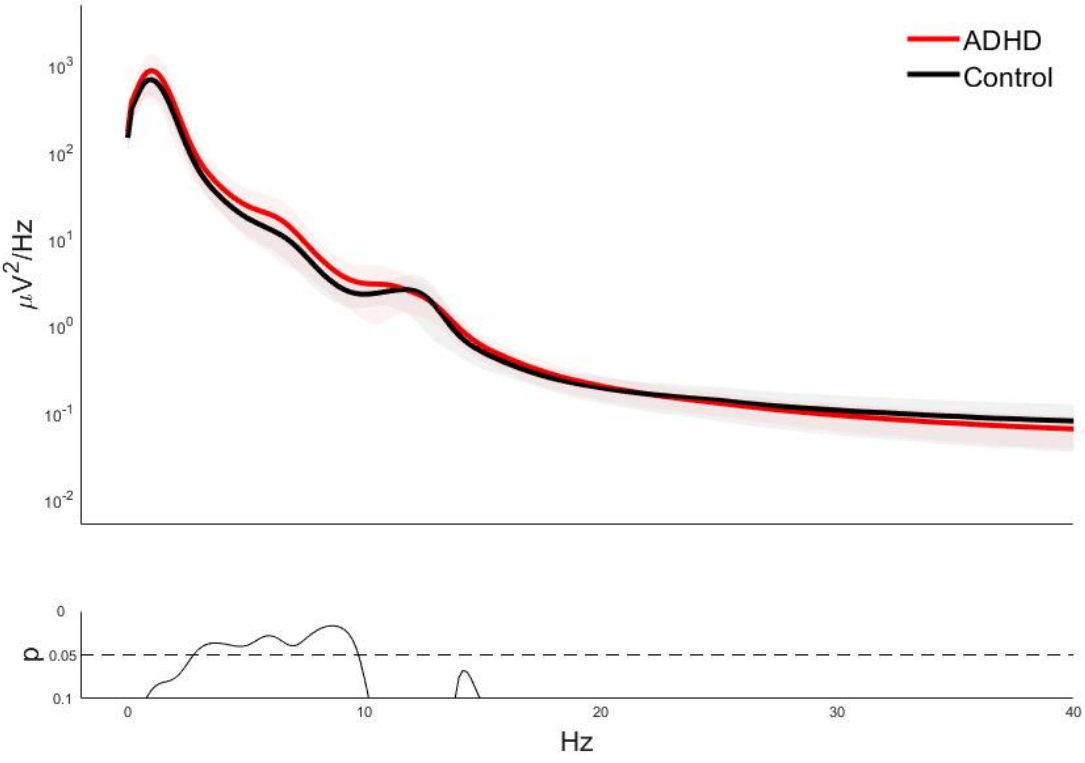

Supplementary Figure 3. Spectral power density average over all artifact free epochs in the attention-deficit/hyperactivity disorder (ADHD) group and in the healthy control group during whole-night non-rapid eye movement (NREM) sleep stage 3 (N3).

Shaded area represents standard error of the mean (SEM). Bottom graph shows p-values, reaching statistical significance between 3 and 10 Hz.

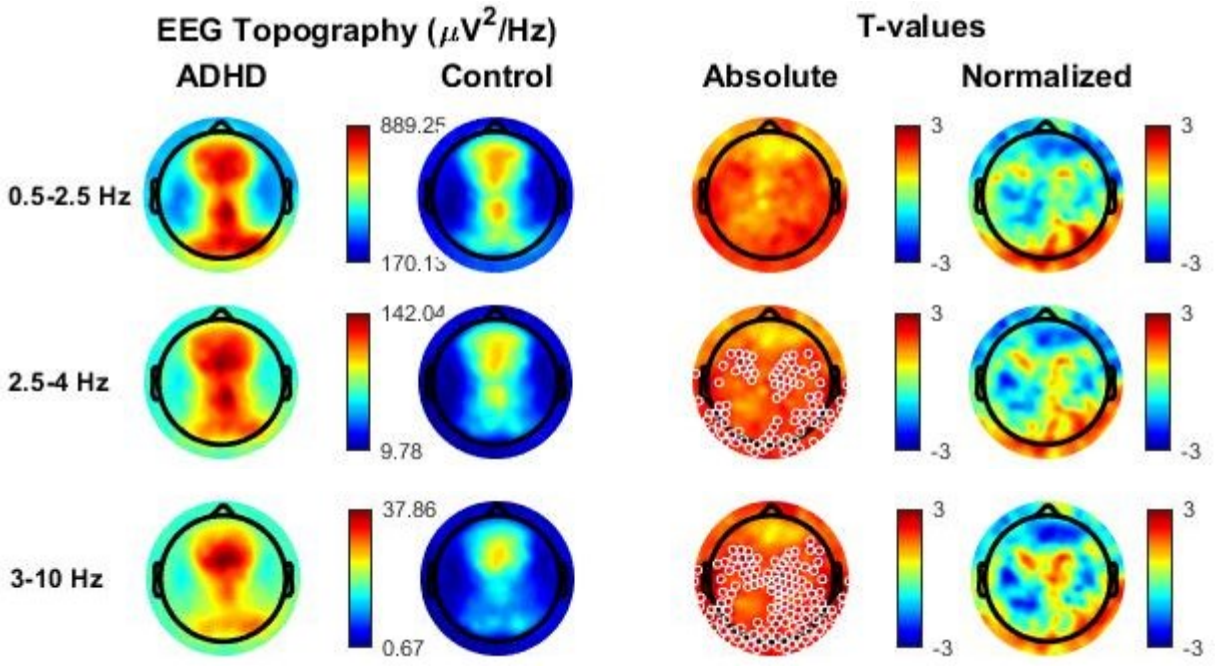

Supplementary Figure 4. Topographical distribution of alternative frequency bands based on whole-night non-rapid eye movement (NREM) sleep stage 3 (N3) in the attention-deficit/hyperactivity disorder (ADHD) group and in the healthy control group.

Values are color coded and plotted on the planar projection of the hemispheric scalp model. Rows represent frequency bands of interest as indicated on the left. The first two rows focused respectively on the low-delta (0.5-2.5 Hz) and high-delta (2.5-4 Hz) frequency ranges. The 3-10 Hz band was selected from the inspection of the average power spectra. First and second column: average N3 sleep EEG topographies across frequency bands for children with ADHD and healthy control matches, respectively. Maxima are shown in red, minima in blue. Third and fourth column: single electrode t-value (two-tailed, unpaired) maps for the comparison between ADHD and control subjects in terms of absolute and normalized (using the z-score across all electrodes) power, respectively. A lower EEG power in patients with ADHD relative to healthy controls (ADHDs < controls) is represented in blue, a higher power (ADHD > controls) in red. White circles indicate significant electrodes ($p < 0.05$, cluster-size correction).

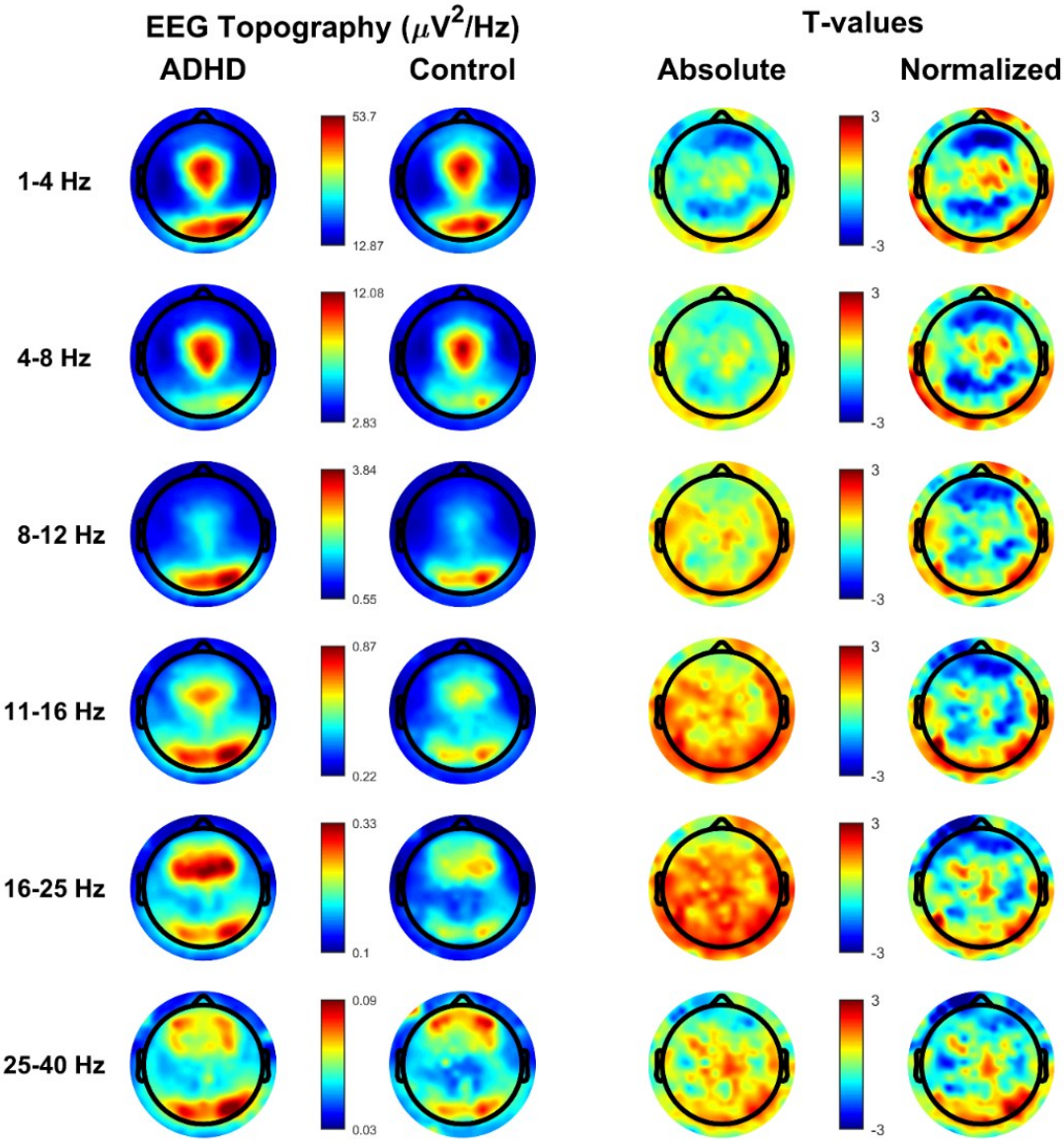

Supplementary Figure 5. Topographical distribution of all frequency bands based on whole-night rapid eye movement (REM) sleep in the attention-deficit/hyperactivity disorder (ADHD) group and in healthy control group.

Values are color coded and plotted on the planar projection of the hemispheric scalp model. Rows represent frequency bands of interest as indicated: Slow wave activity (SWA, 1-4 Hz), Theta (4-8 Hz), Alpha (8- 12 Hz), Sigma (11-16 Hz), Beta (18-25 Hz), Gamma (25-40 Hz). First and second column: average REM sleep electroencephalographic (EEG) topographies across frequency bands for children with ADHD and healthy control matches, respectively. Maxima are shown in red, minima in blue. Third and fourth column: single electrode t-value (two-tailed, unpaired) maps for the

comparison between ADHD and control subjects in terms of absolute and normalized (using the z-score across all electrodes) power, respectively. A lower EEG power in patients with ADHD relative to healthy controls (ADHDs < controls) is represented in blue, a higher power (ADHD > controls) in red. White circles indicate significant electrodes (p < 0.05 cluster-size correction).

Given that the between-subject variability in the number of REM cycles and the fact that the first REM cycle was often very short, we repeated the same analysis on the second/third cycles in 27 patients and 23 control subjects, and again found no significant differences between groups.

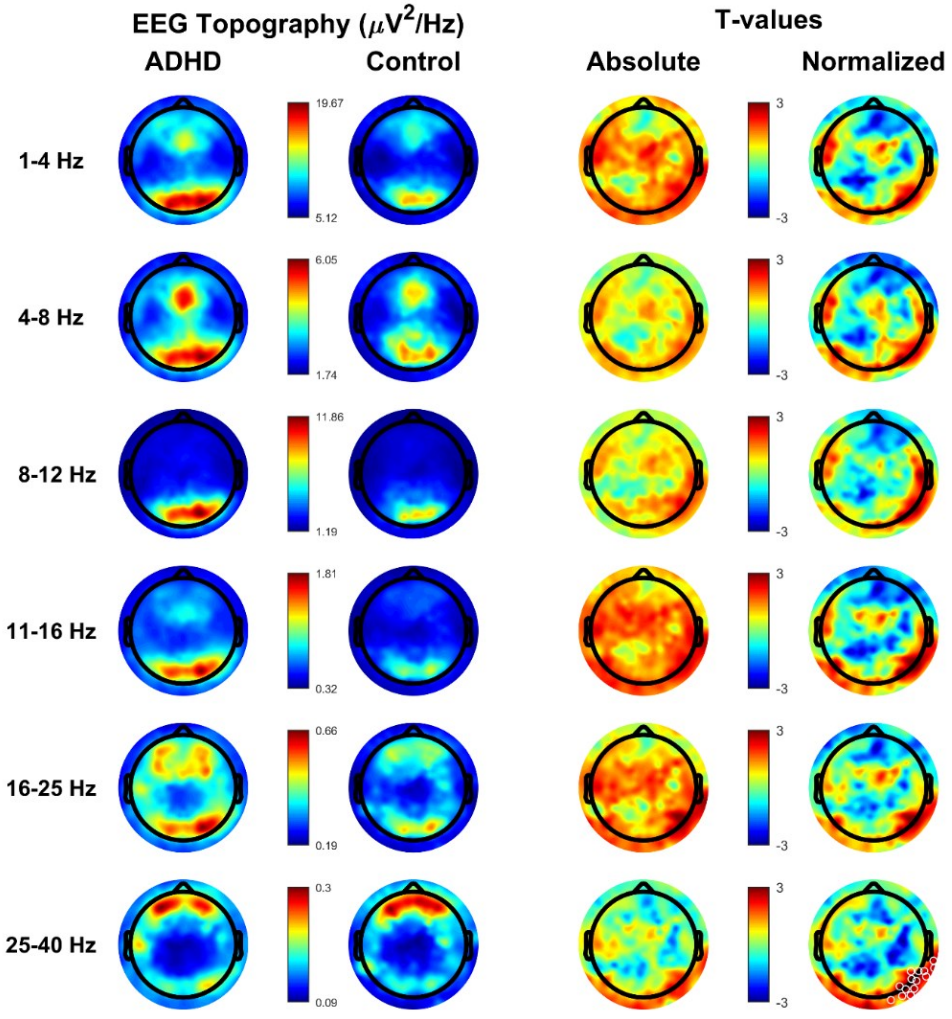

Supplementary Figure 6. Topographical distribution of all frequency bands based on wake before sleep onset in the attention-deficit/hyperactivity disorder (ADHD) group and in healthy control group.

A comparison of pre-sleep signal power between ADHD and control children was performed using all subjects who had a sufficient amount of artifact-free data in the interval comprised between 50 and 10 min before sleep onset (ADHD N = 26, HD N = 18). Three patients and 4 control subjects did not have artifact-free segments of wakefulness before sleep onset longer than 5 minutes and were therefore excluded.

Values are color coded and plotted on the planar projection of the hemispheric scalp model. Rows represent frequency bands of interest as indicated: Slow wave activity (SWA, 1-4 Hz), Theta (4-8 Hz), Alpha (8- 12 Hz), Sigma (11-16 Hz), Beta (18-25 Hz), Gamma (25-40 Hz). First and second column: average wake before sleep onset electroencephalographic (EEG) topographies across frequency bands for children with ADHD and healthy control matches, respectively. Maxima are shown in red, minima in blue. Third and fourth column: single electrode t-value (two-tailed, unpaired) maps for the comparison between ADHD and control subjects in terms of absolute and normalized (using the z-score across all electrodes) power, respectively. A lower EEG power in patients with ADHD relative to healthy controls (ADHDs < controls) is represented in blue, a higher EEG power (ADHD > controls) in red. Significant electrodes indicate as white dots ($p \leq 0.05$ using statistical nonparametric mapping suprathreshold cluster testing).

4.7. References

American Psychiatric Association. (2013). Diagnostic and statistical manual of mental disorders (5th ed.). Washington, DC: American Psychiatric Association.

Baddam, S. K. R., Canapari, C. A., Noordt, S. J. R. van, & Crowley, M. J. (2018). Sleep Disturbances in Child and Adolescent Mental Health Disorders: A Review of the Variability of Objective Sleep Markers. Medical Sciences 2018, Vol. 6, Page 46, 6(2), 46. https://doi.org/10.3390/MEDSCI6020046

Baddam, S. K. R., Canapari, C. A., van Noordt, S. J. R., & Crowley, M. J. (2018). Sleep Disturbances in Child and Adolescent Mental Health Disorders: A Review of the Variability of Objective Sleep Markers. Medical Sciences, 6(2), 46. https://doi.org/10.3390/medsci6020046

Bijlenga, D., Vollebregt, M. A., Kooij, J. J. S., & Arns, M. (2019). The role of the circadian system in the etiology and pathophysiology of ADHD: time to redefine ADHD? ADHD Attention Deficit and Hyperactivity Disorders, 11(1), 5–19. https://doi.org/10.1007/s12402-018-0271-z

Castelnovo, A., Lividini, A., Bernardi, G., Pezzoli, V., Foderaro, G., Ramelli, G. P., Manconi, M., & Miano, S. (2022). Sleep Power Topography in Children with Attention Deficit Hyperactivity Disorder (ADHD). Children (Basel, Switzerland), 9(2). https://doi.org/10.3390/CHILDREN9020197

Caye, A., Swanson, J. M., Coghill, D., & Rohde, L. A. (2019). Treatment strategies for ADHD: an evidence-based guide to select optimal treatment. Molecular Psychiatry, 24(3), 390–408. https://doi.org/10.1038/s41380-018-0116-3

Cortese, S., Faraone, S. V., Konofal, E., & Lecendreux, M. (2009a). Sleep in Children With Attention-Deficit/Hyperactivity Disorder: Meta-Analysis of Subjective and Objective Studies. Journal of the American Academy of Child & Adolescent Psychiatry, 48(9), 894–908. https://doi.org/10.1097/chi.0b013e3181ac09c9

Cortese, S., Faraone, S. v., Konofal, E., & Lecendreux, M. (2009b). Sleep in Children With Attention-Deficit/Hyperactivity Disorder: Meta-Analysis of Subjective and Objective Studies. Journal of the American Academy of Child & Adolescent Psychiatry, 48(9), 894–908. https://doi.org/10.1097/CHI.0B013E3181AC09C9

Díaz-Román, A., Mitchell, R., & Cortese, S. (2018). Sleep in adults with ADHD: Systematic review and meta-analysis of subjective and objective studies. Neuroscience & Biobehavioral Reviews, 89, 61–71. https://doi.org/10.1016/J.NEUBIOREV.2018.02.014

Faraone, S. V., Asherson, P., Banaschewski, T., Biederman, J., Buitelaar, J. K., Ramos-Quiroga, J. A., Rohde, L. A., Sonuga-Barke, E. J. S., Tannock, R., & Franke, B. (2015). Attention-deficit/hyperactivity disorder. Nature Reviews Disease Primers, 1. https://doi.org/10.1038/nrdp.2015.20

Gorgoni, M., D'Atri, A., Scarpelli, S., Reda, F., & de Gennaro, L. (2020). Sleep electroencephalography and brain maturation: developmental trajectories and the relation with cognitive functioning. Sleep Medicine, 66, 33–50. https://doi.org/10.1016/J.SLEEP.2019.06.025

Gruber, R., Xi, T., Frenette, S., Robert, M., Vannasinh, P., & Carrier, J. (2009). Sleep Disturbances in Prepubertal Children with Attention Deficit Hyperactivity Disorder: A Home Polysomnography Study. Sleep, 32(3), 343–350. https://doi.org/10.5665/SLEEP/32.3.343

Hvolby, A. (2015). Associations of sleep disturbance with ADHD: implications for treatment. ADHD Attention Deficit and Hyperactivity Disorders, 7(1), 1–18. https://doi.org/10.1007/s12402-014-0151-0

Konofal, E., Lecendreux, M., & Cortese, S. (2010). Sleep and ADHD. Sleep Medicine, 11(7), 652–658. https://doi.org/10.1016/j.sleep.2010.02.012

Lunsford-Avery, J. R., Krystal, A. D., & Kollins, S. H. (2016a). Sleep disturbances in adolescents with ADHD: A systematic review and framework for future research. Clinical Psychology Review, 50, 159–174. https://doi.org/https://doi.org/10.1016/j.cpr.2016.10.004

Lunsford-Avery, J. R., Krystal, A. D., & Kollins, S. H. (2016b). Sleep disturbances in adolescents with ADHD: A systematic review and framework for future research. Clinical Psychology Review, 50, 159–174. https://doi.org/10.1016/J.CPR.2016.10.004

Polanczyk, G. v., Willcutt, E. G., Salum, G. A., Kieling, C., & Rohde, L. A. (2014). ADHD prevalence estimates across three decades: an updated systematic review and meta-regression analysis. International Journal of Epidemiology, 43(2), 434–442. https://doi.org/10.1093/IJE/DYT261

Sharma, A., & Couture, J. (2014). A Review of the Pathophysiology, Etiology, and Treatment of Attention-Deficit Hyperactivity Disorder (ADHD). Annals of Pharmacotherapy, 48(2), 209–225. https://doi.org/10.1177/1060028013510699

Wajszilber, D., Santiseban, J. A., & Gruber, R. (2018). Sleep disorders in patients with ADHD: impact and management challenges. Nature and Science of Sleep, 10, 453–480. https://doi.org/10.2147/NSS.S163074

Wu, J. C., Gillin, J. C., Buchsbaum, M. S., Chen, P., Keator, D. B., Khosla Wu, N., Darnall, L. A., Fallon, J. H., & Bunney, W. E. (2006). Frontal Lobe Metabolic Decreases with Sleep Deprivation not Totally Reversed by Recovery Sleep. Neuropsychopharmacology 2006 31:12, 31(12), 2783–2792. https://doi.org/10.1038/sj.npp.1301166

5. PROJECT 4

5.1. Preface

In this project, I will present the application of sleep slow wave detection and traveling analysis to the schizophrenia (SCZ) spectrum disorder.

The general idea is to identify specific slow wave properties and traveling features to infer etiopathogenetic mechanisms and track pathology at its earlier stages.

5.2. SCZ

Psychotic Disorders are currently conceptualized as a spectrum of diagnoses, which includes SCZ, Schizotypal Personality Disorder, Delusional Disorder, Brief Psychotic Disorder, Schizophreniform Disorder, Schizoaffective Disorder, Substance/Medication-Induced Psychotic Disorder, Psychotic Disorder Due to Another Medical Condition, Catatonic Disorders and other specified/unspecified Schizophrenia Spectrum Disorders. Moreover, “psychotic features” are considered a specifier for bipolar disorder and depressive disorders (American Psychiatric Association, 2013), highlighting the trans-nosographic nature of psychosis.

The core feature of psychosis is the partial or total impairment of reality testing, i.e., the cognitive function that allows us to distinguish the internal world of thoughts and feelings from the external world. We constantly use this process, for example, to give answer to apparently trivial questions, such as: “what am I seeing? is it really out there or I am just imagining it?”, “does the memory of that episode when I was a child reflect something that

occurred or is it just a by-product of my imagination?". Doubts on the correct answers to these questions are often already observable in prodromal psychotic states. Hallucinations – perceptions without an object - and delusions - beliefs held with strong conviction despite superior evidence to the contrary - usually appear soon after the disruption of this function.

Among psychotic disorders, SCZ is surely the most severe form, as it is by definition also characterized by a progressive decline of cognition and global functioning (Table 1).

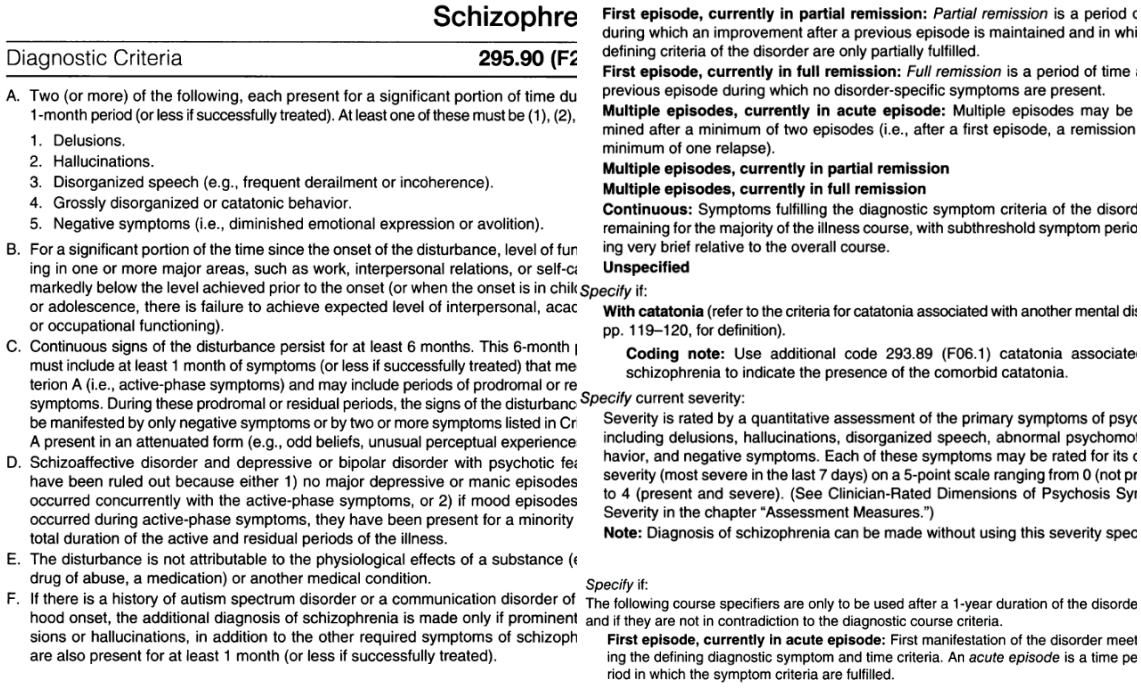

Schizophre

Diagnostic Criteria **295.90 (F2**

A. Two (or more) of the following, each present for a significant portion of time du 1-month period (or less if successfully treated). At least one of these must be (1), (2),
   1. Delusions.
   2. Hallucinations.
   3. Disorganized speech (e.g., frequent derailment or incoherence).
   4. Grossly disorganized or catatonic behavior.
   5. Negative symptoms (i.e., diminished emotional expression or avolition).

B. For a significant portion of the time since the onset of the disturbance, level of fun ing in one or more major areas, such as work, interpersonal relations, or self-ca markedly below the level achieved prior to the onset (or when the onset is in chil or adolescence, there is failure to achieve expected level of interpersonal, acac or occupational functioning).

C. Continuous signs of the disturbance persist for at least 6 months. This 6-month must include at least 1 month of symptoms (or less if successfully treated) that me terion A (i.e., active-phase symptoms) and may include periods of prodromal or re symptoms. During these prodromal or residual periods, the signs of the disturbanc be manifested by only negative symptoms or by two or more symptoms listed in Cr A present in an attenuated form (e.g., odd beliefs, unusual perceptual experience

D. Schizoaffective disorder and depressive or bipolar disorder with psychotic fea have been ruled out because either 1) no major depressive or manic episodes occurred concurrently with the active-phase symptoms, or 2) if mood episodes occurred during active-phase symptoms, they have been present for a minority total duration of the active and residual periods of the illness.

E. The disturbance is not attributable to the physiological effects of a substance (drug of abuse, a medication) or another medical condition.

F. If there is a history of autism spectrum disorder or a communication disorder of hood onset, the additional diagnosis of schizophrenia is made only if prominent sions or hallucinations, in addition to the other required symptoms of schizoph are also present for at least 1 month (or less if successfully treated).

First episode, currently in partial remission: *Partial remission* is a period during which an improvement after a previous episode is maintained and in whi defining criteria of the disorder are only partially fulfilled.

First episode, currently in full remission: *Full remission* is a period of time previous episode during which no disorder-specific symptoms are present.

Multiple episodes, currently in acute episode: Multiple episodes may be mined after a minimum of two episodes (i.e., after a first episode, a remission minimum of one relapse).

Multiple episodes, currently in partial remission

Multiple episodes, currently in full remission

Continuous: Symptoms fulfilling the diagnostic symptom criteria of the disord remaining for the majority of the illness course, with subthreshold symptom perio ing very brief relative to the overall course.

Unspecified

Specify if:

With catatonia (refer to the criteria for catatonia associated with another mental di pp. 119–120, for definition).

Coding note: Use additional code 293.89 (F06.1) catatonia associate schizophrenia to indicate the presence of the comorbid catatonia.

Specify current severity:

Severity is rated by a quantitative assessment of the primary symptoms of psyc including delusions, hallucinations, disorganized speech, abnormal psychomo havior, and negative symptoms. Each of these symptoms may be rated for its severity (most severe in the last 7 days) on a 5-point scale ranging from 0 (not pr to 4 (present and severe). (See Clinician-Rated Dimensions of Psychosis Sy Severity in the chapter "Assessment Measures.")

Note: Diagnosis of schizophrenia can be made without using this severity spec

Specify if:

The following course specifiers are only to be used after a 1-year duration of the disorde and if they are not in contradiction to the diagnostic course criteria.

First episode, currently in acute episode: First manifestation of the disorder meet ing the defining diagnostic symptom and time criteria. An *acute episode* is a time pe riod in which the symptom criteria are fulfilled.

Table 1. SCZ in DSM-5*. Right column: Diagnostic criteria. Left column: Course and severity specifiers. DSM-5* (American Psychiatric Association, 2013) *includes specifiers to identify the observed status (absent, partial or full remission from the acute phase) and the course of illness.*

SCZ has a relatively low prevalence (ranging from 0,3-0,66 to 1%) (Knapp et al., 2004; McGrath et al., 2008a, 2008b; Simeone et al., 2015), but it is ranked by the World Health Organization among the 10 leading causes of disability in adults, given its very high socio-economic costs for patients, their families and the society as a whole (Lora et al., 2012). Thus, in the last 3 decades, increasing attention has been devoted to SCZ prodromal states, in the attempt to improve early-access service provision to those in need of help, clinical management, tailored treatment strategies and follow-up programs to improve the global outcome and decrease transition rates to SCZ (Fusar-Poli et al., 2013).

Although not yet fully embedded within international criteria, the construct of clinical high-risk for psychosis (CHR-P) state for psychosis (also known as the “at-risk mental state” [ARMS], “prodromal,” and “ultra-high-risk” [UHR] state) has been increasingly recognized to describing people that present with potentially prodromal symptoms. High-Risk subjects do not appear to be a homogeneous group and they can be divided in several subcategories as shown in Figure 1. Within the CHR-P group, 3 subgroups are usually recognized: patients at high genetic risk (as SCZ is multifactorial and polygenic with a heritability approaching 80%), attenuated psychotic symptoms (APS), and brief, limited, intermitting psychotic symptoms (BLIPS). Several objective criteria have been proposed over time for the early recognition of APS and BLIPS, although a clear consensus has yet to be reached. Among others, the “Basic Symptoms” (BS) concept is used to define disturbing subjective experiences that can be observed in early-prodromal stages, before and after a first psychotic episode (Gross, 1989), while the *Comprehensive Assessment of at-Risk Mental State (CAARMS*) was developed to include an evaluation of symptoms

duration and frequency to detect later prodromal stages closer to full-blown psychosis (Yung et al., 2016).

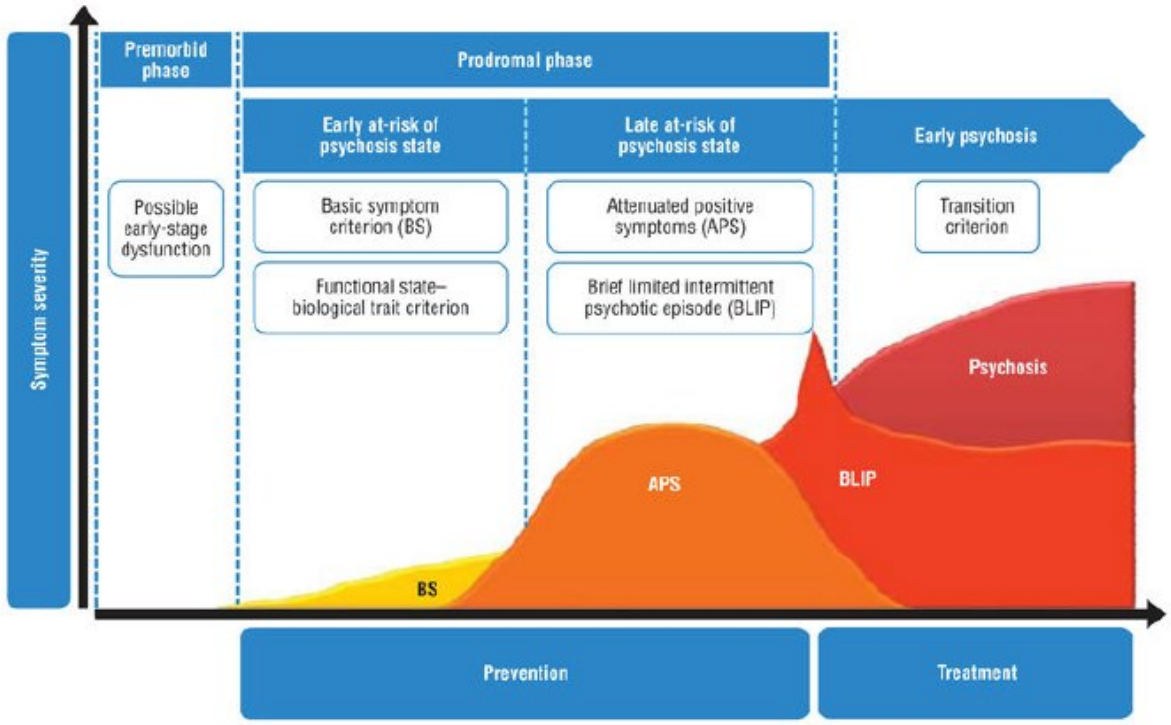

Figure 1. Prodromal stages of Schizophrenia.

During the prodromal stage, subjects can be subdivided according to the following criteria (i) Attenuated Psychotic Symptoms (APS) that must have occurred in the previous year with attenuated intensity (APSa) or frequency (APSb); (ii) Brief Limited Intermittent Psychotic symptoms (BLIP), i.e. symptoms that resolve spontaneously within a year of their onset; (iii) subjects with a SCZ trait carrying a hypothetic vulnerability to psychosis, i.e. an affected FDR and with low socio-functional status for at least a month of the previous year (Fusar-Poli et al., 2013).

5.3. Sleep in SCZ

Sleep disturbances are often subjectively reported by patients with SCZ and other psychotic disorders (Laskemoen et al., 2019). Sleep issues can often be observed in CHR-P even prior to illness onset (Zanini et al., 2015).

A recent meta-analysis concluded that patients with SCZ have consistent abnormalities of sleep continuity parameters such as total sleep time, sleep-onset latency, sleep efficiency. In terms of sleep architecture, patients have decreased slow wave sleep, increased light sleep, decreased REM duration and REM-latency and increased REMs density. Although significant, these results were highly heterogeneous across studies (Chan et al., 2017). Objective sleep abnormalities have also been reported in high-risk populations (Zanini et al., 2013) to the point that it has been suggested that disturbed sleep may help predict those who will develop psychosis among high–risk individuals.

Furthermore, emerging evidence is pointing to more specific abnormalities of sleep spindles and slow waves, the 2 hallmarks of NREM sleep (Castelnovo et al., 2018, 2016). These oscillations have the advantage of being a much more specific target compared to sleep architecture or sleep power, and to be the expression of well characterized neural circuits (see Introduction). Since sleep spindle and slow wave abnormalities appear to be associated to the clinical and cognitive dysfunctions of SCZ, reversing such sleep abnormalities using pharmacological and non-pharmacological interventions, could also have a therapeutic potential. In line with the general goal of my thesis, I herein mainly focus on sleep slow waves. Lower slow wave number/density in NREM sleep in SCZ compared to matched control subjects was previously reported in 4 small-sized studies on drug-free and/or drug-naïve patients with SCZ (Ganguli et al., 1987; Hiatt et al., 1985;

Sekimoto et al., 2011, 2007), and in one larger study on unmedicated patients with a diagnosis of SCZ Spectrum Disorder (Keshavan et al., 1998). More recently, reduced slow wave power was also observed in a sample of 26 drug-naïve early course psychosis patients during NREM sleep stage 2 (Manoach et al., 2014), and reduced slow wave density in a sample of 20 (medicated and unmedicated) early course psychosis patients during NREM sleep (Kaskie et al., 2019). However, other studies failed to report differences in slow wave properties between patients with SCZ and control subjects (Genzel et al., 2015; Göder et al., 2015; Manoach et al., 2014, 2010; Wamsley et al., 2012), perhaps due to the inclusion of a large number of patients treated with Second-Generation Antipsychotics (SGA), which are known to affect slow wave power (Castelnovo et al., 2018). While slow wave power and slow wave density and morphological parameters could be biased by several factors, traveling slow waves properties have a strong potential as they directly reflect the integrity of white matter connections.

5.4. Study aims

Despite extensive research, the pathophysiology of SCZ remains elusive. Specific symptoms, like hallucinations, have been convincingly associated with specific brain structural and functional abnormalities (Dierks et al., 1999; Hubl et al., 2010, 2004). However, SCZ complex and heterogeneous symptomatology could not be localized to specific cortical regions (Andreasen et al., 1986), nor could be attributed to the abnormal activity of the brain cortex alone (Andreasen et al., 1998). Thus, the search of a unifying physio-pathogenetic mechanism to explain the many available and often contradictory

findings remains an open challenge (Castelnovo et al., 2015). The so-called "dysconnectivity hypothesis" (Friston, 1998) offered a possible solution by pointing to a defective integration among distributed brain regions. According to this hypothesis, signs and symptoms of SCZ could be explained by the aberrant connectivity within cortico-cortical and reentrant thalamo-cortical loops, which physiologically integrate and coordinate the function of multiple cortical and subcortical structures. Based on Eugene Bleuler's original conception of disturbed integration of higher cognitive functions as the core of SCZ, this hypothesis has now begun to receive partial confirmation from neuroimaging studies (Canu et al., 2015; Huang et al., 2019; Ramsay, 2019; Sheffield et al., 2020). Given that long-range sleep slow wave traveling seems to be mainly supported by cortico-cortical white matter tracts, I propose slow wave traveling as a candidate marker of aberrant cortico–cortical/thalamocortical connectivity in SCZ.

5.5. Original paper 1

I herein enclose the first original paper that resulted from the current project, published few years ago in Schizophrenia Research (Castelnovo et al., 2020). This article shows for the first time the potential use of slow wave traveling in a sample of 16 SCZ first degree relatives and matched controls.

Schizophrenia Research 221 (2020) 37–43

Contents lists available at ScienceDirect

Schizophrenia Research

journal homepage: www.elsevier.com/locate/schres

Slow wave oscillations in Schizophrenia First-Degree Relatives: A confirmatory analysis and feasibility study on slow wave traveling

Anna Castelnovo [a,b,c,*], Matteo Zago [d], Cecilia Casetta [e], Caroline Zangani [a], Francesco Donati [a], Mariapaola Canevini [a], Brady A. Riedner [f], Giulio Tononi [f], Fabio Ferrarelli [g], Simone Sarasso [h], Armando D'Agostino [a,**]

[a] Department of Health Sciences, Università degli Studi di Milano, Italy
[b] Sleep Center, Neurocenter of Southern Switzerland, Regional Civic Hospital of Lugano, Switzerland
[c] University of Southern Switzerland, Lugano, Switzerland
[d] Department of Electronics, Information and Bioengineering, Politecnico di Milano, Italy
[e] King's College London, Department of Psychosis Studies, Institute of Psychiatry, Psychology & Neuroscience, United Kingdom of Great Britain and Northern Ireland
[f] Department of Psychiatry, University of Wisconsin, Madison, United States
[g] Department of Psychiatry, University of Pittsburgh, United States
[h] "L. Sacco" Department of Biomedical and Clinical Sciences, Università degli Studi di Milano, Italy

ARTICLE INFO

Article history:
Received 6 October 2019
Received in revised form 11 March 2020
Accepted 13 March 2020
Available online 24 March 2020

Keywords:
First-degree relatives
Psychosis
Sleep oscillations
Biomarkers
Dysconnectivity
EEG toolbox
Thalamus

ABSTRACT

Abnormal sleep oscillations have recently been proposed as endophenotypes of schizophrenia. However, optimization of methodological approaches is still necessary to standardize analyses of their microstructural characteristics. Additionally, some relevant features of these oscillations remain unexplored in pathological conditions. Among others, slow wave traveling is a promising proxy for diurnal processes of brain connectivity and excitability. The study of slow oscillations propagation appears particularly relevant when schizophrenia is conceptualized as a dys-connectivity syndrome. Given the rising knowledge on the neurobiological mechanisms underlying slow wave traveling, this measure might offer substantial advantages over other approaches in investigating brain connectivity.

Herein we: 1) confirm the stability of our previous findings on slow waves and sleep spindles in FDRs using different automated algorithms, and 2) report the dynamics of slow wave traveling in FDRs of Schizophrenia patients. A 256-channel, high-density EEG system was employed to record a whole night of sleep of 16 FDRs and 16 age- and gender-matched control subjects. A recently developed, open source toolbox was used for slow wave visualization and detection. Slow waves were confirmed to be significantly smaller in FDRs compared to the control group. Additionally, several traveling parameters were analyzed. Traveled distances were found to be significantly reduced in FDRs, whereas origins showed a different topographical pattern of distribution from control subjects. In contrast, local speed did not differ between groups.

Overall, these results suggest that slow wave traveling might be a viable method to study pathological conditions interfering with brain connectivity.

1. Introduction

At the turn of the 20th Century, Eugen Bleuler coined the term schizophrenia (SCZ) from the greek σχίζω (*schizo*, divided) and φρήν (*phren*, brain/mind), suggesting the presence of a dis-integration of fundamental brain-mind functions in affected patients. Over the past 20 years, a growing number of authors returned to this original conceptualization and described SCZ as a network disorder (Tononi and Edelman, 2000) for which neuroimaging findings are currently laying a biological foundation (Giraldo-Chica and Woodward, 2017; Kambeitz et al., 2016).

Non-Rapid Eye Movement (NREM) sleep brain oscillations, sleep spindles and sleep slow waves, are thought to reflect the anatomical and functional integrity of the thalamocortical system (Steriade, 2003) and have been increasingly associated with neuronal plasticity mechanisms (Diekelmann and Born, 2010). These sleep oscillations may represent a preferential window of observation for dynamic EEG brain

* Correspondence to: A. Castelnovo, Sleep Center, Neurocenter of Southern Switzerland, Regional Civic Hospital of Lugano, Via Tesserete 46, 6900 Lugano, Switzerland.
** Correspondence to: A. D'Agostino, Department of Health Sciences, San Paolo University Hospital, Via Antonio di Rudinì 8, 20142 Milan, Italy.
E-mail addresses: anna.castelnovo@eoc.ch (A. Castelnovo), armando.dagostino@unimi.it (A. D'Agostino).

https://doi.org/10.1016/j.schres.2020.03.025
0920-9964/

connectivity, due to the absence of fluctuating levels of attention and interfering symptoms that are known to influence experimental outcomes during wakefulness.

Sleep spindles typically appear on EEG recordings at the onset of stage 2 NREM sleep (N2) as phasic, waxing-and-waning "spindle"-shaped 12–16 Hz oscillations. These oscillations originate in the Reticular Thalamic Nuclei but are synchronized by a complex excitatory-inhibitory interplay between the thalami and the cortex (von Krosigk et al., 1993; Fuentealba and Steriade, 2005; Timofeev et al., 2000; Bonjean et al., 2011; Piantoni et al., 2016).

Slow waves, the hallmark of NREM stage 3 (N3), are high voltage 1–4 Hz waves arising from the synchronous alternation between active (up) and quiescent (down) firing states of large neuronal ensembles (Steriade, 2003). Slow wave generation has typically been attributed to the cortex (Steriade et al., 1993), although growing literature suggests a role for the thalamus in their full expression (Lemieux et al., 2014; Crunelli et al., 2015; Gent et al., 2018a). Slow waves propagate across the scalp in highly reproducible patterns, typically along the antero-posterior axis (Massimini et al., 2004). These oscillations and their traveling have been linked to the integrity of white matter tracts (Buchmann et al., 2011; Piantoni et al., 2013; Kurth et al., 2017; Schoch et al., 2018) and increasing evidence suggests they might be a fingerprint of brain connectivity (Kurth et al., 2017).

Sleep oscillations have been extensively explored in SCZ, and impaired spindle density has been the most consistent finding (Castelnovo et al., 2016, 2018; Zhang et al., 2019; Kaskie and Ferrarelli, 2019). However, results are not unanimous, especially among the few papers addressing early-course psychosis. The literature on slow waves is less conspicuous and findings lack consistency, perhaps due to pharmacological and/or methodological confounding effects (see Castelnovo et al., 2018 for a discussion on this topic). One study of five unmedicated SCZ patients reported reduced slow wave density and amplitude which was most prominent in the first cycle, in the context of a loss of physiological homeostatic decrease across cycles (Hiatt et al., 1985). Reduced delta power, slow wave number and density (only in the first cycle) were confirmed in a larger sample including 19 drug-naïve patients (Keshavan et al., 1998). A trend towards reduced delta sleep was also reported in another small sample of drug–naïve patients diagnosed with Schizophreniform Disorder (Poulin et al., 2008). A clear slow wave sleep (SWS) deficit was found in 15 unmedicated, chronic SCZ patients with profound disturbances of sleep continuity and architecture (Yang and Winkelman, 2006). Reduced delta power was also reported in a sample of early-course psychosis patients but it did not significantly differentiate SCZ from other psychotic disorders (Manoach et al., 2014). Furthermore, some authors attempted to clarify the relationship between slow waves and cognitive processing in SCZ. Reduced SWS was found to correlate with visuospatial memory impairment in SCZ patients (Göder et al., 2004); the same group also reported a reduction of delta power in the same population, restricted to temporal and occipital channels (Göder et al., 2006). More recently, preserved slow wave densities and amplitudes were reported in chronic, medicated patients who did, however, lack learning-dependent coordination of slow wave activity across the cortex (Bartsch et al., 2019). Notably, a reduced slow wave density in channels overlying a vast prefrontal area has been recently reported using high–density electroencephalography (hdEEG) in early-course psychosis (Kaskie et al., 2019).

Sleep abnormalities have also been investigated in SCZ First-Degree Relatives (FDRs) (D'Agostino et al., 2018; Schilling et al., 2016; Manoach et al., 2014; Sarkar et al., 2010; Keshavan et al., 2004), who exhibit neuroanatomical (Capizzano et al., 2011), neurofunctional (Giraldo-Chica and Woodward, 2017; Kambeitz et al., 2016; Whitfield-Gabrieli et al., 2009), neurophysiological (Earls et al., 2016) and neurocognitive (Sitskoorn et al., 2004; Snitz et al., 2005) profiles similarly to their affected relatives. We previously reported subtle abnormalities of sleep oscillations in this population that may represent a marker of susceptibility to SCZ (D'Agostino et al., 2018).

Despite a generally positive progression, the field of sleep oscillations in the SCZ spectrum remains largely open to debate due to partially inconsistent results. As with several other biomarkers, this might be related to the intrinsic heterogeneity of the selected samples in terms of clinical stage and presentation, genetic load and medication regimens. Moreover, the majority of available studies employed different analysis methods that somewhat limit the possibility of comparing data (Castelnovo et al., 2018).

To address this methodological issue, here we aimed to confirm our previous findings on sleep oscillation abnormalities in FDRs through a standardized and easily reproducible approach which employs a novel and accessible tool for the detection of sleep oscillations. We also aimed to explore the feasibility of adopting slow wave traveling as an effective measure of brain dysconnectivity in SCZ by evaluating its use in FDRs.

2. Materials and method

2.1. Participants

Sixteen adult healthy FDRs of patients diagnosed with SCZ (50% males, age 48.5 ± 14.2) and sixteen age- and gender-matched control subjects (50% males, age 49.8 ± 12.7) with no personal or family history of psychiatric disorders were included in the analyses. History of developmental, neurologic, psychiatric and sleep disorders and use of any drug interfering with CNS functioning were excluded. The same population was used in our previous publication on sleep spindles and slow waves (D'Agostino et al., 2018), where further details on cognition, perceptual experiences and general medical status are available. The study was approved by the San Paolo Hospital ethics committee and by the University of Wisconsin Health Sciences Institutional Review Board.

2.2. Sleep EEG data acquisition

All-night sleep recordings were acquired with a hd-EEG system (Electrical Geodesic Sensor Net for long-term monitoring, 256 channels). Lights-out was within one hour of the participants' reported bedtime, and subjects were allowed to sleep ad libitum. EEG recordings were scored according to AASM criteria (Iber et al., 2007) and reviewed by a sleep expert (AC). All EEG signals were collected at 500 Hz and high-pass filtered at 0.1 Hz. Recording procedures and pre-processing routines used to remove bad channels and artifacts were detailed elsewhere (D'Agostino et al., 2018).

2.3. NREM sleep oscillations analysis

Microstructural sleep oscillatory activity was analyzed with an open-source, Matlab-based user-friendly toolbox that offers the possibility to standardize the detection procedure (Mensen et al., 2016). The toolbox allows us to specify a large number of parameters for the detection of slow waves (e.g. the amplitude threshold, the minimum slow wave length or the minimum traveled distance to classify an EEG oscillation as a slow wave). Thanks to the optimization of its Matlab code, it also offers the possibility to rapidly compare outputs. Results were consistent across methods as assessed by an exploratory preliminary analysis (see Fig. 1). Findings on mastoid-referenced data obtained using parameters proposed as "default" by the toolbox will be presented here. The algorithm and the parameters employed to detect slow waves is detailed extensively elsewhere (Mensen et al., 2016) and will be briefly summarized here.

The canonical wave was derived from the calculation of the negative envelope — i.e. the mean activity of the most negative 2.5% of channels at each sample independently in the time series. Individual slow waves in the canonical wave were detected starting from its local minima, that were also used as initial points to inspect further wave properties. Data-driven, dynamic amplitude thresholds were applied (5 standards

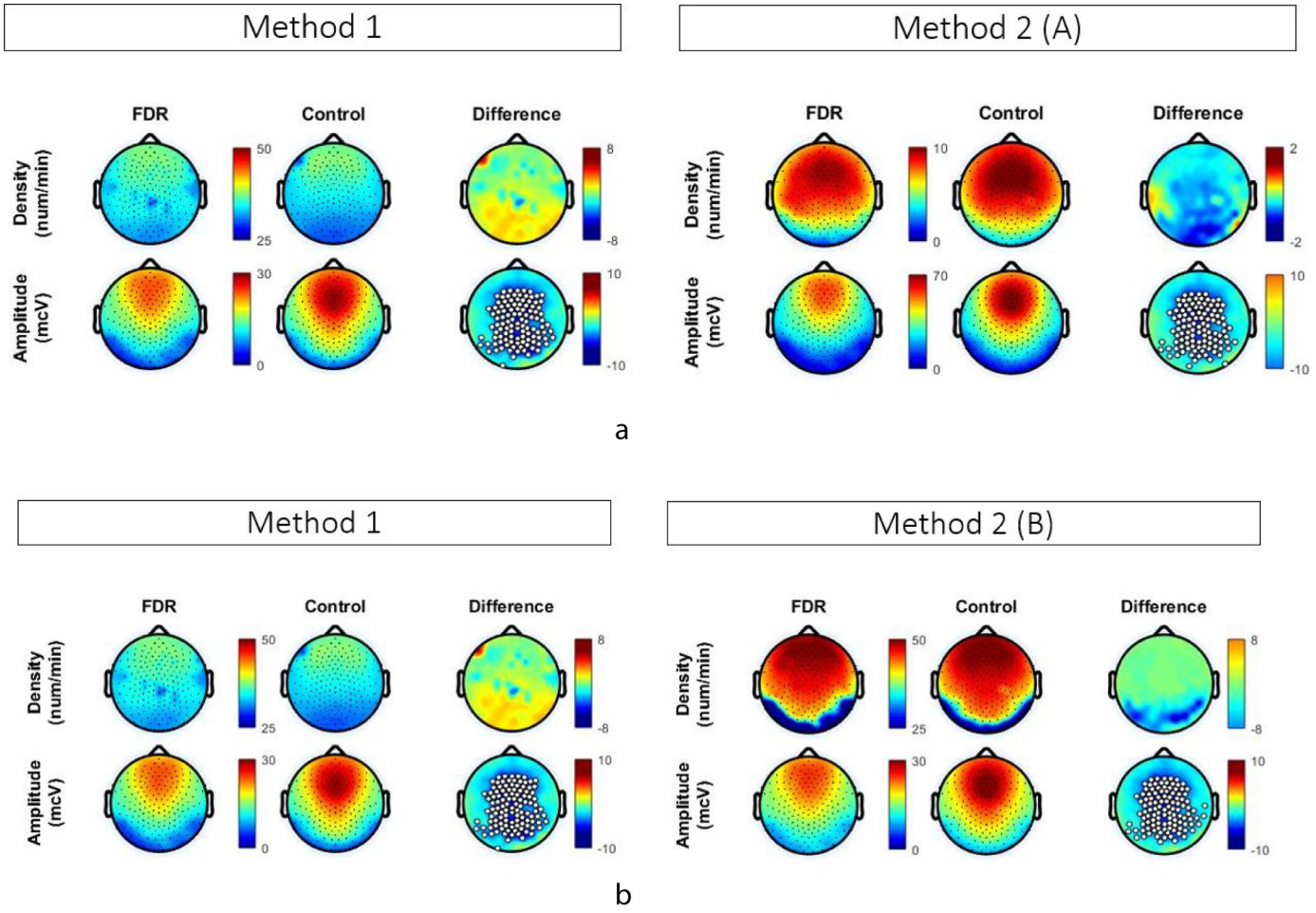

Fig. 1|. A comparison of two slow wave detection methods. Method 1 is based on the slow wave detection algorithm described by Riedner et al., 2007 (Riedner et al., 2007), which was used in our previous work (D'Agostino et al., 2018). Method 2 is the output obtained with the novel toolbox (https://github.com/Mensen/swa-matlab) using default parameters described in Methods section (A) and a set of parameters chosen to reproduce previous analysis as closer as possible to Method 1 (B). Intergroup-comparison results were comparable between the 2 methods. FDR: first degree relatives; Control: age and gender matched control group. Density: number of sleep slow waves over time (minutes). Amplitude: negative peak amplitude in mcV.

deviations of the median amplitude). Defaults for the minimum and maximum wavelength for the canonical wave were 250 ms and 1250 ms, respectively. A correlation method was used for the detection of slow waves at each individual channel, i.e. slow waves at the single-channel level were detected by cross-correlating the negative portion of the canonical wave with the individual channels over a specified time window.

Traveling properties of each slow wave were derived from a delay map obtained interpolating individual delays over the scalp (across "active" channels) on a 40 ∗ 40-unit grid. Although delay maps already offer meaningful information about traveling, average delay maps might be influenced by a number of factors, as the direction of traveling and traveled distance. Therefore, we decided to investigate three other traveling parameters: origins, traveled distance and local speed.

All potential streamlines for each traveling wave were calculated using each channel's coordinates as a seed to examine the optimal streamlines to and from the channel. Only 3 streamlines are retained by the toolbox: (1) the one with the longest linear displacement (the distance between the starting and ending points of the wave), (2) the one with the longest distance traveled (the cumulative sum of all coordinates of the line) if different from the longest displacement, and (3) the stream of most angular deviation from the longest displacement. Given the current lack of a standardized method or theoretical background to choose a streamline over others, we used the first one (1) in line with other authors that previously published on this topic (Massimini et al., 2004; Kurth et al., 2017). All potential waves that traveled for less than a minimum traveling time (set at 40 ms, i.e. approximately 0.8 cm considering a traveling speed of 2 m/s from previous studies) were discarded.

Origins were calculated as the first point of each streamline. As streamlines were calculated on a 40 ∗ 40 grid, in order to plot them we then recalculated the number of origins at each electrode as the sum of the origins in the grid falling within a radius equal to the distance between each neighboring electrode (stable in the system of coordinates adopted for Electrical Geodesic Sensor Net).

To calculate the local speed (i.e. the speed of a wave at each particular electrode), the highest possible number of streamlines was needed to cover the entire scalp. Therefore, we implemented the toolbox saving all streamlines in the final output along with the three described above. Local speed was estimated from the 40 ∗ 40 grid delay map, calculating the space unit grid divided by the time gradient, i.e. the difference between two consecutive tiles of the grid, on the x and y axes. We than calculated the local speed vector in units/s for each tile as the vector sum of the x and y speed vectors.

Of note, we focused our analysis on whole-night stage 3 sleep and repeated an exploratory analysis for sleep stage 3 in first cycle, because this latter sleep period was comparable between the two groups in terms of sleep architecture (see Supplementary Figs. 1 and 2).

Although the main focus of the study was on sleep slow waves, we also performed a confirmatory analysis on sleep spindles (see

Supplementary Fig. 3). The toolbox allows to detect sleep spindles by implementing a published Wavelet-based algorithm that has been found to outperform other 4 (published) automated spindles detectors, including the one reported in our previous study (Warby et al., 2014).

For topographical analysis, we applied statistical nonparametric mapping and a suprathreshold cluster analysis to control for multiple comparisons (Nichols and Holmes, 2002) using an appropriate threshold t-value ($t = 2.042$, corresponding to $\alpha = 0.05$ for the given degrees of freedom) with fixed number of combinations (n = 50,000).

3. Results

Slow wave density during whole-night NREM sleep was comparable between FDRs and the control group, whereas slow wave amplitude was reduced in FDRs with both slow wave detection algorithms (see Fig. 1), validating our previous results. Findings on density (absence of significant differences in absolute and normalized values) and amplitude (a large cluster of 85 channels showing reduced absolute values, $p = 0.0152$) were stable during sleep stage 3 (see Fig. 2). Likewise, we were able to confirm the lack of spindle density deficits in FDRs compared to control subjects, and the reduction of spindle power (see Supplementary Fig. 1 for details) we previously found in the same sample using a completely different algorithm.

Findings related to slow wave traveling during stage N3 are summarized in Fig. 2. FDRs showed increased mean delay values over the midline from central to posterior regions and increased values over frontal regions. However, when looking at absolute topographical maps these findings only showed a trend towards significance (18 channels, $p = 0.0907$ after multiple-comparison correction). Normalized values (z-scores obtained subtracting the mean and dividing for the standard deviation) reached significance over the midline cluster (25 channels, $p = 0.0099$, after multiple comparison correction). No correlation was observed between mean delay and amplitude values.

The topographical map of origins, expressed as a percentage of the sum of values across channels (a measure of normalization), showed a significant increase over frontal regions (n = 13, $p = 0.001$) and a strong decrease over midline central and posterior regions (9 channels,

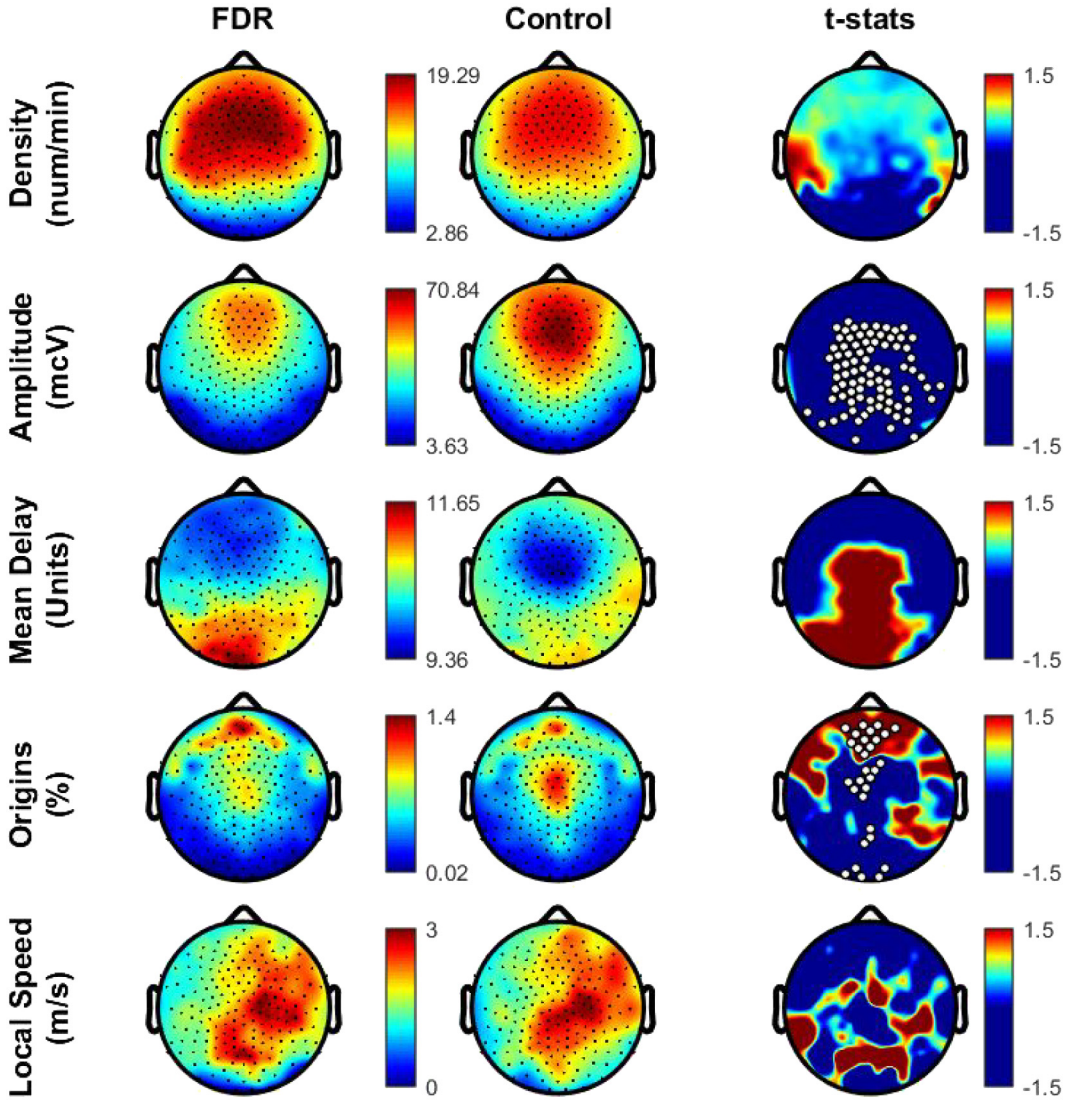

Fig. 2|. Topographical maps of slow wave parameters during whole night sleep stage N3. FDR: schizophrenia first degree relatives. Control: age and gender matched control group. *t*-Stats: map showing the individual electrode *t*-value (two-tailed, unpaired) maps for the comparison between FDR and control subjects in terms of absolute values. First row: slow wave density (number per hour of N3 sleep) at each channel. Second row: slow wave mean amplitude (average of negative peaks values for each channel). Third to six rows: topographical maps of slow wave traveling parameters. Third row: slow wave average delays (delays at individual channels obtained correlating the canonical wave to individual channel slow waves). Fourth row: slow wave origins (expressed as density, i.e. number of slow waves per minute). Fifth row: local speed (the speed of a wave at each particular electrode). Blue: FDR < control. RED: FDR > control. White dots: significance ($p < 0.05$) at the cluster level (after multi-comparison correction).

$p = 0.012$ and 8 channels, $p = 0.021$, respectively). These results paralleled the distribution of the delay maps, that showed much shorter delays in the front compared to the back. In contrast, local speed was no different between groups.

As shown in Fig. 3, traveled distance differed significantly between FDRs and control subjects (2-tailed unpaired t-test, $p = 0.043$). As amplitude and traveled distance are known to be modulated by across-night dynamics, we performed the same analyses during the first NREM sleep cycle, where N3 activity is maximal. We were able to confirm similar findings when N3 sleep of the first NREM sleep cycle was analyzed (see Supplementary Figs. 1 and 2).

4. Discussion

A significant reduction in slow wave amplitude combined with an unaltered slow wave density confirmed our previous slow wave report in SCZ FDRs (D'Agostino et al., 2018). We previously noticed that, unlike the consistency of findings reported across SCZ samples for sleep spindles, slow wave data remain controversial, possibly due to the diverse methodological approaches employed by different groups (Castelnovo et al., 2018). Conducting replication studies is critical to establish credible scientific evidence, even when converging lines of evidence and solid theoretical hypotheses support original data (Nickerson, 2018).

We also observed a reduction of slow wave traveled distances in the FDR sample compared to healthy individuals with a negative familiar history. Shorter propagation distances likely reflect dysfunctional long-range connectivity among distributed cortical regions. Evidence suggest that slow wave propagation parameters are linked to white matter microstructure (Kurth et al., 2017), whereas new research has begun to unveil a role for the thalamus in the coordination of sleep oscillations (Gent et al., 2018a). Specifically, recent optogenetic research revealed that burst activation of centro-medial thalamic neurons mimics Up-states in the cingulate cortex and enhances diffuse synchronization of cortical slow waves during sleep through a relay in the antero-dorsal thalamus (Gent et al., 2018b).

We previously hypothesized that disrupted cortical synchronization might increase the risk of developing SCZ, although thalamic dysfunction reflected by the well-established impairment of sleep spindle generation may be necessary for the disease onset. Current results do not contradict this interpretation as it seems plausible that both cortico-cortical and thalamocortical connectivity regulate slow wave traveling.

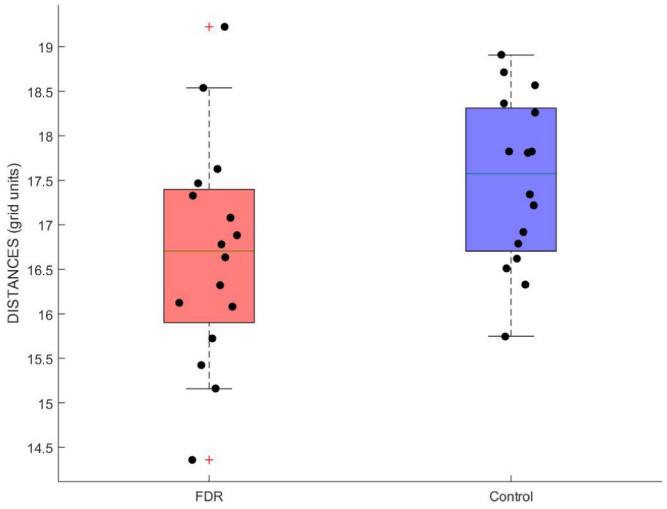

Fig. 3|. Traveled slow wave distance during whole night sleep stage N3. Distance was calculated as the line of longest displacement. Units of measurement are referred to a grid of 40 * 40 tiles. FDR: schizophrenia first degree relatives. Control: age and gender matched control group.

Although further research is needed, a larger impairment in slow wave traveling associated with major abnormalities in sleep spindle density is expected in patients with SCZ.

We also reported abnormality of slow wave origins in FDRs, with an increase over frontal regions and a strong decrease over midline central and posterior regions compared to control subjects. Should these properties of slow wave traveling be confirmed in SCZ patients, they might reflect the connectivity impairment that has extensively been shown during wakefulness. Although several hypotheses remain to be tested and these preliminary results only support a speculative discussion, we suggest that the increased number of slow wave frontal origins in FDRs might be a compensatory mechanism for the relative lack of central and posterior activity and the global reduction of speed and traveled distance. Further studies exploring slow wave traveling and its origins in SCZ patients are necessary to confirm this hypothesis.

Finally, SWS is crucial for the consolidation of memories (Stickgold, 2005) and has been specifically associated with the consolidation of declarative memories (Marshall et al., 2006). Although sleep-dependent consolidation was not tested in our sample, other studies have shown FDRs share similar deficits with patients during a word-pairs association task (Denis et al., 2018) and in declarative memory (Whyte et al., 2005). Future studies should assess whether reduced amplitude and propagation dynamics of slow waves in FDRs also reflect the specific abnormalities of memory processing observed in this population.

The present study has some limitations. First, the sample size was relatively small ($N = 16$ in each group), albeit in line with available studies including whole-night sleep data in FDRs, which range from 13 to 19 (Sarkar et al., 2010; Manoach et al., 2014; Schilling et al., 2016). Furthermore, this has been considered adequate to detect large effect sizes, while desensitizing inference to small effect sizes, for classical inference based on α (Friston, 2012). Another potential limitation was that the sleep macrostructure was found to differ between the two groups. Altered parameters such as duration of stages N2 and N4, reduced TST and low sleep quality have previously been reported in FDRs compared to healthy control populations (Sarkar et al., 2010; Manoach et al., 2014; Schilling et al., 2016). However, we have previously shown that differences in architecture are unlikely to affect slow-wave analysis due to the lack of difference observed between the two samples in terms of density (D'Agostino et al., 2018). In order to control for this potential bias, similar results have been replicated for the first cycle, within which sleep architecture parameters were comparable between groups (see Supplementary Figs. 2 and 3). Finally, although our analysis should be considered confirmatory, we acknowledge that other results might be obtained with different samples even if the same methods are applied. This limitation reflects the intrinsic variability of the population studied, which putatively differs in terms of genetic susceptibility to SCZ across samples.

Despite these limitations, the use of standardized and open source methods for the analysis of sleep oscillations is critical to boost reproducibility of results and comparability across studies. Overall, the results of the current analysis on slow wave traveling are encouraging and could unfold a novel path for future research in patients with SCZ and related disorders. Although functional MRI measures have clearly begun to dissect abnormal connectivity in SCZ, the slow temporal resolution of hemodynamic responses is known to limit this technique (Houck et al., 2017). EEG-based measures can complement imaging findings to capture the full extent of functional connectivity abnormalities in SCZ. In addition to the exquisite temporal resolution of all EEG measures, sleep parameters reflect the spontaneous activity of a brain detached from its environment, which reaches its peak of autonomous "offline" processing during slow waves sleep. Along with several other groups, we encourage access to this privileged window of enquiry to further unravel the neural circuitry underlying SCZ. Emerging findings will eventually allow us to design novel pharmacological and non-pharmacological strategies to alleviate symptoms by targeting sleep abnormalities (Zhang et al., 2019; Kaskie et al., 2019).

5. Conclusions

The study of slow wave traveling is rapidly evolving into a successful, noninvasive analysis method of brain connectivity that might enhance the understanding of neurodevelopmentally abnormal trajectories (Kurth et al., 2017). This pattern has never been studied in disorders typically associated with disrupted brain connectivity such as SCZ.

The refined spatiotemporal resolution of hd-EEG signal coupled with the lack of wake-related confounds during sleep make traveling slow wave oscillations a highly promising candidate marker for SCZ. Future studies will need to confirm the stability of our findings in larger samples of FDR, as well as to assess slow wave traveling deficits in SCZ patients, which may lead to the discovery of pathogenetic and prognostic biomarkers for SCZ and related psychotic disorders.

Contributions

AC and ADA designed the study, wrote the protocol and drafted the manuscript. AC conducted EEG analyses, aided by MZ and BAR. CC, CZ and FD recruited participants and performed sleep EEG recordings. MC guaranteed all sleep recording procedures at her site. BAR and GT provided the EEG equipment across both experimental sites and, together with FF, were responsible of data collected at their location. FF and SS supervised experimental procedures and contributed critical advice on the discussion of findings. All authors critically reviewed the manuscript.

Role of the funding source

The authors received no specific funding for this work.

Declaration of competing interest

The authors have no conflict of interest to declare.

Acknowledgements

We thank all participants and their families; we thank Progetto Itaca Foundation for their support.

We thank Simone Cavallotti and Matteo Marcatili for their contribution to data acquisition in the early stages of the study. We are grateful to Armand Mensen for the development of the toolbox used in for the detection of sleep oscillations and his precious clarifications and advices.

Appendix A. Supplementary data

Supplementary data to this article can be found online at https://doi.org/10.1016/j.schres.2020.03.025.

References

Bartsch, U., Simpkin, A.J., Demanuele, C., Wamsley, E., Marston, H.M., Jones, M.W., 2019. Distributed slow-wave dynamics during sleep predict memory consolidation and its impairment in schizophrenia. NPJ Schizophr. 5 (18).

Bonjean, M., Baker, T., Lemieux, M., Timofeev, I., Sejnowski, T., Bazhenov, M., 2011. Corticothalamic feedback controls sleep spindle duration in vivo. J. Neurosci. 31 (25), 9124–9134. https://doi.org/10.1523/JNEUROSCI.0077-11.2011.

Buchmann, A., Kurth, S., Ringli, M., Geiger, A., Jenni, O.G., Huber, R., 2011. Anatomical markers of sleep slow wave activity derived from structural magnetic resonance images. J. Sleep Res. 20 (4), 506–513. https://doi.org/10.1111/j.1365-2869.2011.00916.x.

Capizzano, A.A., Toscano, J.L.N., Ho, B.C., 2011. Magnetic resonance spectroscopy of limbic structures displays metabolite differences in young unaffected relatives of schizophrenia probands. Schizophr Re 131 (1), 4–10.

Castelnovo, A., D'Agostino, A., Casetta, C., Sarasso, S., Ferrarelli, F., 2016. Sleep spindle deficit in schizophrenia: contextualization of recent findings. Curr Psychiatry Re 18 (8), 72. https://doi.org/10.1007/s11920-016-0713-2.

Castelnovo, A., Graziano, B., Ferrarelli, F., D'Agostino, A., 2018. Sleep spindles and slow waves in schizophrenia and related disorders: main findings, challenges, and future perspectives. Eur. J. Neurosci., 1–21 https://doi.org/10.1111/ejn.13815.

Crunelli, V., David, F., Lőrincz, M.L., Hughes, S.W., 2015. The thalamocortical network as a single slow wave-generating unit. Curr. Opin. Neurobiol. 31, 72–80. https://doi.org/10.1016/j.conb.2014.09.001.

D'Agostino, A., Castelnovo, A., Cavallotti, S., Casetta, C., Marcatili, M., Gambini, O., et al., 2018. Sleep endophenotypes of schizophrenia: slow waves and sleep spindles in unaffected first-degree relatives. NPJ Schizophr. 4 (1), 2. https://doi.org/10.1038/s41537-018-0045-9.

Denis, D., Sato, E., Larson, O., Kohnke, E.J., Parr, E., King, J., et al., 2018. Sleep dependent memory consolidation in early course schizophrenia patients and familial high-risk relatives. Sleep 41 (S1), A369–A370.

Diekelmann, S., Born, J., 2010. The memory function of sleep. Nat. Rev. Neurosci. 11 (2), 114–126. https://doi.org/10.1038/nrn2762.

Earls, H.A., Curran, T., Mittal, V., 2016. A meta-analytic review of auditory event-related potential components as endophenotypes for schizophrenia: perspectives from first-degree relatives. Schizophr. Bull. 42 (6), 1504–1516.

Friston, K., 2012. Ten ironic rules for non-statistical reviewers. Neuroimage 61 (4), 1300–1310.

Fuentealba, P., Steriade, M., 2005. The reticular nucleus revisited: intrinsic and network properties of a thalamic pacemaker. Prog. Neurobiol. 75 (2), 125–141.

Gent, T.C., Bassetti, C., Adamantidis, A.R., 2018a. Sleep-wake control and the thalamus. Curr. Opin. Neurobiol. 52, 188–197. https://doi.org/10.1016/j.conb.2018.08.002.

Gent, T.C., Bandarabadi, M., Herrera, C.G., Adamantidis, A.R., 2018b. Thalamic dual control of sleep and wakefulness. Nat. Neurosci. 21 (7), 974–984.

Giraldo-Chica, M., Woodward, N.D., 2017. Review of thalamocortical resting-state fMRI studies in schizophrenia. Schizophr. Res. 180, 58–63. https://doi.org/10.1016/j.schres.2016.08.005.

Göder, R., Boigs, M., Braun, S., Friege, L., Fritzer, G., Aldenhoff, J.B., Hinze-Selch, D., 2004. Impairment of visuospatial memory is associated with decreased slow wave sleep in schizophrenia. J. Psychiatr. Res. 38 (6), 591–599.

Göder, R., Aldenhoff, J.B., Boigs, M., Braun, S., Koch, J., Fritzer, G., 2006. Delta power in sleep in relation to neuropsychological performance in healthy subjects and schizophrenia patients. J Neuropsychiatry Clin Neurosci 18 (4), 529–535.

Houck, J.M., Çetin, M.S., Mayer, A.R., Bustillo, J.R., Stephen, J., Aine, C., Cañive, J., Perrone-Bizzozero, N., Thoma, R.J., Brookes, M.J., Calhoun, V.D., 2017. Magnetoencephalographic and functional MRI connectomics in schizophrenia via intra- and inter-network connectivity. Neuroimage 145, 96–106 Pt A.

Iber, C., Ancoli-Israel, S., Chesson, A., Quan, S., 2007. The AASM Manual for the Scoring of Sleep and Associated Events: Rules, Terminology and Technical Specifications. First edition. American Academy of Sleep Medicine, Westchester, IL.

Kambeitz, J., Kambeitz-Ilankovic, L., Cabral, C., Dwyer, D.B., Calhoun, V.D., van den Heuvel, M.P., et al., 2016. Aberrant functional whole-brain network architecture in patients with schizophrenia: a meta-analysis. Schizophr. Bull. 42 (S1), S13–S21. https://doi.org/10.1093/schbul/sbv174.

Kaskie, R.E., Ferrarelli, F., 2019. Sleep disturbances in schizophrenia: what we know, what still needs to be done. Curr. Opin. Psychol. 34, 68–71. https://doi.org/10.1016/j.copsyc.2019.09.011.

Kaskie, R.E., Gill, K.M., Ferrarelli, F., 2019. Reduced frontal slow wave density during sleep in first-episode psychosis. Schizophr. Res. 206, 318–324. https://doi.org/10.1016/j.schres.2018.10.024.

Keshavan, M.S., Diwadkar, V.A., Montrose, D.M., Stanley, J.A., Pettegrew, J.W., 2004. Premorbid characterization in schizophrenia: the Pittsburgh high risk study. World Psychiatry 3, 163–168.

von Krosigk, M., Bal, T., McCormick, D.A., 1993. Cellular mechanisms of a synchronized oscillation in the thalamus. Science 261 (5119), 361–364.

Keshavan, M.S., Reynolds 3rd, C.F., Miewald, M.J., Montrose, D.M., Sweeney, J.A., Vasko Jr, R.C., et al., 1998. Delta sleep deficits in schizophrenia: evidence from automated analyses of sleep data. Arch. Gen. Psychiatry. 55 (5), 443–448. https://doi.org/10.1001/archpsyc.55.5.443.

Kurth, S., Riedner, B.A., Dean, D.C., O'Muircheartaigh, J., Huber, R., Jenni, O.G., et al., 2017. Traveling slow oscillations during sleep: a marker of brain connectivity in childhood. Sleep 40 (9). https://doi.org/10.1093/sleep/zsx121.

Lemieux, M., Chen, J.Y., Lonjers, P., Bazhenov, M., Timofeev, I., 2014. The impact of cortical deafferentation on the neocortical slow oscillation. J. Neurosci. 34, 5689–5703.

Manoach, D.S., Demanuele, C., Wamsley, E.J., Vangel, M., Montrose, D.M., Miewald, J., et al., 2014. Sleep spindle deficits in antipsychotic-naive early course schizophrenia and in non-psychotic first-degree relatives. Front. Hum. Neurosci. 8 (762).

Marshall, L., Helgadóttir, H., Mölle, M., Born, J., 2006. Boosting slow oscillations during sleep potentiates memory. Nature 444, 610–613.

Massimini, M., Huber, R., Ferrarelli, F., Hill, S., Tononi, G., 2004. The sleep slow oscillation as a traveling wave. J. Neurosci. 24 (31), 6862–6870.

Mensen, A., Riedner, B., Tononi, G., 2016. Optimizing detection and analysis of slow waves in sleep EEG. J. Neurosci. Methods 274, 1–12. https://doi.org/10.1016/j.jneumeth.2016.09.006.

Nichols, T.E., Holmes, A.P., 2002. Nonparametric permutation tests for functional neuroimaging: a primer with examples. Hum. Brain Mapp. 15 (1), 1–25.

Nickerson, L.D., 2018. Replication of resting state-task network correspondence and novel findings on brain network activation during task fMRI in the human connectome project study. Scient. Report. 8 (17534).

Piantoni, G., Poil, S.S., Linkenkaer-Hansen, K., Verweij, I.M., Ramautar, J.R., Van Someren, E.J., Van Der Werf, Y.D., 2013. Individual differences in white matter diffusion affect sleep oscillations. J. Neurosci. 33 (1), 227–233. https://doi.org/10.1523/JNEUROSCI.2030-12.20h.

Piantoni, G., Halgre, E., Cash, S.S., 2016. The contribution of thalamocortical core and matrix pathways to sleep spindles. Neural Plasticity 3024342.

Poulin, J., Stip, E., Godbout, R., 2008. REM sleep EEG spectral analysis in patients with first-episode schizophrenia. J. Psychiatr. Res. 42, 1086–1093.

Riedner, B.A., Vyazovskiy, V.V., Huber, R., Massimini, M., Esser, S., Murphy, M., Tononi, G., 2007. Sleep homeostasis and cortical synchronization: III. A high-density EEG study of sleep slow waves in humans. Sleep 30 (12), 1643–1657.

Sarkar, S., Katshu, M.Z., Nizamie, S.H., Praharaj, S.K., 2010. Slow wave sleep deficits as a trait marker in patients with schizophrenia. Schizophr. Res. 124, 127–133.

Schilling, C., Schlipf, M., Spietzack, S., Rausch, F., Eisenacher, S., Englisch, S., et al., 2016. Fast sleep spindle reduction in schizophrenia and healthy first-degree relatives:

association with impaired cognitive function and potential intermediate phenotype. Eur. Arch. Psychiatry Clin. Neurosci. 267 (3), 213–224. https://doi.org/10.1007/s00406-016-0725-2.
Schoch, S.F., Riedner, B.A., Deoni, S.C., Huber, R., LeBourgeois, M.K., Kurth, S., 2018. Across-night dynamics in traveling sleep slow waves throughout childhood. Sleep 41 (11). https://doi.org/10.1093/sleep/zsy165.
Sitskoorn, M.M., Aleman, A., Ebisch, S.J., Appels, M.C., Kahn, R.S., 2004. Cognitive deficits in relatives of patients with schizophrenia: a meta-analysis. Schizophr. Res. 71 (2), 285–295.
Snitz, B.E., MacDonald III, A.W., Carter, C.S., 2005. Cognitive deficits in unaffected first-degree relatives of schizophrenia patients: a meta-analytic review of putative endophenotypes.
Steriade, M., 2003. The corticothalamic system in sleep. Front. Biosci. 8, d878–d899.
Steriade, M., Nunez, A., Amzica, F., 1993. A novel slow (<1 Hz) oscillation of neocortical neurons in vivo: depolarizing and hyperpolarizing components. J. Neurosci. 13, 3252–3265.
Stickgold, R., 2005. Sleep-dependent memory consolidation. Nature 437, 1272–1278.
Timofeev, I., Grenier, F., Bazhenov, M., Sejnowski, T.J., Steriade, M., 2000. Origin of slow cortical oscillations in deafferented cortical slabs. Cereb. Cortex 10, 1185–1199.
Tononi, G., Edelman, G.M., 2000. Schizophrenia and the mechanisms of conscious integration. Brain Res. Brain Res. Rev. 31 (2–3), 391–400.
Warby, S.C., Wendt, S.L., Welinder, P., Munk, M.G.S., Carrillo, O., Sorensen, H.B.D., Jennum, P., Peppard, P.E., Perona, P., Mignot, M., 2014. Sleep spindle detection: crowdsourcing and evaluating performance of experts, non-experts, and automated methods. Nat. Methods 11 (4), 385–392.
Whitfield-Gabrieli, S., Thermenos, H.W., Milanovic, S., Tsuang, M.T., Faraone, S.V., McCarley, R.W., et al., 2009. Hyperactivity and hyperconnectivity of the default network in schizophrenia and in first-degree relatives of persons with schizophrenia. Proc. Natl. Acad. Sci. 106 (4), 1279–1284.
Whyte, M.C., McIntosh, A.M., Johnstone, E.C., Lawrie, S.M., 2005. Declarative memory in unaffected adult relatives of patients with schizophrenia: a systematic review and meta-analysis. Schizophr. Res. 78, 13–26. https://doi.org/10.1016/j. schres.2005.05.018.
Yang, C., Winkelman, J.W., 2006. Clinical significance of sleep EEG abnormalities in chronic schizophrenia. Schizophr. Res. 82, 251–260.
Zhang, Y., Quiñones, G.M., Ferrarelli, F., 2019. Sleep spindle and slow wave abnormalities in schizophrenia and other psychotic disorders: recent findings and future directions. Schizophr Res. pii S0920-9964 (19), 30500–30506. https://doi.org/10.1016/j.schres.2019.11.002.

5.6. Supplementary material

Supplementary Figure 1| A comparison of two sleep spindle detection methods.

Method 1 is based on home-made algorithms by Ferrarelli et al., 2007. The corresponding figure is taken from our previous work (D'Agostino, Castelnovo et al., 2018). Method 2 is the output of the Toolbox by Mensen (https://github.com/Mensen/swa-matlab) using default parameters. This method represents an implementation of the Wavelet-based algorithm described by Warby et al, 2014.

FDR: first degree relatives; Control: age and gender matched control group. Density: number of sleep spindles over time (minutes). ISAs: Integrated spindle activity, obtained by integrating spindle amplitude over time. Power: wavelet power in the 10-16 Hz spindle range – the equivalent of integrated spindle activity for the Wavelet-based algorithm. White dots (left) and white crosses (right) represent statistical significance at the single channel le
Method 2 was able to detect a greater number of spindles, as expected from the literature (Warby et al. 2014). However, overall, intergroup-comparison results were comparable between the 2 methods.

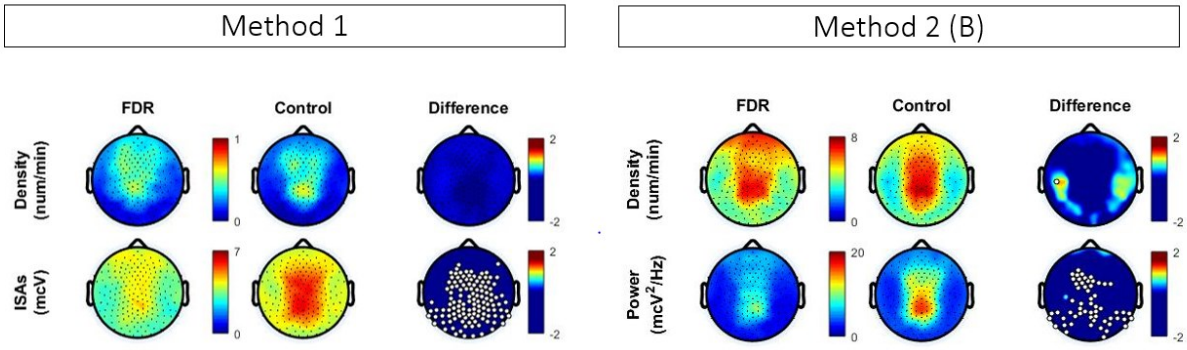

Supplementary Figure 2| Topographical maps of slow wave parameters during the first cycle in sleep stage N3. FDR: schizophrenia first degree relatives. **Control:** age and gender matched control group. **T-stats**: map showing the individual electrode t-value (two-tailed, unpaired) maps for the comparison between FDR and control subjects in terms of absolute values. **First row:** slow wave density (number per hour of N3 sleep) at each channel. **Second row:** slow wave mean amplitude (average of negative peaks values for each channel). **Third to six rows:** topographical maps of slow wave traveling parameters. **Third row:** slow wave average delays (delays at individual channels obtained correlating the canonical wave to individual channel slow waves). **Fourth row:** slow wave origins (expressed as density, i.e. number of slow waves per minute). **Fifth row:** local speed (the speed of a wave at each particular electrode). **BLUE:** FDR < control. **RED:** FDR > control. White dots: significance ($p<0.05$) at the cluster level (after multi-comparison correction).

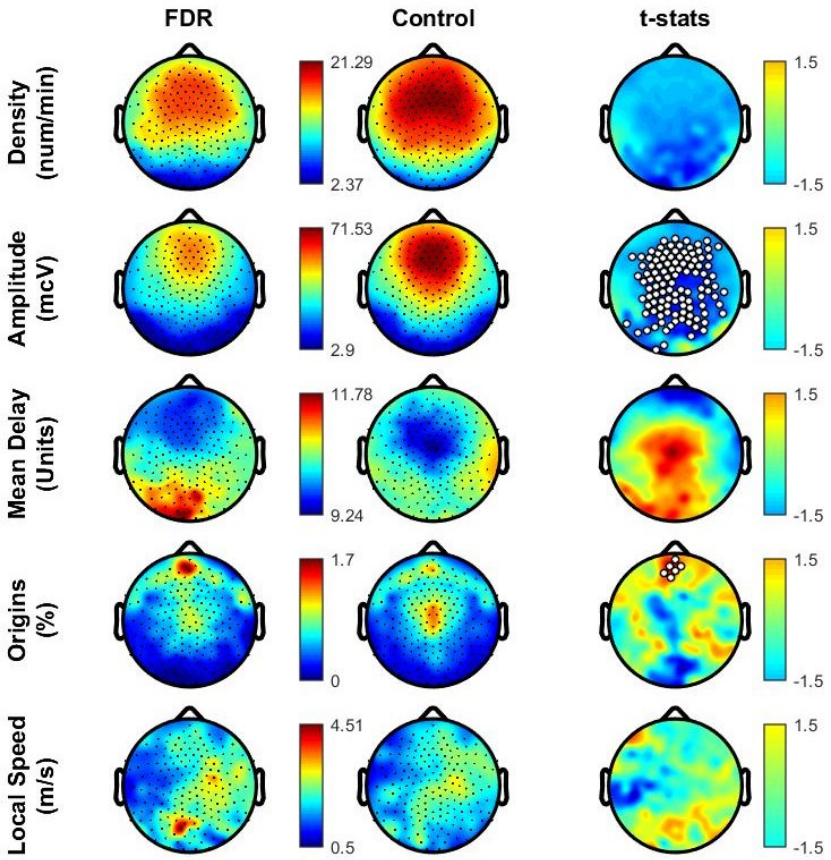

Figure 3| Travelled slow wave distance during the first cycle in sleep stage N3. Distance was calculated as the line of longest displacement. Units of measurement are referred to a grid of 40*40 tiles. **FDR:** schizophrenia first degree relatives. **Control:** age and gender matched control group.

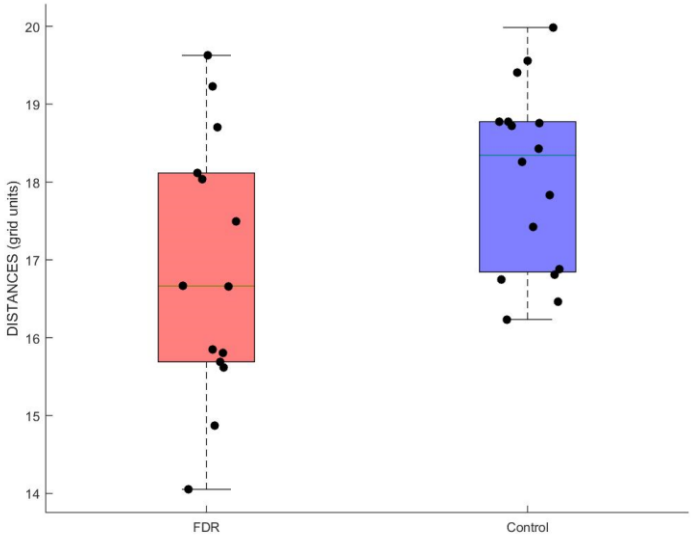

5.7. Original paper 2

I herein also include a preliminary case-control analysis on early course SCZ, under submission, in order to show the potential application of slow wave traveling in early course SCZ.

Proof–of–concept evidence for high–density EEG investigation of sleep slow wave traveling in First-Episode Psychosis

Anna Castelnovo 0000-0002-8875-9657 [a,b,c], Cecilia Casetta 0000-0002-1980-3415 [d,e], Simone Cavallotti 0000-0002-0906-6247 [d], Matteo Marcatili 0000-0002-1436-1961 [f], Lorenzo Del Fabro 0000-0003-1452-9688 [g,h], Mauro Manconi 0000-0002-1849-7196 [a,b], Maria Paola Canevini 0000-0002-2292-4015 [d,i], Simone Sarasso 0000-0001-9984-4710 [l], Armando D'Agostino 0000-0002-2126-799X [d,i]

[a] Sleep Medicine Unit, Neurocenter of Southern Switzerland, Ospedale Civico, Lugano, Switzerland.

[b] Faculty of Biomedical Sciences, University of Southern Switzerland, Lugano, Switzerland.

[c] University Hospital of Psychiatry and Psychotherapy, University of Bern, Switzerland.

[d] Department of Mental Health and Addiction, ASST Santi Paolo e Carlo, Milan, Italy

[e] King's college London, institute of psychiatry, psychology and neuroscience, Dept. of psychosis studies

[f] Psychiatric Department, San Gerardo Hospital, ASST Monza, Monza, Italy.

[g] Department of Pathophysiology and Transplantation, University of Milan, Milan, Italy

[h] Department of Neurosciences and Mental Health, IRCCS Fondazione Ca' Granda Ospedale Maggiore Policlinico, University of Milan, Milan, Italy.

[i] Department of Health Sciences, Università degli Studi di Milano, Milan, Italy

[l] Department of Biomedical and Clinical Sciences, University of Milan, Milan, Italy

Corresponding author: Anna Castelnovo, anna.castelnovo@eoc.ch, Via Tesserete 46, 6900 Lugano

Abstract

As sleep slow waves travel across the brain, they represent an ideal paradigm to study pathological conditions affecting brain connectivity. Here, we provide proof–of–concept evidence for a novel approach to investigate slow wave traveling properties in First-Episode Psychosis with high-density EEG. Slow wave traveled distance was significantly lower in drug-naïve patients who later developed schizophrenia compared to age- and gender-matched healthy control subjects. In a patient who was tested longitudinally during effective clozapine treatment, slow wave parameters partially recovered. These preliminary data suggest that slow wave traveling could be employed in larger samples to detect cortical dysconnectivity at psychosis onset to support early diagnosis and clinical management.

Keywords

electroencephalography; brain plasticity; early course psychosis; oscillations; antipsychotics; synchronization; schizophrenia; classification

Introduction

Psychosis affects the way our brain processes information and cause to lose touch with reality. Schizophrenia (SCZ) is the most severe psychotic disorder (Knapp et al., 2004; McGrath et al., 2008a; Simeone et al., 2015) characterized by perceptive (hallucinations), cognitive (disorganized speech and behavior, delusions, progressive functional impairment) and subtle motor abnormalities (Poletti et al., 2019). According to the so-called “dysconnectivity hypothesis” (Canu et al., 2015; Friston, 1998; Ramsay, 2019), signs and symptoms of SCZ can be explained by the aberrant connectivity within cortico-cortical and thalamo-cortical loops.

Among the many techniques to study brain connectivity in SCZ, sleep electroencephalographic (EEG) recordings offer four major advantages. First, the unique possibility to minimize confounding factors related to waking activities (e.g., the presence of active symptoms). Second, the possibility to relate specific EEG patterns to specific neural circuits and functions (Adamantidis et al., 2019), thanks to the fast-growing advancements in the field of sleep neurophysiology. Third, high-density EEG (hdEEG) techniques have recently advanced the possibility to image the sleeping brain non-invasively, without restriction of nocturnal movements, and with high temporal and spatial resolution (1 cm). Fourth, several studies confirmed the presence of sleep abnormalities in SCZ (Castelnovo et al., 2018a; Ferrarelli, 2021; Lai et al., 2022). Specifically, slow waves, the hallmark of non-rapid eye movement (NREM) sleep, were reported to be reduced in unmedicated patients with SCZ, even at early stages of the disease (Kaskie et al., 2019a). Slow waves appear as continuous high amplitude (>75 μV) slow (1-4 Hz)

oscillations; they reflect the integrity of thalamocortical circuits (Adamantidis et al., 2019; Steriade, 2003), and are implicated in brain plasticity, memory consolidation and several other cognitive functions (Huber et al., 2004). More recently, subcortical white matter tracts (Avvenuti et al., 2020a) were shown to sustain the so-called traveling (Massimini et al., 2004a) of larger slow waves, which typically originate from a definite site and travel over the scalp at an estimated speed of 1.2–7.0 m/sec. The pattern of origin and propagation of slow waves is reproducible across nights and subjects and provides a blueprint of cortical connectivity.

We recently showed that slow wave traveling is a viable method to study connectivity in SCZ first-degree relatives (Castelnovo et al., 2020b) and that slow wave properties are a candidate endophenotype for SCZ (D'Agostino et al., 2018a). Here we propose slow wave traveling as a candidate marker of aberrant cortico–cortical/thalamocortical connectivity at the onset of SCZ and we report an explorative case-control analysis on a small sample of patients as proof–of–concept.

Methods

Participants

All patients who were hospitalized for a first episode of psychosis (FEP) in the psychiatric ward of the San Paolo University Hospital over a period of 1 year were asked to participate in a larger study on sleep EEG that was approved by the local ethics committee. During this time, five drug-naïve patients were recorded overnight with a 256–channel EEG system (Electrical Geodesics Inc., Eugene, OR; 500 Hz, vertex-reference). The diagnosis

of SCZ (American Psychiatric Association, 2013a) was confirmed for all subjects after a two-year follow-up period by at least two expert clinicians through direct interview and medical charts review. Control participants were good sleepers with a negative history of previous or current medical, neurological or psychiatric diagnoses. Written informed consent was provided by each participant. All participants were antipsychotic-naive and free from any other medication that could affect sleep for a minimum of 1 month before the recording.

Patients (n = 5, 100% males, 24.4 ± 3.58 years old) were age– and gender–matched with healthy control individuals (n = 5, 100% males, 24.0 ± 3.32 years old).

FEP clinical features are summarized in Table 1.

Sleep EEG analysis

All subjects underwent an overnight hdEEG recording at T0 or baseline, before starting any treatment.

One patient (PT5), whose clinical history has been detailed elsewhere (Castelnovo et al., 2020a), was assessed also at:

- at T1, after 6 months of pharmacotherapy (3 months of titration and 3 months of clozapine 200 mg/day)
- at T2, after 3 years (last 2 of clozapine at the maintenance dosage of 75 mg/day).

Lights-out fell within 1 hour of the participants usual bedtime. Light-on varied as subjects were allowed to sleep ad libitum. All EEG signals were imported in MATLAB (The MathWorks Inc., Natick, MA) and high-pass filtered at 0.1 Hz, down-sampled to 128 Hz, band-pass filtered (2-way least-squares FIR, 1 – 40 Hz). Sleep staging was performed in Matlab (https://github.com/Mensen/swa-matlab), according to standard criteria (Berry RB,

Brooks R, Gamaldo CE, Harding SM, Lloyd RM, Marcus CL, 2020) by a physician certified in Sleep Medicine (AC). Semiautomatic artifact rejection procedures were utilized to remove channels and epochs with high frequency noise or interrupted contact with the scalp, as done in other recent studies (Castelnovo et al., 2020b, 2016b; D'Agostino et al., 2018b).

Spectral analysis in the slow wave activity range (SWA, 1-4 Hz) was performed using all clean 6-second epochs within NREM sleep (Welch's averaged modified periodogram with a Hamming window) on average-referenced EEG signal. Sleep slow wave detection was conducted on mastoid-referenced signal using an open-source Matlab-based toolbox (Mensen et al., 2016). Parameters of interests were: density (count of slow waves per minute), negative peak amplitude, travelled distance (measured as the line of longest displacement).

Statistical analysis

Between-group statistical comparisons of demographic and sleep architecture variables were performed using unpaired 2-tailed t-tests, Mann–Whitney U tests, or χ^2 tests, as appropriate. For slow wave topographical analysis, we applied non-parametric statistical mapping using a non-parametric suprathreshold cluster analysis to control for multiple comparisons (Nichols and Holmes, 2002), as previously described (Castelnovo et al., 2022c, 2016c).

Results

Sleep Architecture

Sleep architecture parameters are summarized in Table 2.

Topographical maps revealed a non-significant ($p > 0.05$) reduction in SWA power in FEP compared to control group (Figure 1A). The qualitative observation of topographical maps (Figure 2A), suggest lower SWA in PT5 at T0 compared to matched control, and the subsequent progressive normalization of SWA from T1 to T2.

Slow wave analysis showed lower slow wave density at baseline in FEP versus control subjects (Figure 1B). This result remained significant after correction for multiple-comparison. A similar trend was observed for slow wave amplitude (Figure 1B), although group difference was not statistically significant at the topographical level after correction for multiple comparison (Figure 1B). However, when observing channel average amplitude at different percentiles, we could detect a selective reduction of high amplitude slow waves (Figure 1C). Average traveled distance was significantly decreased in FEP vs control participants ($p < 0.05$), with almost no overlap between groups (Figure 1D). At baseline, slow wave density for PT5 was visually lower compared to healthy control subjects. There was a sharp increase at T1 and a return to levels comparable to the control participants at T2 (Figure 2B). Slow wave traveled distance for PT5 was lower compared to healthy control subjects. There was a progressive increase from baseline to T2, yet without a full normalization of this parameter at T2 compared to healthy subjects (Figure 2C).

Discussion

The preliminary results offered by this case–control analysis provide first evidence on slow wave traveling impairment at the onset of psychosis. The lack of overlap between the two groups provides proof-of-concept for the reliability of sleep slow wave traveling as a marker of brain dysconnectivity in SCZ to be tested in large, systematic studies. Interestingly, our observation also raises the question whether the early administration of clozapine may partially reverse slow wave abnormalities after the first psychotic episode. Indeed, baseline traveled distance progressively increased but did not normalize over the course of effective treatment with clozapine in the only subject who was tested longitudinally. It could be speculated that this incomplete recover reflects the underlying white matter damage in early course SCZ (Szeszko et al., 2007) as long-range slow wave traveling is sustained by cortico-cortical connections (Avvenuti et al., 2020a; Bernardi et al., 2021a; Buchmann et al., 2011a; Kurth et al., 2017; Murphy et al., 2009; Piantoni et al., 2013). Instead, slow wave density time-course recorded for this patient seemed to relate more closely to active psychotic symptoms, clozapine dosage, and be partially reversible in SCZ early stages.

Moreover, these preliminary data support the previous observation of an intrinsic deficit of slow wave generation in early course psychosis. Both density and amplitude appeared to be involved, with a significant shift in mean amplitude peak from 40-80 to 20-40 Hz. These observations are in line with the previous literature (Ganguli et al., 1987; Hiatt et al., 1985; Kaskie et al., 2019b; Keshavan et al., 1998; Sekimoto et al., 2011, 2007).

Last but not least, these findings confirm the utility o standardized algorithms and tools for sleep clinical studies as they were obtained using a standardized and open-source toolbox that can be readily employed in clinical contexts with expertise in sleep medicine

and hdEEG analysis. The use of comparable methodologies and tools across studies is critical to guarantee reproducibility of results, especially given the large heterogeneity observed in SCZ (Castelnovo et al., 2020b).

The reported data was derived from a series of only five early-course SCZ patients. Brain connectivity measures may vary across patients, perhaps justifying variable clinical subtypes and the heterogeneity of SCZ.

In conclusion, the preliminary results offered by this case report and case–control analysis: 1) support previous findings on slow wave deficit in early stages of SCZ; 2) provide first evidence on slow wave traveling impairment at the onset of psychosis; 3) raise the question whether the early administration of clozapine may partially reverse slow wave abnormalities after the first psychotic episode; 4) provide proof-of-concept for sleep slow wave traveling as a marker of brain dysconnectivity in SCZ; 5) confirm the utility of standardized algorithms and tools for sleep clinical studies; 6) encourage future systematic studies on larger cohorts of patients.

References

1. Keshavan MS, Diwadkar VA, DeBellis M, et al. Development of the corpus callosum in childhood, adolescence and early adulthood. Life Sci. 2002;70(16):1909-1922. doi:10.1016/S0024-3205(02)01492-3

2. Lynch KM, Cabeen RP, Toga AW, Clark KA. Magnitude and timing of major white matter tract maturation from infancy through adolescence with NODDI. Neuroimage. 2020;212:116672. doi:10.1016/J.NEUROIMAGE.2020.116672

3. Piekarski DJ, Johnson CM, Boivin JR, et al. Does puberty mark a transition in sensitive periods for plasticity in the associative neocortex? Brain Res. 2017;1654(Pt B):123. doi:10.1016/J.BRAINRES.2016.08.042

4. Paus T. Mapping brain maturation and cognitive development during adolescence. Trends Cogn Sci. 2005;9(2):60-68. doi:10.1016/J.TICS.2004.12.008

5. Paus T, Keshavan M, Giedd JN. Why do many psychiatric disorders emerge during adolescence? Nat Rev Neurosci. 2008;9(12):947-957. doi:10.1038/NRN2513

6. Ringli M, Huber R. Developmental aspects of sleep slow waves: linking sleep, brain maturation and behavior. Prog Brain Res. 2011;193:63-82. doi:10.1016/B978-0-444-53839-0.00005-3

7. Ricci A, He F, Fang J, et al. Maturational trajectories of non-rapid eye movement slow wave activity and odds ratio product in a population-based sample of youth. Sleep Med. 2021;83:271-279. doi:10.1016/J.SLEEP.2021.05.002

8. Timofeev I, Schoch SF, LeBourgeois MK, Huber R, Riedner BA, Kurth S. Spatio-temporal properties of sleep slow waves and implications for development. Curr Opin Physiol. 2020;15:172-182. doi:10.1016/J.COPHYS.2020.01.007

9. Gorgoni M, D'Atri A, Scarpelli S, Reda F, de Gennaro L. Sleep electroencephalography and brain maturation: developmental trajectories and the relation with cognitive functioning. Sleep Med. 2020;66:33-50. doi:10.1016/J.SLEEP.2019.06.025

10. Schoch SF, Riedner BA, Deoni SC, Huber R, Lebourgeois MK, Kurth S. Across-night dynamics in traveling sleep slow waves throughout childhood. Sleep. 2018;41(11). doi:10.1093/sleep/zsy165

11. Buchmann A, Kurth S, Ringli M, Geiger A, Jenni OG, Huber R. Anatomical markers of sleep slow wave activity derived from structural magnetic resonance images. J Sleep Res. 2011;20(4):506-513. doi:10.1111/J.1365-2869.2011.00916.X

12. Shaw P, Kabani NJ, Lerch JP, et al. Neurodevelopmental trajectories of the human cerebral cortex. J Neurosci. 2008;28(14):3586-3594. doi:10.1523/JNEUROSCI.5309-07.2008

13. Vyazovskiy V v., Riedner BA, Cirelli C, Tononi G. Sleep homeostasis and cortical synchronization: II. A local field potential study of sleep slow waves in the rat. Sleep. 2007;30(12):1631-1642. doi:10.1093/SLEEP/30.12.1631

14. Riedner BA, Vyazovskiy V v., Huber R, et al. Sleep homeostasis and cortical synchronization: III. A high-density EEG study of sleep slow waves in humans. Sleep. 2007;30(12):1643-1657. doi:10.1093/sleep/30.12.1643

15. Esser SK, Hill SL, Tononi G. Sleep homeostasis and cortical synchronization: I. Modeling the effects of synaptic strength on sleep slow waves. Sleep. 2007;30(12):1617-1630. doi:10.1093/SLEEP/30.12.1617

16. Massimini M, Huber R, Ferrarelli F, Hill S, Tononi G. The sleep slow oscillation as a traveling wave. J Neurosci. 2004;24(31):6862-6870. doi:10.1523/JNEUROSCI.1318-04.2004

17. Murphy M, Riedner BA, Huber R, Massimini M, Ferrarelli F, Tononi G. Source modeling sleep slow waves. Proc Natl Acad Sci U S A. 2009;106(5):1608-1613. doi:10.1073/pnas.0807933106

18. Avvenuti G, Handjaras G, Betta M, et al. Integrity of Corpus Callosum Is Essential for theCross-Hemispheric Propagation of Sleep Slow Waves:A High-Density EEG Study

in Split-Brain Patients. J Neurosci. 2020;40(29):5589-5603. doi:10.1523/JNEUROSCI.2571-19.2020

19. Siclari F, Bernardi G, Riedner BA, LaRocque JJ, Benca RM, Tononi G. Two distinct synchronization processes in the transition to sleep: A high-density electroencephalographic study. Sleep. 2014;37(10):1621-1637F. doi:10.5665/sleep.4070

20. Bernardi G, Siclari F, Handjaras G, Riedner BA, Tononi G. Local and Widespread Slow Waves in Stable NREM Sleep: Evidence for Distinct Regulation Mechanisms. Front Hum Neurosci. 2018;12. doi:10.3389/FNHUM.2018.00248

21. Kurth S, Ringli M, Geiger A, Lebourgeois M, Jenni OG, Huber R. High-Density Sleep Electroencephalogram Study. Journal of Neuroscience. 2010;30(40):13211-13219. doi:10.1523/JNEUROSCI.2532-10.2010.Mapping

22. Jenni OG, Carskadon MA. Spectral analysis of the sleep electroencephalogram during adolescence. Sleep. 2004;27(4):774-783. doi:10.1093/sleep/27.4.774

23. Campbell IG, Feinberg I. Longitudinal trajectories of non-rapid eye movement delta and theta EEG as indicators of adolescent brain maturation. Proc Natl Acad Sci U S A. 2009;106(13):5177-5180. doi:10.1073/PNAS.0812947106

24. Kurth S, Ringli M, LeBourgeois MK, et al. Mapping the electrophysiological marker of sleep depth reveals skill maturation in children and adolescents. Neuroimage. 2012;63(2):959-965. doi:10.1016/J.NEUROIMAGE.2012.03.053

25. Kurth S, Riedner BA, Dean DC, et al. Traveling Slow Oscillations During Sleep: A Marker of Brain Connectivity in Childhood. Sleep. 2017;40(9). doi:10.1093/SLEEP/ZSX121

26. Bernardi G, Siclari F, Handjaras G, Riedner BA, Tononi G. Local and Widespread Slow Waves in Stable NREM Sleep: Evidence for Distinct Regulation Mechanisms. Front Hum Neurosci. 2018;12. doi:10.3389/FNHUM.2018.00248

27. Spiess M, Bernardi G, Kurth S, et al. How do children fall asleep? A high-density EEG study of slow waves in the transition from wake to sleep. Neuroimage. 2018;178:23-35. doi:10.1016/j.neuroimage.2018.05.024

28. Miano S, Amato N, Foderaro G, et al. Sleep phenotypes in attention deficit hyperactivity disorder. Sleep Med. 2019;60:123-131. doi:10.1016/j.sleep.2018.08.026

29. Castelnovo A, Lividini A, Bernardi G, et al. Sleep Power Topography in Children with Attention Deficit Hyperactivity Disorder (ADHD). Children (Basel). 2022;9(2). doi:10.3390/CHILDREN9020197

30. Ferrarelli F, Smith R, Dentico D, et al. Experienced mindfulness meditators exhibit higher parietal-occipital EEG gamma activity during NREM sleep. PLoS One. 2013;8(8). doi:10.1371/JOURNAL.PONE.0073417

31. Dentico D, Ferrarelli F, Riedner BA, et al. Short Meditation Trainings Enhance Non-REM Sleep Low-Frequency Oscillations. PLoS One. 2016;11(2). doi:10.1371/JOURNAL.PONE.0148961

32. Berry RB, Brooks R, Gamaldo CE, Harding SM, Lloyd RM, Marcus CL VB. The AASM Manual for the Scoring of Sleep and Associated Events: Rules, Terminology and Technical Specifications. 2.6 versio.; 2020.

33. Delorme A, Makeig S. EEGLAB: An open source toolbox for analysis of single-trial EEG dynamics including independent component analysis. J Neurosci Methods. 2004;134(1):9-21. doi:10.1016/j.jneumeth.2003.10.009

34. Siclari F, Bernardi G, Riedner BA, LaRocque JJ, Benca RM, Tononi G. Two distinct synchronization processes in the transition to sleep: a high-density electroencephalographic study. Sleep. 2014;37(10):1621-1637F. doi:10.5665/SLEEP.4070

35. Mensen A, Riedner B, Tononi G. Optimizing detection and analysis of slow waves in sleep EEG. J Neurosci Methods. 2016;274:1-12. doi:10.1016/J.JNEUMETH.2016.09.006

36. Bernardi G, Betta M, Cataldi J, et al. Visual imagery and visual perception induce similar changes in occipital slow waves of sleep. J Neurophysiol. 2019;121(6):2140-2152. doi:10.1152/JN.00085.2019

37. Castelnovo A, Riedner BA, Smith RF, Tononi G, Boly M, Benca RM. Scalp and Source Power Topography in Sleepwalking and Sleep Terrors: A High-Density EEG Study. Sleep. 2016;39(10):1815-1825. doi:10.5665/sleep.6162

38. Castelnovo A, Zago M, Casetta C, et al. Slow wave oscillations in Schizophrenia First-Degree Relatives: A confirmatory analysis and feasibility study on slow wave traveling. Schizophr Res. 2020;221:37-43. doi:10.1016/J.SCHRES.2020.03.025

39. D'Agostino A, Castelnovo A, Cavallotti S, et al. Sleep endophenotypes of schizophrenia: slow waves and sleep spindles in unaffected first-degree relatives. NPJ Schizophr. 2018;4(1):2. doi:10.1038/s41537-018-0045-9

40. Massimini M, Huber R, Ferrarelli F, Hill S, Tononi G. The sleep slow oscillation as a traveling wave. Journal of Neuroscience. 2004;24(31):6862-6870. doi:10.1523/JNEUROSCI.1318-04.2004

41. Menicucci D, Piarulli A, Debarnot U, d'Ascanio P, Landi A, Gemignani A. Functional structure of spontaneous sleep slow oscillation activity in humans. PLoS One. 2009;4(10). doi:10.1371/JOURNAL.PONE.0007601

42. Avvenuti G, Handjaras G, Betta M, et al. Integrity of Corpus Callosum Is Essential for theCross-Hemispheric Propagation of Sleep Slow Waves:A High-Density EEG Study in Split-Brain Patients. J Neurosci. 2020;40(29):5589-5603. doi:10.1523/JNEUROSCI.2571-19.2020

43. Schönemann PH. Varism: a new machine method for orthogonal rotation. Psychometrika. 1966;31(2):235-248. doi:10.1007/BF02289510

44. Haxby J v., Guntupalli JS, Connolly AC, et al. A common, high-dimensional model of the representational space in human ventral temporal cortex. Neuron. 2011;72(2):404-416. doi:10.1016/J.NEURON.2011.08.026

45. Richards JE, Sanchez C, Phillips-Meek M, Xie W. A database of age-appropriate average MRI templates. Neuroimage. Published online 2016. doi:10.1016/j.neuroimage.2015.04.055

46. Tzourio-Mazoyer N, Landeau B, Papathanassiou D, et al. Automated anatomical labeling of activations in SPM using a macroscopic anatomical parcellation of the MNI MRI single-subject brain. Neuroimage. Published online 2002. doi:10.1006/nimg.2001.0978

47. Maureen C. An empirical evaluation of free BEM solvers for accurate M/EEG forward modeling. Front Neurosci. Published online 2010. doi:10.3389/conf.fnins.2010.06.00065

48. Pascual-Marqui RD. Standardized low-resolution brain electromagnetic tomography (sLORETA): Technical details. In: Methods and Findings in Experimental and Clinical Pharmacology. ; 2002.

49. Nichols TE, Holmes AP. Nonparametric permutation tests for functional neuroimaging: a primer with examples. Hum Brain Mapp. 2002;15(1):1-25. doi:10.1002/HBM.1058

50. Castelnovo A, Lividini A, Bernardi G, et al. Sleep Power Topography in Children with Attention Deficit Hyperactivity Disorder (ADHD). Children (Basel). 2022;9(2). doi:10.3390/CHILDREN9020197

51. Cohen J. Statistical Power Analysis for the Behavioral Sciences Second Edition.

52. Bernardi G, Avvenuti G, Cataldi J, et al. Role of corpus callosum in sleep spindle synchronization and coupling with slow waves. Brain Commun. 2021;3(2):fcab108. doi:10.1093/braincomms/fcab108

53. Giedd JN, Blumenthal J, Jeffries NO, et al. Development of the human corpus callosum during childhood and adolescence: a longitudinal MRI study. Prog Neuropsychopharmacol Biol Psychiatry. 1999;23(4):571-588. doi:10.1016/S0278-5846(99)00017-2

54. Luders E, Thompson PM, Toga AW. The development of the corpus callosum in the healthy human brain. J Neurosci. 2010;30(33):10985-10990. doi:10.1523/JNEUROSCI.5122-09.2010

55. Giedd JN, Blumenthal J, Jeffries NO, et al. Development of the human corpus callosum during childhood and adolescence: a longitudinal MRI study. Prog

Neuropsychopharmacol Biol Psychiatry. 1999;23(4):571-588. doi:10.1016/S0278-5846(99)00017-2

56. Luders E, Cherbuin N, Thompson PM, et al. When more is less: Associations between corpus callosum size and handedness lateralization. Neuroimage. 2010;52(1):43-49. doi:10.1016/J.NEUROIMAGE.2010.04.016

57. Rajapakse JC, Giedd JN, Rumsey JM, Vaituzis AC, Hamburger SD, Rapoport JL. Regional MRI measurements of the corpus callosum: A methodological and developmental study. Brain Dev. 1996;18(5):379-388. doi:10.1016/0387-7604(96)00034-4

58. Thompson PM, Gledd JN, Woods RP, MacDonald D, Evans AC, Toga AW. Growth patterns in the developing brain detected by using continuum mechanical tensor maps. Nature 2000 404:6774. 2000;404(6774):190-193. doi:10.1038/35004593

59. Westerhausen R, Fjell AM, Krogsrud SK, et al. Selective increase in posterior corpus callosum thickness between the age of 4 and 11 years. Neuroimage. 2016;139:17-25. doi:10.1016/J.NEUROIMAGE.2016.06.008

60. Danielsen VM, Vidal-Piñeiro D, Mowinckel AM, et al. Lifespan trajectories of relative corpus callosum thickness: Regional differences and cognitive relevance. Cortex. 2020;130:127-141. doi:10.1016/J.CORTEX.2020.05.020

61. Mascetti GG. Unihemispheric sleep and asymmetrical sleep: behavioral, neurophysiological, and functional perspectives. Nat Sci Sleep. 2016;8:221-228. doi:10.2147/NSS.S71970

62. Mascetti GG. Unihemispheric sleep and asymmetrical sleep: behavioral, neurophysiological, and functional perspectives. Nat Sci Sleep. 2016;8:221. doi:10.2147/NSS.S71970

63. Tamaki M, Bang JW, Watanabe T, Sasaki Y. Night watch in one brain hemisphere during sleep associated with the first-night effect in humans. Curr Biol. 2016;26(9):1190. doi:10.1016/J.CUB.2016.02.063

64. Gogtay N, Giedd JN, Lusk L, et al. Dynamic mapping of human cortical development during childhood through early adulthood. Proc Natl Acad Sci U S A. 2004;101(21):8174-8179. doi:10.1073/PNAS.0402680101

65. Mensen A, Khatami R. Advanced EEG analysis using threshold-free cluster-enhancement and non-parametric statistics. Neuroimage. 2013;67:111-118. doi:10.1016/j.neuroimage.2012.10.027

66. Riedner BA, Vyazovskiy V v., Huber R, et al. Sleep homeostasis and cortical synchronization: III. A high-density EEG study of sleep slow waves in humans. Sleep. 2007;30(12):1643-1657. doi:10.1093/SLEEP/30.12.1643

67. Kurth S, Achermann P, Rusterholz T, Lebourgeois MK. Development of Brain EEG Connectivity across Early Childhood: Does Sleep Play a Role? Brain Sci. 2013;3(4):1445-1460. doi:10.3390/BRAINSCI3041445

68. Lee GMH, Fattinger S, Mouthon AL, Noirhomme Q, Huber R. Electroencephalogram approximate entropy influenced by both age and sleep. Front Neuroinform. 2013;7(DEC). doi:10.3389/FNINF.2013.00033

69. Spiess M, Bernardi G, Kurth S, et al. How do children fall asleep? A high-density EEG study of slow waves in the transition from wake to sleep. Neuroimage. 2018;178:23-35. doi:10.1016/J.NEUROIMAGE.2018.05.024

70. Metcalf DR, Mondale J, Butler FK. Ontogenesis of spontaneous K-complexes. Psychophysiology. 1971;8(3):340-347. doi:10.1111/J.1469-8986.1971.TB00464.X

71. Kaufmann T, Alnæs D, Doan NT, Brandt CL, Andreassen OA, Westlye LT. Delayed stabilization and individualization in connectome development are related to psychiatric disorders. Nature Neuroscience 2017 20:4. 2017;20(4):513-515. doi:10.1038/nn.4511

5.8. References

American Psychiatric Association, 2013. Diagnostic and statistical manual of mental disorders, 5th ed. ed. Washington, DC: American Psychiatric Association.

Andreasen, N., Nasrallah, H.A., Dunn, V., Olson, S.C., Grove, W.M., Ehrhardt, J.C., Coffman, J.A., Crossett, J.H.W., 1986. Structural Abnormalities in the Frontal System in Schizophrenia: A Magnetic Resonance Imaging Study. Arch Gen Psychiatry 43, 136–144. https://doi.org/10.1001/ARCHPSYC.1986.01800020042006

Andreasen, N.C., Paradiso, S., O'Leary, D.S., 1998. "Cognitive Dysmetria" as an Integrative Theory of Schizophrenia: A Dysfunction in Cortical-Subcortical-Cerebellar Circuitry? Schizophr Bull 24, 203–218. https://doi.org/10.1093/OXFORDJOURNALS.SCHBUL.A033321

Canu, E., Agosta, F., Filippi, M., 2015. A selective review of structural connectivity abnormalities of schizophrenic patients at different stages of the disease. Schizophr Res 161, 19–28. https://doi.org/10.1016/J.SCHRES.2014.05.020

Castelnovo, A., D'Agostino, A., Casetta, C., Sarasso, S., Ferrarelli, F., 2016. Sleep Spindle Deficit in Schizophrenia: Contextualization of Recent Findings. Curr Psychiatry Rep 18, 72. https://doi.org/10.1007/s11920-016-0713-2

Castelnovo, A., Ferrarelli, F., D'Agostino, A., 2015. Schizophrenia: from neurophysiological abnormalities to clinical symptoms. Front Psychol 6. https://doi.org/10.3389/FPSYG.2015.00478

Castelnovo, A., Graziano, B., Ferrarelli, F., D'Agostino, A., 2018. Sleep spindles and slow waves in schizophrenia and related disorders: main findings, challenges and future perspectives. Eur J Neurosci 48, 2738–2758. https://doi.org/10.1111/EJN.13815

Castelnovo, A., Zago, M., Casetta, C., Zangani, C., Donati, F., Canevini, M., Riedner, B.A., Tononi, G., Ferrarelli, F., Sarasso, S., D'Agostino, A., 2020. Slow wave oscillations in Schizophrenia First-Degree Relatives: A confirmatory analysis and feasibility study on slow wave traveling. Schizophr Res 221, 37–43. https://doi.org/10.1016/J.SCHRES.2020.03.025

Chan, M.S., Chung, K.F., Yung, K.P., Yeung, W.F., 2017. Sleep in schizophrenia: A systematic review and meta-analysis of polysomnographic findings in case-control studies. Sleep Med Rev 32, 69–84. https://doi.org/10.1016/J.SMRV.2016.03.001

Dierks, T., Linden, D.E.J., Jandl, M., Formisano, E., Goebel, R., Lanfermann, H., Singer, W., 1999. Activation of Heschl's gyrus during auditory hallucinations. Neuron 22, 615–621. https://doi.org/10.1016/S0896-6273(00)80715-1

Friston, K.J., 1998. The disconnection hypothesis. Schizophr Res 30, 115–125. https://doi.org/10.1016/S0920-9964(97)00140-0

Fusar-Poli, P., Borgwardt, S., Bechdolf, A., Addington, J., Riecher-Rössler, A., Schultze-Lutter, F., Keshavan, M., Wood, S., Ruhrmann, S., Seidman, L.J., Valmaggia, L., Cannon, T., Velthorst, E., de Haan, L., Cornblatt, B., Bonoldi, I., Birchwood, M., McGlashan, T., Carpenter, W., McGorry, P., Klosterkötter, J., McGuire, P., Yung, A., 2013. The Psychosis High-Risk State: A Comprehensive State-of-the-Art Review. JAMA Psychiatry 70, 107–120. https://doi.org/10.1001/JAMAPSYCHIATRY.2013.269

Ganguli, R., Reynolds, C.F., Kupfer, D.J., 1987. Electroencephalographic sleep in young, never-medicated schizophrenics. A comparison with delusional and nondelusional depressives and with healthy controls. Arch Gen Psychiatry 44, 36–44. https://doi.org/10.1001/ARCHPSYC.1987.01800130038006

Genzel, L., Dresler, M., Cornu, M., Jäger, E., Konrad, B., Adamczyk, M., Friess, E., Steiger, A., Czisch, M., Goya-Maldonado, R., 2015. Medial prefrontal-hippocampal connectivity and motor memory consolidation in depression and schizophrenia. Biol Psychiatry 77, 177–186. https://doi.org/10.1016/J.BIOPSYCH.2014.06.004

Göder, R., Graf, A., Ballhausen, F., Weinhold, S., Baier, P.C., Junghanns, K., Prehn-Kristensen, A., 2015. Impairment of sleep-related memory consolidation in schizophrenia: relevance of sleep spindles? Sleep Med 16, 564–569. https://doi.org/10.1016/J.SLEEP.2014.12.022

Gross, G., 1989. The 'Basic' Symptoms of Schizophrenia. The British Journal of Psychiatry 155, 21–25. https://doi.org/10.1192/S0007125000291423

Hiatt, J.F., Floyd, T.C., Katz, P.H., Feinberg, I., 1985. Further Evidence of Abnormal Non-Rapid-Eye-Movement Sleep in Schizophrenia. Arch Gen Psychiatry 42, 797–802. https://doi.org/10.1001/ARCHPSYC.1985.01790310059007

Huang, A.S., Rogers, B.P., Woodward, N.D., 2019. Disrupted modulation of thalamus activation and thalamocortical connectivity during dual task performance in schizophrenia. Schizophr Res 210, 270–277. https://doi.org/10.1016/J.SCHRES.2018.12.022

Hubl, D., Dougoud-Chauvin, V., Zeller, M., Federspiel, A., Boesch, C., Strik, W., Dierks, T., Koenig, T., 2010. Structural analysis of Heschl's gyrus in schizophrenia patients with auditory hallucinations. Neuropsychobiology 61, 1–9. https://doi.org/10.1159/000258637

Hubl, D., Koenig, T., Strik, W., Federspiel, A., Kreis, R., Boesch, C., Maier, S.E., Schroth, G., Lovblad, K., Dierks, T., 2004. Pathways that make voices: white matter changes in auditory hallucinations. Arch Gen Psychiatry 61, 658–668. https://doi.org/10.1001/ARCHPSYC.61.7.658

Kaskie, R.E., Gill, K.M., Ferrarelli, F., 2019. Reduced frontal slow wave density during sleep in first-episode psychosis. Schizophr Res 206, 318–324. https://doi.org/10.1016/J.SCHRES.2018.10.024

Keshavan, M.S., Reynolds, C.F., Miewald, J.M., Montrose, D.M., Sweeney, J.A., Vasko, R.C., Kupfer, D.J., 1998. Delta sleep deficits in schizophrenia: evidence from automated analyses of sleep data. Arch Gen Psychiatry 55, 443–448. https://doi.org/10.1001/ARCHPSYC.55.5.443

Knapp, M., Mangalore, R., Simon, J., 2004. The global costs of schizophrenia. Schizophr Bull 30, 279–293. https://doi.org/10.1093/OXFORDJOURNALS.SCHBUL.A007078

Laskemoen, J.F., Simonsen, C., Büchmann, C., Barrett, E.A., Bjella, T., Lagerberg, T.V., Vedal, T.J., Andreassen, O.A., Melle, I., Aas, M., 2019. Sleep disturbances in schizophrenia spectrum and bipolar disorders - a transdiagnostic perspective. Compr Psychiatry 91, 6–12. https://doi.org/10.1016/J.COMPPSYCH.2019.02.006

Lora, A., Kohn, R., Levav, I., Mcbain, R., Morris, J., Saxena, S., 2012. Service availability and utilization and treatment gap for schizophrenic disorders: a survey in 50 low-and middle-income countries. Bull World Health Organ 90, 47–54. https://doi.org/10.2471/BLT.11.089284

Manoach, D.S., Demanuele, C., Wamsley, E.J., Wamsley, E.J., Montrose, D.M., Miewald, J., Kupfer, D., Buysse, D., Stickgold, R., Keshavan, M.S., 2014. Sleep spindle deficits in antipsychotic-naïve early course schizophrenia and in non-psychotic first-degree relatives. Front Hum Neurosci 8. https://doi.org/10.3389/FNHUM.2014.00762

Manoach, D.S., Thakkar, K.N., Stroynowski, E., Ely, A., McKinley, S.K., Wamsley, E., Djonlagic, I., Vangel, M.G., Goff, D.C., Stickgold, R., 2010. Reduced overnight consolidation of procedural learning in chronic medicated schizophrenia is related to specific sleep stages. J Psychiatr Res 44, 112–120. https://doi.org/10.1016/J.JPSYCHIRES.2009.06.011

McGrath, J., Saha, S., Chant, D., Welham, J., 2008a. Schizophrenia: A Concise Overview of Incidence, Prevalence, and Mortality. Epidemiol Rev 30, 67–76. https://doi.org/10.1093/EPIREV/MXN001

McGrath, J., Saha, S., Chant, D., Welham, J., 2008b. Schizophrenia: A Concise Overview of Incidence, Prevalence, and Mortality. Epidemiol Rev 30, 67–76. https://doi.org/10.1093/EPIREV/MXN001

Ramsay, I.S., 2019. An Activation Likelihood Estimate Meta-analysis of Thalamocortical Dysconnectivity in Psychosis. Biol Psychiatry Cogn Neurosci Neuroimaging 4, 859–869. https://doi.org/10.1016/J.BPSC.2019.04.007

Sekimoto, M., Kato, M., Watanabe, T., Kajimura, N., Takahashi, K., 2011. Cortical regional differences of delta waves during all-night sleep in schizophrenia. Schizophr Res 126, 284–290. https://doi.org/10.1016/J.SCHRES.2010.11.003

Sekimoto, M., Kato, M., Watanabe, T., Kajimura, N., Takahashi, K., 2007. Reduced frontal asymmetry of delta waves during all-night sleep in schizophrenia. Schizophr Bull 33, 1307–1311. https://doi.org/10.1093/SCHBUL/SBL069

Sheffield, J.M., Huang, A.S., Rogers, B.P., Giraldo-Chica, M., Landman, B.A., Blackford, J.U., Heckers, S., Woodward, N.D., 2020. Thalamocortical Anatomical Connectivity in Schizophrenia and Psychotic Bipolar Disorder. Schizophr Bull 46, 1062–1071. https://doi.org/10.1093/schbul/sbaa022

Simeone, J.C., Ward, A.J., Rotella, P., Collins, J., Windisch, R., 2015. An evaluation of variation in published estimates of schizophrenia prevalence from 1990—2013: a systematic literature review. BMC Psychiatry 15. https://doi.org/10.1186/S12888-015-0578-7

Wamsley, E.J., Tucker, M.A., Shinn, A.K., Ono, K.E., McKinley, S.K., Ely, A. v., Goff, D.C., Stickgold, R., Manoach, D.S., 2012. Reduced sleep spindles and spindle coherence in schizophrenia: mechanisms of impaired memory consolidation? Biol Psychiatry 71, 154–161. https://doi.org/10.1016/J.BIOPSYCH.2011.08.008

Yung, A.R., Yung, A.R., Yuen, H.P., Mcgorry, P.D., Phillips, L.J., Kelly, D., Dell'olio, M., Francey, S.M., Cosgrave, E.M., Killackey, E., Stanford, C., Godfrey, K., Buckby, J., 2016. Mapping the Onset of Psychosis: The Comprehensive Assessment of At-Risk Mental States: http://dx.doi.org/10.1080/j.1440-1614.2005.01714.x 39, 964–971. https://doi.org/10.1080/J.1440-1614.2005.01714.X

Zanini, M., Castro, J., Coelho, F.M., Bittencourt, L., Bressan, R.A., Tufik, S., Brietzke, E., 2013. Do sleep abnormalities and misaligned sleep/circadian rhythm patterns represent early clinical

characteristics for developing psychosis in high risk populations? Neurosci Biobehav Rev 37, 2631–2637. https://doi.org/10.1016/J.NEUBIOREV.2013.08.012

Zanini, M.A., Castro, J., Cunha, G.R., Asevedo, E., Pan, P.M., Bittencourt, L., Coelho, F.M., Tufik, S., Gadelha, A., Bressan, R.A., Brietzke, E., 2015. Abnormalities in sleep patterns in individuals at risk for psychosis and bipolar disorder. Schizophr Res 169, 262–267. https://doi.org/10.1016/J.SCHRES.2015.08.023

6. PROJECT 5

6.1. Preface

In this project, I present the last and more complex application of the hdEEG pipeline described in project 1 (see Chapter 2). More specifically, I refined an advanced whole-brain source connectivity analysis, which have been seldom used in the sleep field. This analysis was tested on a single drug-naïve young adolescent affected by sleepwalking (NREM sleep parasomnia), a subtype of the so-called disorders of arousal (DOA).

6.2. DOA

Parasomnias are *"disorders characterized by abnormal behavioral, experiential, or physiological events occurring in association with sleep, specific sleep stages, or sleep–wake transitions. The most common parasomnias – NREM sleep arousal disorders and rapid eye movement (REM) sleep behavior disorder – represent admixtures of wakefulness and NREM sleep and admixtures of wakefulness and REM sleep, respectively. These conditions serve as a reminder that sleep and wakefulness are not mutually exclusive and that sleep is not necessarily a global, whole brain phenomenon"* (American Psychiatric Association, 2013a). Specifically, the disruption of the mechanisms underlying the transition between NREM sleep and wake has been proposed to account for the so-called "Disorders of Arousal" (DOA) (Table 1). Affected patients may exhibit waking behaviors arising abruptly out of NREM sleep, such as sitting-up in bed, screaming, or waking. Despite the variety of displayed behaviors, different subtypes are believed to belong to the

same family of disorders, on the basis of genetic, familiar, electrophysiological and clinical evidence (American Academy of Sleep Medicine, 2014).

DSM-5 **Non-Rapid Eye Movement Sleep Arousal Disorders**	**ICSD-3** **NREM-related parasomnias**
	Disorders of arousal
□ *Recurrent episodes of incomplete awakening from sleep, usually occurring during the first third of the major sleep episode, accompanied by either one of the following:* *1. Sleepwalking: repeated episodes of rising from bed during sleep and walking about. While sleeping, the individual has a blank, staring face; is relatively unresponsive to the efforts of others to communicate with him or her; and can be awakened only with great difficulty.* *2. Sleep terrors: recurrent episodes of abrupt terror arousals from sleep, usually beginning with panicky scream. There is intense fear and signs of autonomic arousal, such as mydriasis, tachycardia, rapid breathing, and sweating, during each episode. There is relative unresponsiveness to efforts of others to comfort the individual during the episodes.*	□ *Recurrent episodes of incomplete awakening from sleep.* *Notes:* *The events usually occur during the first third of the major sleep episode.* *The individual may continue to appear confused and disoriented for several minutes or longer following the episode.*
	□ *Inappropriate or absent responsiveness to efforts of others to intervene ore redirect the person during the episode.*
□ *No or little (e.g. only a single visual scene) dream imagery is recalled.*	□ *Limited (e.g. a single visual scene) or no associated cognition or dream imagery.*
□ *Amnesia for the episodes is present.*	□ *Partial or complete amnesia for the episode.*
□ *The episodes cause clinically significant distress or impairment in social, occupational, or other important areas of functioning.*	
□ *The disturbance is not attributable to the physiological effects of a substance (e.g. a drug of abuse, a medication).* □ *Coexisting mental and medical disorders do not explain the episodes of sleepwalking or sleep terrors.*	□ *The disturbance is not better explained by another sleep disorder, mental disorder, medical condition, medication, or substance abuse.*
Subtypes: • *Sleep terror type* • *Sleepwalking type* * *with sleep-related eating* * *with sleep-related abnormal sexual behavior*	***Subtypes:*** • *Sleep Terror* • *Sleepwalking* • *Confusional Arousal*
	Sleep-related eating disorder

Table 1. International diagnostic criteria for DOA according to DSM-5 and ICSD-3

DSM-5: Diagnostic and Statistical Manual for Mental Disorders, 5th Edition (American Psychiatric Association, 2013b). *ICSD-3: International Classification of Sleep Disorders, 3rd Edition* (American Academy of Sleep Medicine, 2014).

6.3. Sleep in DOA

Even during nights without episodes, patients with DOA have several microstructural sleep abnormalities, like an increased arousal sleep instability (Zucconi et al., 1995), abnormal across-night SWA build-up (Gaudreau et al., 2000), hypersynchronous delta-waves (Pressman, 2004), recurrent local activations as measured by stereo-EEG (Terzaghi et al., 2009), an abnormal topographical distribution of SWA (Castelnovo et al., 2016). However, clear and easily usable objective EEG diagnostic markers to identify DOA in the absence of full-blown episodes during v-PSG recordings are still lacking.

Furthermore, the literature on the neurophysiological correlates during episodes is limited, due to the aforementioned difficulty in catching episodes in laboratory settings and due to methodological issues (like the removal of movement artifacts). It has been hypothesized – and partially demonstrated - that local arousal in the motor and limbic areas, in the context of an otherwise sleeping brain, is at the root of the motor behaviors peculiar of DOA, as illustrated in Figure 1 (Castelnovo et al., 2018). This might represent an exaggeration of the physiological tendency of these networks to exhibit a lower arousal threshold (Nobili et al., 2012), which may have evolved to increase the chance of survival by favoring a prompt motor response in case of danger.

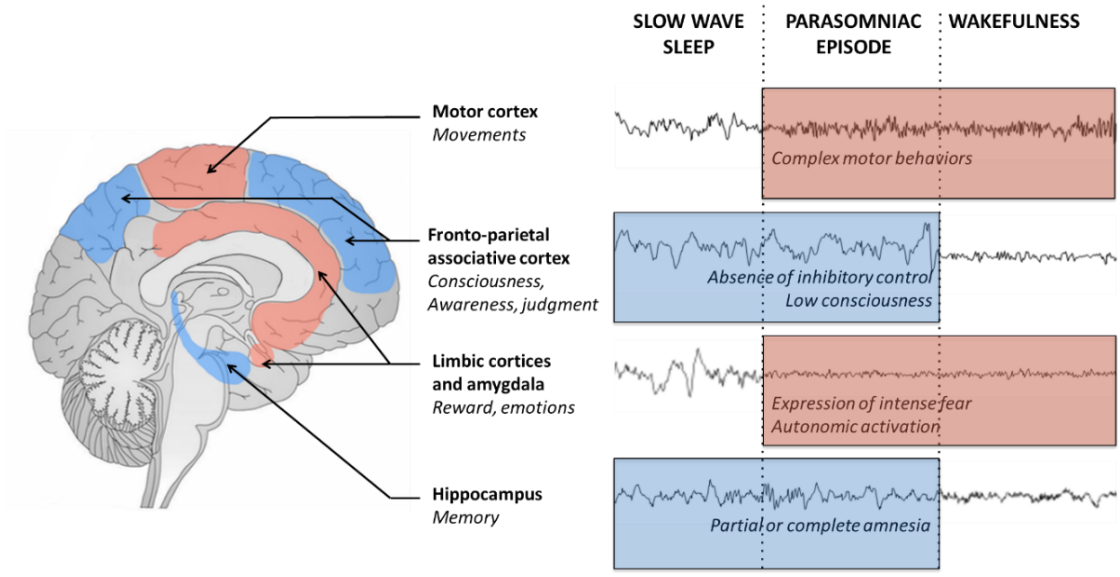

Figure 1. Graphical representation of the functional dissociation between brain regions during DOA episodes. *Taken from* (Castelnovo et al., 2018).

Interestingly, while remaining largely unresponsive to the external environment, DOA patients are able to perform complex behaviors, like wandering around with eyes wide open without tumbling or falling, which imply at least a partial preservation of consciousness. Patients may occasionally report subjective mental experiences associated with their episodes (Oudiette et al., 2009). These experiences usually take the form of fragmentary images or even of complex dreams, sometimes of proper hallucinations where internally generated percepts are mixed with real elements of the external environment (Castelnovo et al., 2021a, 2021b), suggesting that, in parallel with the reactivation of specific brain structures, also consciousness partially re-emerges, although in an unstable form, different from wakefulness and closer to a dream and/or a psychotic state.

6.4. Study aims

The study presented in this section aimed to characterize for the first time the whole brain source EEG activity (in terms of power and connectivity) before and during DOA episodes (n = 20, extracted from 2 consecutive in-laboratory hdEEG sleep recordings) of one single drug-naïve subject (a 12 years old young adolescent) with a long-lasting history of sleepwalking. More specifically, the goal was to find elements in support of the hypothesis that patients are conscious during DOA episodes.

6.5. Original paper

I herein enclose the original paper that resulted from this thesis project, recently published in Cortex (Castelnovo et al., 2022).

CORTEX 155 (2022) 62–74

Available online at www.sciencedirect.com

ScienceDirect

Journal homepage: www.elsevier.com/locate/cortex

Single Case Report

High-density EEG power topography and connectivity during confusional arousal

Anna Castelnovo [a,b,c,*,1], Julian Amacker [d,1], Massimo Maiolo [d,e], Ninfa Amato [a], Matteo Pereno [a], Silvia Riccardi [a], Andrea Danani [f], Simone Ulzega [d] and Mauro Manconi [a,b,g]

[a] Sleep Medicine Unit, Neurocenter of Southern Switzerland, Ospedale Civico, Lugano, Switzerland
[b] Faculty of Biomedical Sciences, University of Southern Switzerland, Lugano, Switzerland
[c] University Hospital of Psychiatry and Psychotherapy, University of Bern, Bern, Switzerland
[d] Institute of Computational Life Sciences, Zurich University of Applied Sciences, Wädenswil, Switzerland
[e] Institute of Pathology, University of Bern, Bern, Switzerland
[f] Dalle Molle Institute for Artificial Intelligence, USI-SUPSI, Lugano, Switzerland
[g] Department of Neurology, University Hospital, Inselspital, Bern, Switzerland

ARTICLE INFO

Article history:
Received 20 February 2022
Reviewed 25 April 2022
Revised 28 April 2022
Accepted 29 May 2022
Action editor Veena Kumari
Published online 22 July 2022

Keywords:
Disorders of arousal
NREM-sleep parasomnia
Somnambulism
Night terror
Pavor nocturnus

ABSTRACT

Confusional arousal is the milder expression of a family of disorders known as Disorders of Arousal (DOA) from non-REM sleep. These disorders are characterized by recurrent abnormal behaviors that occur in a state of reduced awareness for the external environment. Despite frequent amnesia for the nocturnal events, when actively probed, patients are able to report vivid hallucinatory/dream-like mental imagery. Traditional (low-density) scalp and stereo-electroencephalographic (EEG) recordings previously showed a pathological admixture of slow oscillations typical of NREM sleep and wake-like fast-mixed frequencies during these phenomena. However, our knowledge about the specific neural EEG dynamics over the entire brain is limited.

We collected 2 consecutive in-laboratory sleep recordings using high-density (hd)-EEG (256 vertex-referenced geodesic system) coupled with standard video-polysomnography (v-PSG) from a 12-year-old drug-naïve and otherwise healthy child with a long-lasting history of sleepwalking. Source power topography and functional connectivity were computed during 20 selected confusional arousal episodes (from −6 to +18 sec after motor onset), and during baseline slow wave sleep preceding each episode (from − 3 to −2 min before onset).

We found a widespread increase in slow wave activity (SWA) theta, alpha, beta, gamma power, associated with a parallel decrease in the sigma range during behavioral episodes

Abbreviations: BEM, Boundary Element Model; DOA, Disorders of Arousal; EEG, Electroencephalography/ic; FDR, False-discovery rate; NREM, Non-rapid eye movement; PSD, Power Spectral Density; PTE, Phase Transfer Entropy; RDI, Respiratory Disturbance Index; SHE, Sleep-related hyper-motor epilepsy; sLORETA, Standardized low resolution electromagnetic tomography; PLMSI, Periodic Limb Movements Index during Sleep; SPECT, Single photon emission computed tomography; SWA, Slow Wave Activity; vPSG, Video-polysomnography.

* *Corresponding author*. Via Tesserete 46, 6900 Lugano,
E-mail address: anna.castelnovo@eoc.ch (A. Castelnovo).

[1] These two authors contributed equally to the manuscript.

https://doi.org/10.1016/j.cortex.2022.05.021

compared to baseline sleep. Bilateral Broadman area 7 and right Broadman areas 39 and 40 were relatively spared by the massive increase in SWA power. Functional SWA connectivity analysis revealed a drastic increase in the number and complexity of connections from baseline sleep to full-blown episodes, that mainly involved an increased out-flow from bilateral fronto-medial prefrontal cortex and left temporal lobe to other cortical regions. These effects could be appreciated in the 6 sec window preceding behavioral onset.

Overall, our results support the idea that DOA are the expression of peculiar brain states, compatible with a partial re-emergence of consciousness.

1. Introduction

DOA are Non-Rapid Eye Movement (NREM) sleep parasomnias that are thought to derive from incomplete arousal out of NREM sleep (Castelnovo, Lopez, Proserpio, Nobili, & Dauvilliers, 2018; Zadra, Desautels, Petit, & Montplaisir, 2013). Indeed, DOA episodes are characterized by recurrent abnormal sleep-related complex behaviors, lasting from a few seconds to several minutes, associated with various degrees of autonomic activation, and inappropriate or scarce responsiveness to the external environment. These behaviors may range from sitting in the bed quietly with the eyes usually wide open (confusional arousal) to screaming loudly and other fear-related expressions (night terrors) and/or wandering about in the house or even outdoor (sleepwalking). Patients are often amnestic for their events, but when actively probed they may report vivid mental images, thoughts and emotions that are evocative of an hallucinatory/dreaming state (Baldini et al., 2019; Castelnovo, Loddo, Provini, & Manconi, 2021; Castelnovo, Loddo, Provini, Miano, & Manconi, 2021; Mwenge, Brion, Uguccioni, & Arnulf, 2013; Oudiette et al., 2009; Rocha & Arnulf, 2020; Uguccioni et al., 2013).

Severe cases are associated with sleep fragmentation, daytime sleepiness, psychological distress and even with self-harm or legal consequences (Ingravallo et al., 2014). Nonetheless, little progress was made in the last decades in our understanding of DOA neurobiological underpinnings. As a consequence, the diagnosis of these complex manifestations relies solely on clinical criteria.

Sparse evidence suggested that EEG changes precede by a few seconds DOA abnormal behaviors (Desjardins et al., 2017; Espa, Ondze, Deglise, Billiard, & Besset, 2000; Guilleminault, Poyares, Abat, & Palombini, 2001; Jaar, Pilon, Carrier, Montplaisir, & Zadra, 2010; Januszko et al., 2016; Perrault, Carrier, Desautels, Montplaisir, & Zadra, 2014; Terzaghi et al., 2009; Zadra & Nielsen, 1998). Moreover, according to some old qualitative studies based on visual inspection (Schenck, Pareja, Patterson, & Mahowald, 1998; Zadra, Pilon, Joncas, Rompré, & Montplaisir, 2004), as well as quantitative evidence based on one SPECT case report (Bassetti, Vella, Donati, & Wielepp, 2000) and few stereo-EEG case report/series, DOA episodes are states of dissociation characterized by an abnormal coexistence of local sleep-like and wake-like features (Bassetti et al., 2000; Flamand et al., 2018; Sarasso et al., 2014; Terzaghi et al., 2009, 2012). Despite offering remarkable insights, all these studies suffer from limitations connected to the technique they used to investigate these phenomena. More specifically, SPECT low temporal resolution does not allow study of the temporal dynamics of DOA episodes, while stereo-EEG spatial resolution is constrained by the location of the suspected epileptogenic focus. High-density (hd)-EEG is a well-established modern technique that combines the high temporal definition of EEG, with a reasonably high spatial resolution derived by the high-number of scalp electrodes. Interestingly, a first high-density (hd) EEG case report of DOA was reported by our group, which suggested the potential role of the right hemisphere in gating the spreading of abnormal slow wave activity over the left hemisphere, mediating the occurrence of full-blown clinical episodes (Ratti, Amato, David, & Manconi, 2018).

The current work aimed at mapping the EEG dynamics prior and during clinical episodes, at both the scalp and source level, applying spectral and connectivity analyses to 2-night sleep hd-EEG recordings from a single patient with DOA.

2. Case report

2.1. *Clinical history*

The patient is a 12-year-old, Caucasian, right-handed male with a history of DOA - sleepwalking and confusional arousal sub-types (ICSD-3) since the age of 4 years. During his typical sleepwalking episodes, usually about 30–90 min after sleep onset, he quietly wandered around the house with a vacant expression and was apparently unresponsive to his parents. Less frequently, he approached his parents anxiously, mumbling or yelling complex, out-of-context, agitated statements like "You know it, oh, you know it very well!" He usually returned to bed spontaneously or guided by his parents after 1–5 min, falling back to sleep immediately. During minor confusional arousal episodes, he sat up on his bed for few seconds (<1 min), staring at the air or looking around, more often calling his sister and/or talking to her (e.g., "We are trapped in here!") and pointing to non-existent objects in the room. He was usually amnestic for the events, although during the clinical interview he was able to recall 3 episodes associated with dreamlike mental imagery (Castelnovo, Loddo, Provini, Miano, & Manconi, 2021). The family history was positive for NREM sleep parasomnias. The frequency of the episodes had been stable over the years - on average 2–3

major sleepwalking episodes per week and minor episodes almost every night. His personal medical history was unremarkable. Except for frequent sleep-talking and sleep hyperhidrosis, his sleep history was not evocative of any other sleep disorder. Medical and neurologic physical examination showed no abnormalities. Routine hematology testing was normal. The Child Behavior Checklist (Nakamura, Ebesutani, Bernstein, & Chorpita, 2009) did not reveal any behavioral or emotional problem (total score = 11, none of the subscales scored above the pathological threshold). Legal copyright restrictions prevent public archiving of the Child Behavior Checklist, which can be obtained from the copyright holder in the associated reference. Video-Polysomnography (v-PSG) monitoring was planned to exclude mimics or comorbidities. The patient was enrolled in the context of a larger observational, single-center study carried out at the Neurocenter of Southern Switzerland. All study procedures were reviewed and approved by the local Independent Ethics Committee "Comitato Etico Cantonale" (2017-01788 – n.3282, approval date: 15.12.2017), according to the regulatory requirements of Switzerland. The child and his parents provided written consent prior to the beginning of the study.

2.2. *v-PSG recording*

The patient underwent 2 overnight in-laboratory sleep recordings at the Sleep Medicine Unit of the Neurocenter of Southern Switzerland. A full montage with traditional video-PSG channels (electro-oculogram, electromyogram of the submentalis muscle and of the right and left tibialis anterior muscles, electrocardiogram, oral and nasal airflow thermistors, nasal pressure cannula, and wearable piezo-electric bands for thoracic and abdominal movements) was coupled with a high-density EEG system (256 channels; Electrical Geodesics Inc., Eugene, OR, vertex referencing, sampling rate of 500 Hz). Lights-out and light-on were within 1 h of the participant's most consistently reported bedtime. Sleep staging was performed by a board-certified sleep physician, according to standard AASM (Berry et al., 2020) criteria using the EMBLA-RemLogic software based on 30-s epochs for 6 EEG derivations extracted from the high-density EEG system, with bipolar re-referencing (F3/M2, F4/M1, C3/M2, C4/M1, O1/M2, O2/M1), EOG, and submental EMG.

Supplementary video related to this article can be found at https://doi.org/10.1016/j.cortex.2022.05.021

Sleep-disorder breathing (RDI <1) and periodic limb movements (PLMSI <5) were ruled out by concurrent v-PSG. DOA episodes were selected according to the following inclusion/exclusion criteria, which were established before data analysis: 1) episodes must be scored in line with international criteria (Berry et al., 2020) and characterized according to motor video-patterns (Loddo et al., 2018); 2) episodes must not be associated with Mayor Body Movements, as defined by international criteria (Berry et al., 2020); 3) to increase the accuracy and consistency of the evaluation of minor DOA episodes, an episode could only be retained when classified as confusional arousal by 3 independent raters looking at v-PSG, or when an agreement between the raters could be reached after discussion. Twenty behavioral events during sleep stage 3 (9 and 11 per night, respectively) were double-blindly identified by 3 different sleep medicine experts (AC, SR, MM). Episode onset was defined as an abrupt, at least-twofold amplitude increase in EMG channels (the first between chin EMG, arm EMG or leg EMG). All episodes were characterized by non-stereotyped motor behaviors - type I and type II patterns (Loddo et al., 2018). Behaviors ranged from head flexion/extension, limb movements or partial trunk flexion/extension in variable combinations to a complete trunk flexion with patient sitting up in bed with a blind gaze or looking around (see Supplementary Material for an explicative Videoclip). Some episodes were associated with partially intelligible speech. Episodes lasted from about 15 to 30 sec. After episodes, the patient rapidly fell asleep again except for a couple of longer episodes ending with a brief confusional phase and a progressive re-emergence into wakefulness. The subsequent morning the patient did not recall any of the events.

2.3. *Hd-EEG data analysis*

EEG data analysis was conducted with MATLAB (Mathworks Inc., Natick, MA, USA) using the EEGLAB v13 (Delorme & Makeig, 2004) and BRAINSTORM (Tadel, Baillet, Mosher, Pantazis, & Leahy, 2011) toolboxes, and custom scripts. Recordings were off-line high-pass filtered (.1 Hz IIR filter reproducing a single resistor capacity), and subsequently band-pass filtered (.5–45 Hz, Kaiser window-based FIR with zero-phase distortion). From the all-night hd-EEG recordings, segments commencing 3 min before and ending 1 min after each episode onset were selected for further analysis. Data channels and segments containing artifactual activity were visually identified and marked as bad using the BRAINSTORM graphical interface. The signal was then re-referenced to the average of the scalp voltage for all 256 channels. Bad epochs were rejected and the signal for bad channels was reconstructed from the weighted average of neighboring channels using spherical interpolation and with a maximal distance between electrodes of 5 cm.

Source modeling was performed with Brainstorm using an age-appropriate template (Richards, Sanchez, Phillips-Meek, & Xie, 2016), segmented using SPM12/CAT12 Matlab toolbox (Tzourio-Mazoyer et al., 2002). A symmetric BEM of the head having three realistic layers (scalp, inner skull, outer skull) (Maureen, 2010) and a standard co-registered set of electrode positions were used to construct the forward model. The inverse matrix was computed using the sLORETA Minimum Norm (Pascal-Marqui, 2002) with sources constrained to be perpendicular to the cortical surface and retaining only diagonal elements of the noise covariance matrix.

PSD was computed at the scalp level and in source space using Welch's modified periodogram method in 6-s Hamming windows with 50% overlap. The magnitude of the complex PSD was extracted for further analysis. The primary analysis focused on average magnitude of PSD in the .5–4 Hz range, which is associated with slow waves (SWA). A subsequent analysis then explored between-state differences in oscillatory power in theta (4–8 Hz), alpha (8–12 Hz), sigma (12–16 Hz), beta (18–30 Hz) and low gamma (30–45 Hz) frequency bands. For the scalp level both absolute average referenced and subject-normalized (using z-score across

channels) topographic maps were examined, while in source space only the normalized maps (using sLORETA based minimum norm estimates) were considered.

Moreover, Phase Transfer Entropy (PTE) (Lobier, Siebenhühner, Palva, & Palva, 2014), a measure of directed connectivity among neuronal oscillations, was computed at the source level using the average source activity in brain regions defined by the Destrieux atlas for cortical parcellation (Destrieux, Fischl, Dale, & Halgren, 2010). The PTE was normalized according to Hillebrand et al., 2016 (Hillebrand et al., 2016).

The use of PTE as a metric for functional connectivity analysis has several benefits over other methods, namely, it is not biased by artificial zero-lag correlations and it allows interference in the connectivity phase coupling directionality (Hillebrand et al., 2016; Lobier et al., 2014). Thus, PTE is an excellent exploratory method as it does not make any assumptions about the data. Moreover, PTE can detect nonlinear directed information flows, unlike other coherence-based methods, and thus emerges as a very well-suited approach to infer multiple-pathway functional connectivity patterns, typical of brain networks.

Two behavioral states were selected: baseline stage 3 sleep (−180 to −120 sec before onset) and DOA events (from −6 to + 18 sec). DOA events were further subdivided into 3 time-windows: 1) pre-episode (−6 sec from onset to onset), episode T1 (from onset to 6 sec after onset), episode T2 (from 6 to 12 sec from onset), and episode T3 (from 12 to 18 sec from onset). Six-second windows were chosen on the basis of a stereo-EEG study that captured EEG activity changes 5 sec before the start of the clinical onset (Terzaghi et al., 2009) – and to ensure the stability of connectivity results (Fraschini et al., 2016).

Statistical comparisons for sensor and source topographical analysis were made within-subjects and used 2-sided paired t-tests between behavioral states. Group level analyses on the average PSD values were performed separately for each frequency band. Whole cortex analyses were conducted correcting for multiple comparisons using a nonparametric cluster based permutation test (Nichols & Holmes, 2001) with 10000 permutations for scalp power topography and using topological cluster false-discovery rate (FDR) for source power topography and connectivity. Cluster-size tests were used to test for significant regions using a cluster-forming threshold of $p = .05$ and a cluster size threshold of $p < .05$ (cluster corrected).

3. Results

Scalp power analysis. Pre-episode, compared to baseline, was associated with a widespread significant increase in absolute power in SWA. At an exploratory analysis, a similar increase involved theta (Fig. 1, column 1). Normalized maps displayed a significant cluster of relative decrease in sigma and a pattern of relative decrease over frontal areas in lower frequency bands (Supplementary Figure 1, column 1). Episode T1, compared to baseline, was associated with a diffuse increase of absolute power in all frequency bands (Fig. 1, column 2), which decreased over time for lower frequencies in Episode T2 and T3 (Fig. 1, column 3 and 4). The only exception was sigma, which

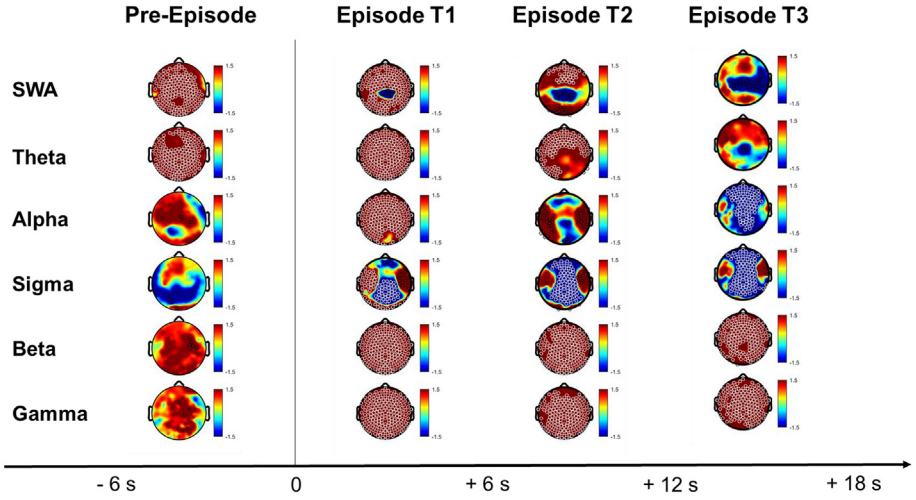

Fig. 1 – Scalp power analysis in all frequency bands. Rows: frequency bands of interest as indicated: SWA (.5–4 Hz), theta (4–8 Hz), alpha (8–12 Hz), sigma (12–16 Hz), beta (18–25 Hz), gamma (25–45 Hz). Columns: comparison between absolute power at baseline and pre-episode, episode T1, episode T2, episode T3. The horizontal black arrow at the bottom defines time in seconds. Baseline: average power from −3 to −2 min before behavioral onset. Pre-episode (column 1): average power from −6 sec prior to onset to onset. Episode T1 (column 2): from onset to 6 sec after onset. Episode T2 (column 3): from 6 to 12 sec after onset. Episode T3 (column 4): from 12 to 18 sec after onset. Blue values: a decrease in absolute EEG power in pre-episode relative to baseline (pre-episode < baseline). Red values: an increase (pre-episode > baseline). White dots: channels that belong to a statistically significant cluster of electrodes ($p \leq .05$) using statistical nonparametric mapping suprathreshold cluster testing. Black dots: individual channels with $p < .05$ (uncorrected). Note: Electrodes on the face and outer ring of the sensor net were eliminated entirely for all participants due to excessive artifacts, yielding a final scalp montage of 186 channels.

displayed a stable decrease over midline brain regions, with a distribution resembling sleep spindle topography in both absolute and normalized power maps (Fig. 1, column 2 to 4).

Of note, in the SWA range, a central cluster of channels was spared by the global power increase (Fig. 1, column 2). This effect became progressively more accentuated over time (Fig. 1, column 3 and 4) and emerged more clearly in normalized maps (Supplementary Figure 1, column 4, 6 and 8). A similar pattern could also be observed in normalized theta values, with a more accentuated antero-posterior discrepancy (Supplementary Figure 1, column 2 to 4).

Cortical source power analysis. No significant differences in band power between pre-episode and baseline were observed in any frequency band at the source level (Fig. 2, column 1). Relative higher SWA power could be observed at the beginning of the episodes (T1) in almost all brain regions except for a centro-posterior zone mainly represented by the precuneus and the superior parietal lobe, bilaterally (Fig. 2, column 2). This increased activity could still be observed mainly over the left hemisphere at T2 in the orbital frontal cortex and gyrus rectus, temporal pole, the anterior, mid and ventral posterior cingulate, the insula, and occipital visual areas (inferior and superior occipital gyri, occipital pole) (Fig. 2, column 3), but not in later stages of the episodes (T3) (Fig. 2, column 4). Compared to baseline, Episode T3 was associated with significantly lower SWA over the right supramarginal and angular gyri, bilateral precuneus (right > left), bilateral paracentral lobule and superior parietal lobule (Fig. 3, column 4).

Exploratory comparisons for other frequency bands are summarized in Supplementary Figure 2, Supplementary Figure 3 and Supplementary Figure 4. Shortly, theta showed a pattern similar to delta, alpha and sigma displayed a relative decrease over midline brain structures and a relative increase over lateral regions, which remained stable over time (from T1 to T2). Finally, beta and gamma source power values were globally and stably increased compared to baseline (from T1 to T2).

3.1. *Connectivity analysis*

The PTE analyses in the SWA range during baseline sleep (Fig. 3A) revealed a rather simple, stereotyped and poorly differentiated pattern of connectivity where almost all information stemmed from 3 main frontal hubs (right middle and inferior frontal gyri > right orbito-lateral frontal cortex > left middle and inferior frontal gyri) and was directed towards almost all brain regions. A disruption of this pattern could be already observed in the pre-episode period (Fig. 3B) that

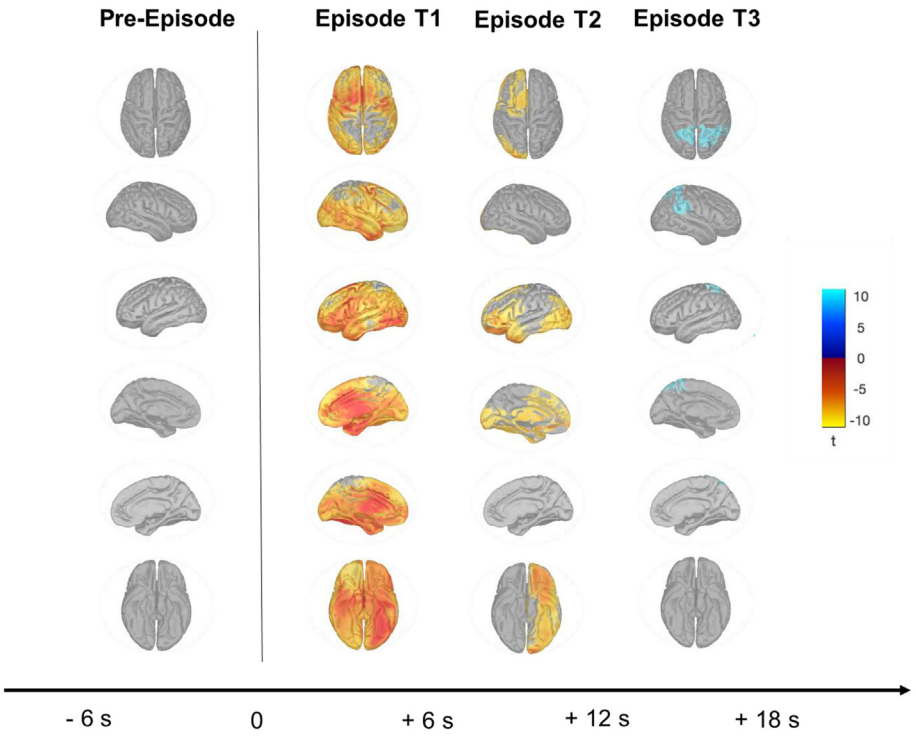

Fig. 2 – SWA source power analysis. Columns: comparison between absolute power at baseline and pre-episode, episode T1, episode T2, episode T3. The horizontal black arrow at the bottom defines time in seconds. Baseline: from −3 to −2 min before behavioral onset. Pre-episode: from −6 sec prior to onset to onset. Episode T1: from onset to 6 sec after onset. Episode T2: from 6 to 12 sec after onset. Episode T3: from 12 to 18 sec after onset. Gray color: non-significant differences after correction for multiple comparison using topological cluster false-discovery rate (FDR). Blue color: a significant decrease in source power in pre-episode or episode relative to baseline (pre-episode/episode < baseline) using FDR. Red color: a significant increase in source power in episode relative to baseline (pre-episode/episode > baseline) using FDR. First row: Horizontal plane (top); second row: sagittal plane, right hemisphere (lateral), third row: sagittal plane, left hemisphere (lateral), fourth row: sagittal plane, right hemisphere (medial), fifth row: sagittal plane, left hemisphere (medial), sixth row: horizontal plane (bottom).

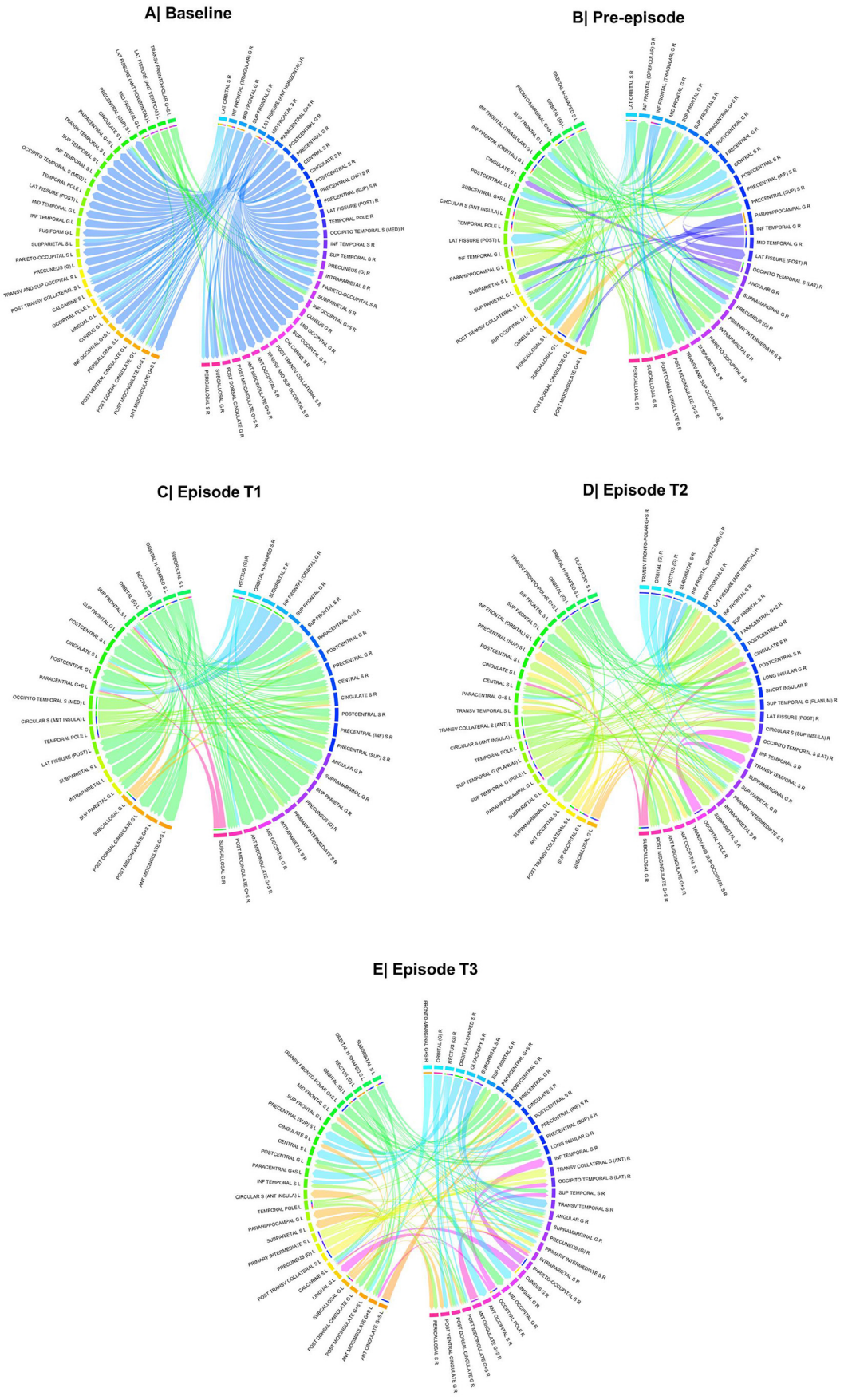
A| Baseline
B| Pre-episode
C| Episode T1
D| Episode T2
E| Episode T3

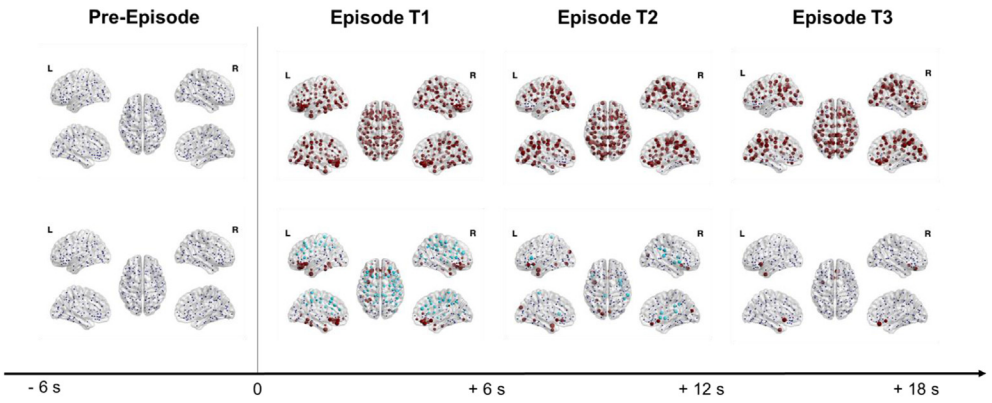

Fig. 4 – Hd-EEG source connectivity analysis (3D representation of mean strength connectivity for each brain region). Columns: comparison between outflow-inflow functional connectivity at baseline and pre-episode, episode T1, episode T2, episode T3. The horizontal black arrow at the bottom defines time in seconds. Baseline: from −3 to −2 min before behavioral onset. Pre-episode: from −6 sec prior to onset to onset. Episode T1: from onset to 6 sec after onset. Episode T2: from 6 to 12 sec after onset. Episode T3: from 12 to 18 sec after onset. Upper rows: statistical comparison of global PTE connectivity (sum of input and output) in each brain region/node. Bottom rows: statistical comparison of global PTE connectivity (different of input and output) in each brain region/node.

displayed a more scattered, integrated and differentiated network of connections originating mainly from: (i) the left temporal lobe: left anterior insula, left temporal pole, left parahippocampal gyrus > (ii) the left frontal lobe (with hubs distributed more anteriorly than during baseline): left orbito-frontal cortex and left gyrus rectus, left orbito-lateral frontal sulcus and to a lesser extent left inferior frontal gyrus (orbital and triangular part) > (iii) the right temporal lobe: lateral inferior, middle and superior temporal gyri as well as para-hippocampal gyrus > (iv) right orbito-lateral frontal sulcus and right inferior temporal lobe (triangular part).

During the episode, PTE connectivity hubs involved the entire orbitofrontal cortices, bilaterally, the left temporal pole, while the right temporal lobe hub was progressively lost, with the concomitant emergence of more scattered connections over parieto-occipital bilateral brain regions (Fig. 3C D and E).

Absolute SWA connectivity (sum of input and output connections from each brain area) was globally increased in pre-episode and during the episode compared to baseline (Fig. 4, upper rows), while net connectivity (meaning the difference between output and input) basically reflected what described for circular plots (Fig. 4, lower rows). At the very beginning of the episode there was a bilateral higher outflow of information from left and right orbitofrontal and inferior lateral frontal brain regions as well as polar and infero/medial temporal areas, and a higher inflow in almost all other brain regions compared to baseline. Subsequently, the increase in outflow persisted bilaterally over basal frontal regions but was skewed towards the left temporal lobe while the increase in inflow displayed the opposite effect.

4. Discussion

This is the first study investigating broad-band brain EEG scalp/source power topography and connectivity prior to and during clinical DOA episodes using hd-EEG, which allowed for a precise analysis of local changes in the space and time domains.

20 confusional arousal episodes (from −6 sec before to + 8 sec after motor onset) were extracted from 2-night recordings in the same subject (a 12-year-old male). The hd-EEG activity in 4-time windows (pre-episode: −6 to 0 sec, episode t1: 0 to + 6 sec, episode t2: from +6 to +12 sec, episode t3: +12 to +18 sec) was extracted and compared to stable slow wave sleep (baseline: −2 to −3 min before onset).

At the scalp level, we found a widespread increase of scalp SWA and theta in pre-episode compared to baseline and an increase in SWA, theta, alpha, beta, gamma, associated with a parallel decrease in sigma during episode compared to baseline. Notably, the increase in SWA power displayed a specific regional pattern that spared bilaterally Broadman area 7 and right Broadman areas 39 and 40.

Functional connectivity in the SWA range underwent drastic changes from pre-episode to episode compared to baseline, with a significant increase in the number and in the distribution of connections. Importantly, the key areas implicated seemed to be the frontal lobes (mainly right infero-lateral prefrontal cortex during baseline and bilateral ventro-medial pre-frontal cortex during clinical episodes) and the left anterior insula/left anterior temporal lobe (mainly infero-

Fig. 3 – Hd-EEG SWA source functional connectivity analysis (circular plots). Circular plots for average functional connectivity (PTE: phase transfer entropy) at A) Baseline: from −3 to −2 min before behavioral onset, B) Pre-episode: from −6 sec prior to onset to onset, C) Episode T1: from onset to 6 sec after onset, D) Episode T2: from 6 to 12 sec after onset, E) Episode T3: from 12 to 18 sec after onset. The direction of the arrow indicates the direction of functional connectivity. Ant: anterior. Post: posterior. Sup: superior. Inf: Inferior. Transv: transverse. G: gyrus. S: Sulcus. L: left. R: right.

lateral, ventral and medial). Overall, during DOA episodes compared to baseline sleep, connectivity seemed to mainly flow from ventral to dorsal, and from left to right brain areas.

4.1. *Comparison with the literature*

Our power results for pre-episode versus baseline are in line with the sparse existing literature, add relevant topographic information and support a consistency of findings in children, previously investigated only by Espa et al. (2000).

At the turn of last century, Zadra and Nielsen reported for the first time a specific increase in SWA prior to night terrors from a single subject compared to average slow wave sleep from a control group (Zadra & Nielsen, 1998). This effect was larger over fronto-central channels and asymmetrically distributed (left > right, 19 channel montage). Subsequently, 4 studies conducted on small groups of patients with sleepwalking and/or sleep terrors (n = 11–22), confirmed an increase in SWA at central or midline leads, with some discrepancies related to the pattern of increase: a progressive increase over the preceding several minutes in a group of children (Espa et al., 2000) versus a clear-cut increase in the few preceding (from 30 to 12) seconds in adults (Desjardins et al., 2017; Guilleminault et al., 2001; Jaar et al., 2010).

The parallel increase in theta prior to episodes compared to baseline was previously described by Desjardins at al., who reported an increase in delta and theta (but not in alpha and beta) in the 20 sec preceding episodes compared to baseline (n = 27, 3 midline leads).

Sigma power - which indirectly represents sleep spindles - tended to decrease just prior to DOA episodes compared to baseline, although at a non-significant level, once again in line with a previous observation of a trend-significance by Desjardin et al. (Desjardins et al., 2017). In our case, the decrease was localized in a central parietal cluster of electrodes resembling the typical distribution of fast spindles.

Finally, beta and gamma tended to be higher in pre-episode versus baseline, reaching significance in the 2-s window prior to onset (data not shown). To the best of our knowledge, gamma activity has not been reported by previous studies, while Januszko et al. found a similar increase in high beta (24–30 Hz), localized at the level of the cingulate motor area when comparing −8 to −4 sec segments to −4 sec to onset segments (Januszko et al., 2016).

At the source level, no significant difference emerged in the power maps of any frequency band during the pre-episode compared to baseline. The only previous hd-EEG study (Ratti et al., 2018) – a case report on a young man suffering from sleepwalking – found an increase of low SWA power in the 5 sec prior to behavioral onset in the right prefrontal cortex (Brodmann's areas 10 and 11). The instability of source findings in the pre-episode period might be related to the different definition of behavioral onset: in the current case report, it was defined as the first EMG movement of chin, legs, or arms, while the previous case report only used chin EMG.

Subsequently, during DOA episodes, absolute SWA power remained globally higher compared to baseline at the scalp level and this effect also turned out to be significant at the source level. Moreover, source analysis revealed a specific regional pattern, not previously described, where parietal higher order associative brain regions (bilateral precuneus and paracentral lobules and right temporo-parieto-occipital junction) were relatively spared by an overwise widespread increase. The previously mentioned hd-EEG case report by Ratti et al. also reported that SWA power, after an initial increase over the right prefrontal cortex just prior to behavioral onset, spread bilaterally and involved the left prefrontal and left temporal cortices in the 0 to 10 sec-span after onset (Ratti et al., 2018). These areas displayed the maximal increase in SWA power in our current analysis. However, Ratti et al. could not detect areas of local relative decrease in SWA power, probably because this latter finding emerged progressively and became significant only between 12 and 18 sec after onset, a time-window not previously investigated. Of note, from 6 to 12 sec after onset, we only found a lateralized effect over the left hemisphere, as in Zadra et al. (Zadra & Nielsen, 1998). Despite the interesting possibility that inter-hemispheric asymmetry plays a role in the development of clinical DOA episodes, the degree of lateralization may vary in different episodes or in different patients.

The scalp and source analysis of other frequency bands during DOA episodes (after behavioral onset) is novel and therefore can't be compared to previous works. It yielded a significant, stable absolute decrease in sigma during DOA episodes compared to baseline, and an absolute increase in theta, alpha, beta and gamma. This increase remained constant throughout the episodes for beta and gamma, while it progressively disappeared for theta and alpha. Beta and gamma were less interpretable because of possible temporal and neck muscle artifacts. However, even considering this limitation, it is interesting to note that central channels (with no artifacts) showed a diffuse increase in high frequencies both at the source and scalp level.

To the best of our knowledge, no previous work investigated EEG connectivity during DOA episodes. Only one study explored connectivity prior to DOA episodes using the imaginary part of the coherence over a longer period of time (20 sec) prior to episode onset, compared to the 20 sec of baseline slow wave sleep occurring 2 min before the episodes (Desjardins et al., 2017). This work revealed a decrease in delta EEG functional connectivity in parietal and occipital regions and in increase of long-range connectivity in alpha and beta range. The use of the imaginary part of coherence (Nolte et al., 2004), as opposed to methods such as Coherency or Phase Locking Value, for evaluating phase coupling between signals, allows circumvention of artificial zero-lag correlations, such as those induced by source leakage (volume conduction problem). However, in general all methods based on coherence estimates, contrary to nonlinear measures of frequency dependence, such as PTE, can be affected by changes in amplitude. Therefore, phase correlated channels, which are not correlated in amplitude, may be lost using a coherence-based approach (Greenblatt, Pflieger, & Ossadtchi, 2012; Pereda, Quiroga, & Bhattacharya, 2005).

4.2. *Interpretation of results*

Current power results during the pre-episode period share similarities with known EEG modifications prior to physiological arousal. More specifically, an increase in fronto-central

SWA and theta activities was previously observed during the 2 sec before arousal onset (Sforza, Jouny, & Ibanez, 2000). Moreover, arousal is known to be associated with a blockage of sleep spindles (Naitoh, Antony-Baas, Muzet, & Ehrhart, 1982; Peter-Derex, Magnin, & Bastuji, 2015), which have been connected with the preservation of sleep continuity (Fernandez & Lüthi, 2020).

The aforementioned similarities between the pre-arousal period and pre-DOA period, on one hand, support a common background, and on the other hand raise concerns about where, when, and how a physiological arousal response becomes dysfunctional in patients with DOA. To date, only 2 studies, based on a limited number of patients ($n = 11–12$) and channels (C3 and/or C4) explored differences between arousals and DOA episodes. These studies found greater SWA and slow oscillation density prior to DOA episodes compared to NREM arousals (Espa et al., 2000) or non-behavioral awakenings (Perrault et al., 2014). However, it remains unclear whether the difference is only related to a different degree of motor activation, as these studies did not make a distinction between motor and non-motor arousals/awakenings. In this regard, our results suggest that an initial arousal-like pattern during pre-DOA episodes later on evolves into a highly disrupted state, different from physiological arousal, leaving our patient "trapped" in a state between sleep and wakefulness. Indeed, while sigma power decreased over a centroparietal cluster of electrodes as during N3 arousal (Peter-Derex et al., 2015), all other frequency bands showed an effect in the opposite direction, meaning a massive global increase. This effect could not be observed during N3 arousal based on the limited available literature. More specifically, a stereo-EEG study (Peter-Derex et al., 2015) detected an overall decrease in delta power in all recorded cortical areas in about 60% of the cases, no changes in the majority of the remaining cases, and a rare paradoxical increase in high-amplitude rhythmic slow wave activity (mainly in frontal but also in parietal dorsolateral cortices). An interesting, although yet speculative hypothesis, could be that DOA episodes arise from an exaggeration or/and an abnormal distribution and persistence of this latter physiological SWA activity.

Taken together, our broad-spectrum power results support the notion of an abnormal and state-specific coexistence of wake-like and sleep-like EEG activity, even in the same brain regions (Flamand et al., 2018).

Another insight is offered by a different aspect of regional dissociation, meaning the observation of brain regions relatively spared by the massive increase in SWA power during episodes (bilateral precuneus and right supramarginal and bilateral angular gyri).

Patients with DOA might be predisposed to this state-specific dissociation, due to a trait-like abnormal distribution of power (relatively lower SWA power over centro-parietal brain regions), as shown in a previous hd-EEG study (Castelnovo et al., 2016). Notably, these trait-like abnormalities in SWA power could be detected also during REM sleep, possibly justifying the occasional description of similar state-dissociations during REM sleep (Bhat, Patel, Rosen, & Chokroverty, 2012; Futenma et al., 2022).

More specifically, the right supramarginal and bilateral angular gyri are cross-modal associative areas implicated in visuo-spatial attention, reorientation of attention towards relevant stimuli, and manipulation of mental representations (Pedrazzini & Ptak, 2019). All these functions are essential to patients in order to navigate through space during clinical episodes. Precuneus, is instead known to be involved in episodic memory, visuospatial processing, reflections upon selfhttps://en.wikipedia.org/wiki/Self_(psychology) (Cavanna & Trimble, 2006), and aspects of conscious experience independently from memory retrieval (Siclari et al., 2017). Thus, the relative decrease in SWA power, typically associated with unconscious states like slow wave sleep or coma, in these brain regions, supports the idea that consciousness reemerges during DOA episodes, although probably in an altered form, during clinical episodes. This hypothesis goes in line with growing evidence pointing to the presence of some form of mental activity during DOA episodes (Baldini et al., 2019; Castelnovo, Loddo, Provini, Miano, & Manconi, 2021; Oudiette et al., 2009). PTE analysis further supports this hypothesis, revealing an increase in integrated and differentiated connectivity from baseline to episodes, typical of wakefulness (Tononi, 2004).

Interestingly, SWA connectivity during baseline sleep displayed an asymmetric frontal right-dominant and antero-posterior pattern. This pattern recalls that observed by studies on slow wave traveling, an indirect measure of brain connectivity during slow wave sleep: larger slow waves are more likely to originate from the right hemisphere (Avvenuti et al., 2020) and to travel antero-posteriorly (Massimini, Huber, Ferrarelli, Hill, & Tononi, 2004). Notably, a bilateral involvement at the beginning of the episode, along with the major involvement of the left temporal lobe, seems to be an essential feature associated with DOA episodes, as in Ratti et al. (2018).

Furthermore, the all-brain and fine-grained connectivity analysis conducted in the source space in this current work allowed for the identification of specific out-flow hubs involved in DOA episodes. Curiously, these hubs mainly involved the ventromedial prefrontal cortex, the left temporal pole, and the left anterior insula, whose function seems to remain deactivated ("sleepier") during DOA episodes. Indeed, the ventromedial prefrontal cortex is thought to represent emotion and reward in decision making as well as facial emotion recognition, theory-of-mind ability processing self-relevant information (Dixon, Thiruchselvam, Todd, & Christoff, 2017; Hiser & Koenigs, 2018), functions that are likely shared with the left temporal pole (Olson, Plotzker, & Ezzyat, 2007). Similarly, the left anterior insula is activated by all valence categories of emotions, and is involved in social emotions, emotional awareness, and switching between the central executive network and the default mode network (Gu, Hof, Friston, & Fan, 2013; Lamm & Singer, 2010). Notably, the right insula was not involved in SWA connectivity (meaning that it is probably more 'active' during DOA episodes). Right insula is specifically involved in the processing of negative emotions (Gu et al., 2013), which are dominantly expressed during clinical behavioral events (Oudiette et al., 2011).

Overall, the knowledge of specific EEG dynamics during DOA episodes provides a plausible explanation for some of the observed behavioral and mental features associated with DOA episodes.

4.3. *Strengths, limitations and future directions*

Of note, we only captured confusional arousal and minor events and not sleep terrors or sleepwalking episodes. This is in line with data from the literature, which suggests that it is difficult to capture major events during vPSG recordings (Loddo et al., 2009). However, although some differences may exist between different DOA manifestations, it is known that they all belong to the same family of disorders and can also coexist in the same subject or family (Petit et al., 2015). Moreover, confusional arousal and minor episodes are those that pose greater issues of differential diagnosis with SHE in clinical practice (Derry, Harvey, Walker, Duncan, & Berkovic, 2009; Zucconi & Ferini-Strambi, 2000). Therefore, the analysis of minor events is essential for the development of objective methods and tools to support the diagnostic process.

The data reported came from the analysis of DOA episodes from one single subject, and therefore they cannot be generalized to the entire DOA population. It is possible that brain activity during clinical episodes varies from patient to patient, justifying different clinical subtypes and the heterogeneity of DOA semeiology. However, this case report clearly demonstrated that hd-EEG analysis of DOA episodes is feasible, and due to its high spatial and temporal resolution could reveal essential pieces of information to clarify these mysterious phenomena. Future studies should strive to collect DOA episodes in a fairly large clinical sample.

Last but not least, functional connectivity results, despite providing the first detailed insight into brain functioning during clinical DOA episodes, are undermined by the lack of literature on physiological data during both sleep and wakefulness. Our case report calls for the urgent need of studies to cover these gaps in our understanding of brain networks across different brain states.

5. Conclusions

DOA events analyzed for this case report were associated with a drastic decrease of sigma activity compared to average slow wave sleep, likely reflecting a suppression of sleep spindles, as in physiological arousal. On the other hand, all other frequency bands displayed a diffuse absolute increase, suggesting a divergence with normal arousal. Interestingly, in the SWA range, a centro-posterior region encompassing precuneus, paracentral parietal lobule and right supramarginal and angular lobule, seemed to be significantly less involved by this massive increase in power. Functional connectivity in the SWA range displayed a clearcut switch from poorly to highly integrated networks where bilateral orbitofrontal and left ventro-medial temporal lobe were the main output hubs.

Overall, these results parallel the observable behavioral expression of DOA episodes, support the idea that DOA are the expression of peculiar brain states, possibly intermediate between sleep and wakefulness, and point to key patterns subserving a partial re-emergence of consciousness.

We envisage that the systematic analysis of DOA episodes and of other sleep events in potential differential diagnosis, such as SHE, will foster the development of specific tools to support the diagnostic process in most difficult and complex cases.

Open practices

The study in this article earned an Open Data – Protected Access badge for transparent practices. Materials and data for the study are available at https://doi.org/10.5281/zenodo.6501824.

Funding

This study was supported by an ABREOC grant (Advisory Board of Scientific Research of the Ente Ospedaliero Cantonale).

Color statement

Color should be used for all figures in print.

Transparency statement

We report all data exclusions (if any), all inclusion/exclusion criteria, whether inclusion/exclusion criteria were established prior to data analysis, all manipulations and all measures in the study.

Data availability statement

The EEG data that support the findings of this study are openly available at https://doi.org/10.5281/zenodo.6501824.

Code availability statement

The code that supports the findings of this study is openly available at https://github.com/AnnaCastelnovo/sleep-EOC.git.

Pre-registration

No part of the study procedures was pre-registered prior to the research being conducted.

No part of the study analyses was pre-registered prior to the research being conducted.

Credit author statement

Anna Castelnovo: Conceptualization, Methodology, Investigation, Project administration, Funding acquisition, Software, Formal analysis, Data Curation, Visualization, Writing- Original draft preparation, Reviewing and Editing. **Julian Amacker:**

Software, Formal analysis, Visualization, Reviewing and Editing. **Massimo Maiolo:** Software, Formal analysis, Visualization, Reviewing and Editing. **Ninfa Amato:** Software, Funding acquisition, Reviewing and Editing. **Matteo Pereno:** Investigation, **Silvia Riccardi:** Reviewing and Editing, **Andrea Danani:** Methodology, Reviewing and Editing, **Simone Ulzega:** Software, Formal analysis, Visualization, Reviewing and Editing. **Mauro Manconi:** Resources, Supervision, Funding acquisition, Reviewing and Editing.

Declaration of competing interest

None to declare.

Acknowledgments

We are deeply grateful to the patient and his family. We also thank the Advisory Board of Scientific Research organized by the Ente Ospedaliero Cantonale (ABREOC) that funded data collection.

Supplementary data

Supplementary data to this article can be found online at https://doi.org/10.1016/j.cortex.2022.05.021.

REFERENCES

Avvenuti, G., Handjaras, G., Betta, M., Cataldi, J., Imperatori, L. S., Lattanzi, S., et al. (2020). Integrity of corpus callosum is essential for the cross-hemispheric propagation of sleep slow waves: A high-density eeg study in split-brain patients. *Journal of Neuroscience, 40*(29), 5589–5603. https://doi.org/10.1523/JNEUROSCI.2571-19.2020

Baldini, T., Loddo, G., Sessagesimi, E., Mignani, F., Cirignotta, F., Mondini, S., et al. (2019). Clinical features and pathophysiology of disorders of arousal in adults: A window into the sleeping brain. *The Florida Nurse, 10*(MAY), 1–9. https://doi.org/10.3389/fneur.2019.00526

Bassetti, C., Vella, S., Donati, F., & Wielepp, P. (2000). SPECT during sleepwalking. *The Lancet, 356*, 484–485.

Berry, R. B., Brooks, R., Gamaldo, C., Harding, S. M., Lloyd, R. M., Quan, S. F., … Vaughn, B. V. (2020). AASM Scoring Manual Updates for 2017 (Version 2.4). *Journal of Clinical Sleep Medicine, 13*(5), 665–666.

Bhat, S., Patel, D., Rosen, D., & Chokroverty, S. (2012). A case of a confusional arousal arising from REM sleep. *Sleep Medicine, 13*(3), 317–318. https://doi.org/10.1016/j.sleep.2011.10.028

Castelnovo, A., Loddo, G., Provini, F., & Manconi, M. (2021). Frequent, complex and vivid dream-like/hallucinatory experiences during NREM sleep parasomnia episodes. *Sleep Medicine, 82*, 61–64. https://doi.org/10.1016/J.SLEEP.2021.03.032

Castelnovo, A., Loddo, G., Provini, F., Miano, S., & Manconi, M. (2021). Mental activity during episodes of sleepwalking, night terrors or confusional arousals: Differences between children and adults. *Nature and Science of Sleep, 13*, 829–840. https://doi.org/10.2147/NSS.S309868

Castelnovo, A., Lopez, R., Proserpio, P., Nobili, L., & Dauvilliers, Y. (2018). NREM sleep parasomnias as disorders of sleep-state dissociation. *Nature Reviews. Neurology, 14*(8), 470–481. https://doi.org/10.1038/s41582-018-0030-y

Castelnovo, A., Riedner, B. A., Smith, R. F., Tononi, G., Boly, M., & Benca, R. M. (2016). Scalp and source power topography in sleepwalking and sleep terrors: A high-density EEG study. *Sleep, 39*(10), 1815–1825. https://doi.org/10.5665/sleep.6162

Cavanna, A. E., & Trimble, M. R. (2006). The precuneus: A review of its functional anatomy and behavioural correlates. *Brain, 129*(Pt 3), 564–583. https://doi.org/10.1093/brain/awl004

Delorme, A., & Makeig, S. (2004). Eeglab: An open source toolbox for analysis of single-trial EEG dynamics including independent component analysis. *Journal of Neuroscience Methods, 134*(1), 9–21. https://doi.org/10.1016/j.jneumeth.2003.10.009

Derry, C. P., Harvey, A. S., Walker, M. C., Duncan, J. S., & Berkovic, S. F. (2009). NREM arousal parasomnias and their distinction from nocturnal frontal lobe epilepsy: A video EEG analysis. *Sleep, 32*(12), 1637–1644. https://doi.org/10.1093/sleep/32.12.1637

Desjardins, M.È., Carrier, J., Lina, J. M., Fortin, M., Gosselin, N., Montplaisir, J., et al. (2017). EEG functional connectivity prior to sleepwalking: Evidence of interplay between sleep and wakefulness. *Sleep, 40*(4), 1–8. https://doi.org/10.1093/sleep/zsx024

Destrieux, C., Fischl, B., Dale, A., & Halgren, E. (2010). Automatic parcellation of human cortical gyri and sulci using standard anatomical nomenclature. *NeuroImage, 53*(1), 1–15. https://doi.org/10.1016/j.neuroimage.2010.06.010

Dixon, M. L., Thiruchselvam, R., Todd, R., & Christoff, K. (2017). Emotion and the prefrontal cortex: An integrative review. *Psychological Bulletin, 143*(10), 1033–1081. https://doi.org/10.1037/bul0000096

Espa, F., Ondze, B., Deglise, P., Billiard, M., & Besset, A. (2000). Sleep architecture, slow wave activity, and sleep spindles in adult patients with sleepwalking and sleep terrors. *Clinical Neurophysiology, 111*(5), 929–939. https://doi.org/10.1016/S1388-2457(00)00249-2

Fernandez, L. M. J., & Lüthi, A. (2020). Sleep spindles: Mechanisms and functions. *Physiological Reviews, 100*, 805–868. https://doi.org/10.1152/physrev.00042.2018

Flamand, M., Boudet, S., Lopes, R., Vignal, J. P., Reyns, N., Charley-Monaca, C., et al. (2018). Confusional arousals during non-rapid eye movement sleep: Evidence from intracerebral recordings. *Sleep, 41*(10), 1–11. https://doi.org/10.1093/sleep/zsy139

Fraschini, M., Demuru, M., Crobe, A., Marrosu, F., Stam, C. J., & Hillebrand, A. (2016). The effect of epoch length on estimated EEG functional connectivity and brain network organisation. *Journal of Neural Engineering, 13*(3), 036015. https://doi.org/10.1088/1741-2560/13/3/036015

Futenma, K., Inoue, Y., Saso, A., Takaesu, Y., Yamashiro, Y., & Matsuura, M. (2022). Three cases of parasomnias similar to sleep terrors occurring during sleep-wake transitions from REM sleep. *Journal of Clinical Sleep Medicine, 18*(2), 669–675. https://doi.org/10.5664/jcsm.9666

Greenblatt, R. E., Pflieger, M. E., & Ossadtchi, A. E. (2012). Connectivity measures applied to human brain electrophysiological data. *Journal of Neuroscience Methods, 207*(1), 1–16. https://doi.org/10.1016/j.jneumeth.2012.02.025

Gu, X., Hof, P. R., Friston, K. J., & Fan, J. (2013). Anterior insular cortex and emotional awareness. *Journal of Comparative Neurology, 521*(15), 3371–3388. https://doi.org/10.1002/cne.23368

Guilleminault, C., Poyares, D., Abat, F., & Palombini, L. (2001). Sleep and wakefulness in somnambulism: A spectral analysis

study. *Journal of Psychosomatic Research*, 51(2), 411–416. https://doi.org/10.1016/S0022-3999(01)00187-8

Hillebrand, A., Tewarie, P., Van Dellen, E., Yu, M., Carbo, E. W. S., Douw, L., et al. (2016). Direction of information flow in large-scale resting-state networks is frequency-dependent. In *Proceedings of the national academy of sciences of the United States of America*. https://doi.org/10.1073/pnas.1515657113

Hiser, J., & Koenigs, M. (2018). The multifaceted role of the ventromedial prefrontal cortex in emotion, decision making, social cognition, and psychopathology. *Biological Psychiatry, 83*(8), 638–647. https://doi.org/10.1016/j.biopsych.2017.10.030

Ingravallo, F., Poli, F., Gilmore, E. V., Pizza, F., Vignatelli, L., Schenck, C. H., et al. (2014). Sleep-related violence and sexual behavior in sleep: A systematic review of medical-legal case reports. *Journal of Clinical Sleep Medicine, 10*(8), 927–935. https://doi.org/10.5664/jcsm.3976

Jaar, O., Pilon, M., Carrier, J., Montplaisir, J., & Zadra, A. (2010). Analysis of slow-wave activity and slow-wave oscillations prior to somnambulism. *Sleep, 33*(11), 1511–1516. https://doi.org/10.1093/sleep/33.11.1511

Januszko, P., Niemcewicz, S., Gajda, T., Wołyńczyk-Gmaj, D., Piotrowska, A. J., Gmaj, B., et al. (2016). Sleepwalking episodes are preceded by arousal-related activation in the cingulate motor area: EEG current density imaging. *Clinical Neurophysiology, 127*(1), 530–536. https://doi.org/10.1016/j.clinph.2015.01.014

Lamm, C., & Singer, T. (2010). The role of anterior insular cortex in social emotions. *Brain Structure & Function, 214*(5–6), 579–591. https://doi.org/10.1007/s00429-010-0251-3

Lobier, M., Siebenhühner, F., Palva, S., & Palva, J. M. (2014). Phase transfer entropy: A novel phase-based measure for directed connectivity in networks coupled by oscillatory interactions. *NeuroImage, 85*(Pt 2), 853–872. https://doi.org/10.1016/j.neuroimage.2013.08.056

Loddo, G., Sessagesimi, E., Mignani, F., Cirignotta, F., Mondini, S., Licchetta, L., et al. (2009). Specific motor patterns of arousal disorders in adults: A video-polysomnographic analysis of 184 episodes. *Sleep, 32*(12), 936–940. https://doi.org/10.1093/sleep/32.12.1637

Loddo, G., Sessagesimi, E., Mignani, F., Cirignotta, F., Mondini, S., Licchetta, L., et al. (2018). Specific motor patterns of arousal disorders in adults: A video-polysomnographic analysis of 184 episodes. *Sleep Medicine, 41*, 102–109. https://doi.org/10.1016/j.sleep.2017.08.019

Massimini, M., Huber, R., Ferrarelli, F., Hill, S., & Tononi, G. (2004). The sleep slow oscillation as a traveling wave. *Journal of Neuroscience, 24*(31), 6862–6870. https://doi.org/10.1523/JNEUROSCI.1318-04.2004

Maureen, C. (2010). An empirical evaluation of free BEM solvers for accurate M/EEG forward modeling. *The Florida Nurse*, (Event Abstract). https://doi.org/10.3389/conf.fnins.2010.06.00065

Mwenge, B., Brion, A., Uguccioni, G., & Arnulf, I. (2013). Sleepwalking: Long-term home video monitoring. *Sleep Medicine, 14*(11), 1126–1228. https://doi.org/10.1016/j.sleep.2013.04.027

Naitoh, P., Antony-Baas, V., Muzet, A., & Ehrhart, J. (1982). Dynamic relation of sleep spindles and K-complexes to spontaneous phasic arousal in sleeping human subjects. *Sleep, 5*(1), 58–72. https://doi.org/10.1093/sleep/5.1.58

Nakamura, B. J., Ebesutani, C., Bernstein, A., & Chorpita, B. F. (2009). A psychometric analysis of the child behavior checklist DSM-oriented scales. *Journal of Psychopathology and Behavioral Assessment, 109*, 103834. https://doi.org/10.1007/s10862-008-9119-8

Nichols, T. E., Holmes, A. P., & Human Brain Mapping. (2001). Nonparametric permutation tests for functional neuroimaging: A primer with examples. *Human Brain Mapping, 15*, 1–25.

Nolte, G., Bai, O., Wheaton, L., Mari, Z., Vorbach, S., & Hallett, M. (2004). Identifying true brain interaction from EEG data using the imaginary part of coherency. *Clinical Neurophysiology, 115*(10), 2292–2307. https://doi.org/10.1016/j.clinph.2004.04.029

Olson, I. R., Plotzker, A., & Ezzyat, Y. (2007). The enigmatic temporal pole: A review of findings on social and emotional processing. *Brain, 130*(Pt 7), 1718–1731. https://doi.org/10.1093/brain/awm052

Oudiette, D., Constantinescu, I., Leclair-Visonneau, L., Vidailhet, M., Schwartz, S., & Arnulf, I. (2011). Evidence for the re-enactment of a recently learned behavior during sleepwalking. *PLoS ONE, 6*(3), 1–8. https://doi.org/10.1371/journal.pone.0018056

Oudiette, D., Leu, S., Pottier, M., Buzare, M. A., Brion, A., & Arnulf, I. (2009). Dreamlike mentations during sleepwalking and sleep terrors in adults. *Sleep, 32*(12), 1621–1627. https://doi.org/10.1093/sleep/32.12.1621

Pedrazzini, E., & Ptak, R. (2019). Damage to the right temporoparietal junction, but not lateral prefrontal or insular cortex, amplifies the role of goal-directed attention. *Scientific Reports, 9*(1), 306. https://doi.org/10.1038/s41598-018-36537-3

Pereda, E., Quiroga, R. Q., & Bhattacharya, J. (2005). Nonlinear multivariate analysis of neurophysiological signals. *Progress in Neurobiology, 77*(1–2), 1–37. https://doi.org/10.1016/j.pneurobio.2005.10.003

Perrault, R., Carrier, J., Desautels, A., Montplaisir, J., & Zadra, A. (2014). Electroencephalographic slow waves prior to sleepwalking episodes. *Sleep Medicine, 15*(12), 1468–1472. https://doi.org/10.1016/j.sleep.2014.07.020

Peter-Derex, L., Magnin, M., & Bastuji, H. (2015). Heterogeneity of arousals in human sleep: A stereo-electroencephalographic study. *NeuroImage, 123*, 229–244. https://doi.org/10.1016/j.neuroimage.2015.07.057

Petit, D., Pennestri, M. H., Paquet, J., Desautels, A., Zadra, A., Vitaro, F., et al. (2015). Childhood sleepwalking and sleep terrors: A longitudinal study of prevalence and familial aggregation. *JAMA Pediatrics, 169*(7), 653–658. https://doi.org/10.1001/jamapediatrics.2015.127

Ratti, P. L., Amato, N., David, O., & Manconi, M. (2018). A high-density polysomnographic picture of disorders of arousal. *Sleep, 41*(11), 1–3. https://doi.org/10.1093/sleep/zsy162

Richards, J. E., Sanchez, C., Phillips-Meek, M., & Xie, W. (2016). A database of age-appropriate average MRI templates. *NeuroImage, 124*(Pt B), 1254–1259. https://doi.org/10.1016/j.neuroimage.2015.04.055

Rocha, A., & Arnulf, I. (2020). NREM parasomnia as a dream enacting behavior. *Sleep Medicine, 75*, 103–105. https://doi.org/10.1016/j.sleep.2020.02.024

Sarasso, S., Pigorini, A., Proserpio, P., Gibbs, S. A., Massimini, M., & Nobili, L. (2014). Fluid boundaries between wake and sleep: Experimental evidence from Stereo-EEG recordings. *Archives Italiennes de Biologie, 152*(2–3), 169–177. https://doi.org/10.12871/0002982920142311

Schenck, C. H., Pareja, J. A., Patterson, A. L., & Mahowald, M. W. (1998). Analysis of polysomnographic events surrounding 252 slow-wave sleep arousals in thirty-eight adults with injurious sleepwalking and sleep terrors. *Journal of Clinical Neurophysiology, 15*(2), 159–166. https://doi.org/10.1097/00004691-199803000-00010

Sforza, E., Jouny, C., & Ibanez, V. (2000). Cardiac activation during arousal in humans: Further evidence for hierarchy in the arousal response. *Clinical Neurophysiology, 111*, 1611–1619. https://doi.org/10.1016/S1388-2457(00)00363-1

Siclari, F., Baird, B., Perogamvros, L., Bernardi, G., LaRocque, J. J., Riedner, B., et al. (2017). The neural correlates of dreaming. *Nature Neuroscience, 20*(6), 872–878. https://doi.org/10.1038/nn.4545

Tadel, F., Baillet, S., Mosher, J. C., Pantazis, D., & Leahy, R. M. (2011). Brainstorm: A user-friendly application for MEG/EEG analysis. *Computational Intelligence and Neuroscience*. https://doi.org/10.1155/2011/879716

Terzaghi, M., Sartori, I., Tassi, L., Didato, G., Rustioni, V., LoRusso, G., et al. (2009). Evidence of dissociated arousal states during nrem parasomnia from an intracerebral neurophysiological study. *Sleep, 32*(3), 409–412. https://doi.org/10.1093/sleep/32.3.409

Terzaghi, M., Sartori, I., Tassi, L., Rustioni, V., Proserpio, P., Lorusso, G., et al. (2012). Dissociated local arousal states underlying essential clinical features of non-rapid eye movement arousal parasomnia: An intracerebral stereo-electroencephalographic study. *Journal of Sleep Research, 21*(5), 502–506. https://doi.org/10.1111/j.1365-2869.2012.01003.x

Tononi, G. (2004). An information integration theory of consciousness. *BMC Neuroscience, 5*, 42. https://doi.org/10.1186/1471-2202-5-42

Tzourio-Mazoyer, N., Landeau, B., Papathanassiou, D., Crivello, F., Etard, O., Delcroix, N., et al. (2002). Automated anatomical labeling of activations in SPM using a macroscopic anatomical parcellation of the MNI MRI single-subject brain. *NeuroImage, 14*(5), 391–398. https://doi.org/10.1006/nimg.2001.0978

Uguccioni, G., Golmar, J. L., Noël de Fontréaux, A., Leu-Semenescu, S., Brion, A., & Arnulf, I. (2013). Fight or flight? Dream content during sleepwalking/sleep terrors vs rapid eye movement sleep behavior disorder. *Sleep Medicine, 14*(5), 391–394. https://onlinelibrary.wiley.com/doi/10.1111/jsr.12219 10.1016/j.sleep.2013.01.014.

Zadra, A., Desautels, A., Petit, D., & Montplaisir, J. (2013). Somnambulism: Clinical aspects and pathophysiological hypotheses. The. *Lancet Neurology, 12*(3), 285–294. https://doi.org/10.1016/S1474-4422(12)70322-8

Zadra, A., & Nielsen, T. (1998). Topographical EEG mapping in a case of recurrent sleep terrors. *Dreaming, 8*, 67–74. https://doi.org/10.1023/B:DREM.0000005897.62698

Zadra, A., Pilon, M., Joncas, S., Rompré, S., & Montplaisir, J. (2004). Analysis of postarousal EEG activity during somnambulistic episodes. *Journal of Sleep Research, 13*(3), 279–284. https://doi.org/10.1111/j.1365-2869.2004.00404.x

Zucconi, M., & Ferini-Strambi, L. (2000). NREM parasomnias: Arousal disorders and differentiation from nocturnal frontal lobe epilepsy. *Clinical Neurophysiology*, (Suppl 2), S129–S135. https://doi.org/10.1016/S1388-2457(00)00413-2

6.6. Supplementary material

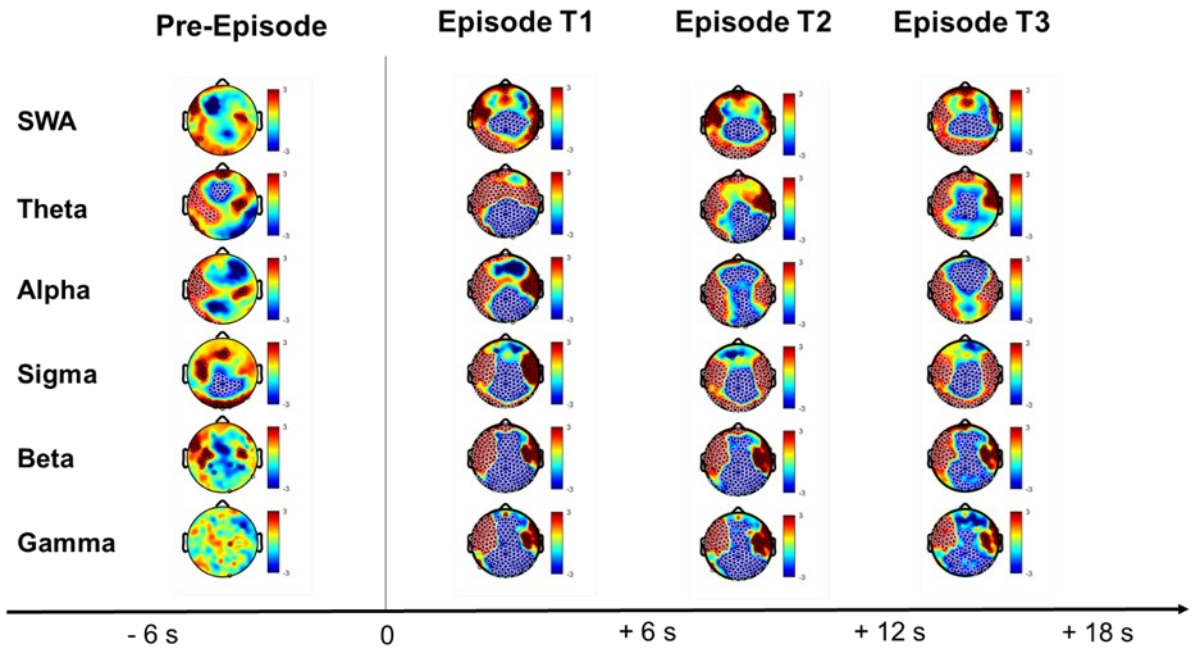

Supplementary Figure 1 | Scalp power analysis in all frequency bands (normalized values)

Rows: frequency bands of interest as indicated: SWA (0.5-4 Hz), theta (4-8 Hz), alpha (8- 12 Hz), sigma (12-16 Hz), beta (18-25 Hz), gamma (25-45 Hz). Columns: comparison between spatially normalized power at baseline and pre-episode, episode T1, episode T2, episode T3. The horizontal black arrow at the bottom defines time in seconds. Baseline: average power from -3 to -2 minutes before behavioral onset. Pre-episode (column 1): average power from -6 seconds prior to onset to onset. Episode T1 (column 2): from onset to 6 seconds after onset. Episode T2 (column 3): from 6 to 12 seconds after onset. Episode T3 (column 4): from 12 to 18 seconds after onset. Blue values: a decrease in absolute EEG power in pre-episode relative to baseline (pre-episode < baseline). Red values: an increase (pre-episode > baseline). White dots: channels that belong to a statistically significant cluster of electrodes ($P \leq 0.05$) *using statistical nonparametric mapping suprathreshold cluster testing. Black dots: individual channels with* $P < 0.05$ *(uncorrected). Note: Electrodes on the face and outer ring of the sensor net were eliminated entirely for all participants due to excessive artifacts, yielding a final scalp montage of 186 channels.*

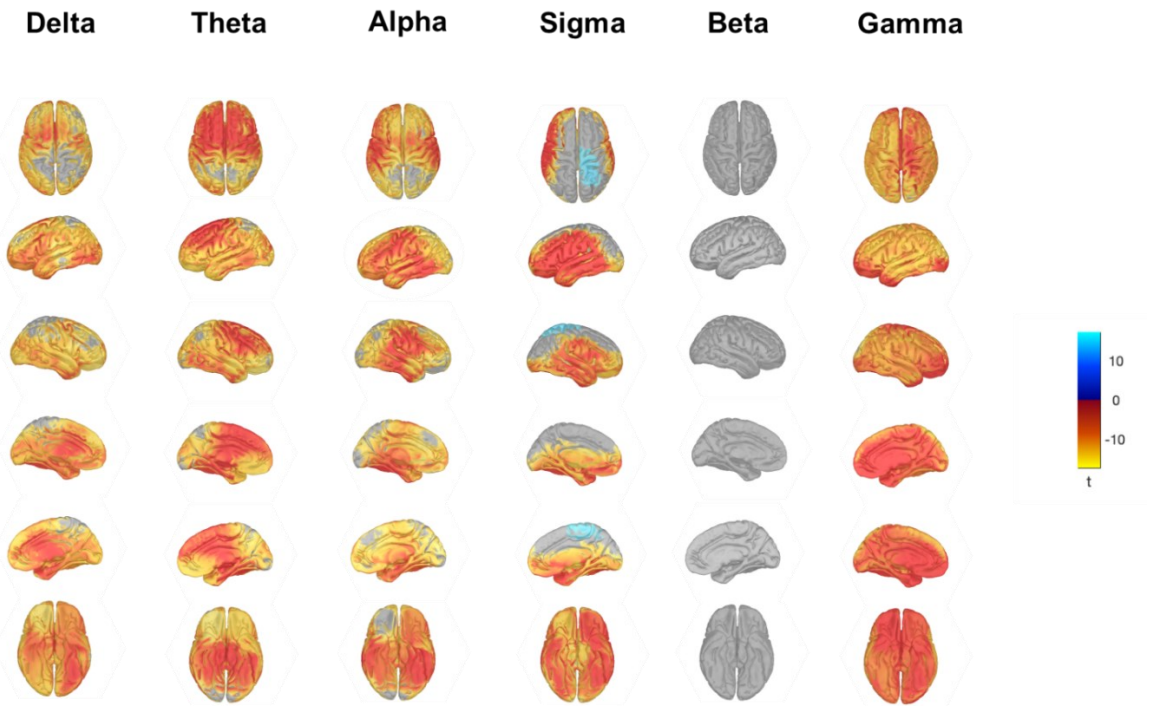

Supplementary Figure 2 | Source power analysis in all frequency bands: Baseline versus Episode T1

Columns: frequency bands of interest as indicated: SWA (0.5-4 Hz), theta (4-8 Hz), alpha (8- 12 Hz), sigma (12-15 Hz), beta (15-25 Hz), gamma (25-45 Hz). First row: Horizontal plane (top); second row: sagittal plane, right hemisphere (lateral), third row: sagittal plane, left hemisphere (lateral), fourth row: sagittal plane, right hemisphere (medial), fifth row: sagittal plane, left hemisphere (medial), sixth row: horizontal plane (bottom). Baseline: from -3 to -2 minutes before behavioral onset. Pre-episode: from -6 seconds prior to onset to onset. Episode T1: from onset to 6 seconds after onset. Episode T2: from 6 to 12 seconds after onset. Episode T3: from 12 to 18 seconds after onset. Gray color: non-significant differences after correction for multiple comparison using topological cluster false-discovery rate (FDR). Blue color: a significant decrease in source power in pre-episode relative to baseline (pre-episode < baseline) after FDR. Red color: a significant increase in source power in pre-episode relative to baseline (pre-episode > baseline) after FDR.

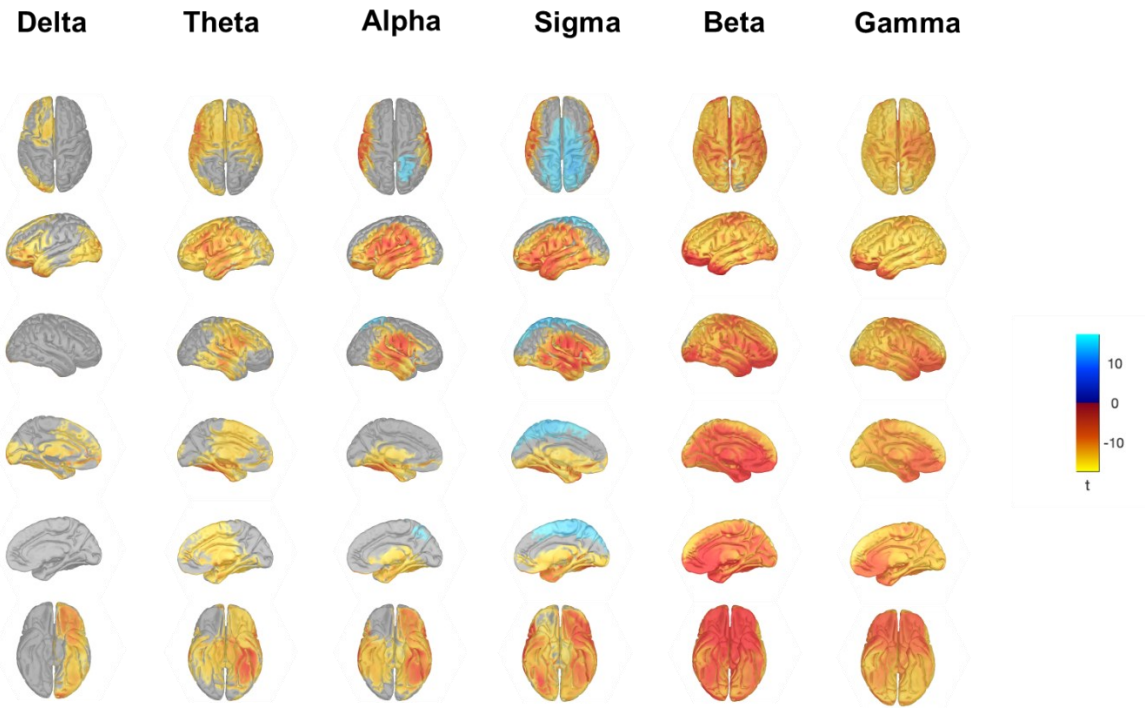

Supplementary Figure 3 | Source power analysis in all frequency bands: Baseline versus Episode T2

Columns: frequency bands of interest as indicated: SWA (0.5-4 Hz), theta (4-8 Hz), alpha (8- 12 Hz), sigma (12-15 Hz), beta (15-25 Hz), gamma (25-45 Hz). First row: Horizontal plane (top); second row: sagittal plane, right hemisphere (lateral), third row: sagittal plane, left hemisphere (lateral), fourth row: sagittal plane, right hemisphere (medial), fifth row: sagittal plane, left hemisphere (medial), sixth row: horizontal plane (bottom). Baseline: from -3 to -2 minutes before behavioral onset. Pre-episode: from -6 seconds prior to onset to onset. Episode T1: from onset to 6 seconds after onset. Episode T2: from 6 to 12 seconds after onset. Episode T3: from 12 to 18 seconds after onset. Gray color: non-significant differences after correction for multiple comparison using topological cluster false-discovery rate (FDR). Blue color: a significant decrease in source power in pre-episode relative to baseline (pre-episode < baseline) after FDR. Red color: a significant increase in source power in pre-episode relative to baseline (pre-episode > baseline) after FDR.

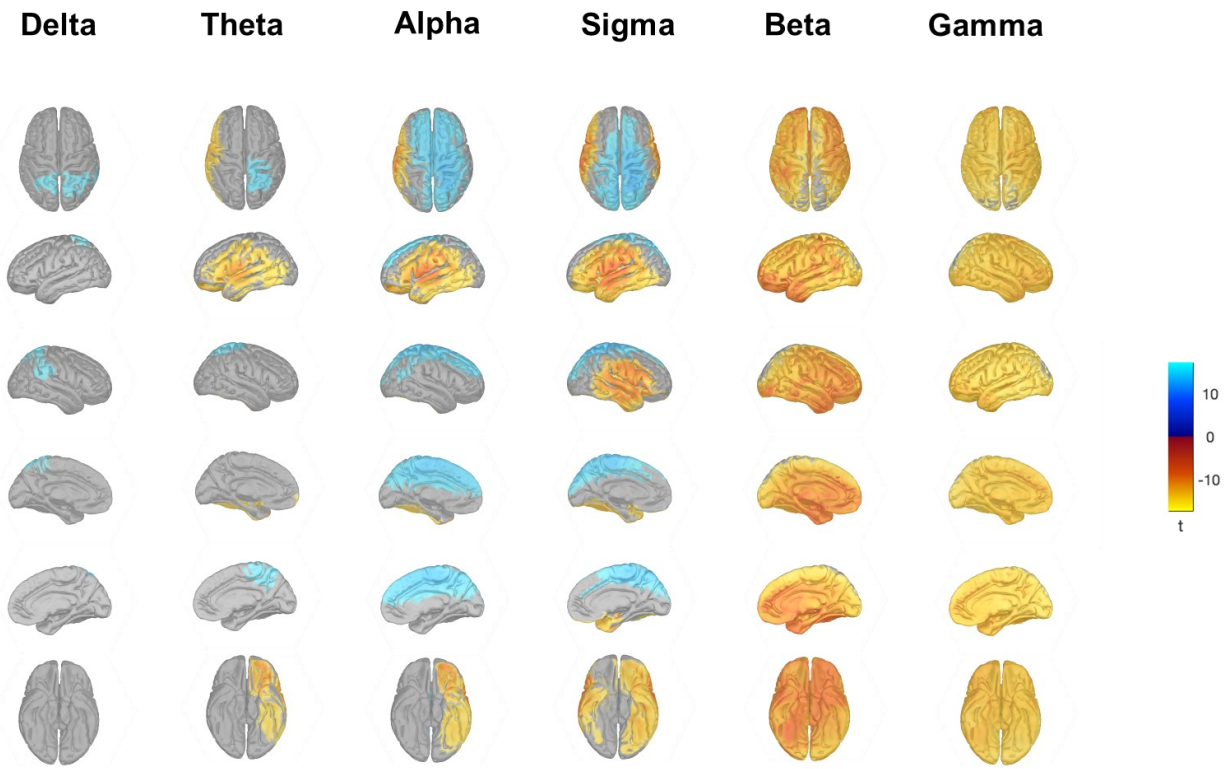

Supplementary Figure 4 | Source power analysis in all frequency bands: Baseline versus Episode T3

Columns: frequency bands of interest as indicated: SWA (0.5-4 Hz), theta (4-8 Hz), alpha (8- 12 Hz), sigma (12-15 Hz), beta (15-25 Hz), gamma (25-45 Hz). First row: Horizontal plane (top); second row: sagittal plane, right hemisphere (lateral), third row: sagittal plane, left hemisphere (lateral), fourth row: sagittal plane, right hemisphere (medial), fifth row: sagittal plane, left hemisphere (medial), sixth row: horizontal plane (bottom). Baseline: from -3 to -2 minutes before behavioral onset. Pre-episode: from -6 seconds prior to onset to onset. Episode T1: from onset to 6 seconds after onset. Episode T2: from 6 to 12 seconds after onset. Episode T3: from 12 to 18 seconds after onset. Gray color: non-significant differences after correction for multiple comparison using topological cluster false-discovery rate (FDR). Blue color: a significant decrease in source power in pre-episode relative to baseline (pre-episode < baseline) after FDR. Red color: a significant increase in source power in pre-episode relative to baseline (pre-episode > baseline) after FDR.

6.7. References

American Academy of Sleep Medicine. (2014). International Classification of Sleep Disorders. Darien, IL: American Academy of Sleep Medicine.

American Psychiatric Association. (2013a). American Psychiatric Association: Diagnostic and Statistical Manual of Mental Disorders Fifth Edition. In Arlington.

American Psychiatric Association. (2013b). Diagnostic and statistical manual of mental disorders (5th ed.). Washington, DC: American Psychiatric Association.

Castelnovo, A., Amacker, J., Maiolo, M., Amato, N., Pereno, M., Riccardi, S., Danani, A., Ulzega, S., & Manconi, M. (2022). High-density EEG power topography and connectivity during confusional arousal. Cortex; a Journal Devoted to the Study of the Nervous System and Behavior, 155, 62–74. https://doi.org/10.1016/J.CORTEX.2022.05.021

Castelnovo, A., Lopez, R., Proserpio, P., Nobili, L., & Dauvilliers, Y. (2018). NREM sleep parasomnias as disorders of sleep-state dissociation. Nature Reviews. Neurology, 14(8), 470–481. https://doi.org/10.1038/s41582-018-0030-y

Castelnovo, A., Riedner, B. A., Smith, R. F., Tononi, G., Boly, M., & Benca, R. M. (2016). Scalp and Source Power Topography in Sleepwalking and Sleep Terrors: A High-Density EEG Study. Sleep, 39(10), 1815–1825. https://doi.org/10.5665/sleep.6162

Gaudreau, H., Joncas, S., Zadra, A., & Montplaisir, J. Y. (2000). Dynamics of slow-wave activity during the NREM sleep of sleepwalkers and control subjects. Sleep, 23(6), 755–760.

Nobili, L., de Gennaro, L., Proserpio, P., Moroni, F., Sarasso, S., Pigorini, A., de Carli, F., & Ferrara, M. (2012). Local aspects of sleep: observations from intracerebral recordings in humans. Progress in Brain Research, 199, 219–232. https://doi.org/10.1016/B978-0-444-59427-3.00013-7

Oudiette, D., Leu, S., Pottier, M., Buzare, M. A., Brion, A., & Arnulf, I. (2009). Dreamlike mentations during sleepwalking and sleep terrors in adults. Sleep, 32(12), 1621–1627. https://doi.org/10.1093/sleep/32.12.1621

Pressman, M. R. (2004). Hypersynchronous delta sleep EEG activity and sudden arousals from slow-wave sleep in adults without a history of parasomnias: clinical and forensic implications. Sleep, 27(4), 706–710. https://doi.org/10.1093/SLEEP/27.4.706

Terzaghi, M., Sartori, I., Tassi, L., Didato, G., Rustioni, V., LoRusso, G., Manni, R., & Nobili, L. (2009). Evidence of dissociated arousal states during nrem parasomnia from an intracerebral neurophysiological study. Sleep, 32(3), 409–412. https://doi.org/10.1093/sleep/32.3.409

Zucconi, M., Oldani, A., Ferini-Strambi, L., & Smirne, S. (1995). Arousal fluctuations in non-rapid eye movement parasomnias: the role of cyclic alternating pattern as a measure of sleep instability. In Journal of Clinical Neurophysiology (Vol. 12, Issue 2, pp. 147–154). https://doi.org/10.1097/00004691-199503000-00005

7. CONCLUSIONS AND FUTURE PERSPECTIVES

7.1. Introduction

This is a methodological cumulative thesis that aims to interrogate sleep in different physiological and pathological conditions to add new pieces of knowledge to the intriguing puzzle of brain development and function.

In this last chapter, I summarize the results of 5 projects conducted for this PhD thesis (described in chapter 2-6) and depict the near-future projects and perspectives derived from the current work.

7.2. Project 1

The Matlab-based hdEEG pipeline created for data pre- and post- processing is currently complete and works smoothly. Working on this pipeline greatly improved my programming skills and my performance in generating efficient algorithms for hdEEG signal analysis.

The following step is to improve the current pipeline in a more user-friendly format, by implementing it with intuitive graphical interfaces able to guide users step by step into the analysis process. In collaboration with the Faculty of Informatics, we planned to create a fast-cleaning toolbox for the manual and automatic detection of artifacts based on spectral analysis. We are applying for grant awarded by the Hasler Foundation to cover up the expenses of this project. Finally, our laboratory will soon

host students from USI to implement the visualization of ICA components (see chapter 2).

7.3. Project 2

Sleep related slow waves originate more posteriorly and have a stronger posterior involvement in young adolescents compared to young adults. While slow waves of adolescents are larger in amplitude and locally more synchronous, they also involve a smaller proportion of electrodes relative to adults. This probably reflects an incomplete synaptic pruning and still immature development of local and long-range white matter connections. Moreover, slow waves tend to originate more often in the right compared to the left hemisphere, and express a higher inter-hemispheric involvement asymmetry, probably due to an incomplete maturation of the corpus callosum. A final proof-of-concept will only be offered by large longitudinal studies combining hdEEG sleep recordings and MRI scans that will require dedicated fundings.

In the near future, I will use the same dataset to explore the unsolved issue of physiological arousal. Technically speaking, an arousal is a brief sleep perturbation defined as an abrupt shift of electrocortical activity into higher frequencies (including alpha, theta, and/or frequencies greater than 16 Hz), with a duration ranging between 3 and 15 seconds. Arousals are considered transient states in between sleep and wakefulness, in which brain undermines sleep continuity and decides to preserve or interrupt sleep depending on the relevance of internal or external stimuli. In particular,

I am planning to use both power and connectivity analytic tools (see project 5) to better explore this transitional state. The detailed characterization of physiological arousal may pave the way to understand pathological arousals. This study will be supported by the EOC Young Researchers Grant 2022.

7.4. Project 3

Children/adolescents with ADHD display higher low-frequency EEG activity during NREM sleep, but not during REM sleep and wakefulness, compared to typically developing peers. Such a difference involves a wide centro-posterior cluster of channels in the 3-10 Hz range (low-alpha, theta and high delta). Between-group differences are maximal in slow wave sleep of the first sleep cycle. Moreover, spectral differences are positively correlated with average total sleep time. These results can be explained by 2 alternative hypotheses: 1) a delay in brain maturation, as suggested by the more posterior distribution of normalized SWA and/or 2) an alteration in sleep homeostasis, as suggest by the increase in absolute SWA, selective for the upper SWA (2.5-4 Hz), which is known to be homeostatically regulated, as opposed to lower SWA (0.5-2.5 Hz). These 2 hypotheses are not mutually exclusive, as sleep abnormalities in ADHD patients (primary or secondary to underlying sleep disorders), can in turn interfere with (and delay) cortical maturation, especially during early developmental phases.

I am currently supervising the thesis of a student in Medicine on the same topic with the aim of providing further support to this framework of interpretation. We are performing a detailed slow wave detection analysis (as described in project 2) on the

same ADHD dataset. I showed in project 2 that in typically developing children/young adolescents, slow wave density, amplitude, origin, synchronization, and distribution is age dependent. According to the maturational delay hypothesis, ADHD subjects, compared to typically developing peers, should have, not only more, higher, more local, and less synchronous slow waves (as also expected by sleep deprivation (Plante et al., 2016)), but also more posterior and right-sided origins and distributions.

7.5. Project 4

SCZ first-degree relatives (FDRs), meaning subjects at SCZ high-genetic risk (who share similar neuro-anatomical, neurofunctional, and neurophysiological profiles to their affected relatives), have significantly smaller slow waves compared to subjects with no family history for psychotic disorders. Additionally, traveled distances is significantly reduced in FDRs. Furthermore, slow wave amplitude and slow wave traveling distance, as well as slow wave density, might reduce in young patients hospitalized at their first psychosis episode. Long–term effective antipsychotic treatment may be associated with an almost complete recover of slow wave density and amplitude, and to a partial normalization of slow wave traveling. The residual deficit in slow wave traveling may reflect the persistent disruption of long-range white matter connections. Taken together, these data offer preliminary but encouraging evidence that slow wave traveling properties could be effectively used in early SCZ. Slow wave traveling could help to interpret anatomical abnormalities, support the early recognition of SCZ patients and definition of their prognosis, and on a wider perspective, to develop new treatment strategies.

To further progress in this direction, larger cohorts of drug-naïve early course psychosis patients are obviously required to confirm current preliminary results. In collaboration with the University of Milan, I am planning to analyse 20 drug-naïve first episode psychosis patients and 20 age and gender matched control subjects recorded with a 64 channel hdEEG system. However, only much larger, longitudinal studies of CHR patients combining MRI and hdEEG will be able to fully assess the prognostic and clinical value of the sleep slow wave deficit and its connection with anatomical white (and grey) matter abnormalities.

Another under investigated area of research that I foresee to explore, is the presence, prevalence, clinical impact and possible negative pathogenetic effect of sleep disorders in patients with psychotic disorders. I will explore this interesting topic if I will obtain the funding from a young researchers grant proposal that I wrote in collaboration with San Raffaele Hospital.

7.6. Project 5

Brain activity at the onset of DOA episodes is characterized by the suppression of sigma activity and by the increase of power in other frequency bands, in line with a recent study we conducted on a larger papulation of DOA patients (N = 53) using traditional low-density EEG (Mainieri et al., 2022). This pattern qualitatively resembles that previously observed at the onset of physiological arousal. This suggests that both physiological and pathological arousals originate by the activation of a common pathway. However, during DOA episodes, bilateral Broadman area 7

and right Broadman areas 39 and 40 are relatively are spared by an otherwise massive and widespread SWA increase. Functional connectivity analysis in the same frequency range reveals a drastic increase in the number, differentiation and complexity of brain networks from baseline sleep to full-blown episodes, in line with the hypothesis that consciousness partially re-emerge during DOA episodes.

Of note, a recently published hdEEG study from another Swiss group revealed no difference between DOA episodes and simple awakenings in adult patients with DOA (Cataldi et al., 2022), The study only found higher delta and lower beta power in the 1-minute window preceding DOA episodes compared to the 1-minute window preceding simple awakenings. It is possible that variability between subjects and episodes reduced the sensitivity of the study to detect differences between the 2 conditions (awakenings vs DOA episodes) and/or that the awakening process itself is altered in patients with DOA.

In this respect, I am planning to conduct two new studies:

First, thanks to a fruitful ongoing collaboration with the Sleep Center of the Bellaria Hospital in Bologna, I will have access to a large dataset of patients with DOA and to age and gender matched healthy subjects, collected with a 20-channel portable EEG system. Thus, I will be able to analyze and compare awakenings from both populations, to explore the possibility of an intrinsic derangement of the arousal/awakening process in patients with DOA.

Second, I will apply the same systematic analysis used in project 5 to study one single case (see chapter 6), on several episodes from different patients that we are currently collecting at the Sleep Medicine Unit in Lugano. The main goal will be to

verify whether the reported results could be generalized to DOA population. In will explore intra and inter-subject statistical variability, as the previous study by Cataldi et al. (Cataldi et al., 2022) did not. Moreover, the current pipeline allows me to study not only EEG power but also more complex measures of brain connectivity, which may add relevant complementary information. This complex analysis will be possible thanks to a collaboration with the University of Applied Sciences of Zurich (ZHAW), which will provide support for the complex and computational demanding source connectivity analyses required for the project.

Finally, I am also planning to study in more detail brain functional connectivity (and more specifically phase transfer energy) during different states of being, meaning during wakefulness, sleep onset, NREM and REM sleep (taking into account different times of the night and sleep cycles), and physiological arousal, in order to have a solid background to interpret results in DOA patients.

7.7. Conclusions

This thesis should be considered as a first step towards the creation of a solid bridge between clinical medicine (in the fields of sleep and psychiatry), and new technological advances employed in the field of neuroscience.

In particular, I implemented the use of advanced technique (hdEEG) in the clinical routine of a sleep medicine unit. HdEEG is a feasible and informative magnifying glass to define with a superlative temporal and good spatial resolution both physiological and pathological brain processes, especially if applied in the stable and

noise-less condition of sleep, where the most crucial neuroplastic events stand out in their clearest purity over the silence of the night.

The hdEEG pipeline that I developed for this thesis works properly, is flexible and user-friendly, and can be successfully used to test specific hypotheses on the pathophysiology of clinical populations.

7.8. References

Cataldi, J., Stephan, A.M., Marchi, N.A., Haba-Rubio, J., Siclari, F., 2022. Abnormal timing of slow wave synchronization processes in non-rapid eye movement sleep parasomnias. Sleep. https://doi.org/10.1093/SLEEP/ZSAC111

Mainieri, G., Loddo, G., Castelnovo, A., Balella, G., Cilea, R., Mondini, S., Manconi, M., Provini, F., 2022. EEG Activation Does Not Differ in Simple and Complex Episodes of Disorders of Arousal: A Spectral Analysis Study. Nat Sci Sleep 14, 1097–1111. https://doi.org/10.2147/NSS.S360120

Plante, D.T., Goldstein, M.R., Cook, J.D., Smith, R., Riedner, B.A., Rumble, M.E., Jelenchick, L., Roth, A., Tononi, G., Benca, R.M., Peterson, M.J., 2016. Effects of partial sleep deprivation on slow waves during non-rapid eye movement sleep: a high density EEG investigation. Clin Neurophysiol 127, 1436. https://doi.org/10.1016/J.CLINPH.2015.10.040